**Nuno César dos Santos Grosso**

Engenheiro do Ambiente

# Development of a satellite based $PM_{10}$ concentration product for urban areas

Dissertação para obtenção do Grau de Doutor em
Engenharia do Ambiente

Orientador: Francisco Manuel Freire Cardoso Ferreira, PhD,
Professor Associado, FCT/UNL

Co-orientadores: Maria Júlia Fonseca de Seixas, PhD,
Professora Associada, FCT/UNL

Júri:

Presidente: António Pereira de Sousa da Câmara

Arguentes: Annette Ladstätter-Weißenmayer
Alexandre Filipe Fernandes Caseiro

Ciência.Inovação 2010

UNIÃO EUROPEIA
Fundo Social Europeu

FACULDADE DE CIÊNCIAS E TECNOLOGIA
UNIVERSIDADE NOVA DE LISBOA

**Janeiro, 2013**

**Development of a satellite based $PM_{10}$ concentration product for urban areas**

*Para os meus pais*

Acknowledgments

During these years many are the ones I have to be thankful to, both at a professional and personal level. I won't do them justice in the next lines. But I will try.

Both my supervisors, Francisco Ferreira and Júlia Seixas, for giving me the opportunity to start working in science, the freedom to develop my own path and the support necessary to finish the thesis.

Dr. Nicolaos Sifakis, of the National Observatory of Athens, for providing me the opportunity to work with him in Athens and introducing me to the subject and method that would become the core of my thesis research.

The Air Quality research group in the FCT/UNL, for all the help, throughout these years, regarding project development, air quality data collection and literature review. I especially would like to thank: Joana Monjardino for the precious help collecting the necessary air quality datasets and for providing me with several of the papers, reports and legislation used during the literature review; Sandra Mesquita, for all the work developed with me in the Aircast project and the help given in the several stages of my thesis; Hugo Tente for his help during the literature review and advices ; Pedro Gomes and Jorge Neto for the provided air quality and meteorological data.

Conceição Capelo and Carina Gomes, for always being available to solve any administrative problem I had with absolute competence and dedication.

For all the contributes during the entire writing process of this document, from the definition of its structure to the discussion of its content and finally its proof reading, I would like to thank Dimitris Paronis, Nuno Carvalhais, Pedro Lourenço, Francisco Ferreira and Júlia Seixas.

The CCIAM research group, especially Prof. Filipe Duarte Santos, the research centre coordinator, Maria João Cruz and Pedro Garrett, coordinators of the projects I'm currently involved, and Luís Dias, my office colleague, for all the support and understanding shown during this last two years, where I had to divide my time between the thesis and everyday work.

Dimitris Paronis, for the continuous exchange of ideas, the willingness to participate in the work being developed and the always insightful advices.

Since 2003, when we first meet in a conference in Crete, he not only opened the door to his office but also the door to his home, both with tremendous generosity. During these last years he became a friend that I truly treasure.

António Rocha and Nuno Pacheco, for their friendship and the work developed in some of the parallel projects that supported my research.

Pedro Lourenço, for his friendship, generosity and for the always interesting inputs to the work being developed.

João Pedro Nunes, who I see not only as one of my friends but also as a role model in terms of scientific research work and to whose advices I've always listened with great attention.

Nuno Carvalhais is another of those role models but mostly is one of my best friends, present in so many great moments of my life in the last 12 years. He was always the right person to discuss everything, from the details of my research to our borderline philosophical problems during the sometimes troublesome PhD years and was therefore an essential part of all this process.

Ricardo Franco, Rui Pimenta and Hugo Tente, who have been constant presences in my life for many years now and, with their endless camaraderie, have helped me to keep sane and to see that there are more important things in life than work.

My grandmother, my sister, my mother and my father. They are the strength behind this thesis. Without their love and support this work would have been impossible. These pages are as much theirs as they are mine.

This work was supported by the Portuguese Foundation for Science and Technology (FCT), the European Union under Operational Program "Science and Innovation" (POCI 2010), PhD grant ref. SFRH/BD/6516/2001

# Abstract

Suspended particulate matter (PM) is one of the most important atmospheric constituents with significant impacts in the climate system and human health. The wide spatiotemporal scale of their effects represents a monitoring challenge that current ground based systems, with limited spatial coverage, cannot fully address. Satellite aerosol optical thickness (AOT) products can complement those monitoring systems by providing, in a periodical basis, spatially resolved ground PM distribution patterns, estimated using linear regression models. Since most satellite AOT products have relevant limitations over high reflective urban areas, where most anthropogenic PM emission sources and world population are concentrated, the development and validation of algorithms to tackle these constraints assumes a paramount importance.

The main objective of this thesis was to assess the suitability of one of those alternative AOT retrieval algorithms, based on the contrast reduction effect measured between two images (one reference and one polluted image), for urban $PM_{10}$ estimation, using MODIS imagery. In order to achieve this objective the work focused primarily on the optimization and validation of a contrast reduction algorithm based on the Differential Texture Analysis (DTA). Several factors were considered such as spatial resolution, reference and polluted viewing geometry similarity and land cover combination to provide more stable and comparable results, while minimizing viewing angle and surface reflectance change effects on algorithm's accuracy. These optimal AOT retrieval conditions

led to a relatively good agreement with the AERONET AOT measurements (r=0.78) for a set of selected European cities and a higher number of valid retrievals when comparing with the MODIS standard aerosol product, supporting the use of this algorithm for urban satellite AOT retrieval. However, the need to define multiple reference images with variable aerosol content as well as the AOT's coarse spatial resolution limits its ability to extract absolute AOT values towards establishing spatially consistent urban aerosol distribution patterns.

The Lisbon Metropolitan air quality stations were used to assess AOT's ability to reproduce $PM_{10}$ concentrations. A characterization of the two variables correlation as a function of $PM_{10}$ time and spatial averaging, season, station type and seasonal reflectance differences between reference and polluted images provided a comprehensive optimal framework for the development of the regression models. This analysis was complemented with the assessment of the relationship of these variables with several other meteorological parameters thus providing additional information to improve $PM_{10}$/AOT correlation or directly estimate $PM_{10}$ concentrations.

Three $PM_{10}$ ground concentration estimation regression models were developed to fully assess AOT's direct capability as the main estimator of daily ground $PM_{10}$ concentration values. Furthermore, the impact of selected meteorological variables was also assessed using a multivariate approach, enhancing the representation of $PM_{10}$ dispersion conditions.

The univariate regression model, using only AOT as an explanatory variable, was able to reproduce between 37 and 61% (95% confidence interval) of the $PM_{10}$ ground concentration variance. Values increased to 50-68%, when wind speed was added to the model and to 53-88% when both variables were used to estimate $PM_{10}$ daily average values, aggregated for all stations. Furthermore the AOT regression coefficients were found to be comparable to other independent studies conducted in different urban regions. $PM_{10}$ underestimation across all models seem to indicate that the satellite based estimations are more representative of background conditions and have a limited capability to reproduce peak concentrations, usually characteristic of smaller areas heavily influence by point sources (traffic or industry).

These results demonstrated the potential of using contrast reduction based AOT values in ground $PM_{10}$ concentration estimation for urban areas, thus helping to establish this AOT retrieval methodology as valid complement to other satellite aerosol products, currently used to assess ground particle concentrations.

However, in order to establish an operational satellite based $PM_{10}$ concentration product for urban areas, future work should focus on: a) removing aerosol residual influence from reference images; b) improving reflectance correction to better account for viewing angle effects introduced by MODIS variable geometries; c) integrating a multi-year dataset to better assess the influence of meteorological variables such as mixing layer height and relative humidity in $PM_{10}$/AOT correlation; d) broaden the development of this algorithm to other sensors to improve spatial (horizontal/vertical) and temporal monitoring capabilities.

# Resumo

As partículas em suspensão (PM) são um dos mais importantes constituintes atmosféricos com impactes significativos no sistema climático e na saúde humana. A ampla escala espaciotemporal destes efeitos representa um desafio em termos de monitorização que as actuais redes de estações de medição de qualidade ao nível do solo não conseguem superar totalmente devido à sua limitada cobertura espacial. Os produtos de Densidade Ótica de Aerossóis (DOA) derivados de imagens de satélite constituem uma fonte de informação complementar aos sistemas de monitorização ao nível do solo. As suas características operacionais permitem a produção cíclica com elevada frequência de padrões espaciais de distribuição de concentrações de PM ao nível do solo, estimados a partir de modelos de regressão linear. A maior parte dos produtos de DOA estimados por satélite possui uma acurácia limitada sobre superfícies urbanas de elevada refletância, onde a maioria da população mundial e das fontes de emissão antropogénicas de PM se concentram. Sob esta perspetiva, o desenvolvimento e validação de algoritmos que superem as limitações de aplicação em zonas urbanas assume uma importância vital.

O objectivo principal desta tese é avaliar a capacidade de estimação de concentrações de PM ao nível do solo a partir de valores de DOA derivados de imagens do sensor MODIS através de algoritmos de regressão baseados no efeito de redução de contraste medido entre duas imagens (uma de referência e outra poluída). Para atingir este objectivo o trabalho desenvolvido foca, numa primeira fase, a optimização e validação de um algoritmo de cálculo de DOA

baseado na redução de contraste, desenvolvido a partir do método de Análise Diferencial da Textura. O estudo considerou diversos factores de optimização do algoritmo, tais como: a resolução espacial; a semelhança de geometria de visualização entre a imagem de referência e a imagem poluída; e a combinação de usos de solo. A consideração destes factores revela-se essencial nos cálculos de DOA, de forma a tornar os resultados mais estáveis e generalizáveis a outras áreas de estudo. As melhorias reflectem-se principalmente na minimização da influência negativa na acurácia do algoritmo introduzida por diferenças nos ângulos de visualização e por alterações sazonais na refletância da superfície. A implementação destas condições ótimas de aplicação do algoritmo de redução de contraste originou numa concordância significativa com as medições de DOA nas estações AERONET (r=0.78) e um número total de medições válidas mais elevado do que o obtido pelo produto standard de DOA do MODIS. Estes resultados sustentam a hipótese de uma maior adequação deste algoritmo para a estimação da densidade óptica de aerossóis em superfícies urbanas. No entanto, observa-se a necessidade de: definir diversas imagens de referência com um conteúdo residual de aerossóis variável (uma para cada grupo de imagens definido com base na semelhança de geometria de visualização); e de considerar a baixa resolução espacial dos valores de AOT ao nível do solo. Estes factores limitam a capacidade de extração de valores absolutos de AOT através de algoritmos baseados em detecção remota por satélite, capazes de definir padrões de distribuição espacialmente consistentes.

A definição de um algoritmo otimizado baseado na redução de contraste permitiu a avaliação da capacidade de reprodução das concentrações de $PM_{10}$ ao nível do solo a partir de valores de DOA. Esta avaliação foi feita através de um caso estudo desenvolvido com base em medições de concentrações de $PM_{10}$ das estações de qualidade do ar da Área Metropolitana de Lisboa. A correlação entre as duas variáveis em é caracterizada em função: do período de agregação temporal para as concentrações de $PM_{10}$; da estação do ano; do tipo de estação ; e das diferenças sazonais de refletância entre imagem de referência e imagem poluída. Os resultados desta análise forneceram um conjunto de condições ótimas para o desenvolvimento dos modelos de regressão linear. Adicionalmente, a avaliação da relação entre estas duas variáveis e diversos parâmetros meteorológicos (por exemplo, intensidade do vento, altura da

camada de mistura e humidade relativa) complementou a análise anterior. A contribuição dos parâmetros meteorológicos para a melhoria da correlação entre concentrações de $PM_{10}$ e valores de DOA forneceu informação adicional relevante para a posterior estimação dos valores de $PM_{10}$.

Foram desenvolvidos três modelos de regressão linear de estimação de concentrações de $PM_{10}$ para avaliar a capacidade directa dos valores de DOA como principal variável preditora desses modelos. A introdução de variáveis meteorológicas foi estudada em esquemas de regressão multivariada, para melhorar a representação das condições de dispersão de $PM_{10}$.

O primeiro modelo univariado desenvolvido só com os valores de DOA como variável independente explicou entre 37% e 61% da variância total das concentrações de $PM_{10}$. Estes valores aumentaram para 53% e 68% ao adicionar a intensidade do vento e para 53% e 88% quando ambas as variáveis foram usadas para estimar valores diários de concentração, agregados para todas as estações. Os parâmetros de regressão estimados para o AOT são comparáveis aos encontrados por outros estudos independentes para diferentes regiões urbanas. A subestimação de concentrações de $PM_{10}$, observável nos três modelos apresentados, parecem indicar que as estimações baseadas em imagens de satélite são mais representativas das concentrações de fundo e possuem uma capacidade limitada de reprodução de concentrações mais elevadas, características de áreas mais restritas, fortemente influenciadas por fontes pontuais (tráfego e indústria)

Os modelos de regressão apresentados demonstram o elevado potencial da utilização de valores de DOA calculados através de um algoritmo de redução de contraste para estimar concentrações de $PM_{10}$ ao nível do solo. Estes resultados sustentam a hipótese de que uma metodologia multivariada para extracção de DOA por detecção remota é um complemento válido a outros produtos de aerossóis derivados por imagens de satélite, actualmente utilizados para avaliar a concentração de material particulado ao nível do solo.

No entanto, para que se possa estabelecer um produto operacional de estimação de concentrações de $PM_{10}$ baseado em imagens de satélite para áreas urbanas, o trabalho a desenvolver no futuro deve focar-se em: a) remover a influência residual de aerossóis das imagens de referância; b) melhorar a

correcção de efeitos relacionados com a geometria de visualização variável característica do MODIS; c) integrar um *dataset* multianual de forma a avaliar mais extensivamente a influência de variáveis meteorológicos como a altura da camada de mistura e a humidade relativa na correlação $PM_{10}$/AOT; d) alargar a aplicação deste algoritmo de extração de AOT a outros satélites de forma a melhorar as capacidades de monitorização em termos de resolução espacial (horizontal/vertical).

**CONTENT**

# List of Figures

# List of Tables

# List of Acronyms

ACS - American Cancer Society

AERONET - Aerosol Robotic Network

AML – Lisbon Metropolitan Area

AMLN – North Lisbon Metropolitan Area

AMLS – South Lisbon Metropolitan Area

ANOVA - Analysis of Variance

AOD – Aerosol Optical Depth

AOD – Aerosol Optical Depth

AOT – Aerosol Optical Thickness

APA – Agência Portuguesa do Ambiente (Portuguese Environmental Agency)

ASTER - Advanced Spaceborne Thermal Emission and Reflection Radiometer

AVHRR - Advanced Very High Resolution Radiometer

BRDF - Reflectance Distribution Function

CAFE – Clean Air For Europe

CALIPSO - Cloud-Aerosol LIDAR and Infrared Pathfinder Satellite Observations

CART - Classification And Regression Trees

CAS - Cascais

CCDR-LVT - Comissão de Coordenação e Desenvolvimento Regional da Região de Lisboa e Vale do Tejo (Regional Development and Coordinating Commission of Lisbon and the Tagus Valley)

CHRIS - Compact High Resolution Imaging Spectrometer

CORINE - Coordination of Information on the Environment

DDV - Dark Dense Vegetation

DL – Decree-Law

DTA – Differential Texture Analysis

EC – European Commission

EEA – European Environment Agency

ENT - Entrecampos

EO – Earth Observation

EPA - Environmental Protection Agency

ESC - Escavadeira

EU - European Union

FAIRMODE - Forum for air quality modelling in Europe

GIS - Geographic Information System

GOES - Geostationary Operational Environmental Satellite

GOES - Goddard Earth Observing System

GPL - Gás de petróleo Liquefeito (Liquefied Petroleum Gas)

HDF-EOS - Hierarchical Data Format - Earth Observing System

HEG - HDF-EOS to GeoTIFF Conversion Tool

HPA – Hazardous Air Pollutants

IM - Insituto de Meteorologia (Portuguese Meteorology Institute)

IM - Instituto da Meteorologia

INE – Instituto Nacional de Estatística (Portuguese National Statistics Institute)

IPCC - Intergovernmental Panel on Climate Change

IQAr – Índice de Qualidade do Ar (Portuguese Air Quality Index)

ISO - International Standard Organization

JJA - June-July-August

LAADSWEB - Level 1 and Atmosphere Archive and Distribution System

LAR - Laranjeiro

LAV - Lavradio

LIB – Avenida da Liberdade

LIDAR - Light Detection And Ranging sensor

LOU - Loures

LVT – Lisboa e Vale do Tejo (Lisbon and Tagus Valley)

MAM - March-April-May

MAR - Quinta do Marquês

MATLAB - Matrix Laboratory software

MEM - Mem-Martins

MERIS - Medium Resolution Imaging Spectrometer

MISR - Multi-angle Imaging Spectroradiometer

MLH - Mixing Layer Height

MODIS - Moderate Resolution Imaging Spectroradiometer

MSG - METEOSAT Second Generation

NAAQS - National Ambient Air Quality Standards

NN - neural network

$NO_2$ - Nitrogen dioxide

NOAA - National Oceanic and Atmospheric Administration

NRMSE - Normalised Root Mean Square Error

ODV - Odivelas

OLV - Olivais

PBL - Planetary Boundary Layer

PM – Particulate Matter

$PM_{10}$ - Particles which pass through a size-selective inlet with a 50 % efficiency cut-off at 10 µm aerodynamic diameter (ISO 7708:1995)

$PM_{2.5}$ - Particles which pass through a size-selective inlet with a 50 % efficiency cut-off at 2,5 µm aerodynamic diameter (ISO 7708:1995)

$P_{mean}$ - Mean Atmospheric Pressure at station level (hPa)

POLDER - Polarization and Directionality of the Earth's Reflectances

r – Pearson correlation coefficient

$r^2$ – Coefficient of determination

REB - Reboleira

RH - Mean Relative Humidity (%)

RMSE - Root Mean Square Error

SeaWiFS - Sea-viewing Wide Field-of-view Sensor

SNR – Signal-to-Noise Ratio

SPOT - Système Pour l'Observation de la Terre

T – Air Temperature

TM – Thematic Mapper

$T_{mean}$ - Mean Air Temperature at station level (º)

TOA – Top-of-Atmosphere

$U_{mean}$ - Mean Wind Speed (m/s)

US – United States

UTC - Coordinated Universal Time

UTM - Universal Transverse Mercator coordinate system

VOC - Volatile Organic Compounds

WHO – World Health Organization

WS – Wind Speed

# List of Symbols

ext(λ,h) - Light extinction coefficient

λ – Wavelength

h - Vertical atmospheric column height

$H_{min}$ – Lower altitude of the vertical atmospheric column

$H_{max}$ – Higher altitude of the vertical atmospheric column

τ - Optical thickness

ρ* - Top of the atmosphere (TOA) reflectance

$\theta_v$ – Sensor zenith angle

$\varphi_v$ - Sensor azimuth ngle

$\varphi_s$ – Solar azimuth ngle

φ – Sensor relative azimuth angle ($|\varphi_v - \varphi_s|$)

$\theta_s$ - Solar zenith angle

$\mu_v$ – Cosine of sensor zenith angle

$\mu_s$ - Cosine of solar zenith angle

$\tau_a$ – Aerosol Optical Thickness

$\rho_a(\mu_v, \mu_s, \varphi)$ - Intrinsic atmospheric reflectance

$T(\mu_s)$ - Total transmission function

$t_{scat}(\mu_v)$ - Diffuse transmission function on the ground-satellite path

s – Atmospheric spherical albedo

$<\rho_s>$ - Target's reflectance

$<\rho_e>$ Mean reflectance of the target's environment

d - distance in pixels

$\Delta\rho_{i,j}^*(d)$ - Difference between the pixel ground reflectances at distance d

$M^{2*}(d)$ - Structure function

σ - Standard deviation

$\overline{\rho}$ - Mean target reflectance

f(RH) - Ratio of ambient and dry extinction coefficients

ρ - Aerosol mass density (g/m)

$Q_{ext,dry}$ - Mie extinction efficiency

$r_{eff}$ - Particle effective radius

α, $\beta_1$, $\beta_2$ – linear regression coefficients fo the $PM_{10}$ concentration estimation models

1

# Chapter 1 - Introduction

## 1.1 Scope and objectives

Aerosols or suspended particulate matter (PM) represent one of the most important atmospheric pollutants worldwide, affecting air quality at local, regional and global scales. Formed by a complex mixture of solid and liquid particles of variable size and composition, PM sources include both natural (e.g., dust from arid areas) and anthropogenic (e.g., traffic, industry and biomass burning) fractions. The main public health effects that have been reported to be associated with PM pollution include the increase of heart and respiratory diseases and premature mortality (Bell *et al.*, 2004; Krewski *et al.*, 2000; Pope and Dockery, 1999; Pope *et al.* 2002; Tran *et al.*, 2008; WHO, 2003). The global distribution of atmospheric PM concentrations also has an important role in climate change processes through direct and indirect radiative forcing mechanisms (IPCC, 2007; Kaufman *et al.*, 2002; King *et al.*, 1999; Solomon *et al.*, 2007).

PM is a highly variable pollutant in both the space and time domains, mainly due to its multiplicity of origins and variable modes of transport, representing a monitoring challenge at different spatial scales. The existing air quality ground station monitoring networks, usually concentrated in urban areas, provide insufficient spatial information to infer local, regional and global distribution patterns. Alternatives like measuring campaigns or physical modelling present restrictions related, in the first case, to high implementations costs and limited temporal representativity and, in the second, to uncertainties relat-

ed to the use of emissions inventories or sparse point ground measurements to characterize initial conditions.

Tropospheric aerosol satellite observations provide good complement to both point ground monitoring and physical modelling. Originally aimed at radiative forcing assessment and climate applications, its potential for air quality monitoring has been a rapidly developing research field in the last years (Hoff and Sundar, 2009). In this context, aerosol remote sensing represents a potential tool to improve the spatial coverage and accuracy of PM concentration estimates, through the use of physically or statistically based algorithms to retrieve PM concentration surrogates. In particular, the Aerosol Optical Thickness (AOT) parameter, which measures aerosol loading in the atmospheric column, can be used as an estimator of PM concentration at ground level.

The several sensors currently in orbit provide global coverage with variable spatiotemporal resolutions and are able to capture monthly, daily and even intra-daily information on aerosol concentration, size and chemical composition. These products, either in standalone approaches or integrated with air quality physical models and ground monitoring data, can improve substantially current knowledge of the aerosol distribution spatial structure at an local, regional, and global scales.

The potential applications of remote sensing to monitor air polluition, also relevant to other atmospheric species (e.g. $SO_2$ and $NO_2$), are summarized in Figure 1.1. They range from improvements in characterization of surface air pollution, air quality forecast, emission inventories and remote location monitoring to support to air quality compliance, model validation and ground air quality network optimization. Aerosol satellite products are already used operationally for the identification of natural dust transport events. Establishment of reliable long term aerosol satellite data series will also provide a positive impact on air pollution emission trends. Nonetheless their widespread use is somewhat restricted due to limitations in product validation, estimation of near surface concentrations from vertically integrated satellite parameters and definition of robust data assimilation approaches for integration with other monitoring tools. These limitations are more relevant for air quality compliance applica-

tions where current legislative frameworks are still strongly dependent on ground data and occasionally on air quality modelling.

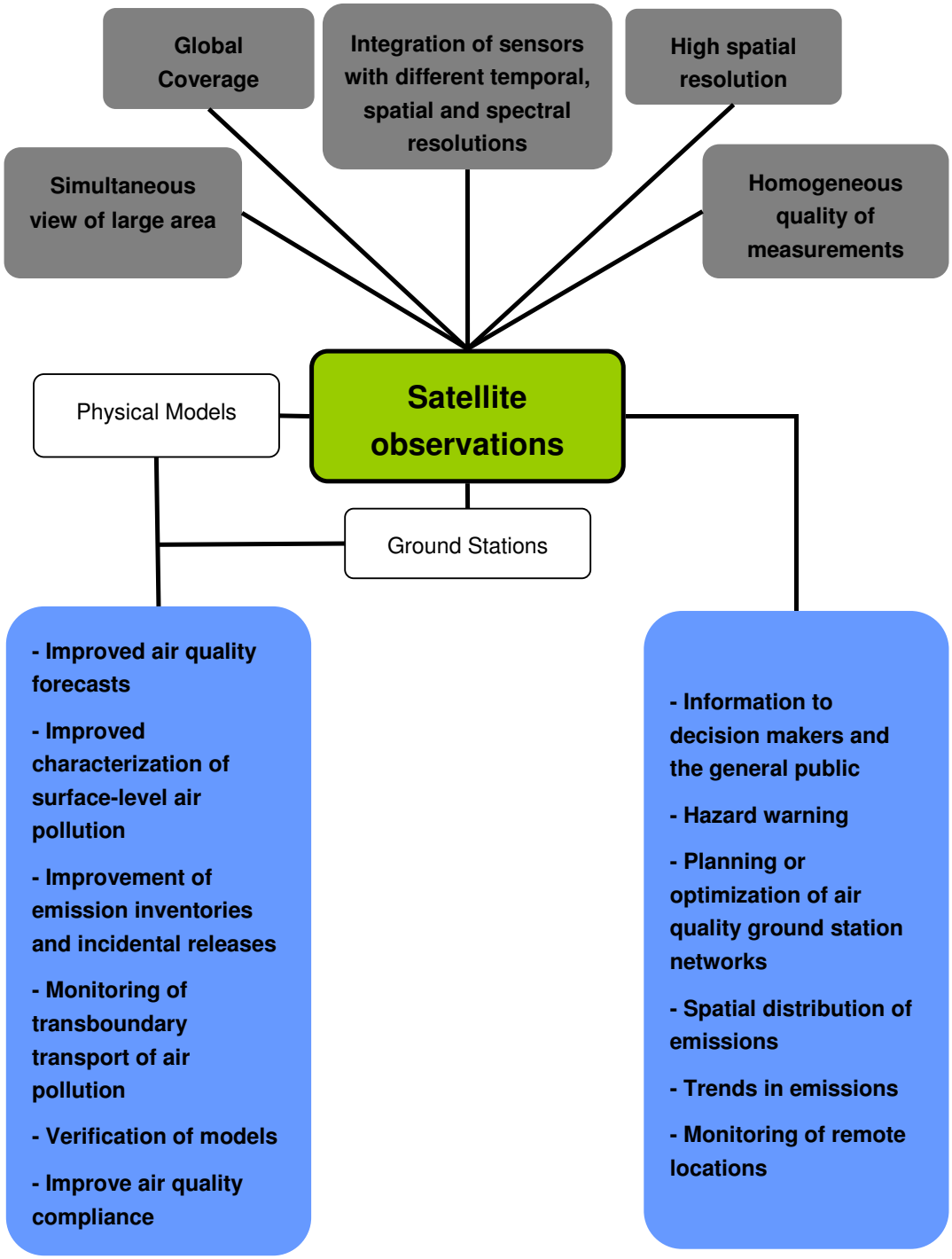


**Figure 1.1 – Advantages and potential applications of satellite remote sensing in the field of air pollution. Adapted from Veefkind *et al.*, 2007.**

In the last decade numerous studies provided empirical relations between $PM_{2.5}$ (particles with an aerodynamic diameter of less than 2.5 μm) and $PM_{10}$

(particles with an aerodynamic diameter of less than 10 μm) ground concentrations, satellite retrieved AOT and several meteorological variables (e.g. the planetary boundary layer height (PBL), relative humidity (RH)), for different sensors and sites around the world. These relations presented very distinct results in terms of correlation strength and PM estimation accuracy (Chu *et al.*, 2003; Engel-Cox, 2004; Gupta *et al.*, 2006, 2009a, 2009b; Liu *et al.* 2005; Paciorek *et al.*, 2008; Wang *et al.*, 2010). Variability in the results demonstrates the need for further improvement in this research area before satellite based quantitative PM estimation can be introduced as a reliable air quality monitoring resource. AOT retrieval accuracy still constitutes one of the main uncertainty sources for PM estimation, recurrently identified in most of these works. Additionally, seasonal aspects, aerosol type, meteorological conditions and station type/location were also identified as relevant uncertainty sources.

Satellite aerosol retrieval methods over land derive AOT from the measured top-of-the-atmosphere radiances, using algorithms that rely on *a priori* definition of certain aerosol properties and correct assessment of surface signal. Most rely on the existence of low and homogeneous surface reflectance pixels (e.g., dark dense vegetation -DDV - approach), to accurately estimate ground reflectance contribution and show a limited accuracy for surface areas with high intrinsic reflectance (Hsu *et al.*, 2004; Kaufman *et al.*, 1997; Levi *et al.*, 2007; Remer *et al.*, 2005). Aerosol retrieval accuracy is particularly problematic for these high reflective areas, such as deserts and urban areas. Since urban areas concentrate most of the world's population and represent the main anthropogenic PM emission source, it is crucial to develop alternative methodologies which address AOT products limitations specifically for these regions..

For high reflective areas a contrast reduction method might complement information given by other AOT retrieval techniques. This method is based on the "blurring effect", present mainly in the visible and near infrared bands, which is linked to the scattering and backscattering induced by aerosols, predominantly in the short wavelengths (Sifakis and Deschamps, 1992). Its application is appropriate for urban areas since it presumes the existence of a heterogeneous and predominantly time invariant surfaces (this last assumption is verified in urban areas at least for short term surface changes). The surface should also present enough contrast to retrieve AOT based on a contrast loss measure

between a pair of images (ideally a reference image, with no aerosol contribution, and a polluted image) with similar viewing geometry. The assumption of time invariance in surface reflectance must be met in order to correctly remove the surface signal influence when calculating contrast differences. For this reason vegetation cover should be accounted for, since, unlike artificial or bare surfaces, these are subject to seasonal reflectance variations which affect the accuracy of contrast reduction based AOT retrieval.

Previous case studies developed in desert and urban areas demonstrate the potential of this method, for high (Landsat and SPOT) to medium/low resolution sensors (MERIS and NOAA AVHRR), when compared to AERONET and ground particulate matter concentration data (Tanre et al, 1988 and 1992, Holben et al, 1992, Sifakis et al, 1992, Lin et al, 2002, Liu et al 2002, Paronis and Sifakis, 2003, Retalis et al 2003, Retalis and Sifakis, 2010).

The main objective of this thesis is to assess the potential of a contrast reduction algorithm for the estimation of $PM_{10}$ concentration levels from MODIS satellite observations over urban areas. The work developed in this thesis is based on MODIS (Moderate Resolution Imaging Spectroradiometer) imagery since it provides a good compromise between spatial resolution (250 m) and temporal resolution (nearly one image per day) to capture $PM_{10}$ spatiotemporal variability features at the urban scale.

To achieve this goal, three distinct partial objectives were defined:

1) Design and implementation of a contrast-reduction algorithm to retrieve optimized AOT estimations from MODIS imagery and evaluation against ground AERONET measurements.
2) Characterization and correlation analysis, for an urban area, of the optimized AOT values, the $PM_{10}$ ground concentrations and several meteorological variables with influence in $PM_{10}$ dispersion and in the definition of the $PM_{10}$/AOT relationship.
3) Definition and evaluation of uni and multivariate linear regression models for $PM_{10}$ concentration estimation based on the combined use of AOT and meteorological variables.

An overview of methodology proposed to achieve these objectives is provided in the following section. The objective of this section is to establish the rationale behind the methodological decisions taken during the development of this thesis and to provide an outline of the respective supporting case studies. Complementary and detailed information about the methodology, case studies and data sets used in this thesis is provided in Chapter 3 and Chapter 4 (Data and Methods" sections) presented as two research publications.

## 1.2 Methodology and case studies overview

The first aforementioned objective aimed at establishing the MODIS optimized contrast reduction technique as a valid methodology to extract AOT values in urban areas and to define its advantages and limitations. It focused on determining optimal AOT retrieval conditions capable of adapting to MODIS variable visualization geometries and to minimize the influence of residual vegetation content in transitional urban areas on the technique's accuracy. These improvements included: 1) definition of the algorithm optimal spatial resolution; 2) calculation of a sensor zenith angle correction term, 3) definition of optimal observation geometry clusters based on their similarity, and 4) characterisation of the most suitable land cover classes to reduce vegetation related reflectance changes.

The impact assessment of the implemented improvements and the evaluation of AOT accuracy were achieved through the development of a case study, which defined a comparison analysis with a one year dataset (2005) of AERONET (Aerosol Robotic Network) sun photometer measurements from five urban European stations. This case study was designed to test and validate the contrast reduction algorithm in similar conditions as the ones presented in the main results chapter, where the optimized AOT values would be used to estimate $PM_{10}$ ground concentrations. The same MODIS datasets were used for the same year (2005) and even the type of AERONET station was chosen to represent comparable urban environment influences to the Lisbon Metropolitan Area. These influences ranged from typical urban centres (Paris and Barcelona) to more transitional suburban areas, interlacing urban and vegetated (forest and agricultural) surfaces (Lille and Modena). A forest influenced site, 50 km west of Lisbon, was included with a twofold objective: providing measurements par-

tially influenced by the same urban centre chosen in the second case study and test the algorithm's resilience to a higher vegetation presence.

The remaining two thesis objectives, aimed at assessing AOT's ability to estimate $PM_{10}$ ground concentrations, were based on a case study developed for the Lisbon Metropolitan Area. This region was chosen due to the fact that it represents the largest Portuguese urban centre, with a population close to two million inhabitants (INE, 2001). In the last ten years it presented, together with the Oporto urban area (the second largest Portuguese city), the highest PM concentration levels in the country, comparable to the most polluted European Cities (APA, 2011). The preference for the urban area surrounding the Portuguese capital was also determined by its denser air quality monitoring network, with the highest number of stations of all Portuguese air quality zones/agglomerations and yearly lower presence of clouds. The first criterion ensures a more comprehensive evaluation of the developed $PM_{10}$ estimation regression models while the second is an essential pre-requisite for an accurate AOT satellite retrieval.

For the development of this case study the following datasets were collected for 2005: a) MODIS imagery to retrieve the AOT values for all $PM_{10}$ air quality stations based on the optimal contrast reduction algorithm; b) $PM_{10}$ hourly ground measurements for those stations; c) meteorological variables (temperature, atmospheric pressure, mixing layer height, relative humidity and wind speed) measured in the Gago Coutinho station located in the Lisbon city centre.

The AOT retrieval from MODIS for the Lisbon Metropolitan Area air quality stations was performed, followed by a characterization and correlation analysis of the $PM_{10}$, AOT values and meteorological variables . This analysis, corresponding to the second defined objective, allowed for a full annual and seasonal characterization and comparison of all the datasets. It also defined the $PM_{10}$/AOT relationship as a function of several factors such as: seasonality, air quality station type (background, traffic and industrial), $PM_{10}$ time averaging period, AOT retrieval accuracy, compatibility between AOT spatial resolution and $PM_{10}$ distribution spatial structure at an urban scale, seasonal AOT and $PM_{10}$ variability and integration with other meteorological variables. Conse-

quently, it allowed the determination of a set of optimal conditions as well as limitations for $PM_{10}$ empirical estimation based on AOT and meteorological variables.

The final objective of this thesis consisted in the definition and evaluation of uni and multivariate linear regression models to estimate $PM_{10}$ ground concentrations from satellite AOT values. The inclusion of non-linear regression $PM_{10}$ estimation schemes (e.g. General Additive Models – GAMs or neural networks) was considered but disregarded since most non-linear relations identified in previous studies (Gupta *et al.*, 2009a, 2009b, Liu *et al.*, 2005) refer to meteorological data and provide no significant additional information on the suitability of the contrast reduction retrieved AOT as a $PM_{10}$ estimator. Furthermore, when using these techniques, it is often more difficult to correctly interpret the role and contribution of each predictor, as intended in this study, and can eventually lead to over fitting issues, which compromise model generalization to a more extended time series or to other urban regions.

On a first stage, a univariate regression model, using only AOT values as the independent variable, evaluated directly the satellite capability to estimate $PM_{10}$. On a second phase, meteorological variables, such as mixing layer height, relative humidity, wind speed, temperature and atmospheric pressure, were added to the regression model, using a stepwise fit technique to assess the influence of each variable on the quality of $PM_{10}$ estimation. In this second stage, two regression models were developed: one for individual ground station concentrations and another for a daily spatial average calculated using all station values. The purpose was to assess their ability to be used, respectively, as a $PM_{10}$ estimator at ground station level or as an overall PM air quality indicator at the urban area level. The definition of confidence intervals for each correlation and error statistics, using a bootstrap technique, provided a comprehensive quantitative model accuracy assessment for each model. The role of each introduced variable was determined by calculation the confidence intervals for their respective regression coefficients. Figure 1.2 summarizes the methodology supporting this research, assigning the different steps to the respective thesis chapters, according to the structure described in more detail in the following section.

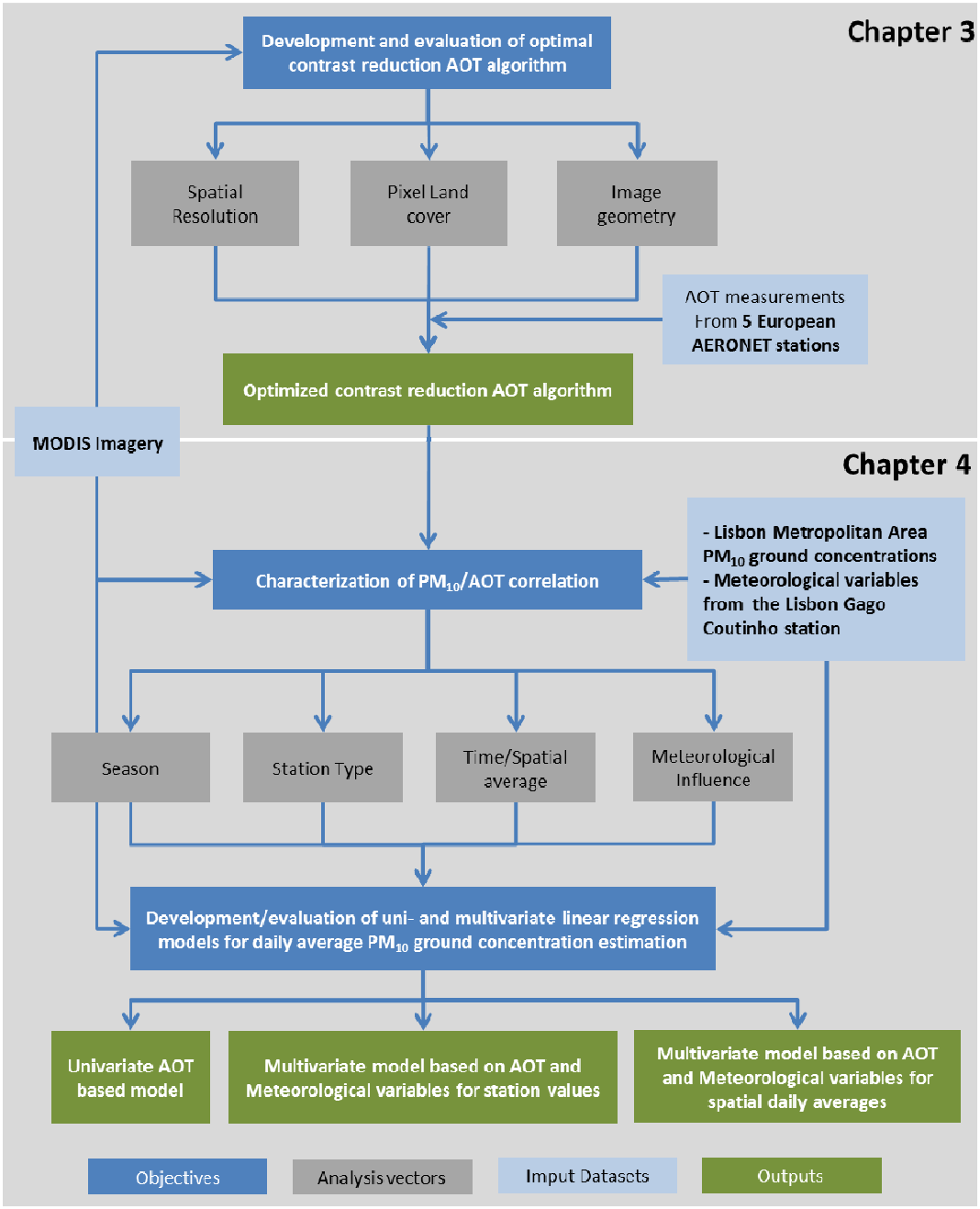


**Figure 1.2 – Overall thesis methodology scheme**

## 1.3 Thesis structure overview

This thesis is divided into five chapters structured around the main results presented in Chapters 3 and 4. Chapter 1 is the current introductory chapter aimed at determining the research scope and objectives.

Chapter 2 contains a comprehensive literature review divided into two sections. The first section provides information on aerosols including definition, main sources, seasonality, related health problems and air quality legislation towards providing a general background to the air pollution problem tackled in this thesis. This framework is followed by a detailed characterization of PM related air quality problems for the Lisbon Metropolitan Area to justify its selection as the main case study developed in the scope of this thesis. It integrates them into a ten year historical context given for the entire Portuguese territory, while conveying information on administrative limits, demography, main emission sources, chemical composition, affected areas, seasonality and ground air quality monitoring network design. The second section briefly discusses the key satellite aerosol retrieval methods over land and then focus on the theory and relevant applications related to the contrast reduction method. Finally it will provide an overview of the main satellite based ground PM estimation studies, including the key achievements and limitations, to establish a comparative framework for the results presented.

In Chapter 3, the main results regarding the definition, implementation and evaluation of the optimized contrast reduction algorithm are presented and discussed. This chapter focus on the comparative analysis of AOT retrieved values for a one year (2005) dataset of MODIS images with the AOT measurements from five European urban AERONET stations. The work described in this chapter is published in a peer reviewed article in "Atmospheric Research" entitled "Comparison of contrast reduction based MODIS AOT estimates with AERONET measurements" (Grosso and Paronis, 2011).

Chapter 4 will build upon the results from the previous chapter to develop linear regression models to estimate $PM_{10}$ that are based on the optimized contrast AOT values for the air quality stations of Lisbon Metropolitan Area. This study will be preceded by a detailed characterization of the times series for $PM_{10}$, AOT and meteorological variables and corresponding correlation analysis.

As mentioned above, Chapter 3 and 4 are both structured as peer reviewed papers with the following sections: 1) introduction, providing a context to the work developed and defining the sub-chapter objectives; 2) data and

methods, describing the key datasets used and the methodology followed; 3) results and discussion, presenting the obtained results and providing an interpretation; and 4) main conclusions, based on those results.

Chapter 5 presents a broader level analysis of all main conclusions provided by the developed work, linking them with the main objectives given in this introductory chapter. In the end, the thesis achievements are summarized and future research directions identified to improve the work presented and the current state of the art in atmospheric pollution monitoring through remote sensing.

2

# Chapter 2 - Literature Review

## 2.1 Aerosol/Particulate Matter

This section provides a comprehensive context to air quality problems related to PM. It introduces a general aerosol definition and classification according to size and emission sources, and establishing a relation between classes and respective global distribution, seasonality and human health effects. Associated with the development of scientific knowledge of those effects, a brief overview of the evolution of European and Portuguese air quality legislation is given this section. This chapter focuses mainly the legal limits of $PM_{10}$ and $PM_{2.5}$ concentrations and on criteria related to the definition of a national air quality monitoring network, with regards to the required station type characteristics and their respective spatial representativeness. This is a relevant issue to be addressed in the scope of a thesis that focuses on estimating point $PM_{10}$ station concentrations from satellite estimates, usually calculated for a wider area. This section finishes with the provision of a historical context of air quality in the Lisbon Metropolitan Area, the main case study for this thesis, integrated within the broader context of the Portuguese territory.

### 2.1.1 Sources and classification

Aerosols, also designated as suspended particulated matter, are generally defined as a complex mixture of solid particle or liquid droplets suspended in a gas with a size lower than 100 μm and greater than individual molecules (Seinfeld and Pandis, 2006). Usually concentrated in the first kilometres of Earth's

atmosphere (2-3 km), they are one of the most important atmospheric constituents with a significant influence in global climate change processes, through direct and indirect radiative forcing mechanisms (IPCC, 2007; Kaufman *et al.*, 2002; King *et al.*, 1999; Solomon *et al.*, 2007), and in local/regional air quality related human health problems (Bell *et al.*, 2004; Krewski *et al.*, 2000; Pope and Dockery, 1999; Pope *et al.* 2002; WHO, 2003). Other impacts related to PM include environmental effects such as visibility degradation (Huang *et al.*, 2009; Husar *et al.*, 1981; Hyslop, 2009) or acid rain formation (Kleinman *et al.*, 1989; Seinfeld and Pandis, 2006).

Due to the multiplicity of components, sources and formation mechanisms it is difficult to classify aerosols. Figure 2.1 and Table 2.1 try to systematize aerosol type information, according to the main categories. There are three main aerosol modes, separated according to size and formation process: 1) nucleation mode, corresponding to particles ranging from 0.005 and 0.1 μm, formed primarily from high temperature gas condensation (e.g., incomplete fuel combustion from diesel vehicles); 2) accumulation mode, with particles ranging from 0.1 to 1 μm, formed mainly through chemical conversion of certain gases (e.g., nitrates, sulphates) followed by nucleation, condensation and coagulation processes; 3) coarse mode, where the mechanically generated aerosols with sizes over 1 μm are included, from either biogenic sources, such as dust transport events, sea, sprays, volcanoes or from anthropogenic emissions. The two first modes are interchangeable and can be aggregated into a wider fine particles mode.

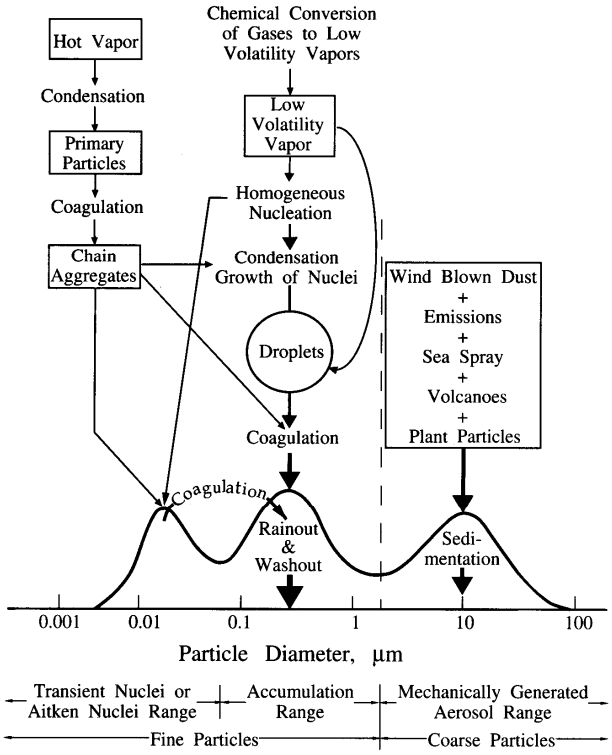


**Figure 2.1 - Principal modes, sources, and particle formation and removal mechanisms. Source: Whitby and Cantrell, 1976**

The coarse particles have a more significant biogenic contribution and represent, according to some estimates, around 85% of the total annual atmospheric aerosol mass (Seinfeld and Pandis, 2006). They are mostly generated by mechanical processes, responsible for their ejection into the atmosphere (primary aerosols). Their main biogenic constituents are crustal elements present in dust, carbonates and sulphates of mineral origin and salt from the sea sprays. The anthropogenic part of this larger type of particles originates from industrial activities like cement and construction and oil or coal based fuel combustion. Coarse particles are usually removed from the atmosphere due to their higher weight through deposition/sedimentation processes.

Fine aerosols have a higher anthropogenic component and originate mainly from industrial activities and traffic emissions. Nevertheless some biogenic input is present from sulphur and nitrogen gases oxidation processes. These aerosols appear mostly through physical and chemical processes (secondary aerosol formation processes), involving nitrate or sulphate but also have other constituents such as ammonium, hydrogen ions and elemental carbon. They

represent a much smaller part of total aerosol mass (around 15%) and are mostly present in the vicinity of large urban centres, where their percentages can be much higher. The main removal mechanism is trough wet deposition processes such as rainout or washout.

**Table 2.1 – Coarse and fine aerosol sources and respective chemical composition Source: Tente, 2005**

| | Coarse particles | | Fine particles | |
|---|---|---|---|---|
| | 0.1 µm 1.0 µm 10 µm 25 µm | | 0.1 µm 1.0 µm 10 µm 25 µm | |
| | Biogenic | Anthropogenic | Biogenic | Anthropogenic |
| Sources | Arid soil dust resuspension.<br>Long range dust transport event.<br>Volcanoes.<br>Marine Sprays.<br>Biological Sources (e.g., spores, pollens). | Industrial activities (e.g., cement, ceramics, construction).<br>Fuel combustion (oil, coal). | Sulfur gases oxidation.<br>Nitrogen gases oxidations (from lightning and soil evapotranspiration.<br>Chemical conversion of organic compounds of biogenic origin. | High temperature industrial activities (e.g., foundry).<br>Traffic emissions associated with chemical conversion of $NO_x$, $SO_2$ and organic compounds. |
| Components | Metallic oxides from crustal elements ($SiO_2$, $Al_2O_3$, $Fe_2O_3$, TiO2)<br>NaCl<br>$CaCO_3$, $Na_2SO_4$, $MgSO_4$, $K_2SO_4$<br>Pollens, spores and micro-organisms | | Sulfate ($SO_4^{2-}$)<br>Nitrate ($NO_3^-$)<br>Amonium ($NH_4^+$)<br>Hidrogen ion ($H^+$)<br>Elemental carbon | |

### 2.1.2 Global distribution and seasonality

Aerosol spatial and temporal impact scales are highly variable and closely related to the nature, seasonality and geographic distribution of their sources (Dubovic *et al.*, 2002; Kaufman *et al.*, 2002; Masmoudi *et al.*, 2003; Remer *et al.*, 2008; Tanré *et al.*, 2001). Unlike greenhouse gases, aerosols are not as well mixed and uniformly distributed in the atmosphere (Solomon *et al.*, 2007). Natural aerosols, from desert dust and sea salts, are mostly composed of coarser particles with a high transport potential across geographic regions and atmospheric layers (Chin *et al.*, 2002; Prospero *et al.*, 1999). Biomass burning particles, associated with forest and grassland fires, although usually smaller, are also able to

penetrate the higher layers of the atmosphere (Kreidenweis *et al.*, 2001; Winkler *et al.*, 2008). Other fine anthropogenic aerosols derived from traffic and industry emissions in populated areas have a more limited range of influence.

Aerosols global geographical distribution and seasonality is presented in Figure 2.2 that shows the MISR Aerosol Optical Thickness (AOT) product, a parameter closely related to aerosol concentration, which definition will be further developed in section 2.2. The observed patterns are mainly associated with four types of aerosols: desert dust, biomass burning, sea sprays and, to a lesser extent, urban anthropogenic fine particles. The high aerosol amounts over homogeneous ice sheets (Antarctica and Greenland) should be disregarded since these result from an artefact related to cloud screening limitations over snow/ice surfaces (Diner *et al.*, 1999).

The main geographical areas responsible for the formation of coarse desert dust particles are the north of Africa (Sahara and Sahel), the Middle East region (Saudi Arabia) and eastern Asia (Gobi Desert in the South Mongolia/Northern China area). Their contribution is higher during the spring (March-April-May or MAM) and the summer (June-July-August or JJA) seasons, with AOT values generally higher than 0.5, usually associated with medium and long range transport events. It is also possible to observe from Figure 2.2 the transport of Saharan dust across the Atlantic to Central and South America (Remer *et al.*, 2008). Additionally the North African dust has a regional effect on particle concentrations in the Mediterranean region, including the Iberian Peninsula (Pandolfi *et al.*, 2011; Rodriguez *et al.*, 2001).

Biomass burning aerosols have a distinct seasonality related to variations in temperature and vegetation. According to Kaufman *et al.* (2002), the areas more affected by smoke from vegetation fires are located in South America (August–October), Central America (April and May), Southern Africa (July–September) and Central Africa (January–March). Their transport range seems to be lower than desert dust but some transatlantic transport can be observed in Figure 2.2 during winter and spring.

Marine aerosol seasonality is more visible along the Southern Ocean, reaching higher levels during autumn and winter due to increased wind speed. North Pacific and Atlantic sea salt aerosol loadings also seem to increase in

spring due to stronger winds, affecting coastal areas in North America and Europe.

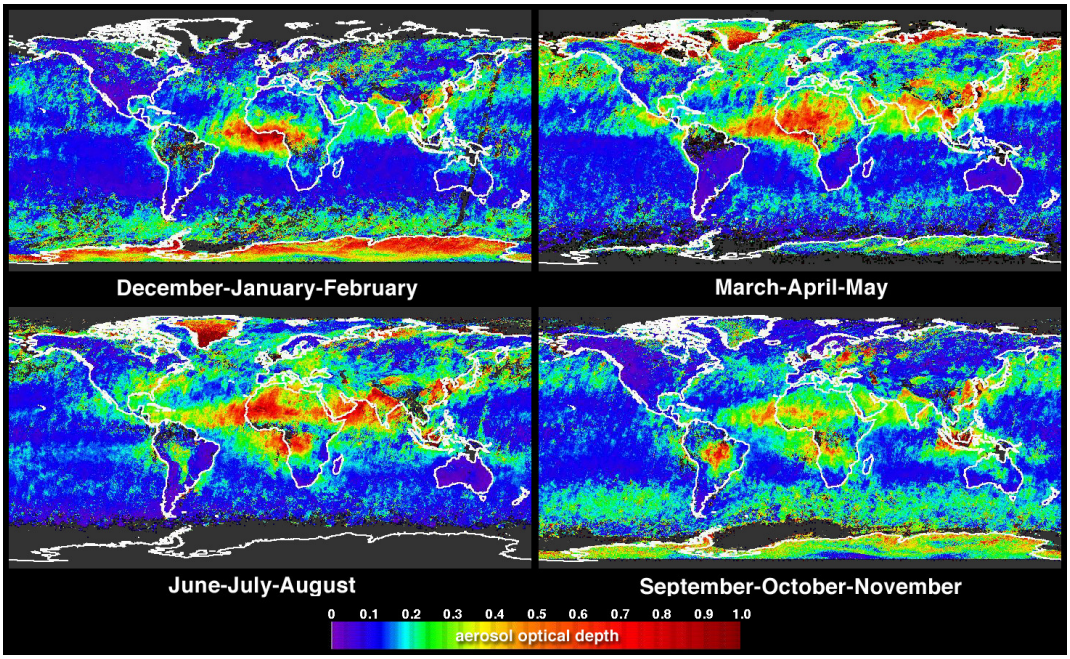


**Figure 2.2 – Aerosol Optical Thickness MISR derived products showing annual aerosol global distribution and seasonality, during the December 2001 through November 2002 time period. Source: http:// http://earthobservatory.nasa.gov.**

Finer anthropogenic aerosols are associated with regional urban and industrial pollution and can be found mainly in developed, developing or densely populated regions, such as Central Europe, eastern North America, the Indian sub-continent and East Asia. Although they usually present a less distinct seasonality than other aerosol types, a specific pattern of higher summertime aerosol loadings and lower in the winter can be found. This conclusion is confirmed by some global climatology studies (Holben *et al.*, 2001; Ichoku *et al.*, 2004; Remer *et al.*, 2008), while more localized studies show different seasonal patterns (Kambezidis, 2008; Kaskaoutis, 2007). These diverse seasonal behaviours are usually related to a higher influence of local and regional emission sources and meteorological parameters. Factors like local traffic and wind patterns, type of industry installed, precipitation, mixing layer height, and relative humidity affect significantly the concentration and dispersion conditions (Barmpadimos *et al.*, 2011; Hooyberghs *et al.*, 2005; Pateraki *et al.*, 2012) and can be responsible for differences in aerosol seasonality between urban regions.

### 2.1.3 Effects on human health

In terms of effects in human health, and even though the outcomes of various epidemiologic and human studies were controversial in the past, there is nowadays strong evidence that both short and long-term exposures to PM are connected with increased morbidity and mortality rates (Anderson, 2009; Bell *et al.*, 2004; Krewski *et al.*, 2000; Pope and Dockery, 1999; Pope *et al.* 2002; Tran *et al.*, 2008; WHO, 2003).

PM health related effects were initially established for short term exposures to high pollution events (e.g., London episodes in 1952 and 1962, described in the works of Bell and Davids (2001) and Lippmann (2001)). Their health effects became progressively more associated with lower particulate pollution levels, during and after the 1990's. This progress was due to an increase in the quantity and availability of epidemiological data and advances in related monitoring technologies (Tente, 2005). As a consequence, several reference studies were presented during that period, relating $PM_{10}$ concentrations with increases in hospital admissions and deaths due to respiratory and cardiovascular diseases (Dockery *et al.*, 1993; Dockery and Pope, 1996; Pope *et al.*, 1995).

During the last 20 years, other studies, conducted for a wide range of time and spatial scales, confirmed these findings. In 2006, Pope and Dockery drafted a review paper where they compiled a substantial part of these studies. Despite a large disparity between the different findings, they found a direct positive trend between increases in $PM_{10}$ short and long term exposure and health effects, such as cardiovascular mortality and hospital admissions or the existence of chronic inflammatory lung injuries.

These effects are illustrated in Figure 2.3, where is possible to infer, from several European and North American studies compiled for a 2004 World Health Organization (WHO) project, statistically significant relationships between mortality and levels of PM in ambient air. In fact, the graph shows that an increase of 10 $\mu g/m^3$ in $PM_{10}$ concentration led to 5 to 20% higher relative mortality risks for all the studied effects (for a 95% confidence interval). Results from North American $PM_{2.5}$ studies seem to imply a higher impact in the relative mortality risk for these smaller size particles, although the uncertainty associated with those results is substantially higher. Anderson (2009) presented

an extensive review of mortality studies related to PM, in which the range of risk increase of the considered studies seems to be less evident. For instance, considering cardiovascular mortality, the risk percentage increase varies between almost zero and 8%.

Relative risks for mortality end-points related to a 10- µg/m³ increase in pollution including 95% confidence intervals. *Left part:* $PM_{10}$, black smoke (BS) and ozone from European studies; *right part:* $PM_{2.5}$ from North American studies.

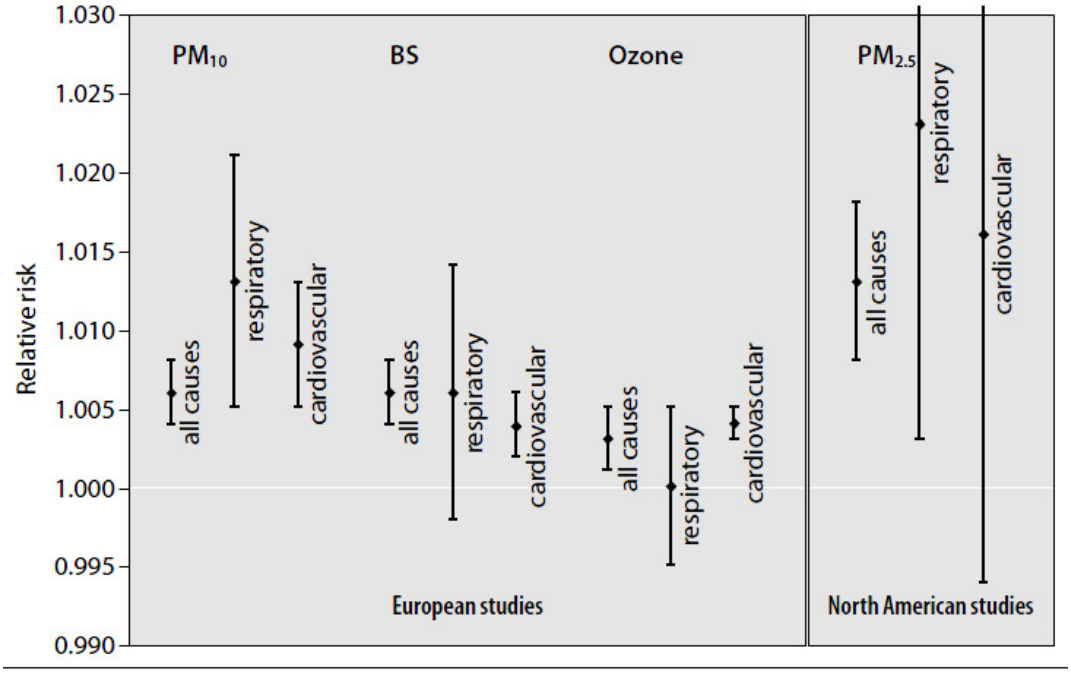


**Figure 2.3 – Relative mortatility risk estimates associated with an 10 µg/m³ increase in $PM_{10}$, PM2.5, black smoke (BS) and Ozone. Source: WHO *et al.*, 2004**

As mentioned above, the range of effects is broad, affecting the respiratory and cardiovascular systems, ranging from children to adults and to a number of large, susceptible groups within the general population. More recently, a growing number evidences is linking a higher incidence of lung cancer and birth related problems with elevated PM concentrations, especially for fine particles ($PM_{2.5}$) (Pope *et al.* 2011; WHO, 2006). A summary of those effects, associated with their respective physiological pathways (Pope and Dockery, 2006), is presented in Figure 2.4.

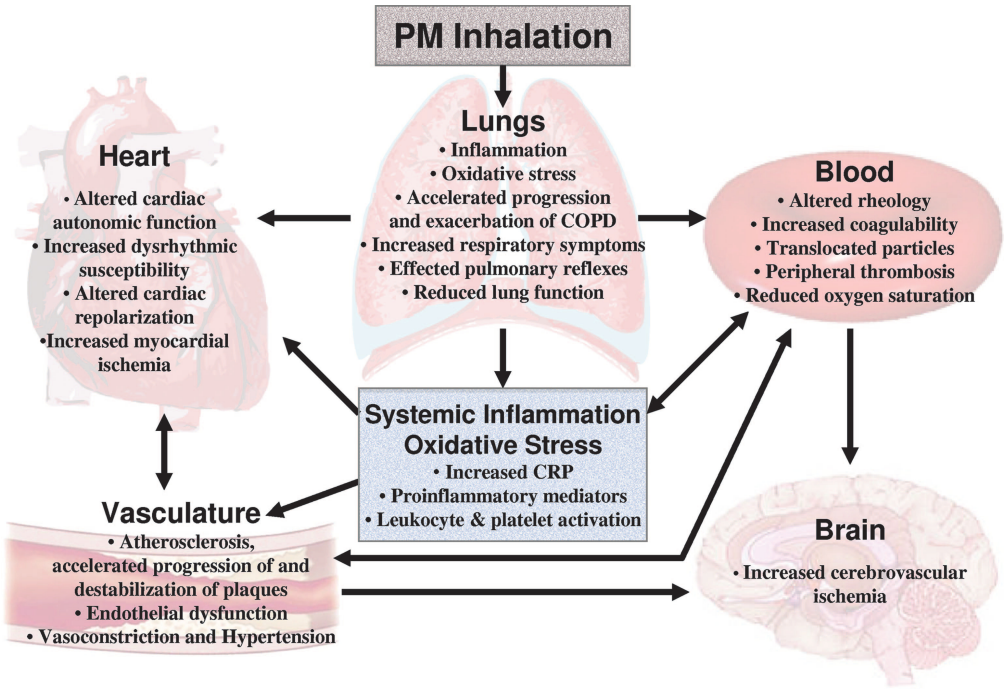


**Figure 2.4 – Main PM related health effects and physiological pathways. Source: Pope and Dockery, 2006.**

The nature and extent of health related PM effects are usually dependent on particle size, chemical composition and duration of exposure.

Particle size determines how far along the physiological pathways, identified in Figure 2.4, can the particle go before deposition occurs. According to the ISO 7708:1995 there are three main particle size fractions: a) the inhalable fraction, corresponding to particles inhaled trough nose and mouth with a diameter lower than 80 µm; b) the thoracic fraction, with a particle diameter lower than 10 µm, equivalent to the $PM_{10}$ size class, which penetrates trough the larynx and ; c) respirable fraction, equal to $PM_{2.5}$ (with a diameter lower than 2.5 µm), able to reach the alveoli region, where most of the gaseous exchanges during respiration are performed. Figure 2.5 shows the probability of reaching the different parts of respiratory tract as a function of particle size.

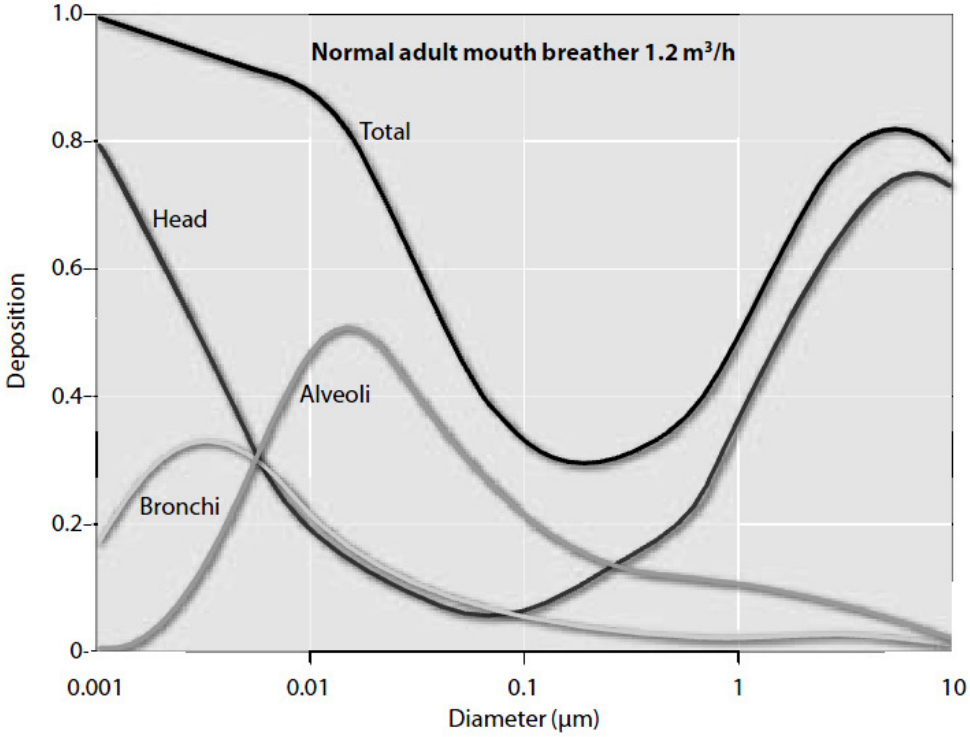


**Figure 2.5 - Deposition probability of inhaled particles in the respiratory tract according to particle size. Source: WHO, 2004**

Smaller particle have the characteristic of reaching further into the respiratory tract and this phenomena seems to be directly linked with an increase in adverse health effects (Pope and Dockery, 2006), as shown in Figure 2.3, by the relative increase in mortality risk estimates seen in PM2.5 epidemiological studies, when compared with $PM_{10}$. Other recent studies seem to extend this conclusions to circulatory system effects, by establishing a more robust link between fine (<2.5 µm) and ultra-fine (<0.1 µm) and several cardiovascular mortality and morbidity indicators for short and long term exposures (Brook *et al.* 2010).

Regarding chemical composition, toxicological studies are inconclusive, stating that although it is "likely that particle toxicology varies, it is not possible to quantify this and that, from a policy perspective, all types need to be considered for regulation" (Anderson, 2009). Nevertheless, the more complex primary combustion-derived fine particles, rich in sulphates, nitrates, acid, metals, organic compounds and other chemicals adsorbed onto their surfaces, seem to present a higher toxic potential, when compared to other single element PM

components like ammonium salts, chlorides, and silicate clays (from wind-blown dust) (Pope and Dockery, 2006; WHO, 2004).

Finally, the duration of exposure is one of the most important aspects of PM health related effects. As mentioned above, the first studies focused on very short term effects (in the order of a few days) of local high PM concentration episodes. As epidemiological data became more readily available and monitoring and statistical techniques developed, analysis gradually progressed to include more extensive time series and case studies. Those time series analysis compared daily variation in $PM_{10}$ concentrations, measured by ground air quality network stations, with population health indicators, such as hospital admissions or death counts (WHO, 2006). They allowed the identification of several acute effects like increase in cardiopulmonary mortality levels but provided little information on more chronic effects, such as reduction in life expectancy, long term mortality rates and incidence of chronic diseases (Pope and Dockery, 2006). Those effects only begun to be identified in the mid 90's, after the results of two long-term prospective cohort studies (Brunekreef, 2003), one by the American Cancer Society (ACS) (Pope *et al.* 1995) and another, often referred as the Harvard Six-Cities Study (Dockery *et al.*, 1993;). For instance, both US studies identified a significant increase in long term mortality rates, between 16 and 26%, due to particulate pollution. These significant links were subsequently confirmed by cohort studies and extended to include other health effects (Anderson, 2009). The main health effects associated with short- and long-term PM exposure are described in Table 2.2. Although higher impacts are associated with long term exposures to high PM concentrations, there is little evidence to suggest a threshold below which no adverse health effects would be anticipated (WHO, 2006).

**Table 2.2 - Important health effects associated with exposure to PM. Source: WHO, 2006**

| Effects related to short-term exposure | Effects related to long-term exposure |
|---|---|
| - Lung inflammatory reactions<br>- Respiratory symptoms<br>- Adverse effects on the cardiovascular system<br>- Increase in medication usage<br>- Increase in hospital admissions<br>- Increase in mortality | - Increase in lower respiratory symptoms<br>- Reduction in lung function in children<br>- Increase in chronic obstructive pulmonary disease<br>- Reduction in lung function in adults<br>- Reduction in life expectancy, owing mainly to cardiopulmonary mortality and probably to lung cancer |

Despite all the advances that occurred in the past 30 years, in the field of PM health related effects, some knowledge gaps still remain and require further research. These include: a) impacts of PM exposure on infant mortality and various birth related problems; b) association between PM and lung cancer; c) definition of the health related impact associated to each component of the PM mixture and their respective source apportionment; d) correct understanding of the major risk groups (Pope *et al.* 2011; Pope and Dockery, 2006).

### 2.1.4 PM air quality guidelines and legislation

The human health impacts described in the previous section have led WHO to propose strict guidelines regarding $PM_{2.5}$ annual mean and 24-hour mean concentrations, where these must not exceed 10 and 25 $\mu g/m^3$, respectively. Threshold values have been selected based on the results of relevant long-term exposure studies such as the ACS (Pope *et al.* 1995) and Harvard Six-Cities Study (Dockery *et al.*, 1993; Kreskwi *et al.* 2000). Although the WHO guidelines are focused primarily on the use of $PM_{2.5}$ and secondarily on $PM_{10}$ as indicators of ambient PM air pollution, the specific air quality guidelines for $PM_{10}$ were adjusted to 20 and 50 $\mu g/m^3$ for the annual and 24-hour mean values, respectively.

The U.S. Environmental Protection Agency (EPA), in compliance with the WHO guidelines, has strengthened the air quality standards related to particle pollution aimed at human health and ecosystem protection. The revised 2006 U.S. National Ambient Air Quality Standards (NAAQS) issued by the EPA tightened the 24-hour standard for $PM_{2.5}$ from 65 $\mu g/m^3$ to 35 $\mu g/m^3$, and re-

tained the annual fine particle ($PM_{2.5}$) standard at 15 µg/$m^3$. As regards $PM_{10}$, EPA has retained the pre-existing 24-hour standard of 150 µg/$m^3$, revoking at the same time the annual standard.

In a similar way, European legislation has been redrafted to better incorporate the WHO recommendations. The Air Quality Framework Directive (1996/62/CE), published in September 27th, 1996, established common policy guidelines for EU countries regarding air quality monitoring, assessment and management.

As shown in Figure 2.6, this directive was followed by four more specific directives, published between 1999 and 2004. They defined limit values for human health protection for all major air pollutants. The upper and lower assessment thresholds were also established, aimed at the definition of particular assessment and management measures (e.g., more detailed measurement or modelling campaigns). For the major pollutants, limit values were introduced for a daily and yearly basis, with the exception of $SO_2$, CO and $O_3$. In the first case, only the daily average values were defined and in the last two, limit and target objective values corresponded to maximum daily eight hour means.

The $PM_{10}$ normative values were defined in Directive 1999/30/EC, published in 22nd of April 1999. The value of 40µg/$m^3$ was set for the yearly average and the value of 50µg/$m^3$ for 24-hour mean values (the latter not to be exceeded more than 35 times a calendar year). From 2001 to January 1st, 2005, progressively lower margin of tolerances were permitted, before reaching those target values. No $PM_{2.5}$ air quality objectives were set at this stage.

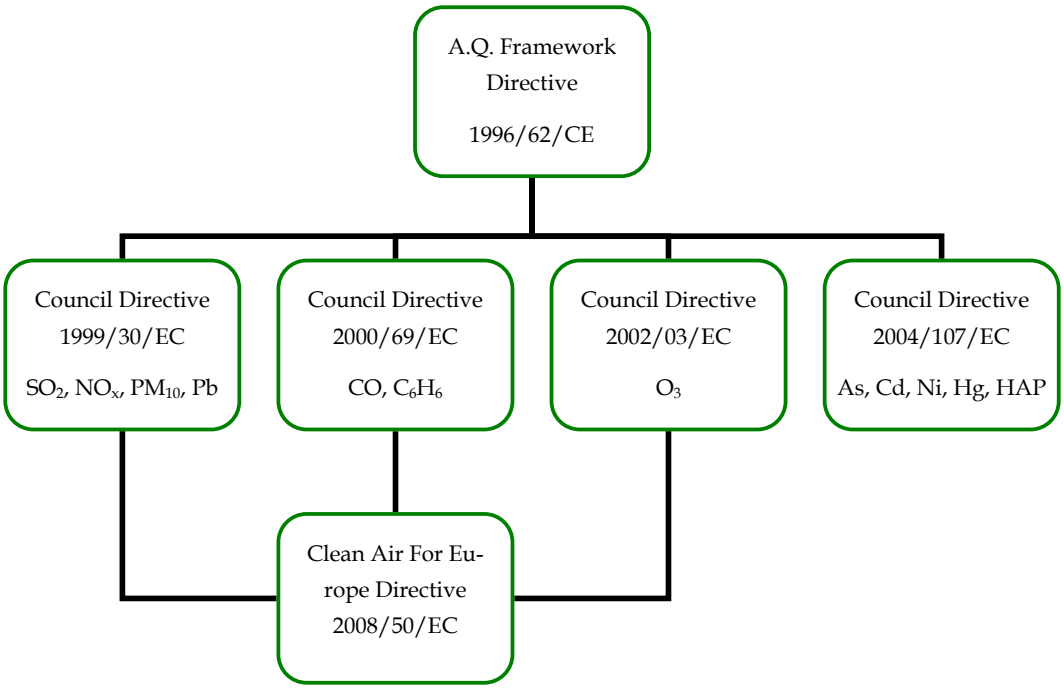


**Figure 2.6 – Main Air Quality European Legislation. Adapted from Ferreira *et al.*, 2009b**

The directive of the European Parliament and the Council of the European Union on ambient air quality and cleaner air for Europe (CAFE directive 2008/50/EC) merged the normative values given by the first three daughter directives (the fourth will be integrated at a later stage). Additionally, it determined: a) air quality objectives for $PM_{2.5}$, including the limit value and exposure related objectives – exposure concentration obligation and exposure reduction target; b) the possibility to remove natural sources of pollution when assessing compliance against limit values; c) the possibility for time extensions of three years ($PM_{10}$) or up to five years ($NO_2$, $C_6H_6$) for complying with limit values, based on conditions and the assessment by the European Commission.

In this latest directive, $PM_{2.5}$ annual mean concentration target limit value for the protection of the human health was set, for the first time, to 25 µg/m$^3$. As in the case of $PM_{10}$, progressively lower yearly margin of tolerances were defined, starting in June 2008, until reaching the target value in January 1, 2015. With regard to $PM_{10}$ values, the pre-existing limits were preserved. Table 2.3 compiles the limit and assessment threshold values for $PM_{10}$ and $PM_{2.5}$, currently present in the CAFE directive.

**Table 2.3 – Limit and assement threshold values for $PM_{10}$ and $PM_{2.5}$ defined in the CAFE directive. Adapted from Brás, 2012**

| Pollutant | $PM_{10}$ | | $PM_{2.5}$ |
|---|---|---|---|
| Objective | Human health protection | | |
| Averaging period | Daily Average | Yearly average | Yearly average |
| Limit value | 50 $\mu g/m^3$ not to be exceeded more than 35 times a calendar year | 40 $\mu g/m^3$ | 25 $\mu g/m^3$ |
| Upper assessment threshold | 70 % of limit value (35 $\mu g/m^3$) not to be exceeded more than 35 times in any calendar year) | 70 % of limit value (28 $\mu g/m^3$) | 70 % of limit value (17 $\mu g/m^3$) |
| Lower assessment threshold | 50 % of limit value (25 $\mu g/m^3$) not to be exceeded more than 35 times in any calendar year) | 50 % of limit value (20 $\mu g/m^3$) | 50 % of limit value (12 $\mu g/m^3$) |
| Target date | January, 1st 2005 | | January, 1st 2015 |

Ground monitoring networks are one of the most common air quality assessment tools used to provide standards compliance data to decision makers and public health related alerts to the general public.

Stations are equipped with analysers that provide continuous measurement of PM and other major pollutants (e.g. $NO_x$, $SO_2$, CO, $O_3$, and heavy metals), concentration levels based on their optical and physical properties (Brás, 2012). Such measurements are primarily used on an operational level by local agencies responsible for air pollution monitoring and control.

The main monitoring objectives of these agencies are the protection of human health, vegetation and ecosystems, trough compliance with EU and national legislation. In parallel they also monitor specific industries/power plants, perform pollutant concentration trend analysis and conduct research (Garber *et al.*, 2002). At the same time, the existing long-term archives serve as input to the various epidemiological and human exposure studies, which aim at analysing the shape of the PM concentration-population mortality and morbidity functions.

In the last ten years a considerable effort has been done towards harmonizing the criteria for design and operation of air quality monitoring present in EU legislation. This harmonization effort ensures that monitoring objectives are

met and provides that information gathered by different EU countries is reliable and comparable. For instance, EC Directive 2001/752 and the subsequent guidance document concerning the Exchange of Air quality information, compiled by Garber *et al.* (2002), establishes criteria for station classification, according to area and pollutant source influence. These criteria are shown in Table 2.4 and Table 2.5

**Table 2.4 – Station classification criteria, according to area of influence. Adapted from Garber *et al.* (2002)**

| Station classification | Description of location according to area of influence |
|---|---|
| Urban | Continuously built-up urban area meaning complete (or at least highly predominant) building-up of the street front side by buildings with at least two floors or large detached buildings with at least two floors. With the exception of city parks, the built-up area is not mixed with non-urbanised areas. |
| Suburban | Largely built-up urban area. 'Largely built-up' means contiguous settlement of detached buildings of any size with a building density less than for 'continuously built-up' area. The built-up area is mixed with non-urbanised areas (e.g. agricultural, lakes, woods). |
| Rural | All areas that do not fulfil the criteria for urban or suburban areas, are defined as rural areas. |
| Rural - Near-city area | area within 10 km from the border of an urban or suburban area. |
| Rural - Regional area | 10-50 km from major sources/source areas |
| Rural - Remote Area | > 50 km from major sources/source areas |

**Table 2.5 - Station classification criteria, according to pollution source influence. Adapted from Garber *et al.* (2002)**

| Station classification | Description of location according to pollution source |
|---|---|
| Traffic | Located such that its pollution level is determined predominantly by the emissions from nearby traffic (roads, motorways, highways). |
| Industrial | Located such that its pollution level is influenced predominantly by emissions from nearby single industrial sources or industrial areas with many sources. Industry source is here taken in its wide meaning including sources like power generation, incinerators and waste treatment plants. |
| Background | Located such that its pollution level is not influenced significantly by any single source or street, but rather by the integrated contribution from all sources upwind of the station (e.g. by all traffic, combustion sources etc. upwind of the station in a city, or by all upwind source areas (cities, industrial areas) in a rural area). |

The implementation of each of these stations classes in a national air quality network serves different monitoring objectives, summarized in Table 2.6.

**Table 2.6 – Main monitoring objectives for each station class. Adapted from Brás, 2012 and Directive 2008/50/EC (the latter was used to add information about station spatial representativeness for some classes).**

| Station Class | | Objectives |
|---|---|---|
| Background | Urban | Average population exposure monitoring to background atmospherical pollution in urban centres. Should be representative of a several square kilometres area |
| | Suburban | Photochemical pollution monitoring, mainly ozone and its precursors and possible primary pollutants. Average population exposure monitoring to background atmospherical pollution in the surroundings of urban centres. |
| | Rural | Average population and ecosystem exposure monitoring to background atmospherical pollution (not influenced by agglomerations or industrial sites in its vicinity), specially regional scale photochemical events |
| Traffic | | Assessment of pollutant concentration associated with maximum population exposure level near main traffic roads (representative of air quality for a street segment no less than 100 m length) |
| Industrial | | Assessment of pollutant concentration associated with maximum population exposure level downwind of main point sources (industries/power plants) due to plume dispersion of accumulation processes (representative of air quality for an area of at least 250 m × 250 m) |

Despite all the efforts to create homogeneous air quality monitoring networks between the different EU countries station representativeness is still an on-going issue. Several studies, scientific papers and reports discuss not only the representativeness values for each station class but also the method used for its calculation. The European Environmental Agency (EEA) technical report on criteria for the establishment of a European wide air quality monitoring network (EUROAIRNET) defined indicative typical ranges of the area of representativeness for each station class. It also recommended station location criteria, including values for area of representativeness, for comparability purposes. These values are summarized in Table 2.7.

**Table 2.7 – Typical ranges of the area of representativeness (radius of area) for various station classes and recommended area values for air quality network design. Source: EEA, 1999.**

| Station class | Typical Radius of area | Recommended area |
|---|---|---|
| Traffic stations | Not applicable | road/street length of some 100 metres or more in central city areas and some 1,000 metres or more in suburban/other areas |
| Industrial stations | 10-100 m | Not provided |
| Background stations: | | |
| - Urban | 100m-1 km | ≥ 3-6 $km^2$ |
| - Near-city | 1-5 km | > 100 $km^2$ |
| - Regional | 25-150 km | > 1000 $km^2$ |
| - Remote | 200-500 km | >10000 $km^2$ |

Some of these criteria were adapted to be included in the first Daughter Directive (1999/30/EC), the Exchange of Air Quality Information EC Decision (97/101/EC), after revised by Decision 2001/752/EC) and the Directive 2008/50/EC (as seen in Table 2.4 and Table 2.5). The report also defines the area of representativeness as the area "within which the concentration does not differ from that at the monitoring station by more than ±20%". The report does not define a reference time period for which this relationship should be valid.

However there is still no agreement regarding European air quality stations classification criteria and definition and quantitative assessment of spatial representativeness. This fact leads, in the opinion of some authors, to misrepresentations of the air quality spatial distribution at national and European levels (Hout and Larssen, 2006).

Recognizing the current discrepancies, the FAIRMODE (Forum for air quality modelling in Europe) project organized a survey based on the opinion of experts from several European institutions in order to assess station spatial representativeness for all major pollutants measured. This study, although limited in scope, not only emphasized differences between legislative and operational air quality monitoring network implementation guidelines but also tackled the importance of considering different time averaging periods, when addressing the issue of station representativeness. In the specific case of $PM_{10}$, the survey results are shown in Table 2.8.

**Table 2.8 - Area of representativeness for $PM_{10}$ monitoring data for the specified station classification and averaging periods. Source: Balaguer and Denby, 2011**

| $PM_{10}$ | | Averaging Period | | |
|---|---|---|---|---|
| | | One hour | One day | One year |
| Station class | Rural background | 10500 m | 19500 m | 29286 m |
| | Suburban background | 5000 m | 6500 m | 11333 m |
| | Urban background | 2940 m | 3383 m | 6629 m |
| | Traffic | 26 m | 91 m | 492 m |
| | Industrial | 260 m | 1025 m | 2400 m |

As expected, time averaging period plays an important role in the definition of station spatial representativeness , with the respective values increasing substantially with this variable, for all station classes.

Several studies and reports proposed alternative ways of aiming at the establishing more uniformly applicable methods at a European scale. According to those studies, station classification could benefit from more detailed information about affected receptors, better emission sources and dispersion conditions characterization and integration of several meaningful time averaging periods (Hout and Larssen, 2006; Spangl *et al.*, 2007). Station representativeness assessment should support that classification and could be achieved by using geostatistical interpolation or data assimilation methods or expert judgement (Balaguer and Denby, 2011; Flemming *et al.*, 2005; Hout and Larssen, 2006; Spangl, 2007). Although relevant, these studies are still not reflected in legislative guidelines.

Contributing to the methodological constraints described above, the deployment of such networks is limited by economical (i.e. equipment cost) and technical factors (i.e. difficulties in maintenance). Therefore, ground networks are mainly deployed in big urban areas leaving at the same time large suburban and rural regions without appropriate surface monitors. The lack of spatial correspondence between high exposure and potentially susceptible populations within cities leads to the introduction of bias in estimates that rely on central monitors to proxy exposure over wide areas (Jerrett *et al.* 2005; Tran *et al.*, 2008). Such limitations can be minimized through coupling of statistical and physical models or introduction of a wide range of satellite air pollution products which can complement ground data. Furthermore satellite and modelling could be used in studies of air quality monitoring network optimization, aimed

at identifying poorly represented areas. These can even be used to redefine station classification criteria or calculation methods linked with the area of representativeness.

### 2.1.5 Aerosol/$PM_{10}$ related Air Quality in Portugal

The EEA report "The European environment – state and outlook 2010" provides a description of the Portuguese country assessment: "Air quality is generally good in Portugal, with the exception of some agglomerations in the north and centre regions, Lisbon and the Tagus valley, where ozone and particle ($PM_{10}$) pollutants represent an atmospheric pollution problem that needs to be tackled". This statement translates, in a simplified manner, the current overall air quality status in Portugal, and is confirmed by the more recent Portuguese air quality index (IQAr) results, published in the last Portuguese State of the Environment Report (APA, 2011).

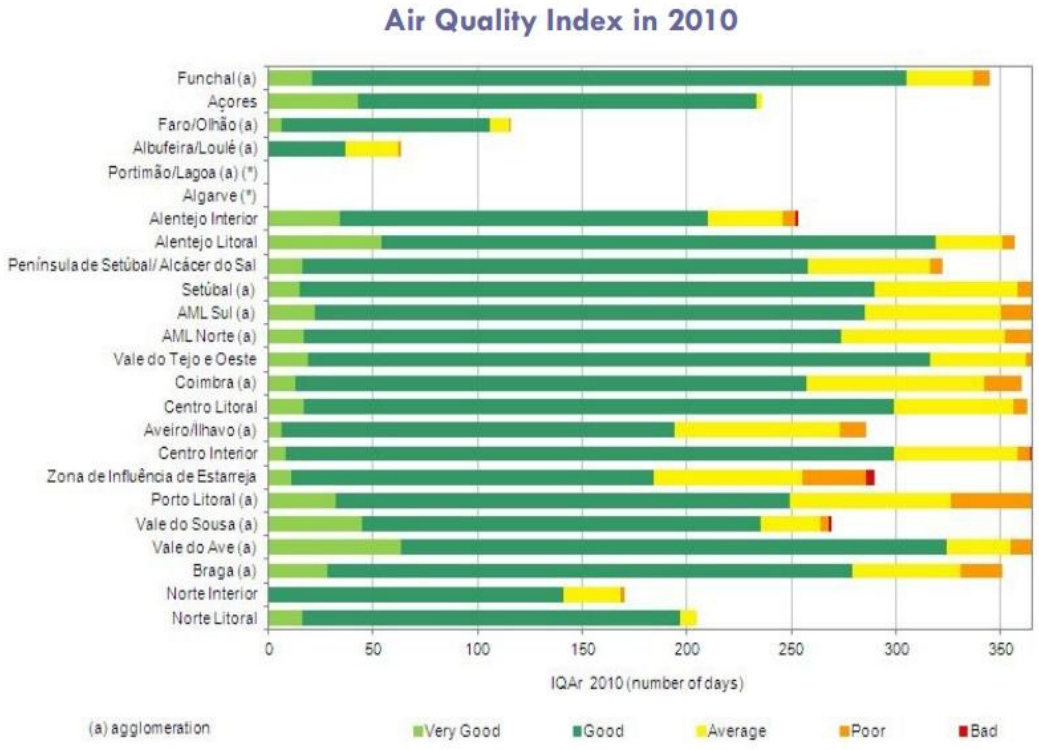


**Figure 2.7 – Air quality index results for all defined zones/agglomerations in the continental Portuguese territory, for the year 2010. Source: APA, 2011. The referred zones/agglomerations were defined in agreement with criteria concerning homogeneity in the measured air quality levels, total population or population density (Decree Law 276/99).**

This index, implemented since 2001 for the Portuguese territory and available at http://www.qualar.org, is calculated from the zone/agglomeration air quality stations average for each pollutant (CO, $NO_2$, $SO_2$, $O_3$ and $PM_{10}$). It is composed of five classes for each pollutant, ranging from "Bad" to "Very Good and based on concentration ranges established according to the legal limit values (APA, 2011). The daily IQAr for a specific zone/agglomeration corresponds to the worst rank obtained from all pollutants. Figure 2.8 provide maps with the location of all current air quality stations (right map) and the delimitation of the zones and agglomerations (left map) for which IQAr is calculated.

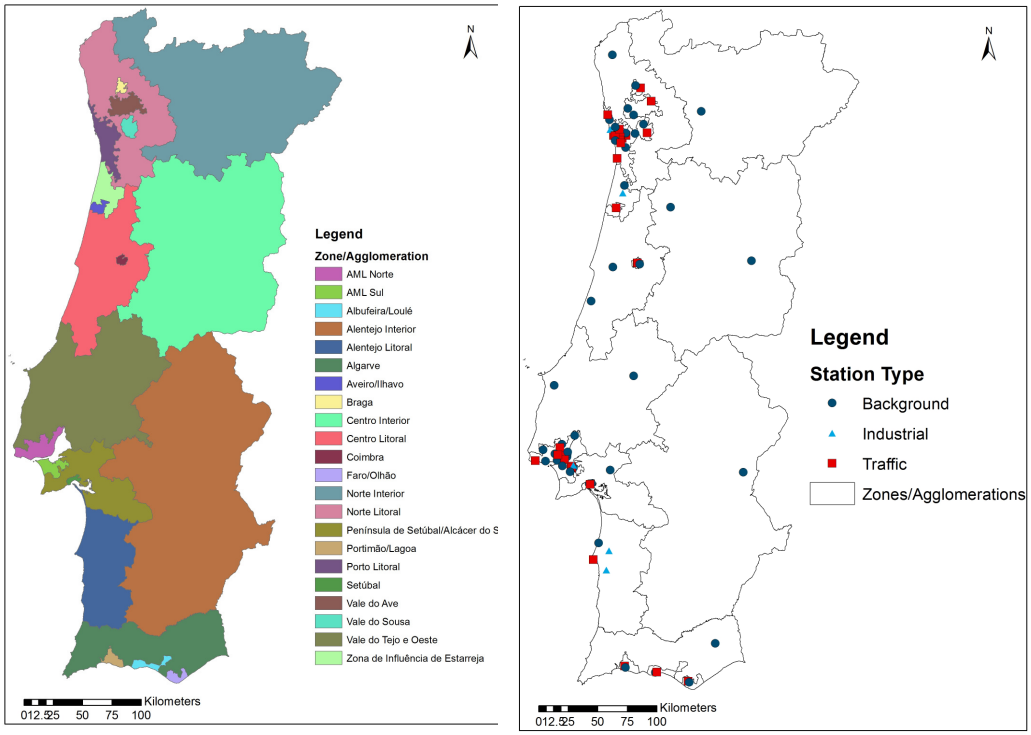


**Figure 2.8 – (a) Delimitation of all air quality zones/agglomerations for the portuguese continental territory; (b) Location of all Portuguese traffic, background and industrial air quality stations**

The 2010 IQAr results for all zones/agglomerations in the continental Portugal (Figure 2.7) shows a clear predominance of days with good air quality index. Nevertheless, as stated in the EEA report, the IQAr in 2010 still presented a significant incidence of days with average to poor air quality in some highly populated coastal areas/cities (North and South Lisbon Metropolitan Area – AMLN and AMLS, Centro Litoral, Lisbon, Oporto - Porto Litoral, Setúbal, Aveiro/Ílhavo and Coimbra,) and industrial areas (Estarreja). These days have

been always associated to either $PM_{10}$ or tropospheric ozone ($O_3$) high concentrations.

In the case of $PM_{10}$, high concentrations are mostly related to industry, road traffic and residential combustion emissions (Alves *et al.*, 2011; Borrego *et al.* 2008a, 2008b, 2010, 2011; Fernandes *et al.*, 2011; Ferreira *et al.* 2006a, 2006c) and desert dust transport events from the North Africa, more frequent during spring and summer (Ferreira *et al.* 2007, 2008, 2009a, 2010, 2011; Franco, 2008; Santos *et al.*, 2007). Also significant are the contributions from marine aerosols (Ferreira *et al.*, 2006b, 2006c; Pereira, 2008), forest fires during summer (Alves *et al.*, 2011; Calvo *et al.*, 2011; Martins *et al.*, 2012; Santos *et al.* 2007) and road and dust resuspension events (Almeida *et al.*, 2006).

Previous APA reports confirm this overall trend of air quality improvement, especially after 2005, in urban/industrial areas such as AMLN and AMLS, Porto Litoral, Setúbal, Braga and Vale do Ave (APA, 2008, 2009). This upward tendency in overall air quality is linked to a decrease in $PM_{10}$ and ozone concentrations, as shown, in the case of $PM_{10}$, by Figure 2.9. It is clear from the figure a significant decrease in the average number of days with a $PM_{10}$ air quality index classified as "Bad" (>120µg/m$^3$), during a period between 2005 and 2008 (EEA, 2010) for Portuguese urban and rural sites. This trend contrasted with the increase verified in the four previous years. In fact, between 2002 and 2005, the average number of exceedance days went from about 10 to 30 days in rural sites and from 30 to 70 days in urban sites. After 2005, it decreased to less than 10 days in rural sites and only 20 days for urban sites.


**Figure 2.9 - Number of days in urban or rural sites with "Bad" $PM_{10}$ air quality index between 2001 and 2008 in Portugal. Source (EEA, 2010).**

During the same interval, annual average $PM_{10}$ concentrations have been decreasing for all station types. In urban sites this trend is more obvious in 2001 and after 2005, where the annual concentration decreased from 35 to 20 µg/m³. In traffic sites the reduction has been steady throughout the seven year period, ranging from 60 to 30 µg/m³. Currently, all values for aggregated station types are below the 40 µg/m³ annual average concentration limit value, set in the Council Directive 2008/50/EC.


**Figure 2.10 – Average annual $PM_{10}$ concentrations for rural, urban and sites between 2001 and 2008. Source (EEA, 2010).**

The limits established in the CAFE Directive (2008/50/EC) for days per year above the daily $PM_{10}$ concentration limit (35) also presents signs of positive development. Figure 2.11 shows a comparison, between 2006 and 2009, of the zones/agglomerations above and below this limit. In 2009 there is a clear increase in the number of compliant areas with emphasis to industrial areas near

Oporto (Vale do Ave e Vale do Sousa) and Aveiro (Estarreja). In the South, the city of Setúbal, near Lisbon, and the agglomeration of Portimão/Lagoa in Algarve also lowered the number of daily exceedances to levels below the 35 day threshold (see map in Figure 2.8 to identify the respective zones/agglomerations).

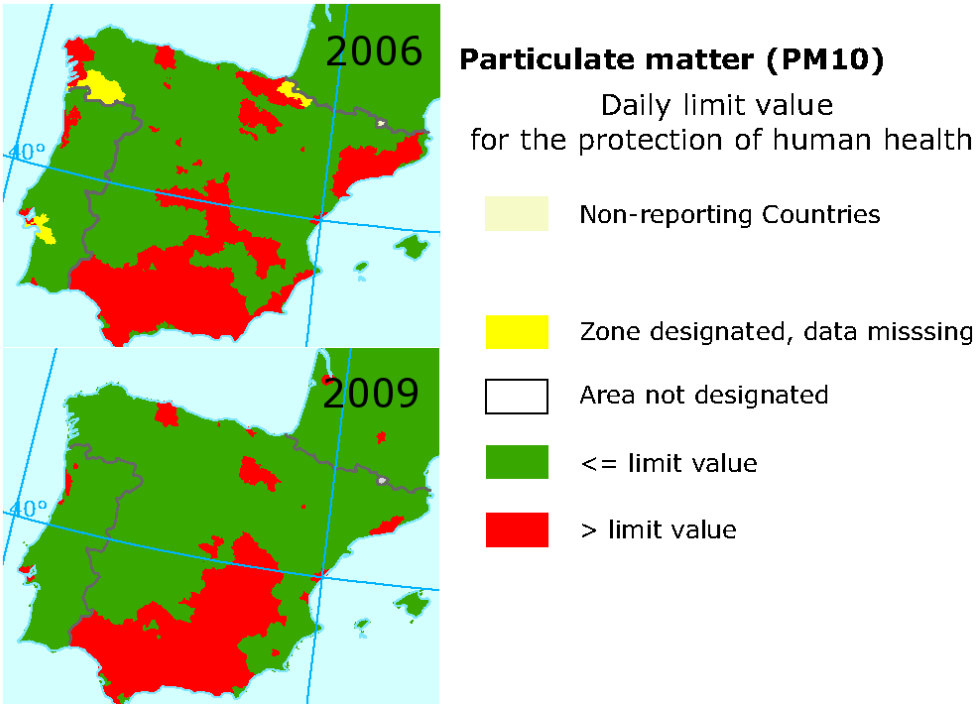


**Figure 2.11 – Maps showing the Portuguese zones/agglomeration with more than 35 days over the $PM_{10}$ daily average limit value (40 µg/m³) for 2006 (top) and 2009 (bottom). Adapted from http://www.eea.europa.eu/data-and-maps/figures/particulate-matter-$PM_{10}$-2007-annual-limit-value-for-the-protection-of-human-health-3**

The progressive improvement in overall air quality in Portugal, specifically when regards to $PM_{10}$, can be justified by measures taken related to the enforcement of national air quality laws and the transposition into national law of the European legislation described in the previous section (APA, 2008).

First the Council Directive 96/62/EC was transposed to the national Decree-Law (DL) 276/99, providing a framework and guidelines for air quality management. In the next years the three directives 1999/30/EC, 2000/69/EC and 2002/03/EC, responsible for setting the limit values for several pollutants, were also implemented through DL 111/2002 ($SO_2$, $NO_x$, $PM_{10}$, Pb, CO, $C_6H_6$) and DL 320/2003 ($O_3$). Those pollutant limit values were defined in Council Di-

rective 96/62/EC as the "level fixed on the basis of scientific knowledge, with the aim of avoiding, preventing or reducing harmful effects on human health and/or the environment as a whole, to be attained within a given period and not to be exceeded once attained". More recently, the CAFE European Directive 2008/50/EC, which aggregates the three mentioned specific directives, was transposed to national law (DL 102/2010), together with a fourth specific directive, responsible for setting the limit values for heavy metals (As, Cd, Ni and Hg) and hazardous air pollutants (HAP). The corresponding limit and assessment threshold values for $PM_{10}$ and $PM_{2.5}$ in Portugal were presented in Table 2.3.

Several instruments were implemented to help define a more integrated air quality management, enforce the stricter pollutants limit values and improve the spatial and temporal coverage of air quality monitoring and reporting, namely:

a) definition of a national air quality strategy;

b) expansion or the air quality network to 72 stations (in 2005), including the creation of a background rural network (see map in Figure 2.8b);

c) significant improvement in station measurement efficiency;

d) definition and implementation of periodically revised regional air quality plans to enforce compliance in zones and agglomerations with pollutant concentrations exceeding the threshold limit value;

e) implementation of the IQAr and respective public information site (htpp://www.qualar.org)

In 2006 a "next day" forecast was implemented applying a "Classification and regression trees – CART" method to construct multiple regression models for each monitoring station (Neto *et al.*, 2004; Neto *et al.*, 2005; Marques *et al.* 2006). The models were developed to predict ozone hourly maximum and daily average $PM_{10}$ based on the respective historical time series and several synoptic and local meteorological variables. Originally developed for the AMLN and AMLS, it has been progressively expanded to other zones and agglomerations and is currently available also for Porto Litoral, Aveiro/Ílhavo, Braga, Coimbra,

Faro/Olhão, Setúbal and the Lisboa e Vale do Tejo (Lisbon and Tagus Valley) Region.

Some of the measures implemented had a relevant impact in PM emission from anthropogenic sources mainly in industrial and urban areas. These included: a) public transport fuel emissions reduction to comply with European standards (Euro norms); b) creation of lower emission areas; c) increase in parking regulations enforcement; d) increase the number of BUS corridors; c) improve industrial PM retention systems; d) reinforcement of the inspection of industry sources; e) establishment of emissions standards for industrial clusters and business activities; f) usage of certified residential combustion appliances with PM emissions reduction (Borrego *et al.*, 2010, 2011; Ferreira *et al.*, 2006a, 2006b).

Regarding biogenic sources, a natural event identification and evaluation methodology was implemented for Portugal in 2006, following the transposition to national law of European Directive 2008/50/EC to DL 102/2010. This methodology, based on the work of Querol *et al.*, 2009, was implemented to quantify and exclude from stations results all natural PM contributions. Those natural events, such as the Saharan dust transport have a strong impact in air quality of Mediterranean countries and can be responsible for over 60% of the total $PM_{10}$ concentrations measured during a strong episode (EC, 2011). When it was first implemented, this measure also included forest fire contributions. They were removed in 2010, due to a clarification by the EC, stating most forest fires originate from human activity and therefore should not count as natural $PM_{10}$ sources (Ferreira and Monjardino, 2011).

Since 2006, this methodology was responsible for a significant reduction of daily average exceedance days in the Portuguese territory. In 2006 the average number of $PM_{10}$ exceedance days per station decreased from 48.7 to 32.5. In 2010 the number of overall exceedance days was substantially smaller, with an average per station of 17.7 days. When accounting for dust transport events there was a reduction to ≈13 days (Ferreira *et al.*, 2007, 2011). Due to the implementation of this methodology APA reported, for the the period between 2006 and 2010, a decrease in $PM_{10}$ annual average concentration ranging from 2 to 4 $\mu g/m^3$ (Ferreira *et al.*, 2007, 2008, 2009a, 2010, 2011).

According to data compiled from the raw $PM_{10}$ concentration values provided by http://www.qualar.org for all stations with measurement efficiencies higher than 75%, the overall impact of these measures can be translated into a reduction of $PM_{10}$ average number of exceedance days per station: from 127 in 2001 to approximately 30 in 2011. During the same period, average station $PM_{10}$ daily concentration decreased from 47.7 to 26.4 $\mu g/m^3$.

The Porto Litoral and North and South AML areas still present a significant number of daily average exceedance days, mostly due to $PM_{10}$. For instance, in 2011 those areas presented an average number of $PM_{10}$ exceedance days per station of, respectively 51.4, 31.8 and 33.2, while in the remaining Portuguese air quality zones/agglomerations averaged around 20. For this reason regional air quality improvement plans were implemented in these problematic areas. These define air quality objectives, establish a set of measures to achieve them and are periodically monitored and revised by regional authorities. Currently there are two regional air quality improvement plans in action since 2001, one for Lisbon and Tagus Valley region and the other for the Northern region. The AMLN and AMLS agglomerations, chosen as a study area in Chapter 4, are included in the Lisbon and Tagus Valley region. Those areas were chosen as the main case study due to its importance, within the national context, as the most populated urban centres in Portugal, with recurring PM related air quality problems. The Peninsula of Setúbal area, which integrates the Lisbon Metropolitan Area, was not included in the case study since it was considered to have a separate air quality dynamics, driven by specific industrial and traffic emission sources. The lack of integration with the remaining Lisbon Metropolitan Area territory is justified by geographical distance and more tenuous socioeconomic link with the capital as shown by lower commuter traffic load to Lisbon, when compared with other areas within the metropolitan area. The next section will provide a general outline and a description of its main characteristics regarding air quality, in particular related with particulate matter.

### 2.1.6 PM Air Quality in the North and South Lisbon Metropolitan Areas

The North and South Lisbon Metropolitan Areas, referred in this chapter as AMLN and AMLS respectively, are two of the air quality agglomerations de-

fined to support the implementation of DL 276/99 (see all zones/agglomerations in Figure 2.8). These are located in the south and north margin of the river Tagus, in a region centred around Lisbon (Figure 2.12). Composed of 13 municipalities (Table 2.9) with a total area of 1450 km² and population of almost 2.4 million inhabitants, these two agglomerations are spread throughout two NUTS III Regions: the Greater Lisbon and the Peninsula of Setúbal. They integrate the Lisbon and Tagus Valley (LVT) NUTS II region.

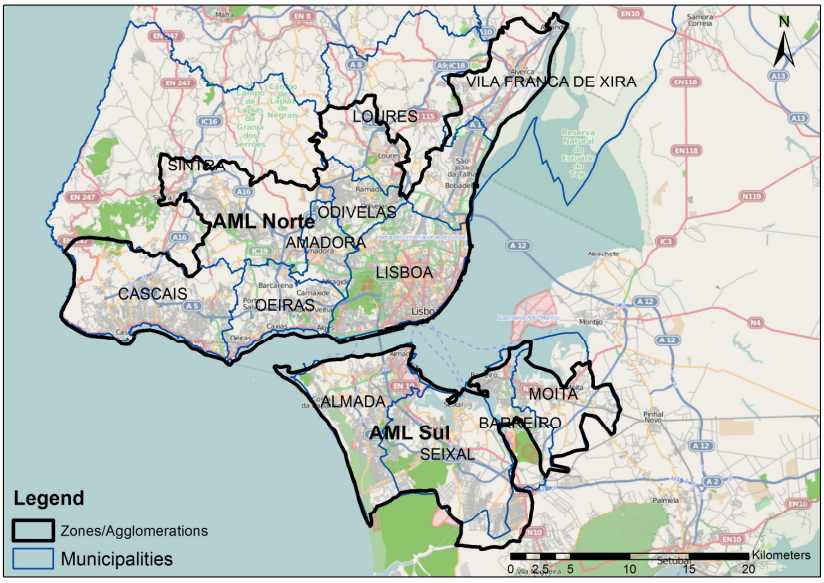


**Figure 2.12 – Map of the North and South Lisbon Metropolitan Areas**

According to the 2001 Census, the most populated urban centre is Lisbon (564 657 inhabitants), followed by Sintra (363 749) and Loures, Amadora, Cascais, Oeiras, Almada, Odivelas and Vila Franca de Xira, with a population ranging from 175 872 to 122 908 inhabitants (INE, 2001).

**Table 2.9 – North and South AML municipalities and respective area and population (INE, 2001)**

| Municipality | Agglomeration | Area (km²) | Population |
|---|---|---|---|
| Amadora | AMLN | 23.8 | 175 872 |
| Barreiro | AMLN | 32 | 79 012 |
| Cascais | AMLN | 97.3 | 170 683 |
| Lisbon | AMLN | 84.6 | 564 657 |
| Loures | AMLN | 167.9 | 199 059 |
| Odivelas | AMLN | 26.6 | 133 847 |
| Oeiras | AMLN | 45.8 | 162 128 |
| Sintra | AMLN | 319.5 | 363 749 |
| Vila Franca de Xira | AMLN | 318.5 | 122 908 |
| Almada | AMLS | 70.1 | 160 825 |
| Moita | AMLS | 54.6 | 67 449 |
| Seixal | AMLS | 95.7 | 150 271 |
| Sesimbra | AMLS | 195.7 | 37 567 |

In the last 30 years, people migrated from Lisbon to more peripheral municipalities like Sintra, Oeiras, Almada, Cascais, Odivelas and Loures. In the last decade, a separate trend was observed with population moving away not only from Lisbon, but also from other densely populated municipalities in the centre of the AMLN and AMLS (Amadora, Odivelas and Oeiras). This movement occurs to more peripheral municipalities like Vila Franca de Xira in the north margin and Mafra, Sesimbra, Montijo, Seixal e Alcochete, in the south. These migrations to more distant urban areas from Lisbon determines an increase in commuter traffic load and mean distance, contributing to an increase in total traffic emissions and in particular PM emissions. This is confirmed by the increase in the number of inter-municipality commuter travels from 483 662 in 1991 to 557 484 in 2001 (Ferreira *et al.*, 2006b).

Looking into the 2000/2001 emission inventory, undertaken in the scope of the air quality improvement plan for Lisbon and Tagus Valley (Ferreira *et al.*, 2006b, Góis *et al.*, 2006), the main regional $PM_{10}$ emission sources were: 54,4% - Industry; 27,6% - Domestic and services; 12.5% - Traffic; 3.5% - Energy production; 1.9% - Aviation. The report also concluded that: a) within the industry related emissions the main contributors are: food (31%), chemical (29%) and paper (21%) industries, followed by thermoelectric power plants (7%) and the cement industry (6%); b) LVT municipalities most responsible for $PM_{10}$ emissions are Lisbon, Amadora, Barreiro and Setúbal (the last two are not part of the study area) (Figure 2.13); c) in the Lisbon municipality the main $PM_{10}$ emission

sectors are Domestic and Services, mostly related to residential combustion and transport (Góis *et al.*, 2006).

Figure 2.13(b) $PM_{10}$ emissions spatialized for the LVT region into a 2x2 km grid (Góis *et al.*, 2005). Its distribution emphasizes the role of the larger urban centres and the most important traffic roadways as the main $PM_{10}$ emission sources (Ferreira *et al.*, 2006c).

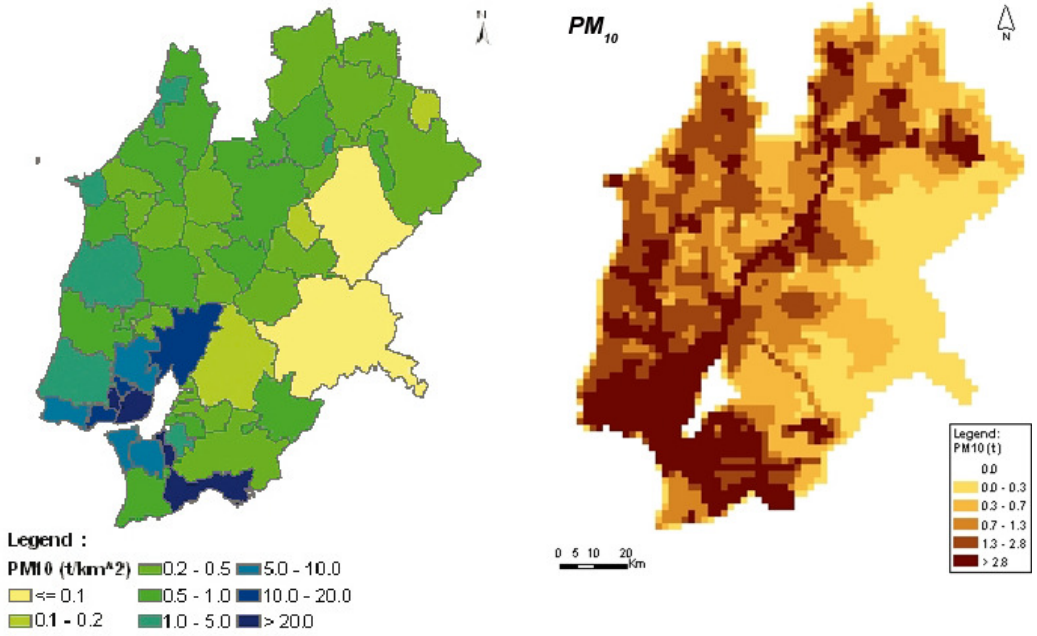


(a) (b)

**Figure 2.13 – (a) $PM_{10}$ Emissions per area for each municipality in the Lisbon and Tagus Valley region. Source: Góis *et al.*, 2005; (b) $PM_{10}$ Emissions per area for a 2x2 km grid covering the Lisbon and Tagus Valley region. Source: Ferreira *et al.*, 2006a.**

A measurement and chemical composition analysis $PM_{10}$ campaign performed from January to October 2003 in the AMLN urban background station of Alfragide (municipality of Amadora) provided additional information on possible $PM_{10}$ sources (Ferreira *et al.*, 2006b). According to the results of this study, 47% of the sampled aerosol derived from traffic emissions, 28% from nitrate and sulphate secondary aerosol formation, also with a traffic related origin, 19% were marine aerosols and the remainder originated from undetermined sources.

Another aerosol speciation study, performed in the Avenida da Liberdade station (Ferreira *et al.*, 2006c), an urban traffic station situated in the centre of

Lisbon, showed a smaller contribution from mobile sources (34-41%), secondary (6-7%) and marine (2.6-4.8%) aerosol and a 11.7 to 15.4% crustal aerosol component, not identified in the previous study, indicating a possible influence from North African dust transport events.

Work developed by Tente (2005) calculated several spatial distribution patterns for $PM_{10}$ urban background average daily concentrations in Lisbon. (Figure 2.14). This study was performed using a kriging geostatistical technique with data from a five day ground measurement campaign in February 2004. Information about wind direction and intensity was also included.

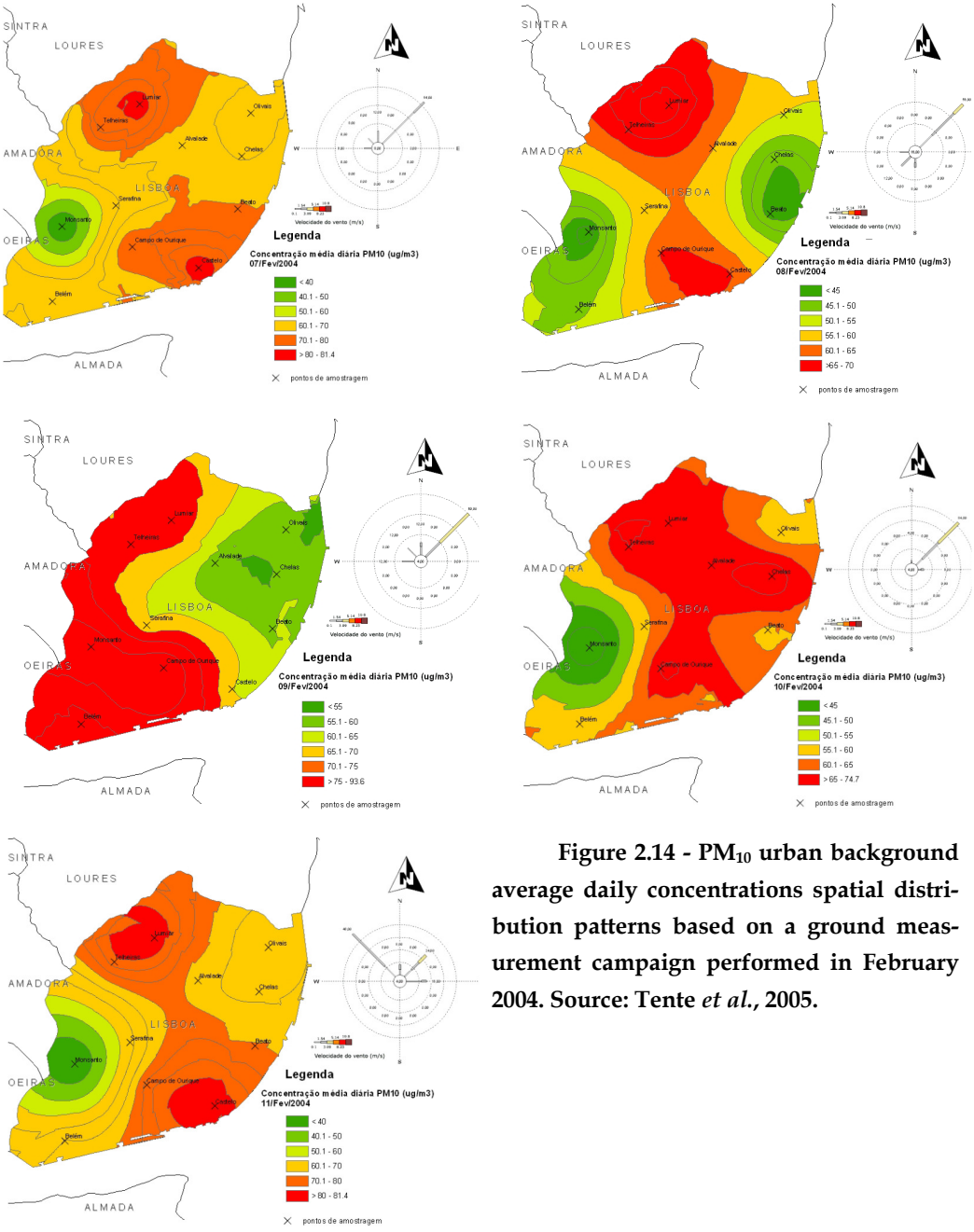


**Figure 2.14 - $PM_{10}$ urban background average daily concentrations spatial distribution patterns based on a ground measurement campaign performed in February 2004. Source: Tente *et al.*, 2005.**

It should be noted that the days presented, especially between the 7th and 9th of February, were influenced by a natural event, which, according to the author, is the main responsible for the observed high concentrations. Nevertheless high $PM_{10}$ values are consistently found along a central axis in the city centre, closely related with the main Lisbon traffic access roads which seem to indicate traffic emissions play a major role in the definition of $PM_{10}$ daily spatial patterns (Tente *et al.*, 2005).

Most air quality studies performed in AML agglomerations are based on pollutant measurements from the LVT air quality ground monitoring network. This network is composed of 24 stations: 14 in AMLN, 6 in AMLS, 3 in Setúbal and 1 in the Vale do Tejo e Oeste region. The main characteristics of the 20 stations from AMLN and AMLS, including station type, zone of influence, measured pollutants and starting date, are presented in Table 2.10.

**Table 2.10 – AMLN and AMLS air quality stations name, zone of influence, station type, main pollutants measured and starting date.**

| Station | Municipality | Zone | Type | Main Pollutants Measured |
|---|---|---|---|---|
| Alfragide | Amadora | Urban | Background | $NO_x$, $O_3$, $SO_2$, $PM_{10}$, $C_6H_6$, $PM_{2.5}$, CO, Pb |
| Beato | Lisbon | Urban | Background | $NO_x$, $O_3$, $SO_2$, $C_6H_6$, CO |
| Fidalguinhos | Barreiro | Urban | Background | $NO_x$, $O_3$, $SO_2$, $PM_{10}$, CO |
| Laranjeiro (LAR) | Almada | Urban | Background | $NO_x$, $O_3$, $SO_2$, $PM_{10}$, $C_6H_6$, $PM_{2.5}$, CO |
| Loures (LOU) | Loures | Urban | Background | $NO_x$, $O_3$, $SO_2$, $PM_{10}$, CO |
| Mem-Martins (MEM) | Sintra | Urban | Background | $NO_x$, $O_3$, $SO_2$, $PM_{10}$, $PM_{2.5}$, CO |
| Olivais (OLV) | Lisbon | Urban | Background | $NO_x$, $O_3$, $SO_2$, $PM_{10}$, $PM_{2.5}$, CO |
| Paio Pires | Seixal | Suburban | Background | $NO_x$, $O_3$, $SO_2$, $PM_{10}$, TSP, CO |
| Quinta do Marquês (MAR) | Oeiras | Urban | Background | $NO_x$, $O_3$, $SO_2$, $PM_{10}$, CO |
| Reboleira (REB) | Amadora | Urban | Background | $NO_x$, $O_3$, $SO_2$, $PM_{10}$, CO |
| Restelo | Lisbon | Urban | Background | $NO_x$, $O_3$, $PM_{10}$, CO |
| Vila Franca de Xira | V. F. Xira | Urban | Background | $NO_x$, $O_3$, $SO_2$, $PM_{10}$, CO |
| Escavadeira (ESC) | Barreiro | Urban | Industrial | $NO_x$, $O_3$, $SO_2$, $PM_{10}$, CO |
| Lavradio (LAV) | Barreiro | Urban | Industrial | $NO_x$, $O_3$, $SO_2$, $PM_{10}$, TSP, CO |
| Alto Seixalinho | Seixal | Urban | Traffic | $NO_x$, $O_3$, $SO_2$, $PM_{10}$, $C_6H_6$, CO |
| Av. da Liberdade (LIB) | Lisbon | Urban | Traffic | $NO_x$, $PM_{10}$ CO |
| Cascais – Mercado (CAS) | Cascais | Urban | Trafic | $NO_x$ , $PM_{10}$, $C_6H_6$, CO |
| Entrecampos (ENT) | Lisbon | Urban | Trafic | $NO_x$, $O_3$, $SO_2$, $PM_{10}$, $C_6H_6$, $PM_{2.5}$, CO |
| Odivelas (ODV) | Odivelas | Urban | Trafic | $NO_x$, $O_3$, $PM_{10}$, CO |
| Sta. Cruz de Benfica | Lisbon | Urban | Trafic | $NO_x$, $SO_2$, $PM_{10}$, CO |

From these 20 stations, 12 are background, two are industrial and 6 are traffic stations (Figure 2.15). Fourteen are located in AMLN: six in the municipality of Lisbon, two in Amadora, and one in Loures, Odivelas, Oeiras, Sintr and Vila Franca de Xira. In the AMLS there are six stations: four in Barreiro, one in Almada and one Seixal. .

The air quality network includes 19 $PM_{10}$ measuring stations, 12 of which presented valid measures for 2005 (marked in grey in Table 2.10 and in blue in Figure 2.15), the year chosen in Chapter 4 for the satellite based $PM_{10}$ estima-

tions in the Lisbon Metropolitan Area. The air quality analysis shown in the following paragraphs will focus mostly in these 12 stations, during a period between 2001 and 2010, to provide a proper context to that case study.

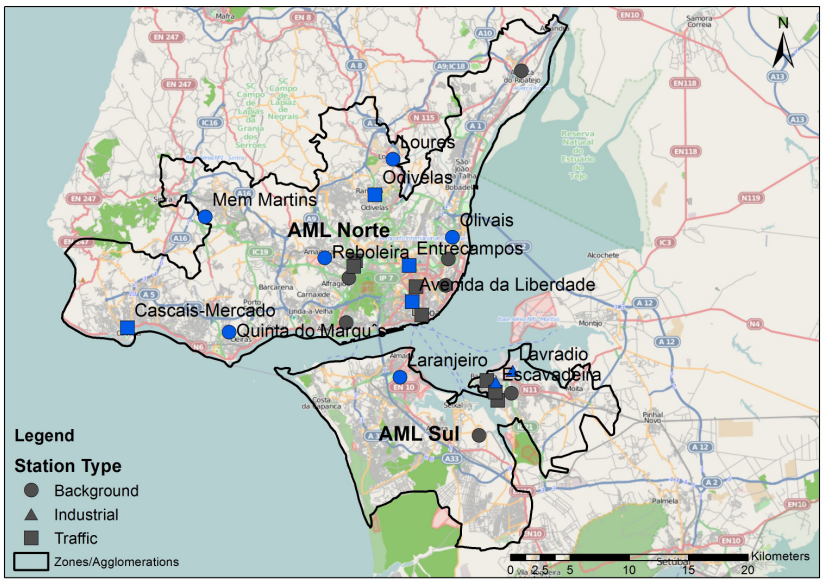


**Figure 2.15 – Location of all current air quality stations for the AMLN and AMLS, including information on station type. 2005 PM stations are marked in blue and labelled with the respective station names**

$PM_{10}$ typical hourly profiles in the stations of the two agglomerations are usually bimodal, with peaks in the early morning (around 9h) and late afternoon (19h), coinciding with the hours of heavier commuter traffic. Two examples are shown in Figure 2.16 for urban traffic (Avenida da Liberdade) and background (Olivais) stations between 2005 and 2010. As expected, the traffic station presents a more a pronounced intra-daily cycle with higher overall and peak concentrations, especially the morning peak, almost imperceptible in the background station.

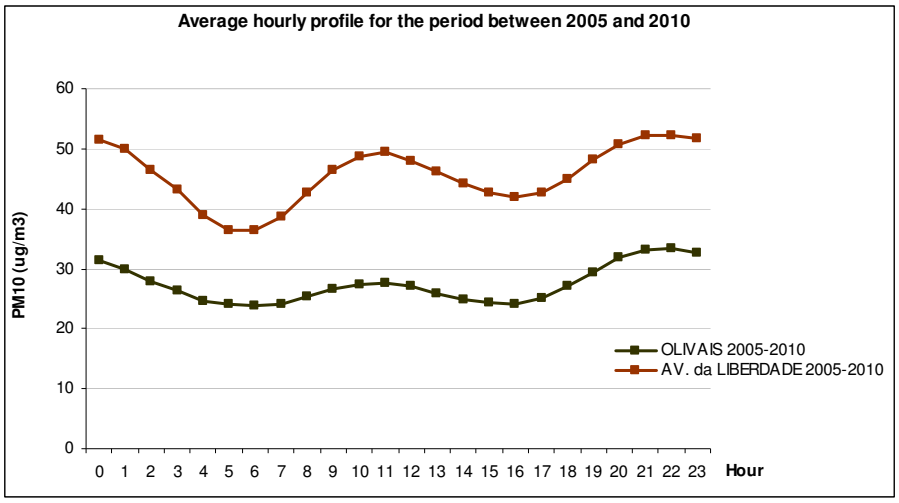


**Figure 2.16 – Example of the average $PM_{10}$ hourly profiles for the 2005-2010 period for an urban background station (Olivais) and an urban traffic station (Avenida da Liberdade). Source: Ferreira *et al.*, 2006b**

While the intra-daily profile in an urban area is driven by traffic load its seasonal variability is more influenced by meteorological factors. Figure 2.17 presents the seasonal profile for the same two stations, established using the monthly mean daily $PM_{10}$ concentrations for the 2001-2010 period. Both present higher and more variable values in winter probably associated with the lower mixing layer heights characteristic of that season. Those lower mixing heights concentrate $PM_{10}$ closer to ground level and are usually responsible for an increase in $PM_{10}$ concentrations measured in ground stations. The monthly mean concentrations decrease steadily, in value and variability until April and remain more or less stable during the next three months. This decrease is probably determined by the influence higher wind speeds and mixing layer heights. August presents higher $PM_{10}$ values with a wider range due to the influence of natural dust events and forest fires. During September and October, concentrations remain at similar levels, followed by an increase in November and a small decrease in December. The $PM_{10}$ seasonal variability will be further explored in Chapter 4.

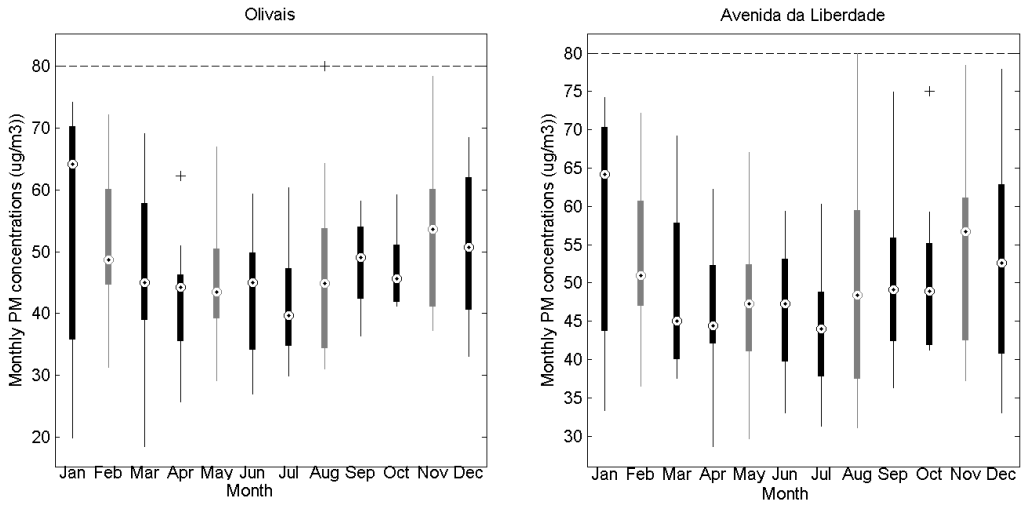


(a) (b)

**Figure 2.17 – Box plot graphs showing the variation of the monthly mean $PM_{10}$ daily concentration considering a period between 2001 and 2010 for: (a) an urban traffic station (Avenida da Liberdade) and; (b) an urban background station (Olivais). The higher and lower bound of each box represent the 25th and 75th percentile and the central value is the 50th percentile (median). Outlier values higher than 80 µg/m³ are not presented to provide a better visualization of the seasonal cycle. Original $PM_{10}$ concentration data downloaded from http://www.qualar.org.**

According to data compiled from the IQAr site (http://www.qualar.org) AMLN and AMLS stations present a constant increase of days with a "Good" air quality index classification, during the 2001-2010 period. This increase is closely correlated with a decrease of "Average" and, to a lesser degree, "Bad" air quality days (Figure 2.18 (a) and (b)). It follows the trend previously observed for the Portuguese territory and translates into an overall improvement of the concentrations of the two main pollutants responsible for "Bad" to "Average" air quality days: $PM_{10}$ and ozone.


(a) (b)

**Figure 2.18 – Evolution of all IQAr air quality index classes for a period between 2001 and 2010, considering only stations from: (a) AMLN; (b) AMLS**

The AMLN and AMLS stations annual average $PM_{10}$ concentrations and number of $PM_{10}$ exceedance days for 2005 also present comparable trends to the remaining Portuguese territory (Figure 2.9 and Figure 2.10). Annual average concentrations kept a constant decrease along the last decade with more relevance in traffic sites. In fact most traffic stations with the exception of Odivelas, presented levels above the current legal limit (40 µg/m$^3$ dashed line, marked in the figure) until 2006. Nowadays only Avenida da Liberdade presents concentrations higher than the legal limit (41.4 µg/m$^3$), whereas most stations present an annual average concentration between 20 and 30 µg/m$^3$.

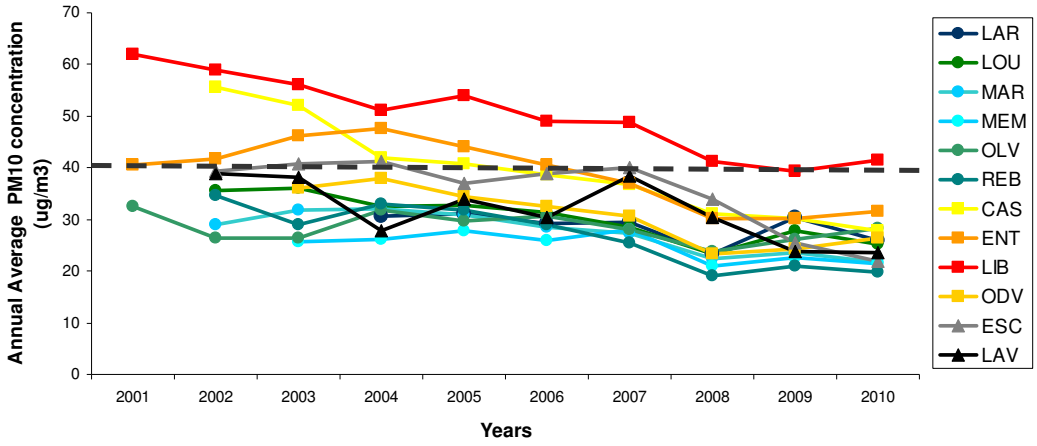


**Figure 2.19 – Annual average $PM_{10}$ concentrations for all 2005 $PM_{10}$ measuring stations during the period between 2001 and 2010. Dashed line marks the current limit value for $PM_{10}$ annual average concentration, as defined in DL 111/2002**

In the number of $PM_{10}$ daily concentration days above the legal threshold (Figure 2.20) most stations show an upward trend until 2005 and a significant decrease after. Between 2004 and 2006 the results were worst, with all traffic and industrial stations and a few background stations above the 35 day value threshold (dashed line). In 2007-2008 the number of non-compliant stations started to decrease significantly until 2010 where only Avenida da Liberdade was above that limit.

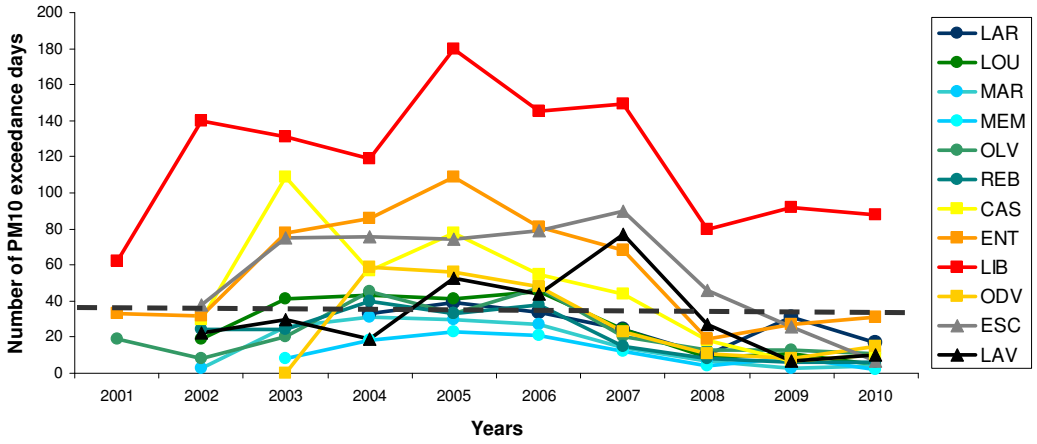


**Figure 2.20 – Number of $PM_{10}$ daily concentration exceedance days for all 2005 $PM_{10}$ measuring stations during the period between 2001 and 2010. Dashed line marks the maximum number of exceedance days per year, permitted in DL 111/2002 (35).**

Several factors contributed to the observed rise in $PM_{10}$ air quality in the last years. The Lisbon and Tagus Valley regional air quality improvement plan, played a decisive role with the definition, implementation and impact evaluation of some important $PM_{10}$ reduction measures. Most of these measures were aimed at bus fleet renovation either by acquiring new buses, installing GPL (Liquefied Petroleum Gas) fuel systems or particle filters. The increase of BUS corridors enhancement of parking regulations also had a significant impact (Ferreira *et al.*, 2006b).

The implementation of low emission zones in the centre of Lisbon, with limitations to vehicle circulation based on non-conformity with Euro emission standards, represents a potential reduction of total $PM_{10}$ traffic related emissions between 8.9% and 35.3%, depending on the severity of the restrictions (Brás, 2012).

Another relevant measure, was the implementation by APA, since 2006, of a dust transport event identification and evaluation procedure (APA, 2006, 2007, 2009, 2010). The yearly impact of this measure on the number of $PM_{10}$ exceedance days and on the average $PM_{10}$ annual concentration is variable and dependent on meteorological conditions. After removing the effect of natural events the number of AMLN and AMLS station exceedance days decreased between 44% to 28% in 2009 and between 100% to 28% in 2010 (APA, 2009, 2010). In terms of average PM annual concentration the impact is also significant varying from 8-15% in 2009 to 64% in 2010.

## 2.2 Aerosol Remote Sensing over Land and PM Air quality

### 2.2.1 Aerosol Optical Thickness

Satellite remote sensing of aerosols delivers global and seasonal coverage of aerosol distribution patterns sorting the spatial and temporal heterogeneities introduced by different sources and thus providing a more accurate quantification and characterization of the presence of aerosols in the atmosphere (King *et al.*, 1999). Data from Earth Observation (EO) satellites has been extensively used for the assessment of suspended aerosol particles in the entire atmospheric column. Several retrieval methods have been operationally implemented for various satellite sensors providing global standard aerosol products. These include:

Aerosol Optical Thickness or Depth (AOT and AOD respectively) and particle size related parameters. AOT is a dimensionless parameter, which provides a measure of the aerosol load on the entire atmospheric vertical column by determining the amount of transmitted light prevented from reaching the satellite sensor due to aerosol scattering and absorption. It's translated by Equation 2.1:

$$AOT(\lambda) = \int_{H\,\min}^{H\,\max} ext(\lambda, h)dh \approx \int_{H\,\min}^{H\,\max} ext(\lambda) f(h)dh \qquad \textbf{Equation 2.1}$$

Where ext(λ,h), expressed in $km^{-1}$, is the light extinction coefficient, for a certain wavelength λ, integrated for the vertical column of height h and lower and upper altitude, $H_{min}$ and $H_{max}$, and a vertical distribution of aerosols represented by the function f(h). AOT is dependent on wavelength and particle size distribution related parameters, as shown in Equation 2.2:

$$AOT(\lambda) = c\lambda^{-\alpha} \qquad \textbf{Equation 2.2}$$

where c is a constant and α is the Angström coefficient, a parameter inversely related to the average size of the particles in the aerosol: the smaller the particles, the larger the exponent. It is also provided as an operational product for several satellite sensors and can be calculated as a function of AOT measured at two different wavelengths, usually within the 440-870 nm range, using Equation 2.3:

$$\alpha = \frac{\log \tau_1}{\log \tau_2} \Big/ \frac{\log \lambda_1}{\log \lambda_2} \qquad \textbf{Equation 2.3}$$

where $\tau_1$ and $\tau_2$ are the optical thickness at wavelength $\lambda_1$ and $\lambda_2$.

Aerosol remote sensing products are well summarized and compared in the work of King *et al.* (1999) and Kokhanosky *et al.* (2007). They include techniques based on: (a) known reflectance ratios between different bands for dark homogeneous surfaces (Moderate Resolution Imaging Spectroradiometer - MODIS) (Chu *et al.*, 2002); (b) reflectance analysis in aerosol sensitive bands (Medium Resolution Imaging Spectrometer - MERIS) (von Hoyningen-Huene *et al.*, 2006; Vidot *et al.*, 2008); (c) multi-angle reflectance analysis (Multi-angle Imaging Spectroradiometer - MISR, Advanced Along-Track Scanning Radiometer - AATSR) (Bevan *et al.*, 2009; Grey *et al.*, 2006; Kahn *et al.*, 2005), CHRIS PROBA (Davies *et al.*, 2010) and (d) quantification of light polarisation by aerosols (Polarization and Directionality of the Earth's Reflectances - POLDER) (Deuzé *et al.*,

2001; Goloub *et al.*, 1999). All these methods separate surface from atmospheric signals by modelling surface contribution. Their accuracy is directly related to the precision with which the reflectance properties of the underlying surface are known (e.g., low surface reflective bands or lower sensitivity to polarised light). With the exception of algorithms developed for multi-angle sensors and specifically the Deep Blue algorithm (Hsu *et al.*, 2006) which is able to retrieve aerosol content over bright and heterogeneous surfaces most operational aerosol products have a limited application for urban, desert or snow covered areas (Hsu *et al.*, 2004; Kaufman *et al.*, 1997; Levi *et al.*, 2007; Remer *et al.*, 2005).

Alternatively, contrast reduction algorithms are based on the principle that image contrast is directly related to aerosol optical thickness. Work developed by Martonchik and Diner (1992) provided an overview regarding expected changes in image contrast with view angle, specifically for multi-angle observations. For single view observations, contrast reduction algorithms retrieve AOT by measuring the contrast differences between a pair of images acquired under the same observation geometry for time invariant heterogeneous surfaces. Contrast reduction algorithms were originally developed for retrieving dust aerosol load from high and medium/low resolution sensors (Tanré *et al.*, 1988 and 1992; Holben *et al.*, 1992). A modified version, named Differential Texture Analysis (DTA), was applied in urban areas with good results using Landsat, SPOT and MERIS data (Paronis and Sifakis, 2003; Retalis *et al.* 2003; Retalis and Sifakis, 2010; Sifakis and Deschamps, 1992). Other revised algorithms have been implemented for urban areas, addressing the issue of optimal spatial resolution (Lin *et al.*, 2002; Liu *et al.* 2002). All these studies apply the contrast reduction method to a very limited number of images for the different referred sensors. Most of them only use the algorithm for air quality studies, only comparing AOT values with $PM_{10}$ ground concentrations and without providing extended validation of the algorithm against other AOT measurements. These approaches will be further discussed detail in section 2.2.3.

### 2.2.2 The Contrast Reduction Algorithm

The top of the atmosphere (TOA) reflectance ($\rho^*$) measured by a satellite sensor in the viewing direction referenced by the sensor zenith angle ($\theta_v$) and

the sensor relative azimuth angle (φ), considering a Lambertian surface, can be described by (Deschamps *et al.*, 1984; Tanré *et al.*, 1988).

$$\rho^*(\tau_a,\mu_v,\mu_s,\phi)=\rho_a(\mu_v,\mu_s,\phi)+\frac{T(\mu_s)\times[\rho_s\times\exp(-\tau/\mu_v)]}{1-s\times\langle\rho_s\rangle}+\frac{T(\mu_s)\times[\langle\rho_e\rangle\times t_{scat}(\mu_v)]}{1-s\times\langle\rho_s\rangle} \quad \textbf{Equation 2.4}$$

where $\theta_s$ is the solar zenith angle, $\mu_v=\cos\theta_v$, $\mu_s=\cos\theta_s$, $\tau$ and $\tau_a$ respectively the optical thickness of the atmosphere and its aerosol component, $\rho_a(\mu_v, \mu_s, \varphi)$ the intrinsic atmospheric reflectance, $T(\mu_s)$ the total transmission function on the Sun-ground path, $t_{scat}(\mu_v)$ the diffuse transmission function on the ground-satellite path, s the atmospheric spherical albedo, $<\rho_s>$ the reflectance of the target and $<\rho_e>$ the mean reflectance of the target's environment. According to Equation 2.4, there are three main components contributing to the TOA reflectance, defined by each one of the right-hand side equation terms: a) the intrinsic atmospheric reflectance ($\rho_a$): its dependence on the surface reflectance is minimal; b) the component related to the direct radiation reaching the sensor from the ground-satellite path: direct radiation reflected on the target is further attenuated by a factor $\exp(-\tau/\mu_v)$ according to Beer's law and c) diffuse radiation is reflected towards the sensor by the target's environment and is further attenuated as prescribed by the diffuse transmittance $t_{scat}(\mu_v)$: this effect is commonly referred to as the adjacency effect. It is noted that the $s\cdot<\rho_e>$ term accounts for the effect of multiple scattering between the ground and the atmosphere.

Most retrieval methods extract aerosol information for low ($\rho_s\approx0$ in Equation 2.4) and homogeneous reflectance surfaces such as deep waters or dark vegetated areas where the atmospheric term ($\rho_a$) is dominant. For high reflective heterogeneous surfaces, as deserts or urban areas, the first component of Equation 2.4 is significantly lower than the other two components and consequently the low signal-to-noise ratio (SNR) leads to less accurate retrievals.

Work developed by Mekler and Kaufman (1982), Deschamps *et al.* (1984), Tanré *et al.* (1988 and 1992) and Sifakis *et al.*(1992) introduced contrast reduction based algorithms which connected an increase in aerosol load with a decrease in the contrast between two pixels (i,j) and (i,j+d) where d is the distance in pixels. In fact, assuming that the underlying surface reflectance is stable and atmospheric background contribution is homogeneous, the first and the third terms of Equation 2.4 cancel out in the calculation of the difference $\Delta\rho_{i,j}^*(d)$ be-

tween the pixel ground reflectances. Δρ* is thus controlled by differences in the second term which is a function primarily of the total atmospheric optical thickness, dominated by the aerosol signal (Tanré *et al.*, 1988):

$$\Delta\rho_{i,\,j*}(\tau_a,\mu_v,\mu_s,\phi)=\rho_{i,\,j+d*}-\rho_{i,\,j*}=\Delta\rho_{i,\,j}\cdot T(\theta_s)\exp(-\tau/\mu_v) \qquad \textbf{Equation 2.5}$$

In the original formulation, contrast variations within a scene containing N pixels over a distance d, were quantified by the introduction of the so called structure function $M^{2*}(d)$ defined as:

$$M^{*2}(d)=\frac{1}{N}\sum_i\sum_j(\rho_{i,\,j+d*}-\rho_{i,\,j*})^2 \qquad \textbf{Equation 2.6}$$

By substituting $\Delta\rho^*$ and $\Delta\rho$ in Equation 2.5 with $M^{*2}(d)$ and $M^2(d)$ respectively, the following equation is derived:

$$M^{*2}(d)=M^2(d)\cdot T^2(\theta_s)\exp(-2\tau/\mu_v) \qquad \textbf{Equation 2.7}$$

According to Tanré *et al.* (1988) when d is large, $M^{*2}(\infty)$ and $M^2(\infty)$ reduce to the standard deviations $\sigma^{*2}$ and $\sigma^2$ of the observed and ground reflectances, and

$$\sigma^{*2}(d)=\sigma^2(d)\cdot T^2(\theta_s)\exp(-2\tau/\mu_v) \qquad \textbf{Equation 2.8}$$

For fixed observation geometry, Equation 2.8 can be rewritten as:

$$\ln[\sigma^{*2}(d)]=\ln[\sigma^2(d)]+\ln[T^2(\theta_s)\cdot\exp(-2\tau/\mu_v)] \qquad \textbf{Equation 2.9}$$

Calculations performed by Tanré *et al.* (1988) for analysing the behaviour of $T^2(\theta_s)\cdot\exp(-2\tau/\mu_v)$ versus τ, for the case of a background desert aerosol model above bright targets, showed that for a large range of τ, the following approximate equation holds:

$$\ln[\sigma^{*2}(d)]\approx\ln[\sigma^2(d)]-\alpha\cdot\tau \qquad \textbf{Equation 2.10}$$

where *a* depends on the observation geometry.

Let $\sigma_1^{*2}(d)$ and $\sigma_2^{*2}(d)$ the local standard deviations of two scenes obtained at times $t_1$ and $t_2$ under the same observation geometry, then Equation 2.9 and Equation 2.10 reduce to:

$$\ln[\sigma_2^*(d)]-\ln[\sigma_1^*(d)]=\ln[T_2(\theta_s)]-\ln[T_1(\theta_s)]-(\tau_1-\tau_2)/\mu_v) \qquad \textbf{Equation 2.11}$$

$$\ln\left[\sigma_2^*(d)\right] - \ln\left[\sigma_1^*(d)\right] \approx a' \cdot (\tau_1 - \tau_2) \qquad \textbf{Equation 2.12}$$

where $a' = a/2$ (9)

Where τ denotes the aerosol optical thickness since other atmospheric components remain constant between acquisitions and therefore their optical thickness difference is approximately zero.

If $T(\theta_s)$ is analytically derived via radiative transfer calculations, Equation 2.11 can be used to retrieve the AOT difference $\tau_1$-$\tau_2$. Alternatively, using a set of images from sites were the values of τ are measured regularly (e.g. AERO-NET sites), the parameter $a'$ can be retrieved on per-site basis and Equation 2.12 can be used subsequently for future retrievals. In both cases, if $\tau_2$ is chosen under low aerosol load then $\tau_2 \approx 0$ and thus $\tau_1$ is approximately the absolute AOT value.

For example, DTA algorithm, first tested by Sifakis *et al.* (1992) with a limited set of high resolution SPOT imagery, assumed that $T(\theta_s)$ does not change significantly for the two images considered and thus it is ignored in Equation 2.11. In this case, Equation 2.11 is equivalent to Equation 2.12 and $a'=1/\mu_v=1/\cos(\theta_v)$. This approach was further applied with good results but for limited datasets of Landsat-TM (Sifakis *et al.*, 1998), AVHRR (Retalis *et al.*, 2003), SPOT (Lin *et al.*, 2002) and MERIS (Retalis and Sifakis, 2010) images. Liu *et al.* (2002) have analytically derived $T(\theta_s)$ and applied Equation 2.11 over Taiwan with AVHRR data for five different days and a 13% average error.

In order to minimize the complexity of the procedure, in the scope of the work developd in this thesis, it was assumed that $a=1/\cos(\theta_v)$. As in the DTA approach described above, the dispersion coefficient $\sigma/\overline{\rho}$ (where $\overline{\rho}$ corresponds to mean reflectance) was used instead of the simple standard deviation), to better account for overall reflectance changes between reference and polluted images, leading to variations in standard deviation not necessarily related to contrast. Those variations might be related to residual cloudy pixels or to different pixel sampling from one image to another (e.g. different pixels are cloud masked in each image, leading to different ground apparent reflectance samples) which modifies the distribution of reflectance values. Other possible causes include calibration and registration errors. These might introduce bias in

standard deviation values, compromising its use as an effective measure of contrast. Although this approach is empirical and not directly derived from theory, the normalization procedure seems to attenuate this effect by bringing the standard deviation values to a common scale and therefore improve algorithm performance. This was verified independently in the work develop by Sifakis and Deschamps (1992) and Lin *et al.* (2002). In the current work the final form of the equation used for the retrievals is:

$$(\tau_1 - \tau_2) = \Delta\tau = \mu_v \cdot \left(\ln\left[\sigma_2^{*}(d)/\overline{\rho_2^{*}}\right] - \ln\left[\sigma_1^{*}(d)/\overline{\rho_1^{*}}\right]\right) \qquad \textbf{Equation 2.13}$$

### 2.2.3 Aerosol Remote sensing based PM ground concentration estimation

The study of aerosols or any other spatiotemporal patterns of atmospheric pollutants at urban or regional scales currently relies on extensive time series obtained from air quality monitoring networks or measurement campaigns. These entail high implementation and maintenance costs and are limited in terms of spatial coverage. Satellite information, characterized by its extentend spatial coverage and the possibility for real-time air-pollution monitoring, is being progressively introduced, especially in the last decade, to complement existing monitoring tools. The use of satellite products provides observations in previously unmonitored sites and a better knowledge of the spatial structure of air pollution and its relevant interactions on global, regional or local scales.

In the last ten years several methods to estimate surface PM concentration levels from aerosol related products have been published. The majority of these are focused on the estimation of $PM_{2.5}$ (and secondarily of $PM_{10}$) surface concentration values from satellite derived AOTs, which provide aerosol loading in the total atmospheric vertical column.

According to theory (Hoff and Sundar, 2009; Koelemeijer *et al.*, 2006; Rohen *et al.*, 2011), PM and AOT relation depends on particle size, their optical properties, vertical distribution and atmospheric conditions. Assuming a cloud free day, homogeneous vertical aerosol mixing and similar aerosol constituents that relation can be expressed as,

$$AOT = [PM] \cdot H \cdot f(RH) \cdot 3 \cdot Q_{ext,dry} / 4 \cdot \rho \cdot r_{eff} \qquad \textbf{Equation 2.14}$$

Source: Hoff and Sundar, 2009

where f(RH) is the ratio of ambient and dry extinction coefficients, ρ is the aerosol mass density (g/m), $Q_{ext,dry}$ is the Mie extinction efficiency (an average measure of the light extinction efficiency of the particles), and $r_{eff}$ is the particle effective radius, calculated from the particle size distribution (a possible theoretical distribution for the different aerosol size modes can be seen in Figure 2.1).

Most of the work developed to estimate PM concentrations from satellite AOTs derives from statistical/empirical models based on variations of this theoretical relation. These mainly consist of linear regression approaches, although some nonlinear and neural network based models have also been developed.

All of these methods have been applied to different sites of the world and are based on aerosol products from various sensors such as MODIS (Chu *et al.*, 2003; Engel-Cox *et al.*, 2004, 2006; Gupta *et al.*, 2006, 2009, 2009b; Koelemeijer *et al.* 2006; Wang *et al.*, 2003, 2010), MISR (Liu *et al.*, 2005; van Donkelaar *et al.*, 2006), MERIS (Retalis and Sifakis, 2010), SeaWiFS (Vidot *et al.* 2006), GOES-12 (Al-Saadi *et al.* 2008; Paciorek *et al.* 2008), Polder (Kacenelenbogen *et al.*, 2006) and also ground photometers (Pelettier *et al.*, 2007).

Hoff and Sundar (2009) did a very comprehensive review of those different AOT/PM correlation and estimation studies. They found a very wide range of regression parameters, with Pearson correlation coefficient (r) varying from low (<0.5) to high values (0.96), regression slopes from 120 to 18.7 and intercepts ranging from -42 to 15. The PM-AOD correlation has been found to vary as a function of the temporal averaging periods (hourly versus 24-hr), season, aerosol type, satellite AOD retrieval accuracy, meteorological conditions, presence of aerosol layers above the boundary layer, station type/location.

Work by Wang and Christopher (2003) and Engel-Cox *et al.* (2004) with MODIS Terra and Aqua AOT products showed a positive effect of time aggregating PM concentrations from hourly to 24h average. The first study covering a specific US County showed a significant effect of PM time averaging, with an increase in correlation from 0.7, for hourly measurements, to 0.98, for daily means. The second study compared results for several sites across the Continental US, during the period of April to September 2002. In this case only a small increase in PM/AOT correlation, from 0.4 to 0.43, was found for sites in-

fluenced by local pollution conditions. This improvement varied from site to site with an overall positive effect although a reduction in correlation was observed for some sites. Time averaging PM concentrations seemed to improve PM/AOT associations by reducing the inherent spatiotemporal representativity discrepancy between the 10 $km^2$ vertically integrated MODIS AOT and the point $PM_{10}$ measurements at ground level.

The 2004 Engel-Cox study included air quality stations across the entire continental US and emphasized differences in correlation due to site location. Those differences could sometimes be accounted to inaccuracies in AOT retrieval in sites with high reflective surface areas or cloud cover. Frequently these were linked to the influence of site specific emission pollution sources and aerosol types. In the referred study higher correlations with $PM_{2.5}$, between 0.4 and 0.6, were found in the northeast US and lower in the northwest, with values ranging from 0.2 to 0.4. The study advances several possibilities to explain these regional correlation disparities, including surface type influence and differences in horizontal and vertical AOT and PM footprint but ultimately found a closer association with aerosol type. According to the authors, the higher correlations are found in regions were the sulphate aerosol type model was used to derive AOT and the poorer correlations are associated with smoke and dust model. They attribute this to the fact that MODIS AOT product was originally designed for aerosol global scale studies and not to monitor urban/regional air pollution and recommend the development of a specific product for this purpose.

A study by Gupta *et al.*, 2006 comparing hourly and daily $PM_{2.5}$ and AOT for 26 cities in five countries also highlighted site differentiation based on the influence of distinct local, regional and even global emission sources. The lower correlations found in Switzerland (0.11) and Sidney (0.35) were attributed to smaller AOT ranges found in some sites, while the higher value for New York (0.6) confirmed the satellite's ability to discern local/regional air pollution. After the 24h average data was homogenised for all sites and binned into 5 $\mu g/m^3$ intervals, overall correlation increased to 0.96. This further emphasizes the importance of spatial and temporal averaging to overcome the natural limitations in PM/AOT comparisons.

The abovementioned paper also introduced a sensitivity study to quantify the effects of cloud cover, relative humidity (RH) and mixing layer height (MLH). As expected, a higher cloud cover fraction led to a decrease in PM/AOT correlation, with values ranging between 0.8 for a 25% cloud fraction and 0.5 for a 75%. This variation is caused by higher AOT retrieval inaccuracies so cloud screening is advised before comparing the two parameters. In the case of RH, high values (from 90% to 100%) originated a pronounced increase in AOT, reaching 25% for RH values from 98 to 99%. The increase was only 5% for RH values ranging from 50 to 80%. The hygroscopic aerosol growth with humidity, leading to a higher particle scattering efficiency is responsible for this increase in AOT (Chin *et al.*, 2002; Malm *et al.*, 2000). Since PM ground measurements are usually performed at dry conditions, the larger AOT values are not accompanied by a PM mass increase, weakening the PM/AOT correlation. Finally tests performed for several MLH classes showed higher correlations (0.8) for low mixing heights, between 100 and 200 m. As height increased, correlation decreased, reaching a minimum (0.36) for values between 800 and 1300 m. This confirms the PM dilution effect along the atmospheric column as MLH increases, causing PM concentrations at ground level to diverge from the vertically integrated AOT values and reducing the correlation.

Several other studies tried to assess or incorporate the influence of these two variables by: a) using Light Detection And Ranging sensor(LIDAR) information to give a more accurate representation of the vertical column and provide a correction factor for the overlying aerosol layer (Al-Saadi *et al.*, 2008; Engel-Cox *et al.*, 2006); b) deriving MLH and RH contributions from Equation 2.14 (Kacenelenbogen *et al.*, 2006; Liu *et al.*, 2005; Paciorek *et al.*, 2008); c) integrating vertical structure information from air quality related models (An *et al.*, 2007; Van Donkelaar *et al.*, 2006); d) introducing them, together with AOT and other relevant variables, in linear or nonlinear multivariate regression models or neural networks (Gupta and Sundar, 2009a, 2009b; Liu *et al.*, 2005).

In general, this approaches improved PM-AOT correlation, demonstrating the importance of considering RH and MLH, as well of other influencing meteorological variables, into satellite based PM estimation schemes. For instance, Paciorek *et al.* (2008) reported an increase in correlation from 0.5 to 0.75 by introducing RH, MLH and seasonality correction factors.

Gupta and Sundar (2009a) reported a 20 to 50% decrease in root-mean square error (RSME), when comparing a simple AOT/$PM_{2.5}$ univariate approach with a multivariate model including temperature (T) and MLH (r=0.68). Results also highlighted seasonal dependences with better estimates for fall and summer days with well mixed aerosol layers (MLH>2 km). The authors also stated that all stations presented a slope lower than one, indicating a systematic underestimation of higher $PM_{2.5}$ concentration values (>45 $\mu g/m^3$). They justified this behaviour with the possible influence of multiple layers of aerosols in the atmosphere or specific pollution events transported from different source regions, leading to a smaller correlation between PM/AOT. No information is provided about the regression coefficients of the meteorological variables to provide further insight on their influence.

The same authors developed a neural network (NN) with AOT, MLH, RH T, Latitude, Longitude, month and wind speed (WS) and input variables. The NN had a better performance than the multivariate model with an overall r of 0.74 for hourly values and 0.78 for daily. Spring and summer presented the best correlation coefficients for daily $PM_{2.5}$ (0.73 and 0.67, respectively). The correlation slope between measured and estimated $PM_{2.5}$ concentrations continues to be lower than one (from 0.28 to 0.54), showing, as in the previous study, a systematic underestimation of higher $PM_{2.5}$ values, especially for winter.

Liu *et al.* (2005) presented one of the few reviewed nonlinear models. It combined, in an exponential model, the MISR AOT product, $PM_{2.5}$ ground measurements from 346 EPA air quality stations in the eastern US, MLH and RH data from the GEOS-3 meteorological model and categorical variables for region, season, station type and distance to coast. All variables were found to be highly significant predictors and the overall model explained 43% of the $PM_{2.5}$ observed variance. AOT regression coefficient was positive and lower than one (0.44), which, according to the authors, indicated a sub linear relation with $PM_{2.5}$ concentrations. This relation was explained by the higher variability of the MISR AOT values, due to the influence of elevated aerosol layers not measured by surface monitors. RH and MLH presented negative exponent values, which is in accordance with the inverse relationship, described earlier, between $PM_{2.5}$ and each of these parameters. Seasonal differences were also significant, with lower AOT/$PM_{2.5}$ associations found during spring, possibly linked with

differences in the vertical aerosol distribution and emission sources. Distinct stations behaviours were attributed to the presence of distinct aerosol types with diverse scattering characteristics.

Seasonality is a recurrent analysis vector in all these studies and, although the results vary significantly, according to site location, main emission sources characterization or meteorological conditions, better results can usually be found in the summer season. This is probably due to smaller influence of cloud cover in summer and to lower AOT values in the remaining seasons, with higher associated uncertainties, especially in winter (Engel-Cox *et al.*, 2004; Gupta and Sundar 2009b).

As previously mentioned, fewer $PM_{10}$ estimation studies are available, when compared with $PM_{2.5}$ since the latter presents an higher scattering efficient and are, therefore, more correlated with satellite AOT values. Nevertheless some $PM_{10}$ estimation works stand out and are considered references in this field. Chu *et al.* (2003), one of the first AOT based air quality studies, demonstrated the potential of this methodology by extracting a strong $PM_{10}$/MODIS AOT linear correlation for a site in Northern Italy (r=0.82). The regression line presented a slope of 54.7 and a positive intercept of 8. The positive intercept is in agreement with the results for the majority of the previously described $PM_{2.5}$ studies, indicating a possible AOT insensitivity to low $PM_{10}/PM_{2.5}$ values.

The work developed for Xia *et al.* (2006), comparing $PM_{10}$ concentrations and ground based AOTs for the Beijing region, emphasized seasonal differences in their correlation. Summer and autumn presented the best correlations, with r values of 0.77 and 0.7, followed by winter, with 0.61 and spring with 0.37. Those results can be partially explained by distinct $PM_{10}$/AOT correlation behaviours, according to differences in seasonal RH and MLH conditions.

Koelemeijer *et al.* (2006) presented a work comparing hourly and daily AIRBASE $PM_{10}$ data for several station types (background, rural background and traffic) for several European stations and MODIS AOT values. Results demonstrated an improvement in linear correlation when correction factors for RH and MLH were applied to AOT. Correlation coefficient for all stations increased from a range of 0.32-0.39 to 0.34-0.54 for hourly values and from 0.21-0.35 to 0.39-0.44 for daily values. For all PM datasets the best correlations were

achieved for rural background stations, followed by background and traffic. Those results were foreseeable since background stations are not influenced by highly variable emission sources such as roads or industries and are therefore representative of wider areas, compatible with MODIS AOT 10 $km^2$ spatial resolution.

Wang *et al.* (2010) showed similar results with $PM_{10}$/AOT correlation improvements from 0.52 to 0.65, after correcting AOT values for MLH and RH and slopes varying, respectively, from 96 to 361 and similar positive intercepts (19-22). Barnaba *et al.* (2010) used LIDAR derived aerosol extinction profiles to correct AOT, extracted from several satellite and ground sensors, for MLH and improve correlation with $PM_{10}$. Dinoi *et al.* (2010) also showed an improvement in MODIS AOT/$PM_{10}$ correlation when AOT was split between the product of mixing layer height and wind speed. For a three year dataset of two sites in southeastern Italy, correlation increased from an interval between 0.34 and 0.57 (depending on the year and the station considered), before the correction, to 0.55-0.66 after. AOT regression coefficients varied from 65 in the first model to 32 in the second and both models showed a positive intercept ranging from 25 to 30.

Pelletier *et al.* (2007) and Vidot *et al.* (2007) developed similar $PM_{10}$ estimation additive linear models integrating AOT from AERONET and SeaWifs, respectively, with several meteorological variables (wind, humidity, pressure, precipitable water) and Julian day. In the first case the authors used a combination of the AOT logarithms for three bands (440, 670, and 870 nm) to better capture aerosol size distribution, while the second only used the 550nm AOT. In both cases initial $PM_{10}$/AOT direct correlations were very low. Nevertheless, after adding the meteorological variables, both final model fits showed a good agreement between measured and observed $PM_{10}$ concentrations. For the first study the final correlation coefficient was 0.87. When applied to a second validation site in Belgium, the value decreased to 0.7. In the second model the final correlation coefficient was lower (0.68) and the presented slope of 0.5 indicated a tendency for $PM_{10}$ underestimation, especially for higher concentrations.

Contrast reduction derived AOTs have been applied in $PM_{10}$ air quality studies for several sensors (Landsat, SPOT, AVHRR, MERIS and MODIS) but

only at a very small scale and a using a very limited number of images (10 to 20 data points) (Grosso *et al.*, 2006; Paronis and Sifakis, 2003; Retalis *et al.* 2003; Retalis and Sifakis, 2010; Sifakis and Deschamps, 1992). Nevertheless, some encouraging results have been found, with $PM_{10}$/AOT correlations coefficients ranging from 0.84 in AVHRR to 0.93 in MERIS and AOT distribution matching with $SO_2$ and smoke patterns

The results compiled in this section demonstrate the potential of satellite based PM estimation but also emphasize the wide heterogeneity of methodologies, algorithms, introduced variables and correlation influencing factors. They reflect the difficulty in relating satellite retrieved parameters with ground air pollutant concentrations and also clarify the relative immaturity of this recent research field, which still requires extensive work before it can contribute significatively to operational methodologies.

3

# Chapter 3 - Design, implementation and evaluation of a new contrast-reduction AOT retrieval algorithm developed for MODIS

## 3.1 Introduction

Aerosols are one of the most important atmospheric constituents with a significant influence in global climate change processes, through direct and indirect radiative forcing mechanisms (IPCC, 2007; Kaufman *et al.*, 2002; King *et al.*, 1999; Solomon *et al.*, 2007). According to several epidemiological studies, high suspended particulate matter concentrations are also responsible for an increase in respiratory and cardiovascular diseases and consequent morbidity and mortality rates in populated areas (Bell *et al.*, 2004; Krewski *et al.* 2000 Pope e Dockery, 1999; Scarrow, 1972; WHO, 2003;). Their suspension and transport potential was well as its relationship with $SO_2$ and $NO_2$ makes aerosols a good indicator of air pollution at urban and regional scales.

Current satellite aerosol retrieval products could be complemented by contrast reduction methods to overcome limitations in highly reflective or heterogeneous surfaces such as urban, desert or snow covered areas. Algorithms based on the contrast reduction principle, define contrast loss in an imageas an exponential function of the Aerosol Optical Thickness (AOT) difference between two images (a reference and a polluted) acquired under similar observation geometry conditions. The main objective of the work presented in this chapter is to develop and evaluate a new contrast reduction algorithm designed

for the MODIS sensor, based on the Differential Texture Analysis (DTA) approach, presented in section 2.2.2. It focuses on algorithm optimization by: a) determining an optimal AOT spatial resolution; b) constraining the relative observation geometry differences between polluted and reference image; c) assessing the influence of several land cover classes on the accuracy of the retrievals.

A comparison of the results obtained for 192 images acquired for the year 2005 with AOT data from five European AERONET (Aerosol Robotic Network) stations is performed to assess overall algorithm accuracy, as well as the impact of the proposed improvements.

Comparative analysis of the results for the various sites showed an optimal algorithm performance for MODIS images using a 39 pixel window, composed of only forest and urban pixels. Comparison with AERONET AOT data showed a good agreement with a correlation coefficient of 0.78. A similar correlation is found when comparing AERONET measurements and MODIS aerosol standard product.

This research supports the establishment of contrast reduction methods as a potential complement to other aerosol retrieval methodologies. Future work should aim at removing the residual aerosol influence from reference images, include BRDF's (Bidirectional Reflectance Distribution Function) to better reproduce surface heterogeneity and observation geometry influences and expand the scope of this study to other AERONET sites so as to further test the algorithm at a global scale.

## 3.2 Data and Methods

### 3.2.1 Ground and satellite data

To evaluate the AOT values retrieved using the contrast reduction algorithm and assess the impact of each proposed improvements, five AERONET stations were selected for this study. AERONET is a world optical ground based aerosol monitoring network consisting of identical automatic sun-sky scanning spectral radiometers owned by national agencies and universities (Dubovic *et al.*, 2002; Holben *et al.*, 1998). Approximately 450 instruments are registered in the network and provide globally distributed near real time obser-

vations of aerosol spectral optical thickness and aerosol size related parameters at several wavelengths. Work developed by Dubovik *et al.* (2000b) defined an AOT accuracy of approximately 0.01, for wavelengths higher than 440 nm, and a 5% uncertainty in measured sky radiances due to calibration errors. More information on accuracy assessments, quality control criteria and data limitations can be found in Holben et al (1998) and Dubovic *et al.* (2000a and 2000b).

Table 3.1 provides a brief description of each of the selected AERONET sites. These stations were chosen according to their land cover typology to provide a wider range of conditions to test the DTA algorithm. Barcelona and Paris can be characterized as more urban influenced sites, while Lisbon is a forest coastal area 50 km from the Portuguese capital city. Lille and Modena are transitional areas, mixing agricultural and urban land covers. All sites are mainly influenced by urban/industrial aerosols, although Lisbon and Barcelona also have a significant marine and North African dust contribution (Pandolfi *et al.*, 2011; Rodriguez *et al.* 2001; Santos *et al.*, 2007). Saharan dust may also be transported to the Modena region.

**Table 3.1 - Description of the AERONET stations used in this study**

| Site | Location | Site Description |
|---|---|---|
| Barcelona | Latitude:41.4° North<br>Longitude: 2.1° East<br>Elevation: 125 m | Located 5 km west of the city centre. The surrounding is mostly urban with a mountain range 2 km from the site location in the north-northeast quadrant. |
| Lille | Latitude: 50.6° North<br>Longitude: 3.1° East<br>Elevation: 60 m | Located at Villeneuve d'Ascq, southeast of the city of Lille, is on the fringe of the urban perimeter and is surrounded by agricultural lands. |
| Lisbon/ Cabo da Roca | Latitude: 38.8° North<br>Longitude: 9.5° West<br>Elevation: 140 m | Located at the most western point of the European continent, on the Atlantic coast of Portugal, a typical coastal area with shrub and forest surroundings, at 30 km North west of Lisbon. |
| Modena | Latitude: 44.6° North<br>Longitude: 10.9° East<br>Elevation: 56 m | Similar to Lille, this site is also located in the fringe of Modena's urban perimeter in a southeast suburb and is surrounded by agricultural areas mainly to the south. |
| Paris | Latitude: 48.9° North<br>Longitude: 2.3° East<br>Elevation: 50 m | Located in the city centre near the Seine's north bank is almost exclusively surrounded by urban areas. |

The AERONET data was collected using the web tool available in http://AERONET.gsfc.nasa.gov/. Only cloud-screened and quality-assured Level 2.0 measurements were included. The considered AOT field for validation referred to the 675 nm band since the contrast reduction algorithm was applied for band 1 (620–670 nm) MODIS Terra images. After a dataset analysis for all selected stations, the year 2005 was chosen for all subsequent data collection. The year of 2005 was chosen only to match temporally the work developed in the next result chapter.

Satellite imagery used to calculate the contrast reduction based AOT values is provided by the MODIS sensor, on-board of the Terra earth observation NASA satellite, launched in 1999. A similar sensor is also on-board the NASA satellite Aqua, launched in 2002, but the products used in this study refer only to the Terra MODIS sensor. Terra's sun synchronous polar orbit covers the entire Earth surface every one to two days and crosses the equator from north to south in the morning (10:30 am). The MODIS sensor acquires data in 36 spectral

bands, ranging from the visible to the thermal infrared spectra (440 nm to 14400 nm).. MODIS imagery spatial resolution varies according to the spectral bands: 250 m for bands 1 and 2; 500 m in bands 3 through 7; and 1000 in bands 8-36.

MODIS geolocated radiance fields from band 1 (620–670 nm) at 250 m spatial resolution (MOD02QKM) for the year 2005 were extracted from Level 1B HDF files. Other ancillary products included a cloud mask product (MOD35_L2), geolocation fields to characterize observation geometry (MOD03) and the MODIS standard aerosol product (MOD04_L2) for comparison purposes. Further information on each product content, methodology, accuracy assessment and limitations is given in the respective "Algorithm Technical Basis Document" (ATBD) or Product's User Guide documents (MOD02QKM: MODIS Level 1B Product User's Guide, 2006; MOD35_L2: Ackerman *et al.*, 2006; MOD04_L2: Remer *et al.*, 2006) and in the NASA's sensor website (http://modis.gsfc.nasa.gov).

**Table 3.2 - Description of MODIS main and auxiliary datasets**

| Product Name | Fields | Spatial Resolution (m) |
|---|---|---|
| MODIS Level 1B calibrated radiances (MOD02QKM) – Collection 5 (C005) | Earth View 250M Reflective Solar Bands Scaled Integers | 250 |
| Modis Cloud Mask (MOD35) | Cloud Mask<br>Quality Assurance | 1000 |
| Modis Geolocation Fields (MOD03) | Sensor Zenith<br>Solar Zenith<br>Sensor Azimuth<br>Solar Azimuth | 1000 |
| Modis Aerosol Product (MOD04_L2) | Aerosol Optical Thickness at 0.66 µm | 10000 |

All data pre-processing stages were performed using the HDF-EOS to GIS Format Conversion Tool (HEG) and included: 1) extraction of all MODIS data subsets for each AERONET site in UTM coordinate system; 2) application of the MODIS cloud mask product to remove cloudy pixels ; 3) construction of appropriate AERONET- MODIS (including both reflectance and MODIS AOT values) match up datasets according to the satellite's overpass time; 4) establish clusters of MODIS images based on viewing geometry similarity, according to predefined maximum differences between images for each solar and viewing angle

(further details are given in section 3.3.1). Images acquired with a time difference higher than 60 minutes of the closest AERONET measurement or under high cloud content, even after the cloud masking, were excluded.

The final MODIS dataset comprised 270 images (78 of those were used as reference, as described in section 3.2.2). Cloud cover was especially noticeable in the Lille and Paris sites where the number of available images is therefore smaller (24 and 39, respectively). The number of available images differs considerably from one site to the other (Barcelona, 97 images; Lille, 24; Lisbon, 63; Modena, 47; Paris, 39). Since this affects conclusions at a per site basis, results were analysed in aggregated form, even though some site specific information is provided throughout the following sections.

## 3.3 Methodology

All processing phases required to apply the contrast reduction algorithm based on the DTA approach, are presented in Figure 3.1.

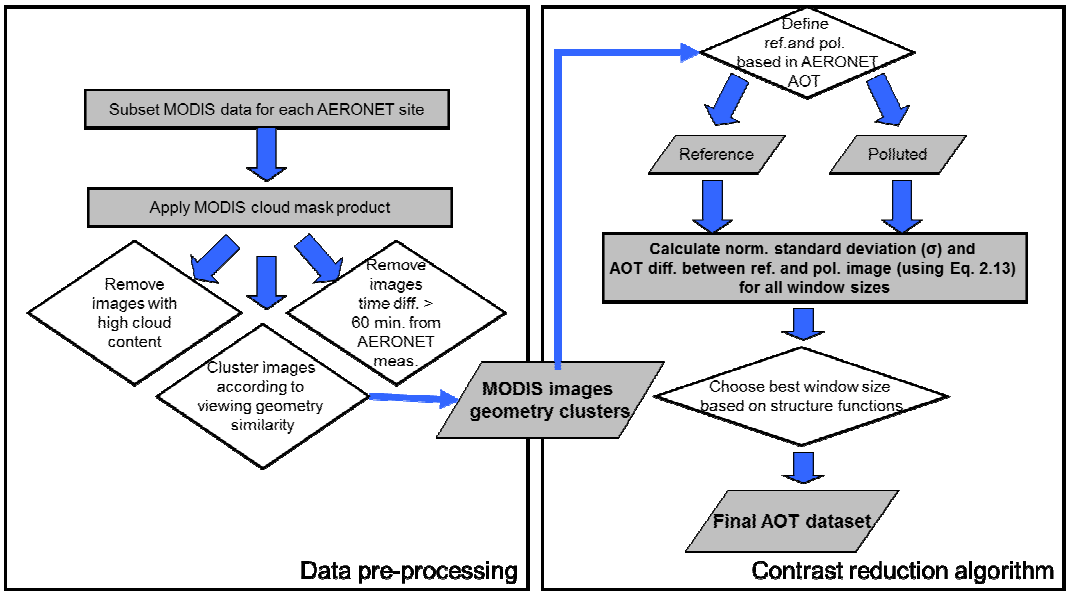


**Figure 3.1 – Contrast reduction algorithm processing steps**

They include all the pre-processing stages already described in the previous section (left side of Figure 3.1) and the AOT calculation steps (right side of Figure 3.1), according to the previously defined equation (section 2.2.2):

$$(\tau_1 - \tau_2) = \Delta\tau = \mu_v \cdot \left(\ln\left[\sigma_2^*(d)/\overline{\rho_2^*}\right] - \ln\left[\sigma_1^*(d)/\overline{\rho_1^*}\right]\right) \qquad \textbf{Equation 3.1}$$

Where $\tau_1$, $\tau_2$ are the aerosol optical thickness and $\sigma_1/\rho_1$, $\sigma_2/\rho_2$ are the normalized standard deviation for the polluted and reference images, respectively. It should be considered that, although ideally $\tau_2$ is $\approx 0$, some residual aerosol load is usually present and so the retrieve AOT value will not be an absolute value, but the relative difference between the two images (as shown in the equation).

The normalized standard deviation, calculated for both images, is the measure of contrast between the adjacent pixels centred at the location of the AERONET site. The number of adjacent pixels is determined by a window, also centred at site coordinates, with a specific radius size, defined by pixel distance to the centre (Figure 3.2). In this study, both normalized standard deviation and respective AOT will be calculated for several window sizes, ranging from 1 to 39 pixel distance, in order to assess the best window size for applying the contrast reduction algorithm. Further details are given in sections 3.3.2 and 3.4.1.

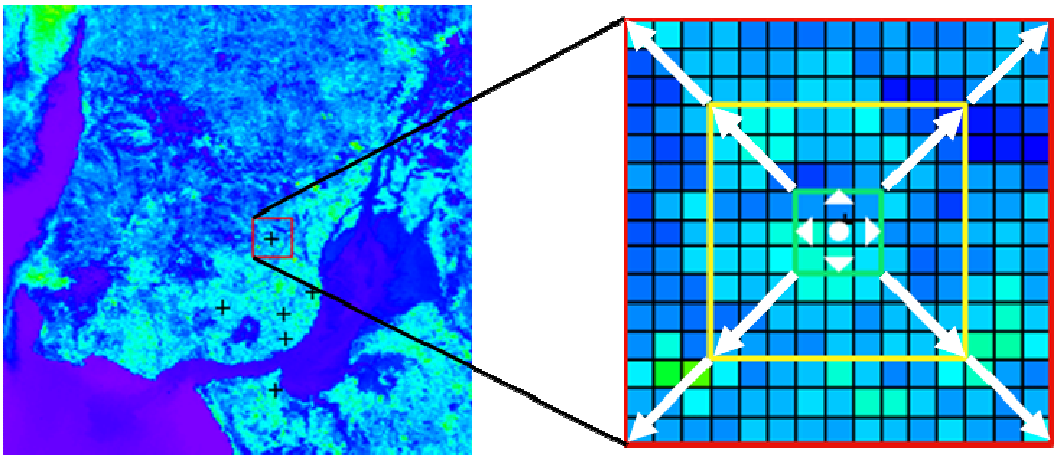

**Figure 3.2 – Definition of the pixel window used for DTA AOT calculations.**

### 3.3.1 Selection of observation geometry clusters

MODIS can acquire images from the same target at different observation geometries which presents a problem since algorithm accuracy is highly dependent on the geometry similarity between reference and polluted images. The basic assumption of the DTA algorithm is that the different image acquisitions are made under identical observation geometries (i.e. solar zenith angle, sensor zenith angle and sun-sensor relative azimuth), minimizing the effects related to the anisotropic reflectance of the underlying surface.

For this reason, the observation geometries of the available dataset were classified into distinct clusters by combining the following criteria:

- Two separate clusters for $|\varphi_v - \varphi_s| > 90º$ and $|\varphi_v - \varphi_s| < 90º$ geometries, where $\varphi_v$ and $\varphi_s$ represents the sensor and solar azimuth respectively;
- Sensor zenith angle groups from $0^o$ to $90^o$ with a $15^o$ interval;
- Solar zenith angle groups from $0^o$ to $90^o$ with a $20^o$ interval;

The first criterion was selected to process separately acquired images in the forward and backscattering direction. The second and third criteria defined above were chosen to concurrently constrain sensor and solar zenith angle differences and maximize the number of available images per cluster.

Subsequently reference image for each cluster was selected based on AERONET AOT values, corresponding to a minimum aerosol load.Table 3.3 provides an overview of total and per site number of reference images, their AOT range and the respective mean. In total, 78 images were chosen as reference with AERONET AOT values ranging from 0.179 to 0.007 and a mean of 0.061. As expected, Lisbon presented the lowest reference AOT mean value (0.026), characteristic of a typical forest site, with almost no urban influence and therefore a smaller anthropogenic aerosol contribution. All other sites present a wider reference AOT range and a higher mean value. For Barcelona, Lille and Modena the values are very similar (0.051, 0.077 and 0.072, respectively) whereas Paris, an urban site, presents the highest mean reference AOT (0.106).

**Table 3.3 - Total number of reference images and corresponding range and mean AERONET AOT (675 nm) per site and for all sites**

| Site | Num. of Ref. images | Max. AERONET AOT | Min. AERONET AOT | Mean AERONET AOT |
|---|---|---|---|---|
| Barcelona | 25 | 0.119 | 0.016 | 0.051 |
| Lille | 8 | 0.140 | 0.035 | 0.077 |
| Lisbon | 18 | 0.066 | 0.007 | 0.026 |
| Modena | 13 | 0.162 | 0.025 | 0.072 |
| Paris | 14 | 0.179 | 0.064 | 0.106 |
| All | 78 | 0.179 | 0.007 | 0.061 |

### 3.3.2 Selection of the DTA optimal window size and spatial resolution

Optimal window size selection should consider an area large enough to hold sufficient surface texture but sufficiently small to assume a homogeneous

atmospheric composition so as to minimize errors (Tanré *et al.*, 1988; Retalis and Sifakis, 2010). The subjectivity in choosing an optimal window size and its influence on the quality of the results is evident in previous works, where errors ranging from 0.15 to 0.3 in AOT retrieval are reported due to an inadequate choice (Lin *et al.*, 2002; Paronis and Sifakis, 2003). The current work proposes the combined use of two distinct window selection methods to establish a DTA optimal window size range.

In the first method window choice is made based on interpretation of the structure function. The structure function shows the variation of apparent reflectance differences between adjacent pixels (given by the normalised standard deviation) as a function of window size. It provides information on the surface structure and atmospheric composition. In a typical structure function, the initial normalised standard deviation values will exhibit an irregular behaviour due to a higher sensitivity to ground structure changes, after which the values will tend to increase with window size, following a more regular pattern, until they stabilize when all ground structure is incorporated. This inflection point provides a more consistent measure of surface heterogeneity and is used, in this first method, to select the optimal window size.

The second method is based on the assumption of the aerosol layer homogeneity. Considering that the local variance of the AOT in general depends on the size of the spatial window adopted, the method retrieves the AOT over a site for various window sizes consecutively. For each window size, AOT is retrieved for one pixel and its 8 neighbours, by moving the centre of the DTA window one pixel at a time. The optimal window size corresponds to the minimum AOT local variance (Paronis and Sifakis 2003). The results given by this second method are closely related to the first, since constant normalized standard deviation values will more likely provide less variable AOT retrievals, but will tend to be more conservative.

After applying the DTA algorithm to several window sizes, two mean curves were calculated per site (e.g. Figure 3.3 and Figure 3.4 in page 95), using all images, one for the normalised standard deviation of the reflectance and a second for the AOT local variance, and plotted as a function of window size.

These two curves were used to select, per site, an optimal window for each method.

### 3.3.3 Site land cover influence in algorithm accuracy

A decrease in algorithm performance is expected from more urban influenced datasets to the more vegetation dominated ones since the latter are subject to more significant surface reflectance changes. For example, man-managed vegetated land uses, such as agricultural areas, present the highest temporal variability in terms of texture, due to annual crop cycles, when compared to forest and especially urban pixels. Therefore, in order to perceive differences in the algorithm accuracy due to land cover changes between the reference and polluted images, the algorithm was applied to the following four distinct pixel groups, according to the CORINE 2000 product classification (Bossard *et al.*, 2000): (a) vegetation pixels (agriculture and forest); (b) vegetation and urban pixels; (c) forest and urban pixels; (d) urban pixels. The order in which the four groups are presented corresponds to a gradual decrease in the influence of vegetated pixels and consequently to an expected increase in texture temporal stability. The study focused on a comparative correlation analysis of the algorithm for the four datasets previously defined, based on r, NRMSE (defined as RMSE normalised by the mean of the observed values) and average pixel percentage. NRMSE was considered more appropriate since it provided a comparable error measure for sites with different AOT levels. The results are presented combined for all stations per site and also dividing the stations in two groups, according to dominant land cover typology: urban (Barcelona and Paris) and transitional for mixed vegetated/urban stations (Lille and Modena).

## 3.4 Results and Discussion

### 3.4.1 Selection of the DTA optimal window size and spatial resolution

Individual images and mean structure functions, presented for all sites in Figure 3.3, exhibit a similar behaviour: a higher and more irregular increase rate of normalized standard deviation values for smaller window sizes, which is progressively reduced until it stabilizes. Although similar, the inflection point location differs significantly from site to site, ranging from a window size of 15

pixel distance in Modena to a 30 pixel distance in Lisbon. The selection entails some subjectivity, especially in the cases of Lille and Paris. In the first case, the mean structure function shows a stable behaviour for window sizes starting from a 10 pixel distance. Nevertheless, the individual structure functions still indicate some variability, which only decreases after the chosen 18 pixel distance window. As for Paris, a first stable range of values is observed between the 10 and 15 pixel distances. However, the standard deviation differences between the individual structures functions are not as marked or stable as the second range, starting at the chosen 28 pixel window size, indicating a possible higher AOT retrieval accuracy.

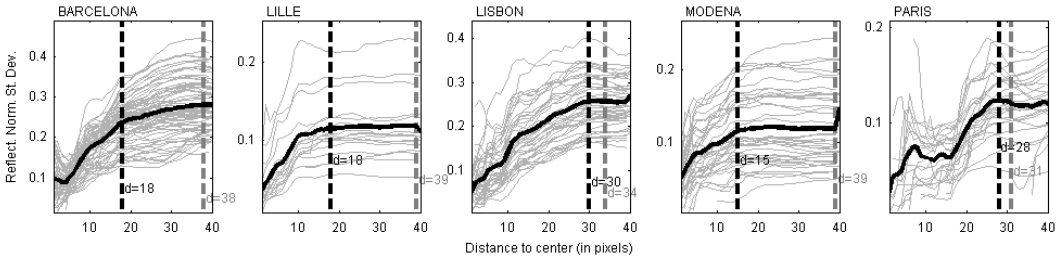


**Figure 3.3 - Structure function for all sites: variation of the standard deviation of the pixel reflectance for each window size. The chosen distance is given by the black dashed line, whereas the grey line represents the window size selected using the alternative method. The mean structure function is represented by the thicker black line.**

Figure 3.4 shows the standard deviation of the DTA AOT (a measure of AOT local variance) calculated for nine pixels (station location and its 8 neighbours) as a function of the window size. The AOT standard deviation decreases sharply until reaching a window size after which those values are almost invariable. The chosen window size, according to the minimum AOT standard deviation criterion (marked by black vertical lines), usually corresponds to window sizes higher than a 30 pixel distance.

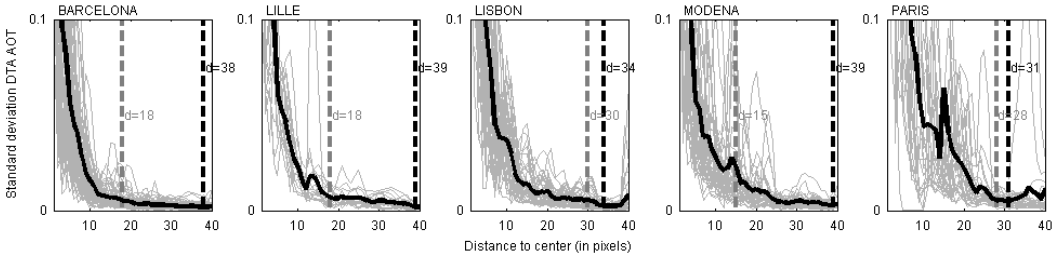


**Figure 3.4 - Standard deviation of AOT estimates for the station location and its neighbour pixels as a function of window size. The chosen distance is given by the black dashed line where as the grey line represents the window size selected using the alternative method. The mean AOT standard deviation curve is represented by the thicker black line.**

The optimal window sizes given by the first method under examination are smaller and present a larger inter-site variability, when compared with the second method. In fact, the structure function analysis seems to be more sensitive to site characteristics, providing a more specific solution, while establishing a minimum AOT standard deviation criterion offers a more general solution, closer to an optimal common window size.

In Figure 3.4 a significant overall decrease in AOT variability is observed after reaching the optimal window retrieved by the first method, which is maintained over the subsequent sizes until reaching its minimum value. The window sizes given by the two methods defines the lower and upper limits of an interval where image contrast is high, almost constant and AOT standard deviation is minimal, providing the ideal conditions for AOT estimation.

Figure 3.5 depicts r and NRMSE values for the correlation between AOT DTA estimates and AERONET measurements as a function of window size, shown in Figure 3.5. For most sites the selected window sizes for the two methods are within the interval where higher correlation coefficients and lower normalized root mean square error (NRMSE) lower are found (area delimited by the two grey vertical solid lines in the figures below). The exception is Lille where the window size identified by the first method is outside of this interval. In this case the effectiveness of the first method might be affected by the limited sample size (16 images).

Furthermore, r and NRMSE analysis show that an unsuitable window size might lead to a significant increase in error usually associated with smaller windows sizes. The error range differs significantly from site to site, with

NRMSE values in Paris ranging from 30 to almost 1, while in Modena the values only vary from around 3 to 1. Results demonstrate an improvement in DTA performance for windows starting from a 20 to 25 pixel distance, depending on the site, with the exception of Barcelona, where the algorithm shows consistent results around a 15 pixel distance. A similar performance is achieved when a common window size solution for all sites is tested (last graph of Figure 3.5). In this case the optimal range starts at a 20 pixel distance window and is maintained, with almost constant r and NRMSE values, until reaching the best results for the 39 pixel distance window. This also confirms the interpretation given above regarding the greater proximity of the window sizes provided by the second method to a more general solution.

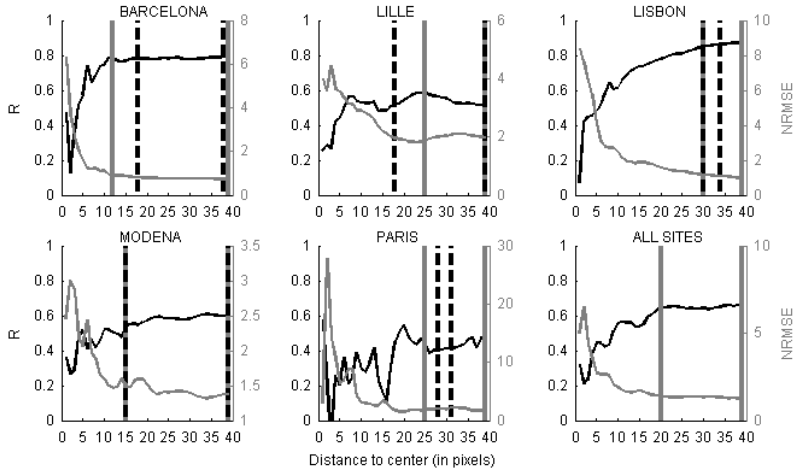


**Figure 3.5 - Variation of the NRMSE and R with window size: for each site (identified in the title of each subplot) and considering all sites together (last graph). Black dashed lines define the window size interval given by the two methods and grey solid lines the two methods and grey solid lines the interval of optimal NRMSE and R values.**

Finally, three sets of results were compared considering all sites together: 1) and 2) a site specific window size according to the assessment given by the first and second methods;3) a 39 pixel distance common window size. The main calculated correlation parameters for the three sets are summarized in the table below. All of them demonstrate a good adjustment between measured and estimated AOT values with a slight tendency for overestimation (average error is positive for all sets and the correlation slope is higher than one). The two methods present similar performances to the observed for a common window size of 78 by 78 pixels (corresponding to the 39 pixel distance) which confirms their

suitability to determine the most appropriate window size per site when using the DTA algorithm.

**Table 3.4 - Correlation parameters for three sets of results: site specific window size according to the assessment given by the first (1) and second (2) methods, respectively; a 39 pixel distance common window size (3)**

| Method | Slope | Y Origin | r | Average Error | RMSE | NRMSE | N |
|---|---|---|---|---|---|---|---|
| 1 | 1.17 | 0.01 | 0.74 | 0.01 | 0.09 | 1.09 | 191 |
| 2 | 1.16 | 0.00 | 0.74 | 0.02 | 0.09 | 1.10 | 192 |
| 3 | 1.15 | 0.00 | 0.78 | 0.01 | 0.09 | 0.99 | 192 |

For the subsequent sections, the 39 pixel distance common window was adopted. The choice of a common window size better suits the purpose of this paper, an evaluation of the DTA algorithm for several sites, since it provides the best fit between measurements and estimates. Such approach also embeds the advantage of establishing more easily comparable AOT estimates by minimizing the influence of pixel sample size variability between locations as a possible source of inter-site error differentiation.

### 3.4.2 Site Land Cover influence in algorithm accuracy

An overall comparative correlation analysis, as well as per site and site group (Transitional/Urban), is presented in Table 3.5 for four datasets.

**Table 3.5 - r, NRMSE, average pixel percentage relative to the number of pixels inside the 39 pixel distance window and number of estimated values (N) for all sites, per site group (Urban – Barcelona, Paris; Transitional – Lille and Modena) and per site for the for the four constructed datasets which included: a) vegetation pixels (agriculture and forest); b) vegetation and urban pixels; c) forest and urban pixels; d) urban pixels.**

| | Land Cover | All | Urban | Transit. | Barcelona | Lille | Lisbon | Modena | Paris |
|---|---|---|---|---|---|---|---|---|---|
| r | a) | 0.70 | 0.64 | 0.70 | 0.75 | 0.50 | 0.88 | 0.71 | 0.51 |
| | b) | 0.77 | 0.77 | 0.74 | 0.80 | 0.60 | 0.88 | 0.76 | 0.72 |
| | c) | 0.78 | 0.77 | 0.75 | 0.80 | 0.43 | 0.88 | 0.80 | 0.72 |
| | d) | 0.71 | 0.74 | 0.75 | 0.80 | 0.51 | 0.68 | 0.77 | 0.72 |
| NRMSE | a) | 1.31 | 1.28 | 1.42 | 0.88 | 2.43 | 0.90 | 1.19 | 2.26 |
| | b) | 1.00 | 0.84 | 1.14 | 0.72 | 1,86 | 0.93 | 0.98 | 1.22 |
| | c) | 0.88 | 0.86 | 0.81 | 0.74 | 1.53 | 1.03 | 0.64 | 1.22 |
| | d) | 0.98 | 0.80 | 0.81 | 0.64 | 1.32 | 1.62 | 0.70 | 1.25 |
| Pixel % | a) | 29.98 | 14.76 | 64.76 | 19.53 | 44.74 | 23.78 | 74.18 | 0.46 |
| | b) | 55.50 | 49.89 | 89.78 | 44.93 | 95.94 | 29.49 | 86.89 | 64.16 |
| | c) | 33.16 | 44.30 | 23.58 | 37.54 | 46.92 | 19. 78 | 12.61 | 63.77 |
| | d) | 23.60 | 33.68 | 22.06 | 23.39 | 44.08 | 3.55 | 11.70 | 63.32 |
| N | | 192 | 97 | 50 | 72 | 16 | 45 | 34 | 25 |

A tendency in improvement of DTA performance is observed in Table 3.5, as vegetation influence is reduced. With the exception of Lisbon, a strongly vegetated site, all other columns show a decrease in NRMSE from dataset (a) to (b). When agriculture related pixels are also removed (dataset (c)), results considering all sites together continue to improve mainly based on the NRMSE decrease for transitional sites. The algorithm performance for the last dataset where only urban pixels are considered is compromised by the poor performance for the Lisbon forest site, with an average urban pixel percentage of 3.55%. Such low pixel count affects the reliability of the algorithm and justifies the increase of NRMSE from 1.03 to 1.62 when comparing datasets (c) and (d). Although not presented in Table 3.5, removing Lisbon from the analysis improved significantly the performance of the algorithm for dataset (d), considering all other four sites, with an increase of r to 0.75 and a decrease of NRMSE to 0.81, confirming a progressively lower downward tendency going from dataset (a) to (d).

The improvement is more evident for transitional sites where the NRMSE decreases steadily across the first three datasets from 1.41 in dataset (a) to 0.81 for dataset (c) and (d). Urban sites show a more consistent behaviour with similar error levels for the last three datasets. Even the poor results observed using dataset (a) are partially explained by a very low presence of vegetated pixels in the Paris station, leading to higher error levels. Nevertheless, NRMSE values for urban and transitional sites are very similar for the last two datasets (although per site analysis shows differences for each site) which can be interpreted as sign of algorithm robustness even when applied to for areas where urban influence is less visible. Nevertheless a minimum valid pixel sample size must be observed to guarantee consistent results.

These results confirm the impact of possible surface reflectance changes in DTA performance, especially in managed land covers, such as agricultural areas, where spatial changes are more abrupt and extensive. In forest areas the impact might be less significant depending on the forest type, as confirmed by the good results obtained for Lisbon. Another feature highlighted in Table 3.5 is the apparent robustness in algorithmic performance with small valid pixel samples. Average pixel percentages of 12% still provided good quality results, as demonstrated in the case of datasets (c) and (d) for Modena. This aspect might

constitute a valuable asset when dealing with cloud cover contamination. Nevertheless in some cases the pixel count was too low (datasets (a)) for Paris and (d) for Lisbon), causing a considerable DTA result degradation. These results seem to indicate that implementing a minimum pixel count threshold will improve algorithm reliability, since lower valid pixel percentages are prone to worst window representativeness. Such approach can be important for the establishment of *a priori* confidence in AOT estimates (e.g. quality control flags). The site-to-site variability of these results depends on the different contributions of vegetated versus urban areas locally. Ultimately, these observations suggest that an overall a priory assessment of algorithmic robustness should mandatorily include information on the land cover mixtures locally. Further developments should integrate additional AERONET sites with different urban and vegetation contributions in order to assess the sensitivity of the algorithm to these two factors.

Taking into consideration this analysis and to minimize land cover influence while maximizing the number of available pixels, the results shown in the next section refer to dataset (c). The overall correlation and error analysis between the AERONET measurements and the DTA estimates, for a 39-by-39 pixel distance window size dataset (c), is presented in Figure 3.6 and Table 3.6. The negative AOT values observed in Figure 3.6 occur when the reference image chosen for each geometry class, based on the AERONET values, presents a lower contrast than the polluted. These values have no physical meaning but are included in this study to provide a more comprehensive analysis of the error associated to the DTA algorithm.

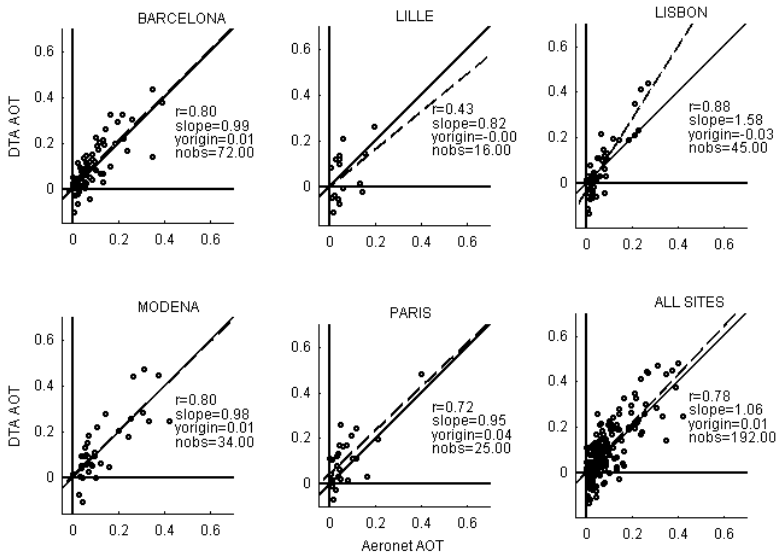


**Figure 3.6 – Scatter pot between AERONET measurements and DTA algorithm estimates for dataset c) considering all sites and a 39-by39 window size. Calculated parameters are: r – correlation coefficient; slope – correlation slope; yorigin – correlation origin in the Y-axis; nobs – number of observations.**

The correlation coefficient shows a good agreement with observations when considering all stations (r=0.78). The regression line depicted in Figure 3.6 (all sites) with a slope higher than 1 (1.06) and a small positive offset (0.01) seem to indicate a slight tendency for AOT overestimation. This is confirmed by comparing the mean estimated (0.10) and observed AOT (0.08) values given in Table 3.6. Nevertheless the error measures are high (NRMSE=0.88 and RMSE=0.08). This might be related to a high frequency of negative retrieved AOT values and low AERONET AOT in the original dataset. The relative errors for these points are generally very high and have significant negative impact on the RMSE and NRMSE values. Imposing two separate constraints (retrieved AOT values > 0 and AERONET AOT values > 0.05) a significant improvement is observed in error analysis (see values in parentheses in Table 3.6) with overall NMRSE dropping from 0.88 to 0.58. These might reflect the inability of the algorithm to extract very low AOT values. A site error analysis shows that, for both sets of results, the algorithm seems to perform better for the Barcelona and Modena stations, with a NRMSE of 0.74 (0.55) and 0.64 (0.52), respectively, contrasting with the results for Lille and Paris, where the NRSME is 1.53 (0.76) and

1.22 (0.62), Although these could lead to the conclusion that the algorithm is not efficient over these sites, their limited datasets (many images were rejected due to high cloud cover values), comprised of low AOT values do not allow any statistically robust conclusions.

**Table 3.6 - Number of polluted images (N), RMSE, NRMSE, mean AERONET AOT and mean DTA AOT per site and for all sites considering all values and imposing two separate constraints (retrieved AOT values > 0 and AERONET AOT values > 0.05, bracketed values)**

| Site | N | RMSE | NRMSE | Mean Obs. AOT | Mean Retrieved AOT |
|---|---|---|---|---|---|
| Barcelona | 72 (40) | 0.06 (0.07) | 0.74 (0.55) | 0.08 (0.13) | 0.10 (0.15) |
| Lille | 16 (4) | 0.10 (0.10) | 1.53 (0.76) | 0.06 (0.13) | 0.05 (0.15) |
| Lisbon | 45 (20) | 0.07 (0.08) | 1.03 (0.65) | 0.07 (0.12) | 0.07 (0.17) |
| Modena | 34 (24) | 0.08 (0.09) | 0.64 (0.52) | 0.13 (0.16) | 0.14 (0.18) |
| Paris | 25 (10) | 0.09 (0.09) | 1.22 (0.62) | 0.07 (0.14) | 0.11 (0.17) |
| All | 192 (98) | 0.08 (0.08) | 0.88 (0.58) | 0.08 (0.14) | 0.10 (0.17) |

Figure 3.7 shows a comparison of the DTA and AERONET AOT time series for the Barcelona station, confirming a good agreement between the two datasets. Nevertheless, the results given between July and December seem to indicate a relative loss in algorithm accuracy. A baseline of AERONET values for the corresponding reference images is provided (black asterisk markers) to emphasize the variability of reference conditions.

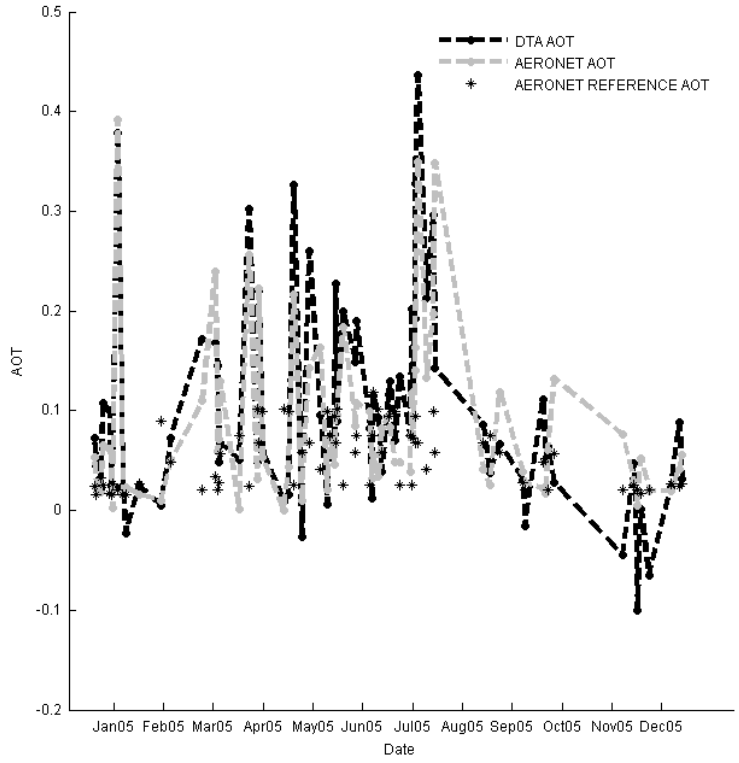


**Figure 3.7 - Time series plot of AERONET AOT (black dashed line) and DTA AOT (grey dashed line) for the Barcelona station. Reference AOT value for each polluted image is also given (black asterisk markers).**

Figure 3.8 shows a box plot of the absolute error as a function of the time difference in days between the polluted and reference images. This plot was derived by grouping the time differences in 60 day intervals. A small cyclical pattern is observed as error reaches the maximum for the 120-180 day cluster, and then decreases in the subsequent clusters to initial error levels. Such pattern can be attributed to seasonal reflectance changes, implying some residual influence from the image vegetation content.

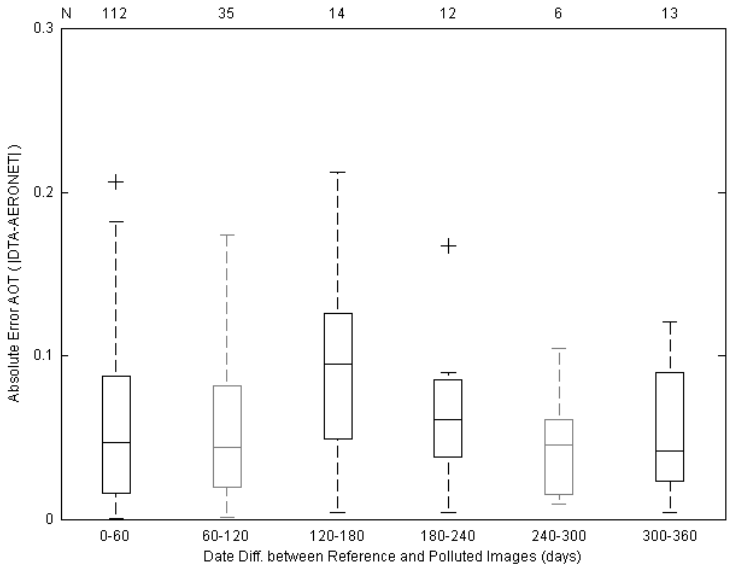


**Figure 3.8 - Absolute Error Box plot as a function of 60 days clusters of the date difference between the polluted and reference images.**

Finally, Figure 3.9 shows the scatter plots of DTA and MODIS aerosol standard product AOT against the respective AERONET values for all overlapping acquisition dates with valid values for both products. In order for the two AOT datasets to be comparable, AOT values from the reference days were also subtracted from the polluted images for the MODIS standard product. The overall performance of the two products is very similar with identical r (0.75) and a slightly smaller NRMSE value for the contrast based results (0.90 for DTA and 0.97 for MODIS). The most significant difference is related to the number of valid points. The MODIS standard product only presented 76 valid AOT values for the same acquisition dates, with Barcelona and Lisbon only with two and ten images. For this reason, further comparisons between the two products considering, for instance, different site groups, according to their main land use typology (urban/transitional), could not be performed.

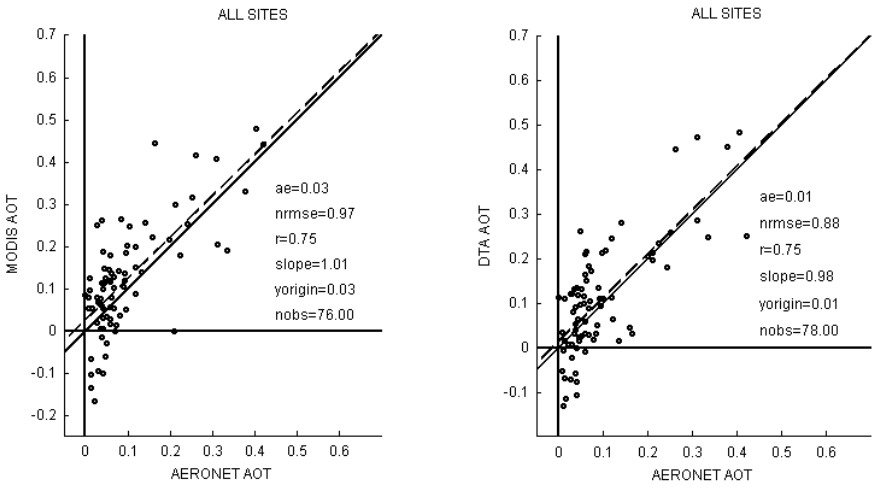


**Figure 3.9 – Scatter plot between AERONET measurements and: DTA algorithm results (left graph); MODIS aerosol standard product AOT (right graph). Calculated parameters are: ae – average error; nrmse – normalised root mean square error; r – correlation coefficient; slope – correlation slope; yorigin – correlation origin in the Y-axis; nobs – number of observations.**

### 3.4.3 Observation geometry

As referred in Equation 2.12, DTA AOT retrieval is dependent on coefficient *a*, where, $a=1/\cos(\theta_v)$. Omitting this term introduces a significant increase in the error (NRMSE increases from 0.88 to 1.53) especially for angles higher than $30^o$, as observed in Figure 3.10.

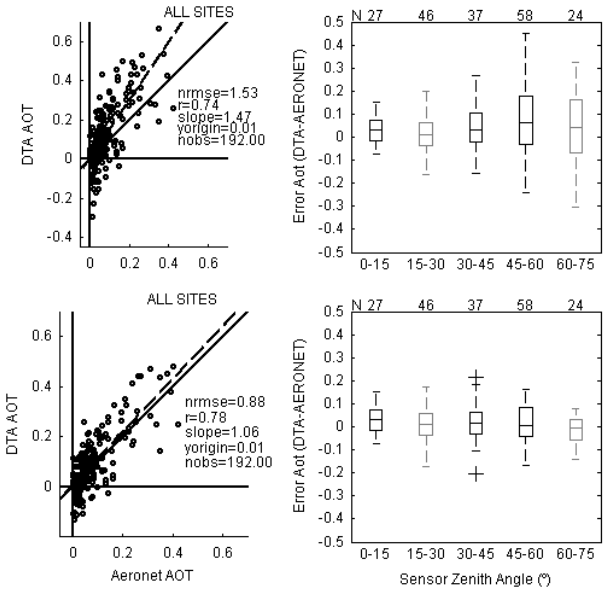


**Figure 3.10 - Correlation between DTA and AERONET AOT values and respective error plots as a function of the defined sensor zenith angle clusters before (top row) and after (bottom row) applying the cosine of sensor zenith angle term.**

To further explore the performance of DTA as a function of observation geometry to the remaining viewing and solar angles, one must consider that these can influence the algorithm at two different levels: 1) absolute angles (Figure 3.11, left) ; and 2) angle difference between reference and polluted images (Figure 3.11, right).

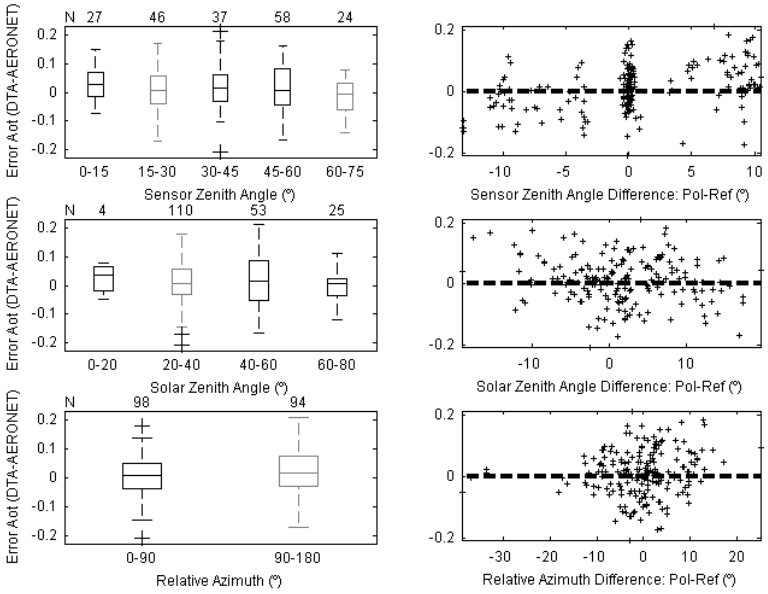


**Figure 3.11 - DTA AOT error plots according to the different sensor zenith, solar zenith and relative azimuth absolute angles clusters (left column) and angle differences (polluted minus reference, right column)**

Only a weak statistical association can be established between DTA AOT errors and relative observation geometries (Figure 3.11, right). However, a tendency for AOT underestimation is observed when the polluted image sensor zenith angle exceeds the reference image sensor zenith angle by more than 3º. AOT overestimation is observed when this relation is inverted (sensor zenith angle difference < -3º; Figure 3.11, top right). In fact, performing an one-way ANOVA (Hogg and Ledolter, 1987) followed by a multiple comparison test, considering three groups, one with zenith angle differences lower than -3º, a second with differences higher than 3º and a third for angle differences within those two values, showed that, although only 17% of the total error variance is explained by this factor, the differences between these groups means are statistically significant. Furthermore, as shown in Figure 3.12, when all images with an absolute zenith angle difference higher than 3º were removed, r increased to 0.83 and NRMSE decreased to 0.7. Therefore a further constraint of sensor zenith angle differences when applying the DTA algorithm is advisable. Nevertheless it should be noted that adding this constraint generally reduces significantly the sample size (in this case to 87 images). Results are encouraging in terms of algorithm applicability since they imply that, if this basic assumption of the

DTA is fulfilled, the error is greatly minimized approaching levels compatible with those observed for other algorithms.

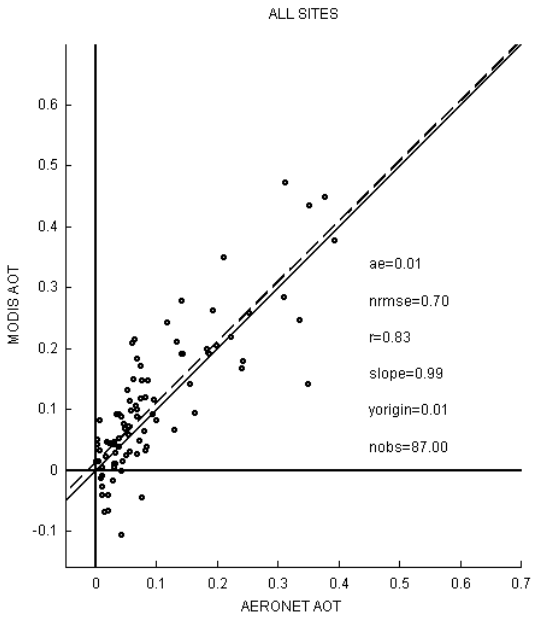


**Figure 3.12 – Scatter plot between AERONET measurements and DTA algorithm estimates for sensor zenith angle differences lower than 3º. Calculated parameters are: ae – average error; nrmse – normalised root mean square error; r – correlation coefficient; slope – correlation slope; yorigin – correlation origin in the Y-axis; nobs – number of observations.**

## 3.5 Conclusions

The comparison of a one year dataset of DTA algorithm MODIS AOT estimates with *in situ* AERONET data for five different European stations expands on previous studies: 1) by first applying a contrast reduction based algorithm to an extended set of MODIS imagery; as well as 2) by allowing a more systematic analysis of the algorithm's accuracy and robustness to less-optimal conditions.

The current research introduced a modified version of the DTA algorithm. It focused on optimization for three important factors: a) window size and spatial resolution; b) pixel land cover influence; c) ability to cope with different observation geometries.

The following sections present the main conclusions for each of those improvements, following the same structure as in the result section.

### 3.5.1 Selection of the DTA optimal window size and spatial resolution

The study allowed the definition of two separate methodologies to define optimal site spatial resolution. The first method is based on the interpretation of the structure function, given by the variation of the normalized standard deviation across the several window sizes. It provided smaller and more site specific window sizes, varying between 15-by-15 and 30-by-30 pixels. The second method relied on the minimization of the variability of AOT estimates, calculated for all pixels adjacent to the site location, as presented by Paronis and Sifakis (2003). This method established wider window sizes, usually higher than 30-by-30 pixels, and closer to a common window size solution. For the subsequent studies, developed in the scope of the thesis, preference was given to a common 39-by-39 window size for all sites, nearer to the common window size approach given by the second method.

Work developed by Retalis and Sifakis (2010) with MERIS images for the Athens region, of similar spatial resolution (300 m), provided a smaller window size of 13-by-13 pixels. This discrepancy might be partially explained to differences between the two sensors but it is mostly related to the reduced scope of the MERIS study. The authors only used five summer images from the Athens area. The dataset variability is therefore much smaller and unable to capture the seasonal, land cover and even aerosol load variations represented in the MODIS study. Larger window sizes capable of integrating all these variations and provide stable AOT calculations for a wide range of conditions. Nevertheless, the coarse resolution needed to retrieve valid AOT values restricts its ability to extract the aerosol spatial distribution features for environments where particle concentrations vary significantly at smaller spatial scales, like urban areas.

### 3.5.2 Site Land Cover influence in algorithm accuracy

The second improvement was the definition of an optimal land cover combination for AOT calculation. The objective of this improvement was to choose the land cover combination which minimized the influence of change in the vegetation content between reference and polluted images in the algorithm's accuracy, while maximizing the number of available pixels for AOT retrieval. Correlation analysis with the AERONET measurements for the different

land cover classes confirmed the impact of vegetation related surface reflectance changes in the algorithm performance. These impacts were reflected in the occurrence of higher errors and lower correlations, especially in sites more influenced by managed vegetation land covers (Modena and Lille) where those changes are more abrupt and extensive. Lower errors were found when only urban land cover was considered, except when the number of pixels in these classes was too low to provide a correct AOT retrieval ( as it was the case with Lisbon). In order to extent the algorithm applicability to those regions and since forest influenced sites revealed to be more resilient to reflectance changes, the final land cover combination included both urban and forest classes.

### 3.5.3 Observation geometry

Optimal image geometry clusters were defined to minimize the influence of differences in reference and polluted visualization geometries, by combining the maximum difference criteria for the sensor zenith, solar zenith and sensor and solar azimuth angles.

Some residual influence of sensor zenith angle differences still remained after defining these intervals. For angle differences (polluted-reference) higher than $3^o$ and lower than $-3^o$ a positive and negative offset was identified. In fact after removing those higher differences correlation increased from 0.78 to 0.83 and NRMSE decreased from 0.88 to 0.7. Nevertheless the original zenith angle intervals were maintained because applying these stricter differences reduced significantly the number of available images (87). The reduction of those visualization geometry intervals would require a longer image time series for each cluster, which can only be achieved, in the future, by using a multi-year dataset to expand on the results presented here. Another limitation introduced by these geometry clusters is the need to define, for each one, a reference image. Considering that each reference image has a different residual aerosol load this limits the algorithm's ability to extract absolute AOT values for the polluted images. It might also be responsible for some discrepancies in AOT retrieval error.

Parallely, a coefficient $a=1/\cos(\theta_v)$, where $\theta_v$ is the sensor zenith angle, was integrated into the algorithm to improve its capability to deal with different viewing angles, making the corresponding AOT retrievals more comparable. The introduction of this term didn't improve correlation between AERO-

NET and MODIS AOTs but it reduced significantly the overall error (NRMSE decreases from 1.53 to 0.88), especially the ones associated with more oblique views, for sensor zenith angles higher than $30^{o}$.

### 3.5.4 General conclusions

Overall DTA estimates for a MODIS dataset with a 78 pixel window (approximately 20 km) composed of only forest and urban pixels present a good overall agreement with AERONET measurements with a correlation coefficient of 0.78 and a RMSE of 0.08 (corresponding to an NRMSE of 0.88). If the unrealistic negative AOT values as well as the small AERONET AOT values (< 0.05) are excluded, a significant improvement is observed in error analysis with overall NRMSE dropping from 0.88 to 0.58. The error is significantly reduced if the basic assumption of identical observation geometries for the reference and polluted image is fulfilled. DTA showed also a similar performance to MODIS aerosol standard product with comparable r and error levels but presented a significantly higher number of images, reflecting as expected higher ability of the contrast reduction to extract AOT values in high reflective urban areas. Nevertheless, to confirm these findings a full comparison between the two products should be performed using a more extensive data time series.

These findings support the establishment of contrast reduction methods as a potential complement to other aerosol retrieval methodologies. However some limitations inherent to the nature of this algorithm need to be addressed. The inclusion of BRDF's, able to reproduce non-Lambertian surface behaviour, must be studied in order to better account for surface heterogeneity and observation geometry influences. Current work could also be expanded to other AERONET sites so as to further test the algorithm at a global scale.

4

# Chapter 4 - Estimation of $PM_{10}$ concentrations through AOT-based regression models

## 4.1 Introduction

Particulate matter is one of the major air pollutants responsible for human health problems related with the respiratory and cardiovascular systems (Bell *et al.*, 2004; Krewski *et al.*, 2000; Pope and Dockery, 1999; Pope *et al.* 2002; WHO, 2003) and are also related with several climate change inducing mechanisms (IPCC, 2007; Kaufman *et al.*, 2002; King *et al.*, 1999; Solomon *et al.*, 2007). Their suspension and transport potential as well as its relationship with precursor species such as $SO_2$ and $NO_2$ (Kim et. al., 2011; Putaud *et al.*, 2010; Seinfeld and Pandis, 2006) makes aerosols a good indicator of air pollution at urban and regional scales thus emphasizing the importance of developments in satellite aerosol retrieval.

The study of aerosols, or any other atmospheric pollutant, dispersion patterns relies on spatial and temporal data series obtained from air quality monitoring networks or measurement campaigns that entail high implementation and maintenance costs and are limited in spatial coverage. Such limitations can be minimized through the integration of statistical and physical modelling and introduction of a wide range of satellite sensors that can complement ground data. Satellite imagery can be used to better assess the spatial structure of air pollution and interactions on global, regional or local dispersion patterns. In fact, as shown in several studies, referenced in section 2.2.3, satellite derived

aerosol optical thickness can be used as an estimator of $PM_{10}$ ground concentrations, if several constraints associated with the different nature of the two variables are taken into account. AOT is a measure of light extinction due to the presence of aerosols in the total atmospheric column. $PM_{10}$ is a point ground measurement corresponding to an air quality station with a spatial representativity that can vary from an area of a few hundred meters in the case of traffic stations to thousands of square kilometres for rural background stations (Garber *et al.*, 2002). Several factors can influence the correlation between these two variables. For instance, low mixing layer heights can improve $PM_{10}$/AOT correlation, since most vertical aerosol content is concentrated in first few hundred meters above ground. High relative humidity can decrease this correlation due to aerosol hygroscopic growth which changes its optical properties and causes AOT overestimation.

Following the definition of the new optimized DTA algorithm for the MODIS sensor, the work presented in this chapter tries to assess the suitability of using the derived DTA AOT in air quality studies at the urban scale. In particular the study will focus on the ability of the DTA AOT algorithm to estimate $PM_{10}$ concentrations for the Lisbon Metropolitan Area by defining and evaluating several univariate and multivariate (together with meteorological variables) linear regression models. The algorithmic evaluation will be preceeded by a characterization and correlation analysis between retrieved AOT values and $PM_{10}$ ground measurements for several air quality stations in the Lisbon Metropolitan Area will be performed to fully assess their relationship.

As explained in section 2.2.2 and in Chapter 3, DTA AOT values do not correspond to absolute AOT values, since some residual aerosol load is always present in the reference image. For that reason, to determine correctly the regression models, the independent variable to be estimated will correspond, not to the absolute ground $PM_{10}$ concentration in the polluted image, but to its difference to the reference concentration value, calculated for each station and time average.

A comparison of a one-year dataset (2005) of DTA derived MODIS AOT values with $PM_{10}$ data from twelve air quality stations in the North and South

Lisbon Metropolitan Areas (AMLN and AMLS) air quality agglomerations was performed.

These air quality agglomerations are part of a wider region called Lisbon Metropolitan Area, which includes also the Setúbal Peninsula. Although the Setúbal region was not included, the study area, for the purposes of this study and as a matter of convenience, will be referred to as Lisbon Metropolitan Area.

The year of 2005 was chosen because it presented a significant range of $PM_{10}$ ground measurements concentrations for the study area in order to assess satellite AOT suitability as a $PM_{10}$ estimator. In fact, according to the characterization done in section 2.1.6, the PM air quality in the Lisbon Metropolitan Area has improved significantly in the period between 2005 and 2010. Choosing a year within this period would result in a smaller range of $PM_{10}$ values and might have limited the study conclusions, while a year before this period would probably be less representative of the current air quality situation.

$PM_{2.5}$ was, theoretically, the PM size range with the closest association with satellite AOT because of its higher light scattering efficiency (see section 2.2.3). The preference for $PM_{10}$ is explained by the higher number of monitoring stations with measurements for this pollutant, especially in 2005, where only three $PM_{2.5}$ stations were available, against the twelve $PM_{10}$ sites. This provides, not only a larger dataset but concentration estimates for a pollutant more representative of the overall air quality of the study area.

This work demonstrates the significant potential of using a contrast reduction based AOT product in urban $PM_{10}$ related air quality studies. The DTA AOT showed a moderate ability to reproduce air quality stations daily $PM_{10}$ concentrations, with a $PM_{10}$ explained variance confidence interval between 37 and 61%. Explained $PM_{10}$ variance values increased 10% when wind speed was added as an independent variable. The best results were obtained when all stations AOT and $PM_{10}$ daily average values were averaged per day (between 53 and 88% $PM_{10}$ explained variance). This suggests DTA AOT might be more adequate as an overall urban $PM_{10}$ air quality indicator by characterizing the mean daily conditions at the urban scale.

Nevertheless, this work identified some limitations to this product. On one hand, the coarse resolution of the product (≈20km) limits its use at an urban

scale. On the other hand, the presence of a significant and variable $PM_{10}$ content in reference images hinders the extraction of absolute $PM_{10}$ concentration values and meaningful $PM_{10}$ spatial patterns.

For these reasons, future work should be directed at attempting to establish absolute reference images with almost no $PM_{10}$ content by using, in conjunction with the DTA, other AOT and surface reflectance products. DTA should also be applied to higher spatial resolution sensors and to geostationary satellite imagery. In the first case, this would improve the AOT spatial resolution to scales more compatible with urban air quality studies. In the second case, it would provide some insight on intra-daily $PM_{10}$ variations, since geostationary satellites such as the METEOSAT Second Generation (MSG) series, although with a spatial resolution even lower then MODIS (pixel size in the order of a few kilometres), have revisit periods as low as 30 minutes.

## 4.2 Data and Methods

### 4.2.1 Ground and satellite data

The work presented in this chapter comprised five datasets collected for 2005:

a) Hourly ground measurements $PM_{10}$ concentration from monitoring stations of the Lisbon Metropolitan Area air quality network;

b) meteorological data from the Lisboa/Gago Coutinho station
    a. mixing layer height, MLH (m);
    b. mean atmospheric pressure at station level, $P_{mean}$ (hPa);
    c. mean relative humidity, RH (%);
    d. mean wind speed, $U_{mean}$ (m/s);
    e. mean air temperature at 1.5 m height from ground, $T_{mean}$ ($^{o}$);

c) Three different MODIS Terra products, already used in the work developed in the previous chapter (Table 3.2), namely:

a. geolocated radiance fields from band 1 (620–670 nm) – (MOD02QKM, Collection 5 - C005);

b. cloud mask (MOD35);

c. geolocation fields (MOD03);

The Lisbon Metropolitan Area air quality ground network, described in more detail in section 2.1.6, included, in 2005, 12 PM10 measuring stations. Their location and main characteristics are provided in Figure 4.1 and Table 4.1. All PM10 air quality stations are situated in an urban environment and include six background stations, four traffic and two industrial stations, according to the classification given by European Commission, following the work developed by Garber et al. (2002) (further details in section 2.1.4).

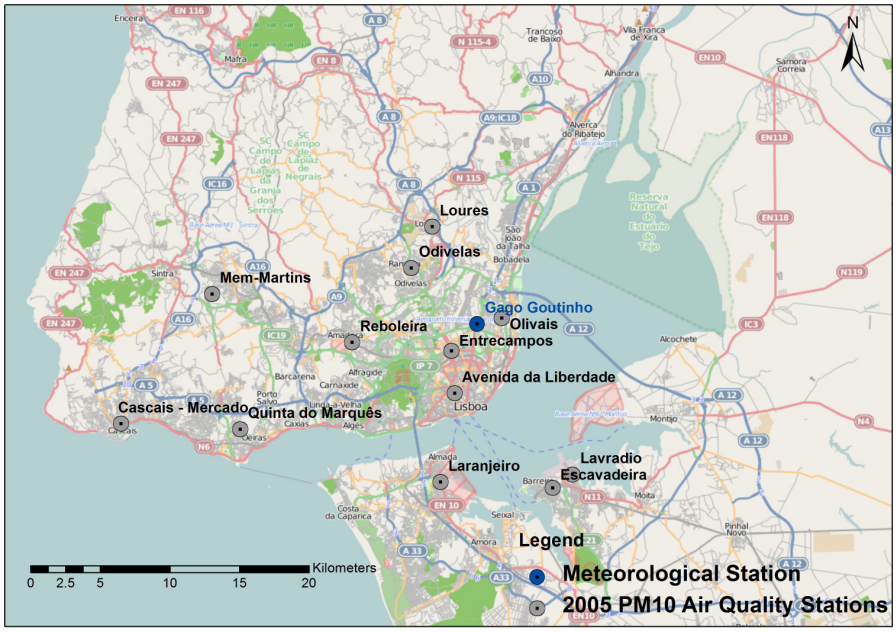


**Figure 4.1 – Location of the Lisbon Metropolitan Area $PM_{10}$ air quality stations network in 2005 and the Gago Coutinho meteorological station.**

**Table 4.1 – Description of the 2005 $PM_{10}$ measuring stations from the Lisbon Metropolitan Area air quality network (adapted from www.qualar.org)**

| Station | Zone | Station Type | Altitude (m) | Station Coordinates |
|---|---|---|---|---|
| Laranjeiro (LAR) | Urban | Background | 63 | Latitude: 38° 39' 49" N<br>Longitude: 9° 9' 28" W |
| Loures (LOU) | Urban | Background | 100 | Latitude: 38° 49' 44 " N<br>Longitude: 9° 9' 55" W |
| Mem-Martins (MEM) | Urban | Background | 173 | Latitude: 38° 47' 6" N<br>Longitude: 9° 20' 51" W |
| Olivais (OLV) | Urban | Background | 34 | Latitude: 38° 46' 12" N<br>Longitude: 9° 6' 26" W |
| Quinta do Marquês (MAR) | Urban | Background | 48 | Latitude: 38° 41' 51" N<br>Longitude: 9° 19' 24" W |
| Reboleira (REB) | Urban | Background | 30 | Latitude: 38° 45' 15" N<br>Longitude: 9° 13' 51" W |
| Escavadeira (ESC) | Urban | Industrial | 30 | Latitude: 38° 39' 36" N<br>Longitude: 9° 3' 54" W |
| Lavradio (LAV) | Urban | Industrial | 31 | atitude: 38° 40' 7" N<br>Longitude: 9° 2' 55" W |
| Avenida da Liberdade (LIB) | Urban | Traffic | - | Latitude: 38° 43' 16" N<br>Longitude: 9° 8' 46" W |
| Cascais – Mercado (CAS) | Urban | Traffic | 5 | Latitude: 38° 42' 05" N<br>Longitude: 9° 25' 16" W |
| Entrecampos (ENT) | Urban | Traffic | 86 | Latitude: 38° 44' 55" N<br>Longitude: 9° 8' 56" W |
| Odivelas (ODV) | Urban | Traffic | - | Latitude: 38° 48' 7" N<br>Longitude: 9° 10' 56 " W |

The network is maintained by the Comissão de Coordenação e Desenvolvimento Regional da Região de Lisboa e Vale do Tejo (CCDR-LVT), responsible also for the air pollution data collection, validation, reporting and distribution. $PM_{10}$ is measured continuously using automatic beta radiation particle monitors (Tente, 2005). The 15-minutes average period data are stored into the memory of the analyser. This data is periodically sent to a CCDR-LVT server and included in a centralized air quality database (Brás, 2012). The data is then validated and several related statistical parameters are calculated, according to the directives set by the European Commission after the work developed by Graber *et al.* (2002). Hourly average $PM_{10}$ concentrations are available, in excel format, through the internet portal www.qualar.org, maintained by the Portuguese Environmental Agency (APA).

All daily average meteorological variables listed above were collected in the Gago Coutinho station, located at the northeast part of Lisbon (Figure 4.1

and Table 4.2) and part of the meteorological station network maintained by the Meteorology Institute (IM). The selection of variables was made based on their possible influence on air pollution dispersion. Precipitation was disregarded because only clear days were selected in the satellite dataset. Most variables at station level are measured with corresponding sensors. Variables in altitude are recorded using radio sounding equipment. Mixing layer height values were calculated indirectly from vertical temperature profiles at 12h UTC, using the Holzworth method (Neto *et al.*, 2009).

**Table 4.2 – Main characteristics of the Gago Coutinho meteorological station**

| Station | Altitude (m) | Variables measured | Station Coordinates |
|---|---|---|---|
| Gago Coutinho | 104 | - Mean Air Temperature (º)<br>- Mean Atmospheric Pressure (hPa)<br>- Relative Humidity (%)<br>- Precipitation (mm)<br>- Temperature and Pressure at different atmospheric levels (hPa)<br>- Wind direction<br>-Wind Speed (m/s) | Latitude: 38º 45′ 58′′ N<br>Longitude: 9º 7′ 39′′ W |

Finally the Collection 5 MODIS Terra products were collected through the LAADSWEB service (http://ladsweb.nascom.nasa.gov). As referred above, only mostly cloud free days were selected. As mentioned earlier the main characteristics of each collected product are described in Chapter 3 (Table 3.2). The MOD02QKM radiance product (Figure 4.2) was used to calculate DTA AOT values, while MOD35 and MOD3 products were used in pre-processing to mask cloudy pixels and characterize solar and sensor geometry.

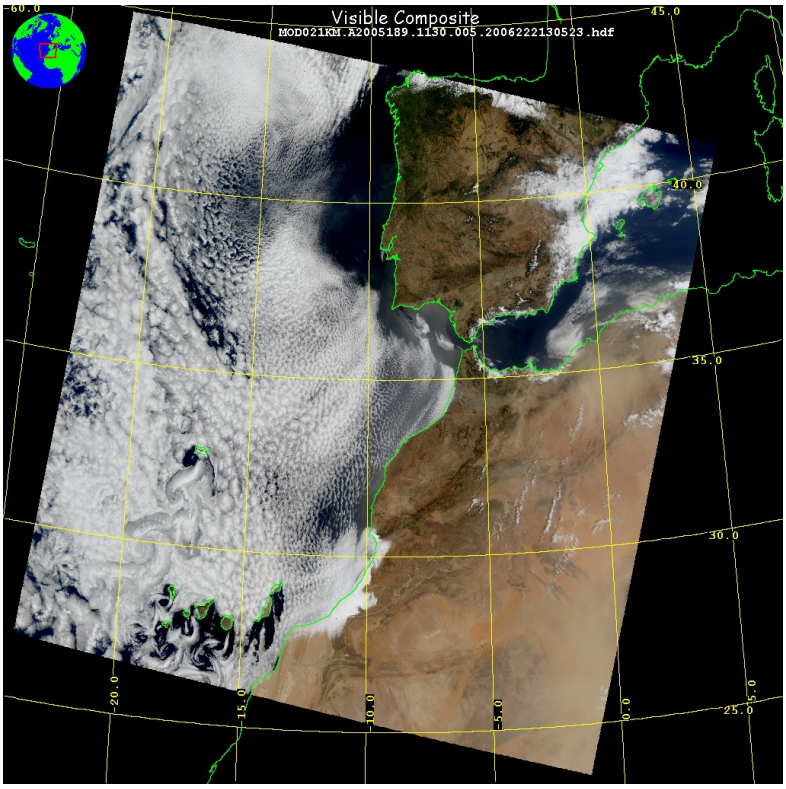


**Figure 4.2 – RGB example of MOD02QKM product taken from the LADSWEB service**

A CORINE 2000 land cover product (Bossard *et al.*, 2000) was used to remove MODIS pixels corresponding to agricultural land uses. These pixels were removed because, according to the work presented in Chapter 3, they might decrease DTA AOT accuracy, due to significant vegetation content changes between the reference and polluted images. Figure 4.3 gives an overview of that CORINE land cover product for the Lisbon Metropolitan Area. The map shows an almost continuous urban fabric within the city of Lisbon (urban land cover is identified as "Artificial Surfaces"). The fabric becomes more discontinuous and interlaced with patches of forested and agricultural, in the suburban areas to north, west and south of the city centre. The retrieval of AOT values for those areas, where stations like Loures, Quinta do Marquês, Mem Martins and Odivelas are included, could, therefore, be more affected by residual vegetation content.

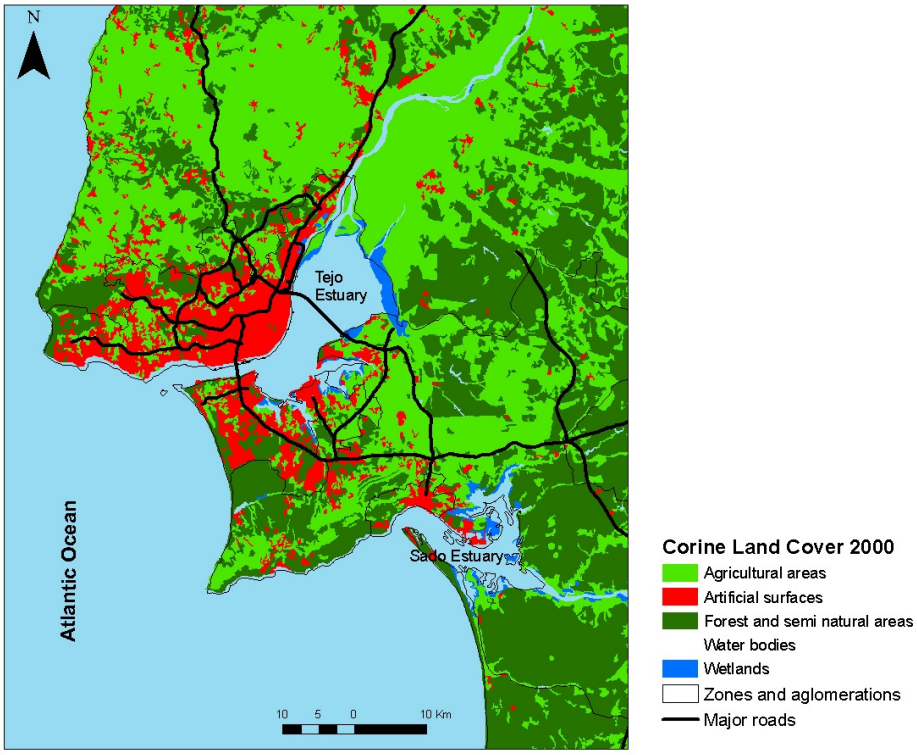


**Figure 4.3 – CORINE 2000 land cover product for the Lisbon Metropolitan Area**

### 4.2.2 Dataset collection and pre-processing

The MODIS dataset pre-processing stages were similar to the ones described in Chapter 3 (see Figure 3.1 in page 90).

HDF-EOS to GIS Format Conversion Tool (HEG) was used to define and extract a subset, previously reprojected to the UTM coordinate system. The subset was approximately a 60x60 km area centred in Lisbon, an area sufficiently large to accommodate the pixels required for the DTA AOT calculation for all air quality stations. The subsequent processing steps were performed using MATLAB programmed functions, including: a) removing cloud pixels from the Lisbon Metropolitan Area MOD02QKM subsets using the MOD035 corresponding product; b) and c) removing pixels corresponding to agricultural land cover and performing DTA AOT calculations for all air quality stations using a window size, centred at their respective location, of 78x78 pixels (approximately 20x20 km), according to the optimal conditions for algorithm performance defined in the previous chapter (Grosso and Paronis, 2011); d) matching up

MODIS polluted and reference images with the $PM_{10}$ ground measurements and daily meteorological variables close to the satellite time of passage.

Images were matched according to sensor and solar viewing geometry similarity, also following the clusters defined in MODIS DTA AOT/AERONET presented earlier:

- Two separate clusters for $|\varphi_v - \varphi_s| > 90^o$ and $|\varphi_v - \varphi_s| < 90^o$ geometries, where $\varphi_v$ and $\varphi_s$ represents the sensor and solar azimuth respectively, to represent ;
- Sensor zenith angle groups from $0^o$ to $90^o$ with a $15^o$ interval;
- Solar zenith angle groups from $0^o$ to $90^o$ with a $20^o$ interval;

The more restrict $3^o$ sensor zenith difference, identified in Chapter 3, section 3.4.3 (Grosso and Paronis, 2011), was not used since it limited significantly the number of available images.

Reference images were selected after clustering the images according to their visualization geometry. Their selection is a more difficult process than in the previous chapter, because, instead of a single site, they should be representative of the entire study area. Therefore the following criteria were used::

1) images should have $PM_{10}$ concentration data for all available $PM_{10}$ stations;

2) images should correspond, if possible, to the lowest average $PM_{10}$ concentration, in each geometry cluster, calculated using all available station measurements for the hour closest to the satellite time of passage.

These criteria were selected to maximize the number of available $PM_{10}$ and AOT values but some problems arose from their application. Since reference selection is based on an average overall value, some individual stations $PM_{10}$ concentration values are higher in the reference day, when compared to the polluted day, leading to the existence of negative values in the final $PM_{10}$ dataset. Furthermore, some polluted days can even present an overall $PM_{10}$ concentration lower than the corresponding reference image but could not be selected because they present a lower number of stations with valid $PM_{10}$ measurements.

The final list of MODIS images (42 polluted and 30 reference), including dates and respective date difference in days is presented in Table 4.3. The total

number of available valid air quality station points varied between 382 and 414, depending on the time average. The limited number of polluted images of the final dataset highlights the difficulty in establishing polluted/reference pairs with limited cloud content and similar visualization geometry. This low number of images might limit conclusions in terms of spatiotemporal representativity of the achieved results and the ability of extracting AOT based $PM_{10}$ spatial patterns for urban areas. Nevertheless these were not the main objectives of this study. The central objective of this work is to determine if the DTA AOT can be used as a $PM_{10}$ concentration estimator in urban areas and the final number of points is still sufficient to allow conclusions regarding that purpose.

**Table 4.3 – Polluted and reference MODIS image dates used in DTA AOT calculations**

| Polluted Image Date | Reference Image Date | Difference (in days) |
|---|---|---|
| 07-01-2005 12:05 | 09-12-2005 12:05 | 336 |
| 09-01-2005 11:55 | 11-12-2005 11:55 | 336 |
| 11-01-2005 11:40 | 13-12-2005 11:40 | 336 |
| 28-01-2005 12:25 | 05-11-2005 12:15 | 281 |
| 01-02-2005 12:00 | 17-02-2005 12:00 | 16 |
| 03-02-2005 11:45 | 19-02-2005 11:45 | 16 |
| 10-02-2005 11:55 | 25-01-2005 11:55 | -16 |
| 17-03-2005 12:25 | 04-10-2005 12:15 | 201 |
| 11-04-2005 10:40 | 27-04-2005 10:40 | 16 |
| 27-04-2005 12:20 | 01-08-2005 12:20 | 96 |
| 29-04-2005 12:05 | 03-08-2005 12:05 | 96 |
| 06-05-2005 12:10 | 26-08-2005 12:10 | 112 |
| 20-05-2005 12:25 | 05-06-2005 12:25 | 16 |
| 01-06-2005 11:10 | 19-07-2005 11:10 | 48 |
| 06-06-2005 11:30 | 05-05-2005 11:30 | -32 |
| 09-06-2005 12:00 | 24-05-2005 12:00 | -16 |
| 21-06-2005 12:25 | 05-06-2005 12:25 | -16 |
| 22-06-2005 11:30 | 05-05-2005 11:30 | -48 |
| 01-07-2005 11:25 | 15-06-2005 11:25 | -16 |
| 02-07-2005 12:05 | 16-06-2005 12:05 | -16 |
| 07-07-2005 10:45 | 05-06-2005 10:45 | -32 |
| 07-07-2005 12:25 | 05-06-2005 12:25 | -32 |
| 10-07-2005 11:15 | 23-05-2005 11:15 | -48 |
| 16-07-2005 12:20 | 05-06-2005 12:25 | -41 |
| 18-07-2005 12:05 | 16-06-2005 12:05 | -32 |
| 23-07-2005 12:25 | 05-06-2005 12:25 | -48 |
| 02-08-2005 11:25 | 15-06-2005 11:25 | -48 |
| 04-08-2005 11:10 | 19-07-2005 11:10 | -16 |
| 17-08-2005 10:40 | 27-04-2005 10:40 | -112 |
| 17-08-2005 12:20 | 01-08-2005 12:20 | -16 |
| 24-08-2005 12:25 | 01-08-2005 12:20 | -23 |
| 29-08-2005 11:05 | 13-08-2005 11:05 | -16 |
| 13-09-2005 12:00 | 28-08-2005 12:00 | -16 |
| 18-09-2005 10:40 | 02-09-2005 10:40 | -16 |
| 18-09-2005 12:15 | 11-04-2005 12:20 | -160 |
| 30-09-2005 11:05 | 14-09-2005 11:05 | -16 |
| 05-10-2005 11:20 | 19-09-2005 11:20 | -16 |
| 09-11-2005 11:55 | 25-01-2005 11:55 | -288 |
| 14-11-2005 12:10 | 30-01-2005 12:10 | -288 |
| 24-11-2005 11:10 | 10-12-2005 11:10 | 16 |
| 15-12-2005 11:30 | 29-11-2005 11:30 | -16 |
| 16-12-2005 12:10 | 30-11-2005 12:10 | -16 |

Time averages for $PM_{10}$ ground measurements were also calculated. The total number of hours included in the calculations, varied between 4 and 24 hours, considering an interval centred in the hourly $PM_{10}$ ground measurement

closest to the satellite passage. Only values from the same day were considered in the averaging process. Therefore the 24h value is equivalent to the daily average for a specific point.

A Lisbon Metropolitan Area daily spatial average was also calculated for AOT and $PM_{10}$, corresponding to a single daily value calculated averaging data from all available stations. Time aggregation was only performed if, for each date, station and time aggregation period, more than half of the measurements were valid, following the directives for calculation of daily means defined in the guidance document established by the European Commission Decision 97/101/EC on Exchange of Information (Garber *et al.*, 2002).

### 4.2.3 Regression model related methodologies

Both $PM_{10}$ and AOT correlation analysis and the development and evaluation of $PM_{10}$ concentration estimation uni and multivariate regression models were performed using MATLAB© programmed functions.

Three $PM_{10}$ concentration differences estimation regression models were developed in the scope of this work. Model A is a univariate model where AOT is the only independent variable used to estimate $PM_{10}$ concentrations. The objective of this model is to assess directly the satellite AOT's capability to estimate ground level particle concentrations. Model B is a multivariate model where the most significant meteorological variables are added, together with AOT, to optimize $PM_{10}$ estimation. Model C is also a multivariate model, with both AOT and meteorological variables. Its aim is to estimate the daily spatial average of $PM_{10}$ at Lisbon's Metropolitan Area instead of individual $PM_{10}$ values at air quality stations, as in the previous models. It will serve to assess the ability of those independent variables to be used as an overall air quality indicator for an urban area.

To test the robustness of the derived regression models, and considering limited sample size, a bootstrapping technique was applied to all presented regression models to infer confidence intervals for several regression parameters (Efron, 1979). Bootstrapping is a broadly applicable, nonparametric approach to statistical inference that can be used in regression modelling to derive accurate standard errors, confidence intervals, and hypothesis tests for most statistics (Fox, 1997). The confidence intervals are derived by resampling the original da-

ta multiple times, in this case 1000, using random sampling with replacement, and determining, for each set of sampled data, the required parameters of the regression model. The final 95% confidence interval is derived by the 2.5$^{th}$ and 97.5$^{th}$ percentiles of each parameter distribution. (Efron 1982).

The multivariate regression model was developed following a two-step methodology. First, a stepwise fit procedure was used to add or remove independent variables from the multilinear regression model based on their regression statistical significance and avoid collinearity between them. Statistical significance is given by the p-value of an F-statistical test, which provides a measure of the increment in the regression explanatory power given by each potential term (Draper and Smith, 1998). If p-value is lower than 0.05 the term is added to the model.

The stepwise fit was associated to a bootstrapping technique to repeat the procedure for several resampled datasets (1000) and determine the number of times each parameter was chosen as a significant regression model independent variable. Results were analysed to establish which variables were selected for the second stage, where, the bootstrapping technique was used to resample the original dataset multiple times (1000), determine the regression model for each resampled dataset and establish confidence intervals for the respective regression coefficients and correlation and error statistics.

## 4.3 Results and Discussion

### 4.3.1 Characterization of the $PM_{10}$ and AOT datasets

Figure 4.4 provides an overview of daily, weekly and monthly average Lisbon Metropolitan Area air quality stations $PM_{10}$ concentrations for the year 2005. It also shows the daily average $PM_{10}$ concentrations, corresponding to the reference and polluted MODIS images passage time and their respective difference. As explained earlier, there are some negative concentration differences, due to lower station values in polluted images, when compared with the reference.

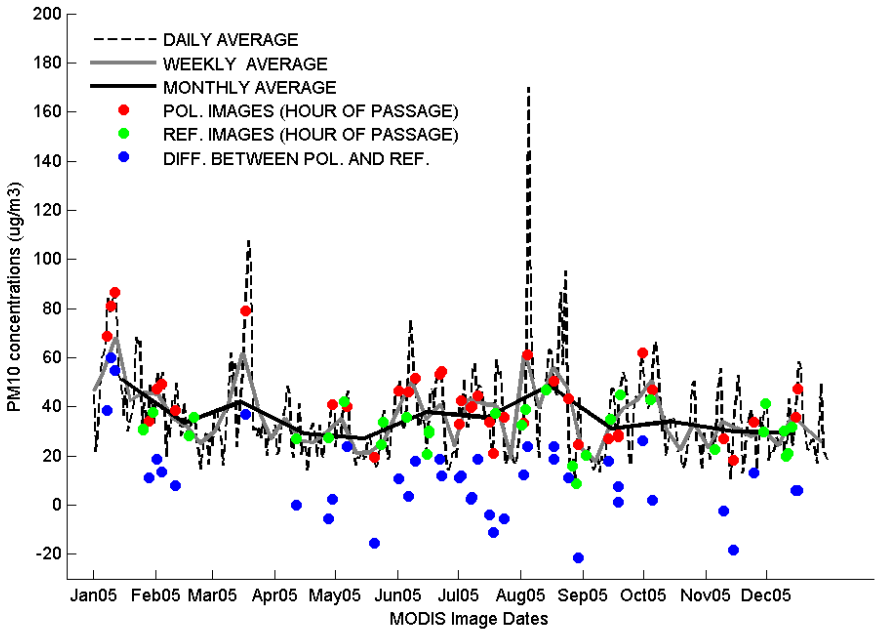


**Figure 4.4 - $PM_{10}$ daily mean concentrations for the year 2005, considering all stations from Lisbon Metropolitan Area (black line). Red and green dots refer to the mean $PM_{10}$ concentrations for the day and hour of passage for all available reference and polluted MODIS images, respectively. Blue dots refer to the $PM_{10}$ concentration difference between the polluted and reference**

An overall analysis of the daily averaged $PM_{10}$ concentrations (dashed line) shows a range of values between 10 and 170 µg/m$^3$ with a distinct seasonal cycle. January higher values (51 µg/m$^3$) progressively decrease until mid-May (29 µg/m$^3$), with the exception of some peak values in the beginning of March (monthly mean, 43 µg/m$^3$). After that point they begin rising until reaching a peak mean value of 49 µg/m$^3$ in August, followed by a steady decrease until December (29 µg/m$^3$). This annual cycle is mostly driven by differences of emission sources and meteorological conditions, as discussed in section 2.1.6. For instance, higher concentrations in winter are often associated with low mixing layer heights originated by colder air masses at lower altitudes. The higher values in March could be due to the influence of Saharan dust transport events, which are also partially responsible for the summer peak, together with the higher influence of road and dust resuspension events and forest fires. A further discussion about the influence of meteorological factors is given in section 4.3.3.

Table 4.4 presents the mean and standard deviation (Std1) values for daily $PM_{10}$ concentration values, discriminated per station and season. It also provides information on mean intra-daily standard deviation (Std2). This parameter is presented not only to help characterize station and seasonal differences but also because higher intra-day variability might have a negative effect on AOT/$PM_{10}$ correlation.

Seasonal analysis, shown in the last rows, confirms the higher winter and summer daily averages, respectively of 38.38 and 40.24 µg/m$^3$. It also highlights the similar inter-daily variability for all seasons (Std1≈21 µg/m$^3$) and the higher mean winter intra-daily variability (Std2=15.24 µg/m$^3$).

**Table 4.4 - $PM_{10}$ Conc. (µg/m$^3$) mean daily average (Mean), standard deviation (Std1) and mean intra-daily standard deviation (Std2) for all days of the year and for all polluted, reference and respective difference per station and season (Win – Winter; Spr – Spring; Sum – Summer; Aut – Autumn). Thicker lines separate background, traffic and industrial stations (in this order). For the reference column, season does not refer to its own date but to date of corresponding polluted image**

| Station | $PM_{10}$ Conc. (µg/m$^3$) Daily Average | | | | | | | | | | |
|---|---|---|---|---|---|---|---|---|---|---|---|
| | All Year | | | Polluted | | | Reference | | | Difference | |
| | Mean | Std1 | Std2 | Mean | Std1 | Std2 | Mean | Std1 | Std2 | Mean | Std1 |
| LAR | 31.10 | 18.70 | 10.93 | 38.23 | 18.33 | 13.42 | 26.42 | 6.64 | 9.76 | 13.03 | 19.36 |
| LOU | 32.79 | 15.84 | 9.53 | 38.65 | 14.24 | 9.93 | 28.63 | 7.89 | 8.92 | 10.02 | 14.33 |
| MAR | 30.80 | 16.31 | 8.59 | 40.95 | 15.18 | 11.38 | 28.99 | 4.52 | 8.27 | 18.53 | 14.75 |
| MEM | 27.62 | 20.05 | 9.10 | 33.11 | 14.49 | 10.78 | 24.70 | 12.02 | 9.73 | 8.69 | 16.83 |
| OLV | 29.74 | 18.34 | 9.72 | 36.82 | 20.46 | 14.61 | 23.34 | 13.02 | 8.69 | 13.83 | 22.13 |
| REB | 31.73 | 7.55 | 9.54 | 37.59 | 14.16 | 10.13 | 26.59 | 7.46 | 8.33 | 11.23 | 14.55 |
| CAS | 40.77 | 15.19 | 15.55 | 43.80 | 15.95 | 16.63 | 36.54 | 8.27 | 15.12 | 7.61 | 15.17 |
| ENT | 44.05 | 19.76 | 15.23 | 52.78 | 24.47 | 18.98 | 37.16 | 6.12 | 14.31 | 15.62 | 26.01 |
| LIB | 53.78 | 18.77 | 18.92 | 63.75 | 21.16 | 22.89 | 50.46 | 10.53 | 19.91 | 13.30 | 22.20 |
| ODV | 34.46 | 18.06 | 10.79 | 40.24 | 17.83 | 12.96 | 27.07 | 8.35 | 10.43 | 14.62 | 20.14 |
| ESC | 36.93 | 17.03 | 12.47 | 44.58 | 18.97 | 15.82 | 33.61 | 10.03 | 13.66 | 10.97 | 21.51 |
| LAV | 33.90 | 25.31 | 12.89 | 42.20 | 18.20 | 15.68 | 28.51 | 12.83 | 13.97 | 10.72 | 22.32 |
| Win | 38.38 | 21.19 | 15.24 | 55.41 | 24.15 | 23.98 | 26.46 | 14.92 | 18.58 | 25.18 | 24.78 |
| Spr | 33.32 | 21.11 | 10.21 | 40.06 | 22.47 | 14.59 | 24.00 | 14.70 | 17.95 | 8.64 | 19.65 |
| Sum | 40.24 | 21.06 | 11.53 | 42.27 | 13.66 | 11.16 | 26.21 | 16.24 | 17.88 | 8.77 | 13.82 |
| Aut | 32.00 | 21.09 | 11.12 | 33.19 | 16.72 | 11.46 | 22.84 | 14.48 | 16.57 | 6.10 | 15.66 |

The air quality stations annual mean daily average $PM_{10}$ concentration (Table 4.4) shows a clear distinction between station types. Background stations, representative of urban background conditions not associated with specific pollution sources, present similar lower daily average values, varying between 27.62 µg/m$^3$ in Mem Martins and 32.79 µg/m$^3$ in Loures. They also have

a limited range of annual mean intra-daily standard deviation (Std2), between 9.10 and 10.93 μg/m$^3$.

On the other hand, traffic stations, influenced by high traffic volume roads, present a higher and wider range of annual mean daily average values. Odivelas presents clearly the lowest mean (34.46 μg/m$^3$) and intra-daily standard deviation (10.79 μg/m$^3$). The behaviour and consequent spatial representativity of this station is in fact more consistent with a background station. For that reason in all subsequent results Odivelas is considered a background station. The remaining stations present a $PM_{10}$ daily mean range between 40.77 (CAS) and 53.78 μg/m$^3$ (LIB) and an intra-daily standard deviation range from 15.23 (ENT) to 18.92 μg/m$^3$ (LIB).

Industrial stations, Escavadeira (ESC) and Lavradio (LAV), in the vicinity of major industries, are characterized by an intermediate range of $PM_{10}$ values and corresponding intra-daily variability usually related to the operation regimes of those point sources and predominant wind directions. In 2005 these presented an annual mean daily average and standard deviation of 36.93 and 33.90 μg/m$^3$ and 12.47 and 12.49 μg/m$^3$, respectively.

Daily $PM_{10}$ concentration standard deviation values (Std1) are similar for most stations, varying between 15 and 20 μg/m$^3$. The exceptions are Reboleira (REB), which presents a very low inter-daily variation (7.55 μg/m$^3$) and Lavradio, with the highest value (25.31 μg/m$^3$).

Overall $PM_{10}$ daily values follow a weekly pattern usually associated with traffic pollution, highlighted in Figure 4.5. Sundays characteristic low $PM_{10}$ concentrations (average: 25 μg/m$^3$) are followed by a gradual increase until Wednesday (38 μg/m$^3$) and a subsequent decrease until Saturday (30 μg/m$^3$).

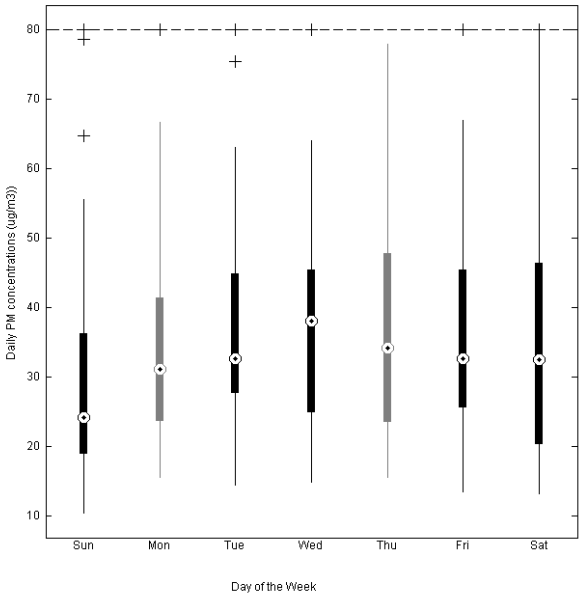


**Figure 4.5 - $PM_{10}$ daily Concentration grouped according to weekday**

When comparing the 42 valid MODIS polluted images selected for this study (Figure 4.4, red dots) we can identify that, although preserving some of the characteristics described for the full year, there are some evident differences. $PM_{10}$ daily concentration ranges between 18 and 87 $\mu g/m^3$. There is an high number of images in the summer (June, July, August) with 19 polluted images, 9 images in winter (December, January, February) and 8 in both spring (March, April, May) and Autumn (September, October, November). The least represented months are February, March and October.

Some of the seasonal variations identified earlier are captured in the satellite polluted dataset: higher concentrations in January, June and August and lower in the remaining months (Figure 4.4, red dots and Figure 4.6, top left). Nevertheless some differences can be found such as the lower values in July when compared to June, and a few high values in February and October. Winter and spring daily $PM_{10}$ mean, inter and intra-daily standard deviation values, shown in Table 4.4, are significantly higher than annual statistics. On the other hand, summer and autumn present a mean and an intra-daily standard deviation similar to the annual values but a lower inter-daily variation.

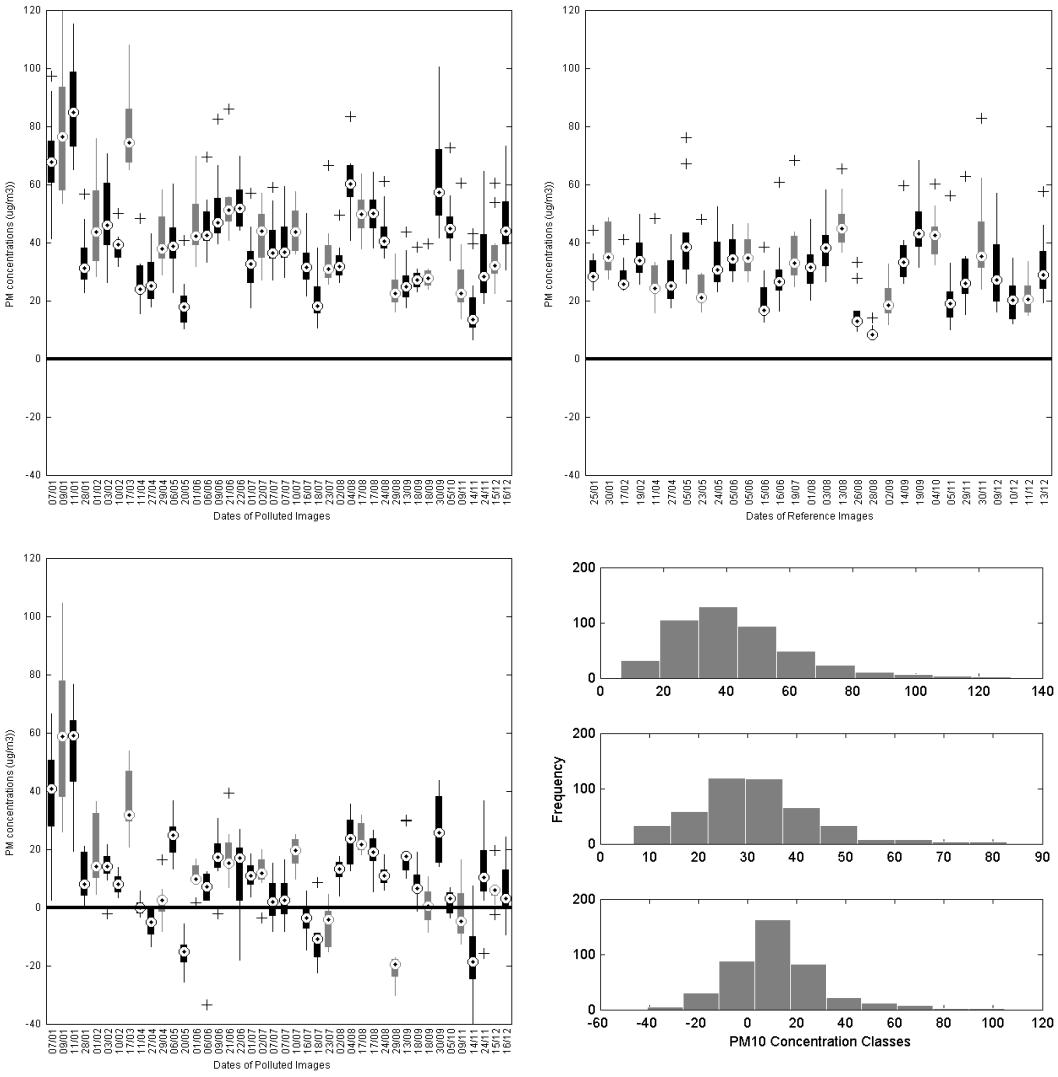


**Figure 4.6 - $PM_{10}$ concentrations range for all available polluted (top right) and reference (top left) MODIS images, the difference between the two (bottom left) and the respective histograms (bottom right: polluted – top; reference – middle; difference – bottom)**

The dataset with 30 reference images (Figure 4.4, green dots, Figure 4.6, top right) shows a significantly smaller daily mean $PM_{10}$ values, ranging from 9 to 47 $\mu g/m^3$. They display a less marked seasonality, with the exception of some marginally higher values in August and October and lower values for the winter months. They also show very similar inter and intra-daily seasonal variations (Table 4.4), ranging from 14.48 to 16.24 $\mu g/m^3$ in the first case and 16.57 to 18.58 $\mu g/m^3$, in the second.

These are desired characteristics in a reference dataset since DTA AOT values and subsequently the $PM_{10}$ values being estimated do not correspond to the ideal absolute values but to the difference between the polluted and reference concentrations for each day and air quality station. A reference image with low $PM_{10}$ mean and intra-daily standard deviation values limits their impact on DTA AOT calculation and AOT/$PM_{10}$ correlation.

Nevertheless reference images still present significant $PM_{10}$ concentrations, often above 20 $\mu g/m^3$, and some intra-daily variability. An example of its effect can be given by comparing, in Table 4.4, the absolute concentration values in background and traffic stations with their respective concentration differences.

Traffic stations $PM_{10}$ concentration values in reference images have a mean value interval between 36.54 $\mu g/m^3$ in Cascais and 50.46 $\mu g/m^3$ in Avenida da Liberdade (LIB) and mean intra-daily standard deviation ranging from 11 to 15 $\mu g/m^3$. On the other hand, background stations present a lower average $PM_{10}$ reference range, from 23.34 $\mu g/m^3$ in Olivais (OLV) to 28.99 $\mu g/m^3$ in Quinta do Marquês (MAR) and a lower mean daily standard deviation, around 9 to 10 $\mu g/m^3$. As a consequence, the distinction in $PM_{10}$ concentrations between background and traffic stations is diluted when concentration differences between polluted and reference images are calculated. Some traffic and background stations present similar mean concentration difference values and in some cases, like Quinta do Marquês, even present a higher mean (18.53 $\mu g/m^3$) than all traffic stations.

Another effect of variable reference conditions is the significant increase in daily $PM_{10}$ concentration differences standard deviation (last column of Table 4.4), observed for each station and season, when compared with the original polluted values. These station spatiotemporal variations also limit the possibility of extracting meaningful spatial $PM_{10}$ concentration patterns for a specific set of days, since the spatial relation between those values might vary significantly, depending on the reference values used.

Figure 4.7 presents information on the DTA AOT Lisbon Metropolitan Area daily mean time series and Table 4.5 on the corresponding station means,

for all polluted images. They range from –0.08 to 0.36 and -0.16 to 0.5 (histogram in Figure 4.7), respectively, with an average AOT of 0.08 in both cases.

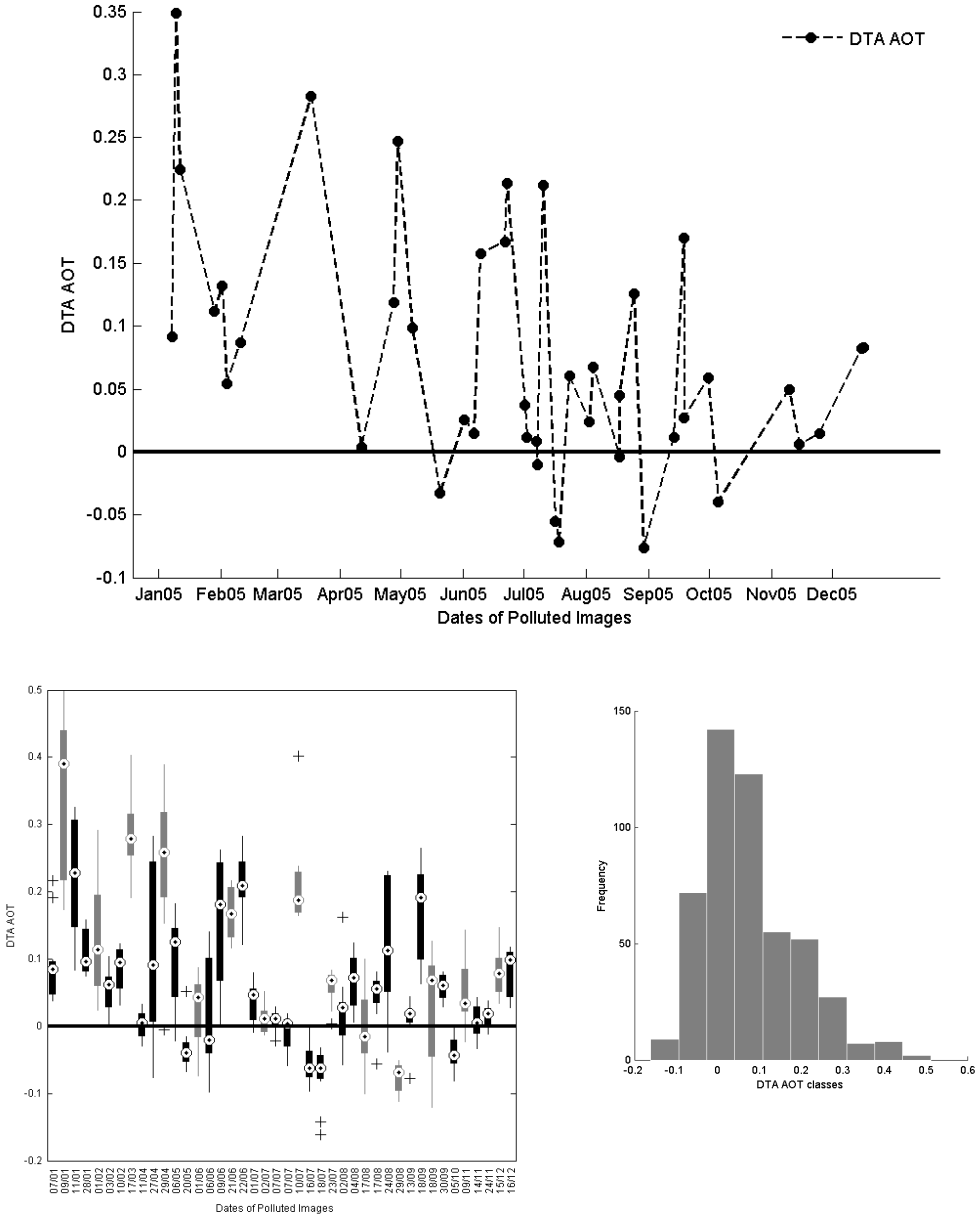


**Figure 4.7 – Top: DTA AOT time series (top); Bottom: DTA AOT box plot (left) and station DTA AOT histogram (right)**

In terms of seasonal variation, the time series and box plot graphs in Figure 4.7 shows that DTA AOT follows the $PM_{10}$ downward trend in the six images corresponding to the first two months of the year. This trend shifts, during spring, to a more irregular inter-daily pattern of high and low AOT daily mean

images with a wide daily spread. June's upward trend is followed by a sequence, in July, of very low AOT images with small intra-daily variation. Mean daily AOT increases in August but, contrarily to $PM_{10}$, the overall levels are lower than June. The last four months are characterized by a decrease from September to November and a slight increase in December. Overall AOT seasonal values (Table 4.5), when compared to $PM_{10}$, maintain the higher mean winter levels (0.14) but seem to present higher spring values (0.12). Discrepancies in DTA AOT and $PM_{10}$ values, especially in summer and spring, could be attributed to the presence of overlying aerosol layers associated with desert dust transport events which affect more the vertically integrated AOT values than the ground $PM_{10}$ levels.

**Table 4.5 – MODIS DTA AOT mean and standard deviation per station and season**

| Station | AOT | |
|---|---|---|
| | Mean | Standard Deviation |
| LAR | 0.08 | 0.10 |
| LOU | 0.06 | 0.08 |
| MAR | 0.08 | 0.13 |
| MEM | 0.04 | 0.08 |
| ODV | 0.05 | 0.08 |
| OLV | 0.10 | 0.14 |
| REB | 0.06 | 0.08 |
| CAS | 0.08 | 0.12 |
| ENT | 0.09 | 0.12 |
| LIB | 0.09 | 0.12 |
| ESC | 0.10 | 0.13 |
| LAV | 0.10 | 0.14 |
| Win | 0.14 | 0.11 |
| Spr | 0.12 | 0.14 |
| Sum | 0.05 | 0.10 |
| Aut | 0.04 | 0.07 |

Background stations present a wider range of AOT mean and standard deviation values, with lower bound values in Mem-Martins (MEM) (mean=0.04 and standard deviation=0.08) and an upper bound in Olivais (0.10 and 0.14).

Industrial stations present values closer to this upper bound with a mean value of 0.1 and a standard deviation between 0.13 and 0.14.

Traffic stations present slightly lower mean and standard deviation values and very similar between them (mean between 0.08 and 0.09 and an equal standard deviation of 0.12 for all three stations). Station comparison of $PM_{10}$ concentration differences and AOT mean values seem to be in moderate agree-

ment. Nevertheless, AOT values for Cascais and the industrial stations are relatively higher than their respective $PM_{10}$ mean concentrations. These are relatively lower for background stations Quinta do Marquês and Odivelas.

### 4.3.2 $PM_{10}$/AOT correlation

Table 4.6 presents the correlation coefficients and corresponding number of observations between AOT and different time averaged $PM_{10}$ concentration values for the entire dataset. These values are mean daily averages (identified in the table as LMA Daily Avg.) per station type and season, for the Lisbon Metropolitan Area. As mentioned in the data and methods section, time averages included in the analysis vary between four and 24 hours, centred on the measurement hour closest to the satellite time of passage.

For these subdivisions correlation statistics were calculated considering all available images, designated by "full" or "original dataset", and considering only polluted/reference image pairs from the same season, referred as "same season dataset". This was done in order to determine the possible effect of reflectance differences caused by seasonal land use changes, discussed in the previous result chapter.

The different station types (background, traffic, industrial) and $PM_{10}$ time aggregation periods were included to integrate into the analysis part of the variability introduced by the different spatial and temporal nature of the satellite derived AOT and the ground $PM_{10}$ measurements. AOT is an atmospheric vertical column integrated variable calculated using pixels in a 10 km radius from the location of the air quality station. $PM_{10}$ measurements are point values corresponding to the concentration of an air pollutant at almost ground level. Averaging the ground $PM_{10}$ values to progressively higher time periods might increase $PM_{10}$ spatiotemporal representativity, and improve AOT correlation (Engel-Cox *et al.*, 2004; Gupta *et al.*, 2006). For the same reason, correlation between station's average values of AOT and $PM_{10}$ instead of individual values, should improve results significantly. The division into station types accounts for the different behaviour observed in traffic, background and industrial air quality stations. As seen in the previous section, background stations usually present a smaller temporal variability and are representative of a larger spatial

area when compared to traffic and industrial stations and are therefore expected to present a better correlation with AOT values.

**Table 4.6 - Correlation coefficients (r) and respective number of observations (N) between different temporally averaged $PM_{10}$ concentrations and DTA AOT considering all stations, per station type group (Background, Traffic and Industrial), per season and DTA AOT daily average. The first line for each group corresponds to the values obtained using the entire dataset, while the second is using only pairs of reference/polluted images from the same season**

| Aggregation Period | Same Hour | | 4h | | 8h | | 12h | | 16h | | 20h | | 24h | |
|---|---|---|---|---|---|---|---|---|---|---|---|---|---|---|
| Sample | N | R | N | R | N | R | N | R | N | R | N | R | N | R |
| All | 382 | 0.48 | 392 | 0.51 | 397 | 0.54 | 408 | 0.55 | 413 | 0.56 | 414 | 0.57 | 414 | 0.58 |
| | 214 | 0.59 | 218 | 0.61 | 222 | 0.65 | 229 | 0.67 | 230 | 0.69 | 230 | 0.70 | 230 | 0.71 |
| Background | 210 | 0.49 | 215 | 0.52 | 219 | 0.57 | 230 | 0.56 | 233 | 0.57 | 234 | 0.58 | 234 | 0.58 |
| | 115 | 0.60 | 117 | 0.64 | 120 | 0.68 | 127 | 0.67 | 128 | 0.68 | 128 | 0.69 | 128 | 0.69 |
| Traffic | 110 | 0.52 | 114 | 0.54 | 115 | 0.55 | 115 | 0.58 | 116 | 0.59 | 116 | 0.61 | 116 | 0.62 |
| | 62 | 0.68 | 64 | 0.68 | 65 | 0.71 | 65 | 0.74 | 65 | 0.74 | 65 | 0.75 | 65 | 0.75 |
| Industrial | 62 | 0.45 | 63 | 0.52 | 63 | 0.52 | 63 | 0.52 | 64 | 0.53 | 64 | 0.54 | 64 | 0.54 |
| | 37 | 0.49 | 37 | 0.54 | 37 | 0.58 | 37 | 0.61 | 37 | 0.65 | 37 | 0.68 | 37 | 0.69 |
| Dec- Feb | 85 | 0.51 | 89 | 0.55 | 92 | 0.63 | 96 | 0.64 | 98 | 0.68 | 98 | 0.69 | 98 | 0.69 |
| | 57 | 0.49 | 59 | 0.52 | 62 | 0.63 | 64 | 0.64 | 65 | 0.67 | 65 | 0.68 | 65 | 0.68 |
| Mar- May | 55 | 0.58 | 55 | 0.62 | 56 | 0.60 | 57 | 0.60 | 58 | 0.60 | 58 | 0.60 | 58 | 0.59 |
| | 9 | -0.63 | 9 | -0.19 | 9 | -0.20 | 9 | -0.23 | 9 | -0.03 | 9 | -0.17 | 9 | 0.02 |
| Jun- Aug | 167 | 0.46 | 169 | 0.49 | 170 | 0.51 | 172 | 0.52 | 173 | 0.51 | 173 | 0.50 | 173 | 0.51 |
| | 120 | 0.55 | 121 | 0.58 | 122 | 0.58 | 124 | 0.59 | 124 | 0.60 | 124 | 0.59 | 124 | 0.58 |
| Sep-Nov | 75 | 0.07 | 79 | 0.11 | 79 | 0.14 | 83 | 0.15 | 84 | 0.14 | 85 | 0.16 | 85 | 0.16 |
| | 28 | 0.13 | 29 | 0.11 | 29 | 0.14 | 32 | 0.12 | 32 | 0.08 | 32 | 0.08 | 32 | 0.07 |
| LMA Daily Avg. | 42 | 0.66 | 42 | 0.67 | 42 | 0.68 | 42 | 0.67 | 42 | 0.65 | 42 | 0.65 | 42 | 0.65 |
| | 24 | 0.79 | 24 | 0.80 | 24 | 0.81 | 24 | 0.80 | 24 | 0.80 | 24 | 0.81 | 24 | 0.82 |
| LAR | 33 | 0.59 | 34 | 0.65 | 34 | 0.67 | 36 | 0.64 | 36 | 0.63 | 36 | 0.63 | 36 | 0.64 |
| | 21 | 0.65 | 21 | 0.70 | 21 | 0.71 | 21 | 0.72 | 21 | 0.74 | 21 | 0.75 | 21 | 0.77 |
| LOU | 38 | 0.38 | 38 | 0.42 | 39 | 0.47 | 42 | 0.49 | 42 | 0.50 | 42 | 0.50 | 42 | 0.49 |
| | 21 | 0.67 | 21 | 0.68 | 22 | 0.70 | 24 | 0.71 | 24 | 0.70 | 24 | 0.69 | 24 | 0.70 |
| MAR | 16 | 0.73 | 16 | 0.62 | 16 | 0.62 | 18 | 0.57 | 18 | 0.61 | 18 | 0.65 | 18 | 0.66 |
| | 6 | 0.93 | 6 | 0.88 | 6 | 0.88 | 8 | 0.63 | 8 | 0.68 | 8 | 0.73 | 8 | 0.75 |
| MEM | 40 | 0.41 | 40 | 0.46 | 40 | 0.44 | 41 | 0.45 | 41 | 0.47 | 41 | 0.45 | 41 | 0.43 |
| | 22 | 0.56 | 22 | 0.57 | 22 | 0.56 | 23 | 0.57 | 23 | 0.57 | 23 | 0.55 | 23 | 0.54 |
| ODV | 31 | 0.61 | 31 | 0.64 | 31 | 0.66 | 33 | 0.65 | 33 | 0.63 | 33 | 0.61 | 33 | 0.60 |
| | 16 | 0.83 | 16 | 0.86 | 16 | 0.88 | 18 | 0.81 | 18 | 0.80 | 18 | 0.79 | 18 | 0.79 |
| OLV | 20 | 0.51 | 23 | 0.51 | 25 | 0.71 | 25 | 0.72 | 27 | 0.73 | 27 | 0.73 | 27 | 0.73 |
| | 11 | 0.66 | 12 | 0.66 | 13 | 0.84 | 13 | 0.83 | 13 | 0.81 | 13 | 0.78 | 13 | 0.76 |
| REB | 32 | 0.46 | 33 | 0.51 | 34 | 0.49 | 35 | 0.44 | 36 | 0.44 | 37 | 0.43 | 37 | 0.44 |
| | 18 | 0.63 | 19 | 0.66 | 20 | 0.62 | 20 | 0.60 | 21 | 0.62 | 21 | 0.63 | 21 | 0.66 |
| CAS | 31 | 0.56 | 32 | 0.61 | 32 | 0.62 | 32 | 0.65 | 32 | 0.66 | 32 | 0.67 | 32 | 0.68 |
| | 17 | 0.63 | 17 | 0.70 | 17 | 0.71 | 17 | 0.71 | 17 | 0.73 | 17 | 0.75 | 17 | 0.77 |
| ENT | 39 | 0.61 | 41 | 0.65 | 41 | 0.62 | 41 | 0.62 | 42 | 0.64 | 42 | 0.63 | 42 | 0.64 |
| | 23 | 0.76 | 24 | 0.77 | 24 | 0.74 | 24 | 0.74 | 24 | 0.74 | 24 | 0.74 | 24 | 0.75 |
| LIB | 40 | 0.42 | 41 | 0.38 | 42 | 0.43 | 42 | 0.49 | 42 | 0.51 | 42 | 0.55 | 42 | 0.57 |
| | 22 | 0.65 | 23 | 0.59 | 24 | 0.69 | 24 | 0.76 | 24 | 0.78 | 24 | 0.81 | 24 | 0.81 |
| ESC | 41 | 0.42 | 41 | 0.49 | 41 | 0.47 | 41 | 0.45 | 42 | 0.45 | 42 | 0.45 | 42 | 0.45 |
| | 24 | 0.41 | 24 | 0.51 | 24 | 0.53 | 24 | 0.57 | 24 | 0.62 | 24 | 0.66 | 24 | 0.67 |
| LAV | 21 | 0.53 | 22 | 0.57 | 22 | 0.60 | 22 | 0.63 | 22 | 0.66 | 22 | 0.70 | 22 | 0.70 |
| | 13 | 0.61 | 13 | 0.57 | 13 | 0.64 | 13 | 0.68 | 13 | 0.72 | 13 | 0.76 | 13 | 0.77 |

Time averaging $PM_{10}$ concentrations to progressively higher time periods improved overall correlation from 0.48 to 0.58 in the full dataset and from 0.59 to 0.71 in the seasonal dataset. It also increases the number of points, 382 to 414, in the first case and 214 to 230 in the second, since stations previously with no data at the hour of measurement closest to the satellite time of passage can now be included in the analysis. The same occurred for most individual stations when the dataset was divided according to season and station type . For those reasons, all subsequent results will be presented using station daily average $PM_{10}$ concentration values (corresponding to the 24h time period).

Considering only polluted images with a reference image from the same season also improved considerably the individual stations, station types and overall AOT/$PM_{10}$ correlation (0.58 to 0.71) but decreased the number of points from 414 to 230. Correlation strength depended heavily on winter and summer results, with a significant increase in this last season, from 0.51 to 0.58 and very similar values for both datasets in winter (0.69 and 0.68). Both autumn and spring presented negligible correlations, 0.02 and 0.07, respectively, and a significant decrease in the number of available images.

In fact, dividing the dataset per season made evident seasonal differences in AOT/$PM_{10}$ correlation strength and respective slopes (see also Figure 4.8).

Winter days, with the broadest daily average $PM_{10}$ range and highest mean, from -10 to 100 $\mu g/m^3$, for the full dataset, and an average of 25.18 $\mu g/m^3$, presented the best AOT/$PM_{10}$ fit (r=0.69). It also presented the highest slope (152.13), corresponding to an increase of 15 $\mu g/m^3$ per each 0.1 in AOT. The range, correlation coefficient and slope are similar for the same season dataset.

Summer points, with a mean of 8.77 $\mu g/m^3$ and a range between -30 and 50 $\mu g/m^3$, showed a lower correlation coefficient (0.51) and slope (71.70), lowering the AOT/$PM_{10}$ increase rate to half of the winter rate. Introducing the reference/polluted same season criteria, improved AOT/$PM_{10}$ correlation coefficient (r=0.58) and increased slope to 99.83, a value closer to the observed for the winter images.

Spring and autumn presented a more erratic behaviour. The first, with a mean of 8.64 $\mu g/m^3$ and a range between -30 and 50 $\mu g/m^3$ for the full dataset,

presented a correlation coefficient of 0.59 and a slope of 86.93. Both parameters decreased significantly to negligible values in the second dataset, due mainly to the reduction of the spring dataset to a single image of low and limited range.

Finally, autumn presents an almost negligible correlation in both datasets, 0.16 and 0.07, respectively, slope (33.12 and 8.93) and the lowest mean daily average $PM_{10}$ concentration (6.10 $\mu g/m^3$).

The correlation behaviour in spring and autumn for both datasets might be associated to two factors: a) the narrow AOT value, with a higher incidence of low AOT values, as seen in other PM/AOT studies (Engel-Cox *et al.*, 2004 and Gupta *et al.* 2006); b) the higher short term vegetation related reflectance changes, characteristic of these transitional seasons (Brest, 1987; Zhou *et al.*, 2003). Regarding the second reason, air quality stations in the Lisbon Metropolitan Area are implemented in urban areas and, before DTA calculations, agriculture related pixels were masked. Nevertheless, the presence of some residual pixels from this class and some forest content, mainly agro-forested areas and shrublands, might cause DTA AOT to lose accuracy. These land cover types are more influential in suburban areas affecting the vicinity of stations like Loures, Odivelas, Quinta do Marquês and Mem-Martins. For this reason, using polluted/reference pairs from different seasons might result in less optimal AOT estimates. Since the main objective of this study is to retrieve significant relations between AOT and $PM_{10}$ the regression model results presented in the next sections refer only to the same season dataset.

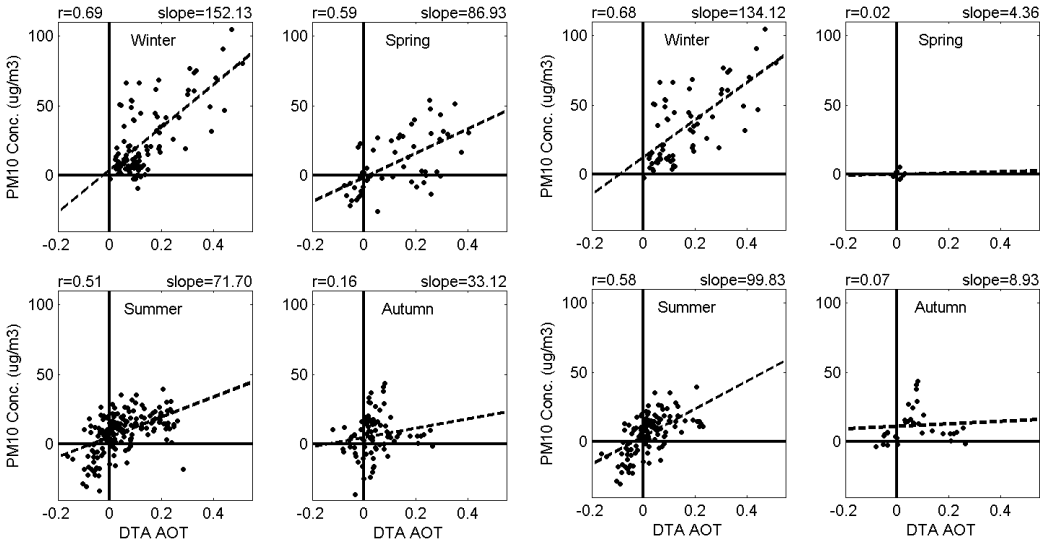


**Figure 4.8 - AOT/$PM_{10}$ Daily Average Scatter plot per season, including information on correlation coefficient (r) and slope. Right graphs refer to results using the entire dataset, left graphs is using only pairs of reference/polluted images from the same season. Solid lines correspond to the x and y axis and dotted line to the regression line.**

Results according to station type for the original dataset (Table 4.6 and Figure 4.9) presented a very similar behaviour for background, traffic and industrial stations. The higher $PM_{10}$ daily average variability of traffic and industrial stations and consequent lower spatial representativity, didn't affect the respective correlation, with obtained values similar to the ones from background stations. The predominance of lower $PM_{10}$ values, heighten by the need to subtract reference values, is evident in the scatter plot that includes data from all stations (bottom right), showing a significant cluster of values bellow 25 $\mu g/m^3$. Slope values are also similar, ranging from 88 to 114, which corresponds to an increase of about 9 to 11 $\mu g/m^3$ for each 0.1 increase in AOT, while intercept values range from 2 to 5 $\mu g/m^3$.

Conclusions for the same season dataset are similar, although correlation coefficients and corresponding slope for all station types increased significantly, to a range of 0.69-0.75 and 149.58-108.66. When analysing the same season dataset correlation, and by comparing with the full dataset (bottom right graph of each column in Figure 4.9), the most distinctive trace is the lower number of

high AOT/low $PM_{10}$ points, which increases slope and provides a better fit for higher $PM_{10}$ values.

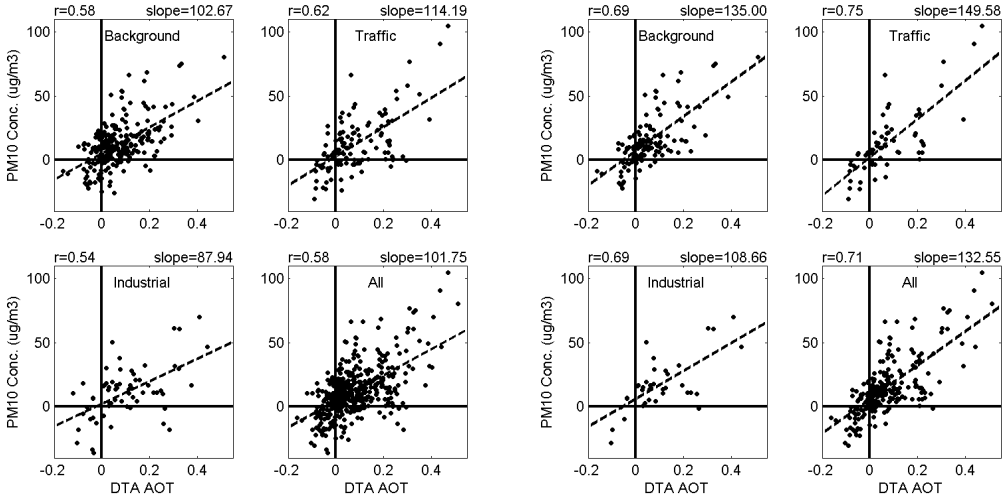


**Figure 4.9 – AOT/$PM_{10}$ Daily Average Scatter plot per station type, including information on correlation coefficient (r) and slope. Right graphs refer to results using the entire dataset, left graphs is using only pairs of reference/polluted images from the same season. Solid lines correspond to the x and y axis and dotted line to the regression line.**

The maps in Figure 4.10 and Figure 4.11 provide a per station analysis of mean $PM_{10}$ and AOT as well as correlation strength and slope for the two datasets.

The two first parameters (Figure 4.10) show a similar spatial behaviour for both datasets: higher $PM_{10}$ values for stations within Lisbon city perimeter (Avenida da Liberdade, Entrecampos e Olivais), decreasing as you move outwards to the south of the city into the urban/industrial areas in the south margin of the Tagus estuary (Laranjeiro, Escavadeira e Lavradio) and to the suburban areas into the northwest (Loures, Odivelas, Reboleira). The lowest values are reported in the west and northwest fringe of the metropolitan area, in the stations of Mem-Martins and Cascais. The exception to this pattern is Quinta do Marquês, to the west of the city, presenting $PM_{10}$ values comparable to the city centre and even higher AOT values. An overall increase in mean $PM_{10}$ and AOT values is observed from one dataset to the other, as previously mentioned.

Correlation slope (Figure 4.11, last pair of images) shows a similar pattern of decreasing values as urban content decreases, for both datasets, implying a lower AOT sensitivity to $PM_{10}$ changes in suburban areas.

Correlation coefficient (Figure 4.11, first pair of images) shows a more homogeneous pattern, with most values concentrated in the 0.5-0.6 and 0.6-0.7 classes. Nevertheless lower values can be found in the Loures, Mem-Martins and Reboleira, typical suburban areas in the north and northwest part of the Lisbon Metropolitan Area, and Escavadeira, an industrial site to the south. Correlation coefficient improves for all stations in the second dataset, with values concentrated in the 0.6-0.7 and 0.7-0.8 classes, but the lower relative values in the referred suburban stations are maintained. These results seem to emphasize the importance of the predominance of an urban land cover for the successful implementation of the DTA algorithm. Even though significant correlations are obtained for suburban areas around the city centre, the influence of forest and residual agricultural areas seem to have an negative effect in the quality of AOT retrievals, lowering the overall AOT/$PM_{10}$ correlation.

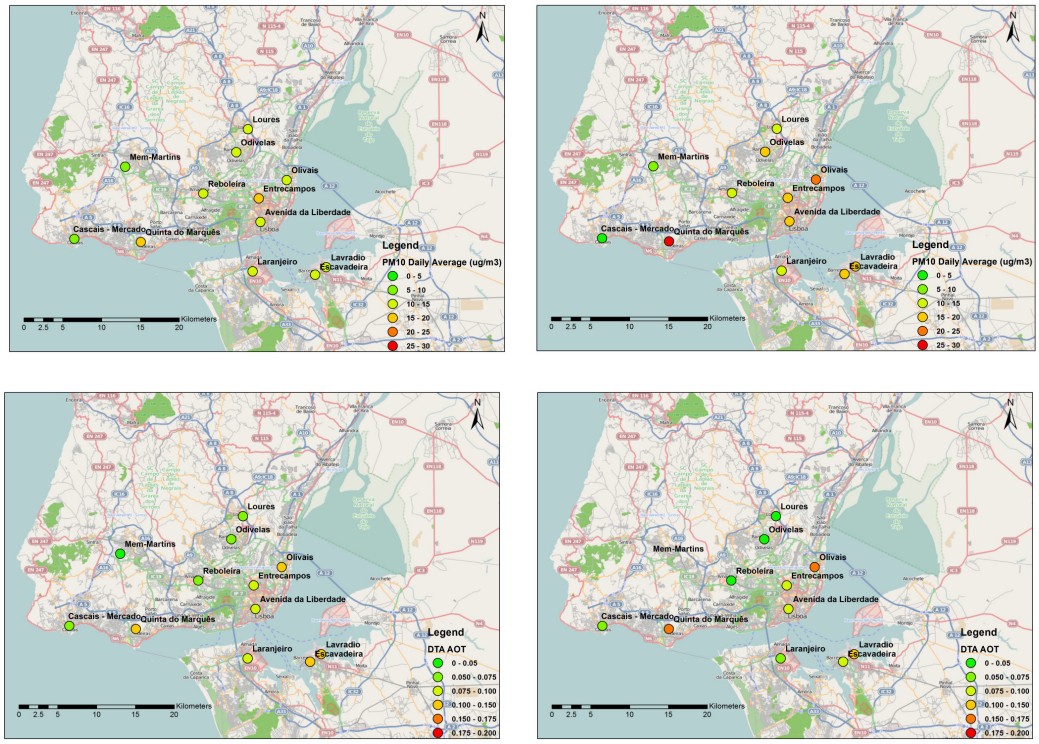


**Figure 4.10 – Air quality network maps showing, from top to bottom, the mean $PM_{10}$, the mean AOT. Left column refers to the full dataset and right to the dataset only with polluted/reference image pairs from the same season**

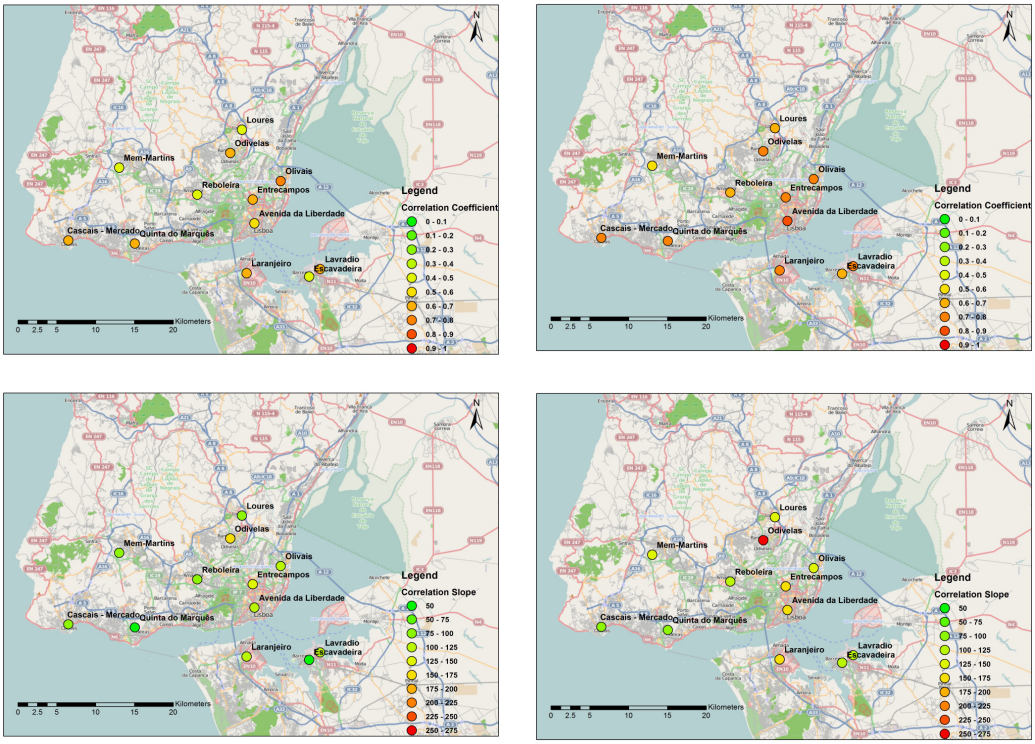


**Figure 4.11 – Air quality network maps showing, from top to bottom, the correlation coefficient and regression slope between AOT and $PM_{10}$ daily average concentration per station. Left column refers to the full dataset and right to the dataset only with polluted/reference image pairs from the same season**

Finally, averaging all station values for AOT and $PM_{10}$ for each day in the full and same season dataset improved correlation from 0.58 and 0.71 to 0.65 and 0.82, respectively. This was expected since, as stated in the data and methods section, it provides a daily spatial average of both variables which partially attenuates the differences in spatial representativity inherent to their respective nature. As observed for previous results the gain in correlation from the full to the same season dataset seems to be achieved mainly through the removal of high AOT/low $PM_{10}$ points, indicating a possible tendency for AOT overestimation due to seasonal reflectance differences when reference/polluted image pairs from different seasons are used.

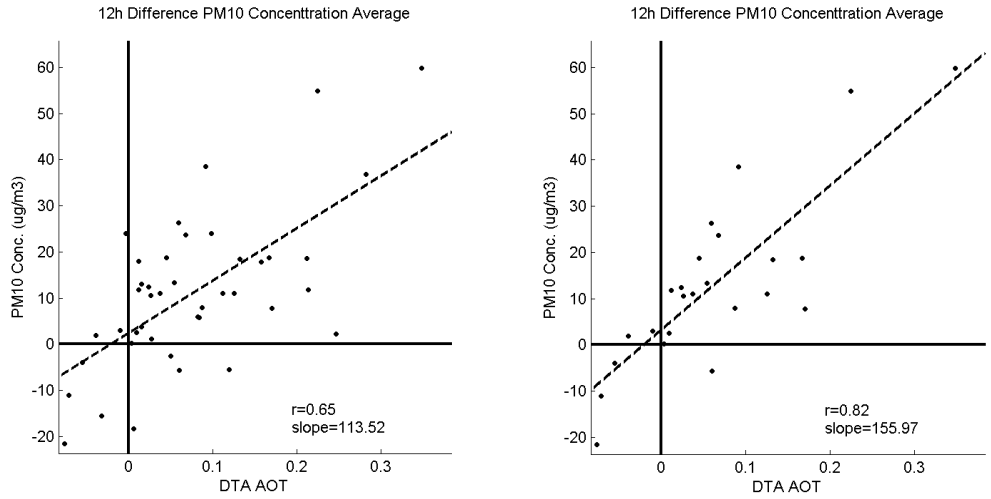


**Figure 4.12 - AOT/$PM_{10}$ mean daily average scatter plot, including information on correlation coefficient (r), slope (slope). Right graphs refer to results using the entire dataset, left graphs is using only pairs of reference/polluted images from the same season. Solid lines correspond to the x and y axis and dotted line to the regression line.**

### 4.3.3 Characterization of the meteorological datasets and their relationships with $PM_{10}$ and AOT

This section will characterize a set of meteorological parameters daily values, measured in the Gago Coutinho meteorological station in the city centre. It will also try to determine how those meteorological variables affect daily average $PM_{10}$ concentrations and daily DTA AOT values. The parameters were chosen based on their influence in air pollution dispersion, as explained in the texts associated with the graphs presented below.

Results presented include, for each parameter, the full annual time series aggregated daily and monthly and the time series of days with AOT measurements (only for reference/polluted same season dataset), plotted together with the respective $PM_{10}$ values.

A second set of graphs include scatter plots of each meteorological parameter plotted against daily $PM_{10}$ values, also for the full annual dataset and the days with AOT measurements. For this last group, scatter plots were made not only for $PM_{10}$ polluted image values but also for $PM_{10}$ polluted/reference concentration differences and the respective AOT values.

This set of graphs will provide information on: a) the yearly relation between the two variables; b) differences between the $PM_{10}$ yearly relation and the relation considering only the dataset of images with AOT measurements; c) possible relationship differences when considering $PM_{10}$ concentration differences and d) possible differences between AOT and $PM_{10}$ dependence.

The objective is not only to investigate the nature of the relationship between the different involved variables for the satellite dataset but also to offer insight on the representativeness of those relationships in a yearly context. This representativeness analysis is relevant considering satellite data covers less than 10% of all days of the year and corresponds to cloud free days, which might skew considerably the $PM_{10}$ dispersion conditions.

**Table 4.7 – Main statistics (minimum Min; maximum – Max; mean – Mean and standard deviation – Std. Dev.) calculated for all meteorological variables considering the full yearly dataset and only the dates with DTA AOT estimates**

| | Year | | | | Dates with DTA values | | | |
|---|---|---|---|---|---|---|---|---|
| Variables | Min | Max | Mean | Std.Dev. | Min | Max | Mean | Std.Dev. |
| P (hPa) | 989.70 | 1024.90 | 1006.22 | 5.68 | 1000.20 | 1023.00 | 1008.40 | 6.81 |
| $T_{mean}$ (ºC) | 4.90 | 31.40 | 16.64 | 5.48 | 7.30 | 31.40 | 19.14 | 6.56 |
| $U_{mean}$ (m/s) | 1.00 | 8.90 | 3.36 | 1.16 | 1.20 | 5.30 | 3.33 | 1.16 |
| RH (%) | 22.00 | 97.00 | 67.31 | 14.69 | 22.00 | 81.00 | 57.54 | 15.23 |
| MLH (m) | 139.00 | 3207.00 | 1263.69 | 544.85 | 384.00 | 2682.00 | 1311.69 | 684.99 |

Table 4.7 presents minimum, maximum, mean and standard deviation values for all meteorological variables used, as measured in the Gago Coutinho meteorological station. A more detailed description of the provided information, together with the graphs for each meteorological parameter, is presented in the following pages.

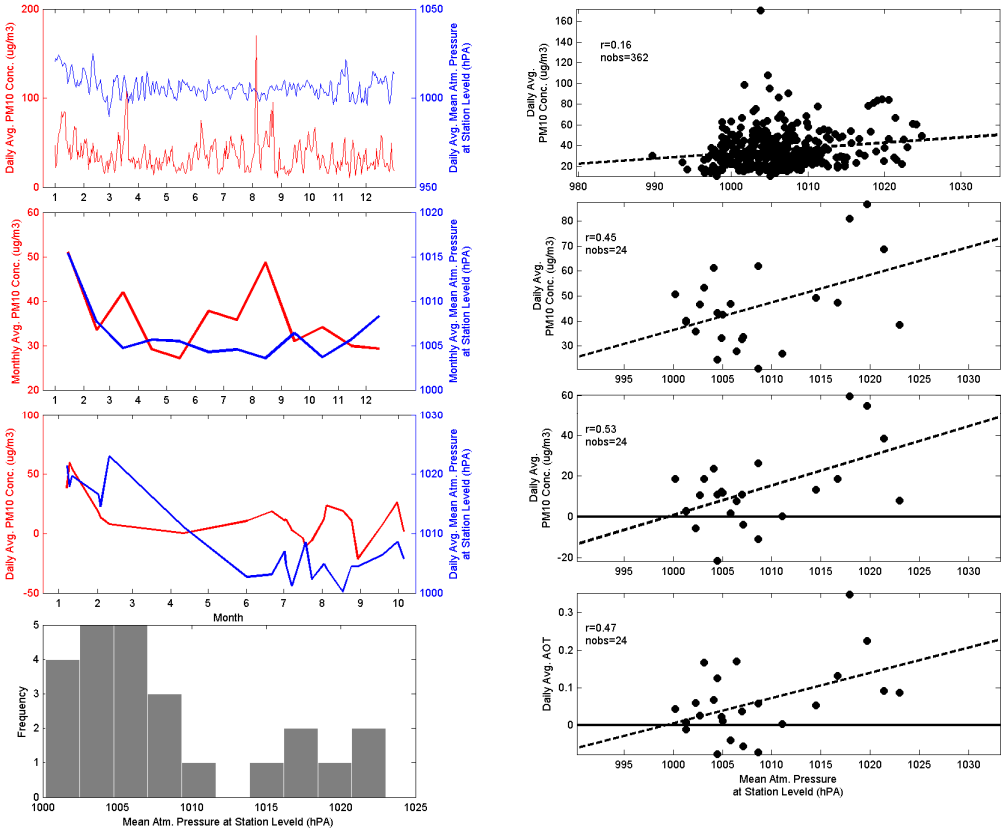


(a) (b)

**Figure 4.13 – (a) Left side -Daily and monthly Mean Atmospheric Pressure at Station Level Time Series and respective daily histogram (from top to bottom); (b) Right side: Scatter plot relating Mean Atmospheric Pressure at Station Level with daily average $PM_{10}$ concentration for all days of the year, all polluted images, daily $PM_{10}$ concentration differences and daily AOT.**

Annual mean atmospheric pressure values at station level varied in 2005 between 980 and 1024 hPa with an average of 1006 hPa and a standard deviation of 5.68 hPa (Table 4.7). The range for the MODIS images dataset is a slightly lower, between 1000 and 1023 hPa, but corresponds to a higher mean of 1008 hPa and standard deviation (6.81 hPa). Both datasets show a tendency for air pressure values below the average pressure level at sea level (1013.25 hPa).

Time series analysis shows that lower pressure values and inter-daily variations are usually associated with summer conditions. Mean atmospheric pressure tends to increase during spring and autumn and reach maximum values and variability during winter (Figure 4.13(a), first two graphs). This result is

consistent since usually higher atmospheric pressures are associated with colder and denser air masses at ground level, characteristic of winter and lower values with warmer and lighter summer air masses.

Analysing the evolution of daily $PM_{10}$ averages with atmospheric pressure for the entire year (Figure 4.13(b), top graph) and considering only the MODIS image dates (Figure 4.13(b), second graph), a positive correlation can be found between the two variables. This correlation seems to be more evident for pressure values higher than 1005-1010 hPa. This can be attested by the increase in correlation coefficient from the yearly dataset (r=0.16) to the MODIS dataset (r=0.45), where those higher atmospheric pressure values are more frequent.

This relationship is maintained and even strengthened for $PM_{10}$ concentrations differences (r=0.54) (Figure 4.13(b), third graph) and DTA AOT (r=0.47) (Figure 4.13(b), bottom graph). It can be partially explained by the relationship between higher atmospheric pressure values and more stable air dispersion conditions given by colder air masses at surface level, more frequent during winter. These circumstances can sometimes even be associated with thermal inversion phenomena, leading to extremely low mixing layer heights and higher air pollutant concentrations at ground level. These conditions are ideal for AOT/$PM_{10}$ correlation, since most atmospheric aerosol content is concentrated near ground level.

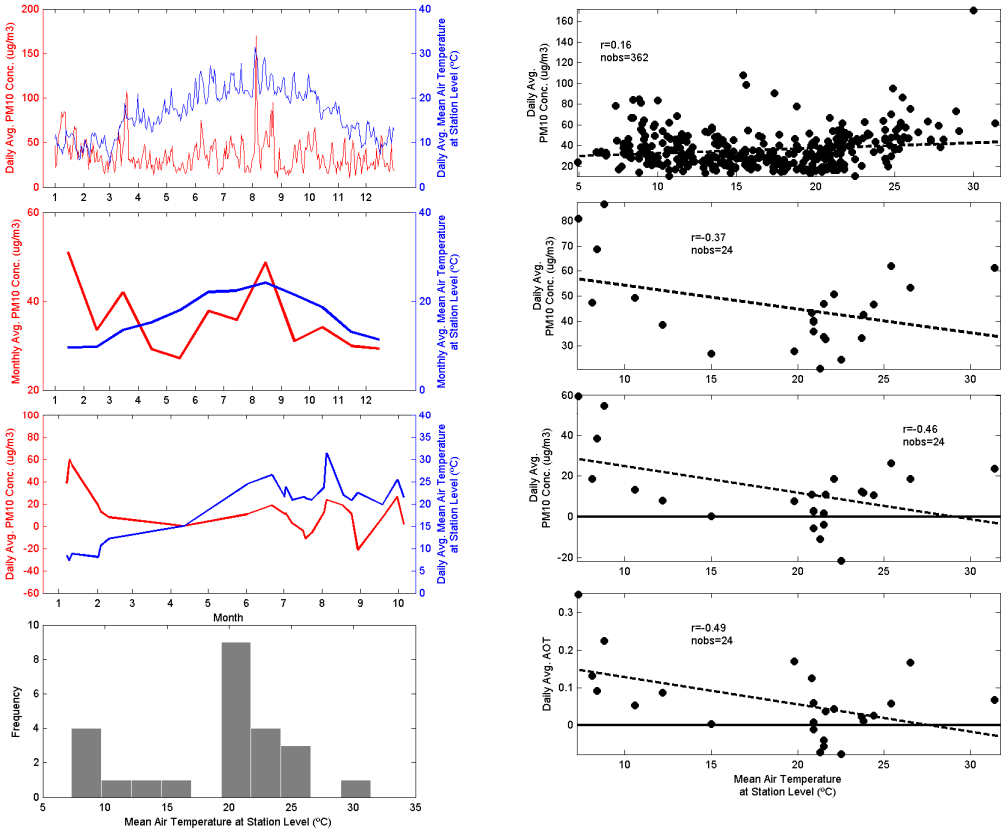


(a) (b)

**Figure 4.14 – (a) Right Side: Daily and monthly average Mean Air Temperature at Station Level Time Series and respective daily histogram (from top to bottom); (b) Left side: Scatter plot relating daily average Mean Air Temperature at Station Level with daily average $PM_{10}$ concentration for all days of the year, all polluted images, daily $PM_{10}$ concentration differences and daily AOT (from top to bottom).**

Table 4.7 shows 2005 daily mean temperature values at station level for the Lisbon Metropolitan Area, ranging from a minimum 4.9ºC to a maximum of 31.4ºC, with an average value of 16.64ºC and a standard deviation of 5.48ºC. In comparison, the MODIS dataset presents a higher minimum, mean and standard deviation values, 7.30, 19.14 and 6.56ºC, respectively.

As expected, higher temperature values could be found during summer, which progressively decreased trough spring and autumn, reaching minimum values in winter (first two graphs in Figure 4.14(a)).

Meaningful associations between $PM_{10}$ and mean air temperature at ground level were found in the full year dataset for both low and high ranges of

temperature values (Figure 4.14(b), top graph). Low temperature/high $PM_{10}$ association can be explained by the presence of winter colder air masses during high pressure events, as previously explained. The high temperature/high $PM_{10}$ concentration events might be attributed to several factors, usually associated with summer: a) lower precipitation (especially in 2005), leading to higher PM accumulated concentrations and a higher influence of road and soil particle resuspension events (Barmpadimos *et al.*, 2011); c) higher production of secondary aerosols associated with the increased production of biogenic Volatile Organic Compounds (VOC) (Barmpadimos *et al.*, 2011) b) Sahara dust transport events, more frequent during spring and summer (Franco, 2008, Santos *et al.*, 2008); c) higher influence of forest fire related biogenic aerosols (Franco, 2008, Santos *et al.*, 2008, Calvo *et al.*, 2011). In the MODIS dataset the relationship between low temperatures and high $PM_{10}$ concentrations prevail (Figure 4.14(b)), when considering either absolute polluted concentrations (r=-0.37), concentration differences (r=-0.46) or AOT values (r=-0.49), contrarily to what happens in the full dataset (r=0.16).

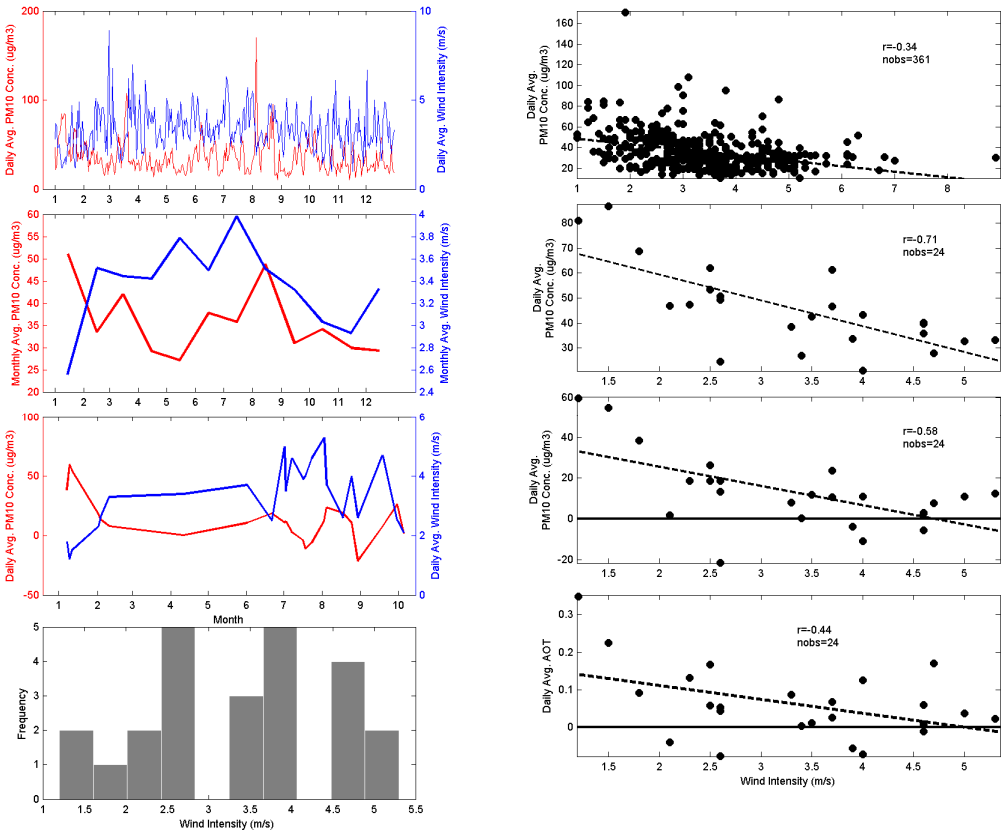


(a) (b)

**Figure 4.15 – (a) Left side: Daily and monthly average Wind Speed Time Series and respective daily histogram (from top to bottom) for the year 2005; (b) Right Side: Scatter plots relating daily average Mean Air Temperature with daily average $PM_{10}$ concentration for all days of the year, all polluted images, concentration differences (polluted –reference) and daily AOT (from top to bottom) for the year 2005.**

Wind speed values for the year 2005 vary between 1 and 8.9 m/s and present an average value of 3.36 m/s and a standard deviation of 1.16 m/s (Table 4.7). By comparison, the MODIS dataset presents a lower maximum value (5.30 m/s) and average (3.33 m/s).

As the first two graphs in Figure 4.15(a) show, higher wind intensities can be found during February, all through spring and early summer (peaking in July).

As anticipated, $PM_{10}$ and wind speed establish a significant negative correlation for all datasets (first three graphs of Figure 4.15(b)), since wind operates as one of the main air pollution dispersion factors. In the yearly dataset, the cor-

relation is nearly linear for wind intensities lower than 3.5 m/s and loses significance after that threshold. The $PM_{10}$ polluted concentrations MODIS dataset, presents an even higher correlation (r=0.71) and a strong linearity in its entire domain. The correlation coefficient decreases to 0.58 for $PM_{10}$ polluted/reference concentration differences and to 0.44 for DTA AOT. This lower correlation with AOT was foreseeable since wind speed is only characteristic of dispersion conditions at ground level and might not as representative of conditions in the entire atmospheric column.

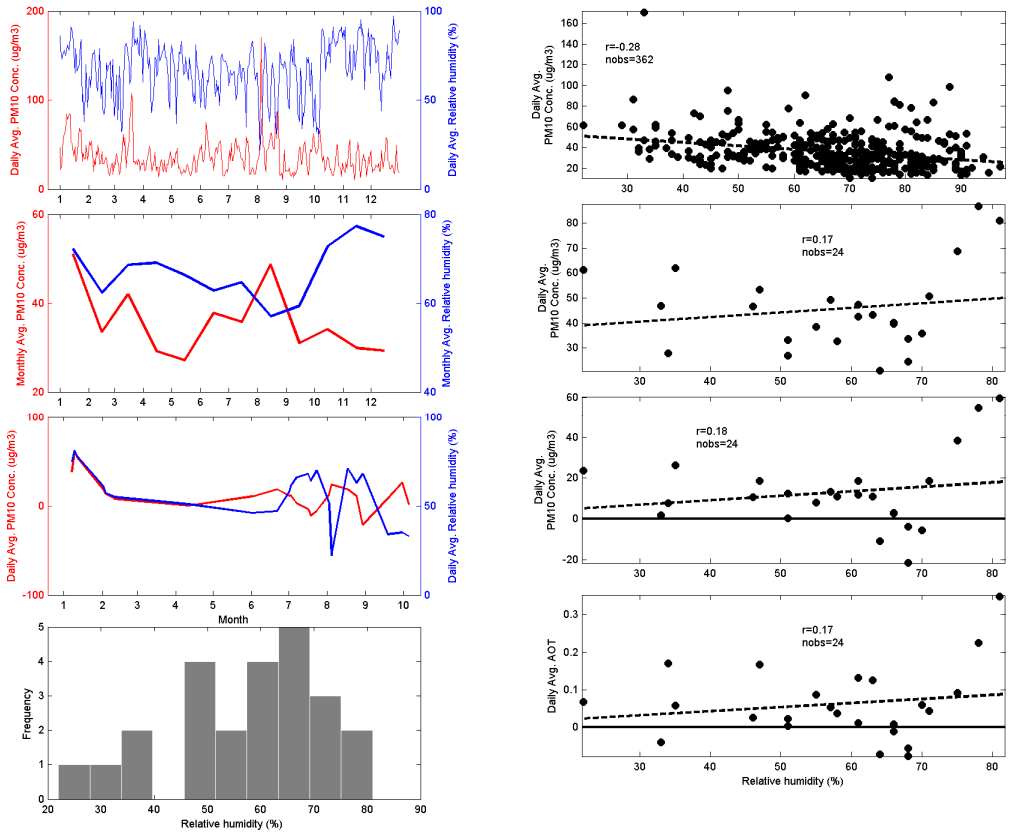


(a) (b)

**Figure 4.16 – (a) Left side: Daily and monthly average Relative Humitidy Time Series and respective daily histogram (from top to bottom); (b) Right Side: Scatter plot relating daily average Relative Humitidy with daily average $PM_{10}$ concentration for all days of the year, all polluted images, daily $PM_{10}$ concentration differences and daily AOT (from top to bottom).**

Annual relative humidity statistics, presented in Table 4.7, show a wider range (22-97%) and a higher mean (67.31%), when compared to the MODIS datsaset (range – 22-81% and mean-57.54%).

Seasonal variations, shown in Figure 4.16(a), are characterized by an overall decrease from a 70% monthly mean in December to 55% in August and an abrupt increase in October to values around 75%, maintained through November and December.

The yearly dataset shows a negative correlation between relative humidity and $PM_{10}$ concentration (r=-0.28, Figure 4.16(b), top graph). This might related to the same drivers behind the high temperature/high $PM_{10}$ concentration

events, namely, resuspension, forest fires and dust transport events, usually associated with low relative humidity mean daily values. Nevertheless for the MODIS dataset some high relative humidity (>70%) days show a very strong positive correlation with $PM_{10}$ values (Figure 4.16(b), second graph). They mask the prevailing opposite effect seen in the yearly dataset and establish a relationship where no significant linear correlation can be found between the two parameters (r=0.17). This effect is also seen for concentration differences and AOT.

This increase in both AOT and $PM_{10}$ for high relative humidity values might be associated with a hygroscopic aerosol growth phenomenon. In fact several studies show that, due to the hygroscopic properties of aerosols, relative humidity can significantly change their size and composition, resulting in differences in the light scattering properties of aerosols (Robles González *et al.* 2003, Meier *et al.*, 2009, Flores *et al.*, 2012). Properties like the scattering coefficient or the growth factor of aerosols increase exponentially when the relative humidity reaches a certain threshold. The definition of this threshold is not simple and depends on the many factors including the nature of the aerosols in terms of chemical composition. For instance, sea salt aerosols are more hygroscopic than dust or carbonaceous aerosols and therefore more sensitive to changes in light scattering properties due to water vapour. Nevertheless usually this relative humidity threshold varies between 70 and 80% for urban aerosols. After reaching this threshold the optical thickness increases significantly, making it impossible to distinguish the aerosol from the water vapour contribution. This phenomenon can also be responsible for an overestimation of $PM_{10}$ concentrations since beta ray attenuation monitors, used in the Lisbon Metropolitan Area, can also be influenced by high relative humidity (Gobeli *et al.*, 2008). Nevertheless, there is insufficient data to attribute this higher $PM_{10}$ and AOT values to the effect of aerosol hygroscopic growth.

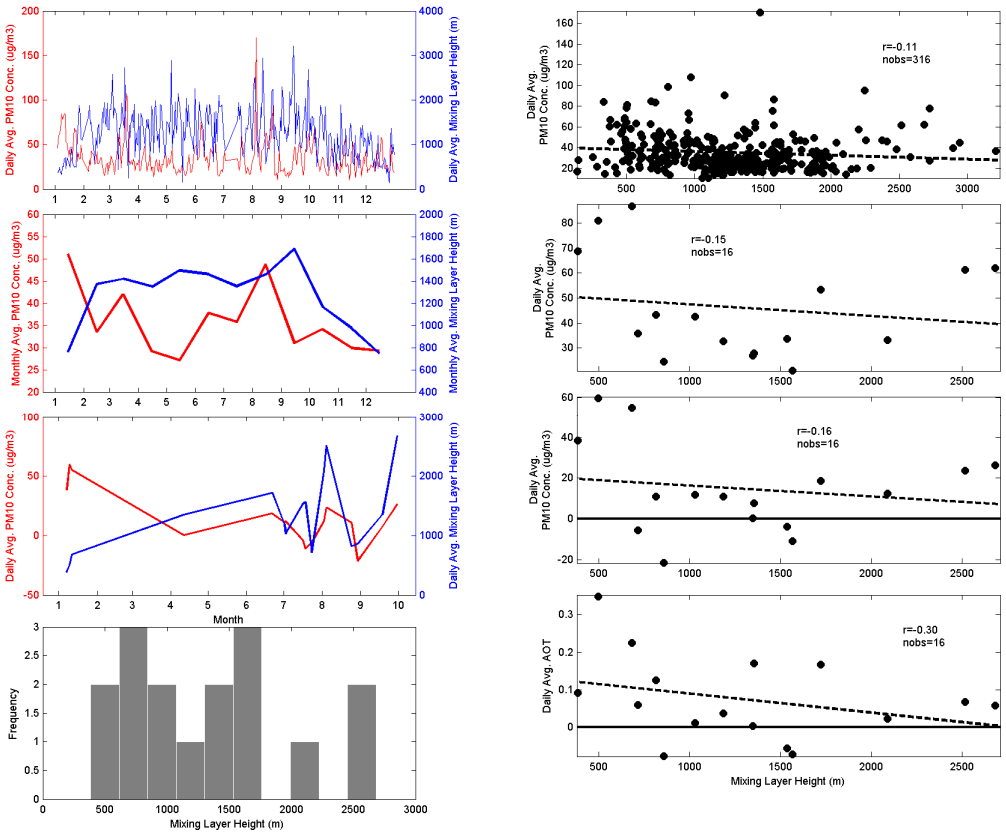


(a) (b)

**Figure 4.17 – (a) Left side: Daily and monthly average Mixing Layer Height Time Series and respective daily histogram (from top to bottom); (b) Right Side: Scatter plot relating daily average Mixing Layer Height with daily average $PM_{10}$ concentration for all days of the year, all polluted images, daily $PM_{10}$ concentration differences and daily AOT (from top to bottom).**

According to Table 4.7, mixing layer height values vary between 139 and 3207 m, presenting a mean value of 1263.69 m and a standard deviation of 544.85. This range decreases in the MODIS dataset to 384-2682 m, although mean and standard deviation increase to 1311.69 and 684.99 m.

This variable presents a pronounced intra-daily cycle, closely related to air temperature daily variation, with lower values during the nocturnal cycle, which progressively increase during the morning, reaching a peak around noon that is maintained until it starts to decrease during late afternoon. A similar temperature driven evolution can be found seasonally (Figure 4.17(a)), with lower mixing layer heights means (near 700 m) during the coldest months, Jan-

uary and December. Those values increase significantly to 1300 m in February, a level that remains more or less stable until August. After this month values rises again, reaching a 1700 m peak monthly mean value in September and decreasing abruptly in the following months until reaching December levels.

Therefore the relationship with yearly $PM_{10}$ concentrations (Figure 4.17(b), top graph) is similar to the one observed for temperature, approximating a quadratic curve form, with increasing $PM_{10}$ values for mixing layers lower than 1000 m and higher than 2000 m. This can be explained by combining two factors. On one hand, lower mixing layer heights lead to higher $PM_{10}$ values since most particles remain concentrated in the atmospheric levels near the ground (Rost *et al.*, 2009). On the other hand, higher mixing layer heights are associated with warmer days, characterized with a higher incidence of resuspension, forest fire and dust events, responsible for higher $PM_{10}$ levels.

The MODIS dataset seems to replicate this behaviour, (Figure 4.17(b), second and third graphs) but with a higher predominance of low mixing layer height days. The linear correlation, considering the entire domain of layer height values, is not significant, with correlation coefficients of 0.17 and 0.16 for absolute and difference $PM_{10}$ concentration values, respectively. AOT presents a higher negative correlation coefficient (r=-0.3), since, contrarily to $PM_{10}$, it shows a small sensitivity to higher mixing layer heights. Although the image dataset is too small to reach any conclusion this might be due to the nature of the phenomena responsible for the increase in $PM_{10}$ at higher layer heights (eg., road resuspension events). Those types of phenomena produce a higher impact at ground level, whilst having a more limited effect in the total aerosol content of the atmospheric column.

As referred several times in this section, these meteorological parameters present some degree of dependence. Table 4.8 presents a correlation matrix for DTA AOT and each of those parameters to assess those dependences and identify possible collinearity problems that might arise when defining the multiple linear regressions models presented in the next sections. The lower part of the matrix refers to all days of the year and the upper part to days with MODIS images. The purpose of this comparison is, as in the previous figures, to assess if

the dependence relationships identified for the 24 image MODIS datasets are representative of their annual behaviour.

**Table 4.8 – Correlation matrix for all independent variables (daily values: upper part, for days with AOT values and lower part for all days of the year, identified by a bold font)**

| Variables | AOT | $U_{mean}$ | RH | MHL | $T_{mean}$ | P |
|---|---|---|---|---|---|---|
| AOT | - | -0,44 | 0,17 | -0,30 | -0,49 | 0,47 |
| $U_{mean}$ | **-** | - | -0,22 | 0,32 | 0,52 | -0,57 |
| RH | **-** | **-0,10** | - | -0,83 | -0,56 | 0,28 |
| MHL | **-** | **0,10** | **-0,44** | - | 0,75 | -0,46 |
| $T_{mean}$ | **-** | **0,08** | **-0,32** | **0,36** | - | -0,85 |
| P | **-** | **-0,29** | **-0,11** | **-0,17** | **-0,29** | - |

When comparing the two datasets is possible to verify that correlation signs are maintained for all entries but values are consistently higher for the MODIS dataset.

This feature could be attributed to the more limited set meteorological conditions present in the MODIS dataset. In fact, all of those images correspond to clear days, a requirement to extract optimal DTA AOT values, with typical profiles and relationships between meteorological parameters.

For instance, atmospheric pressure and temperature at ground level are inversely correlated in both datasets but the strength of the correlation is much higher in the MODIS dataset (r=-0.85). Typical summer unclouded days have a higher near surface temperature which causes the air to rise and pressure to drop. Those are the majority of days present in the satellite dataset. On the other hand, clean winter days are characterized by descending colder air masses, causing pressure near ground level to rise and temperature to drop.

This might also explain other high correlations involving mixing layer height with mean air temperature (r=0.75) and relative humidity (r=-0.83). For example, clear days with low mixing layer heights usually originate from descending colder air masses characterized by lower temperatures and higher relative humidity.

The three mentioned pairs of meteorological variables were the only to present correlation values indicative of possible collinearity problems. All other remaining independent variable pairs show overall low to medium correlation values.

### 4.3.4 Regression model for daily average $PM_{10}$ concentration estimation based on AOT values

During the previous result sections, some limitations were found regarding the required assumptions to implement a linear regression model, namely, the observed non-linearity in the relationships between $PM_{10}$ measured concentrations and some independent meteorological variables. Nevertheless the final set of results will attempt to derive $PM_{10}$ concentration estimation multiple linear regression models, for all stations daily average and Lisbon Metropolitan Area daily averages. It should be stated once more, before presenting the regression model results, that the $PM_{10}$ concentrations being estimated are not absolute values for the polluted images but their difference with $PM_{10}$ reference values.

All results refer only to the same season dataset. To test the robustness of the derived regression models and considering limited sample size (n=230), a bootstrapping technique was applied to resample the original dataset 1000 times to infer confidence intervals for several regression parameters. This technique was explained in more detail in the data and methods section.

The first regression model (Model A) includes only AOT as an explanatory variable. It will provide a first approach determine its ability to reproduce $PM_{10}$ station concentration measurements and provide information on the influence of each meteorological parameter on residuals behaviour.

The general regression formula for Model A is given by Equation 4.1

$$[PM10]_{\mu g/m^3} = \alpha + \beta_1 AOT \qquad \textbf{Equation 4.1}$$

The AOT and constant regression coefficients as well as correlation coefficient, root mean squared error (RMSE) and normalized root mean squared error (NRMSE) obtained for Model I and respective 2.5$^{th}$ and 97.5$^{th}$ percentile confidence interval are shown in Table 4.9.

Figure 4.18 presents the scatter plot of measured against estimated $PM_{10}$ concentrations and respective number of observations, $PM_{10}$, correlation coefficient, slope and intercept of the regression line between the two and the NRMSE.

**Table 4.9 – Model parameters obtained for Model A and respective 2.5th and 97.5th percentile confidence intervals obtained using a bootstrapping technique.**

| | Confidence intervals | | |
|---|---|---|---|
| Model parameter | 2.5th Percentile | Original dataset | 97.5th Percentile |
| $\alpha$ | 3.44 | 5.33 | 7.38 |
| $\beta_1$ | 110.51 | 132.55 | 152.17 |
| r | 0.61 | 0.71 | 0.78 |
| $r^2$ | 0.37 | 0.50 | 0.61 |
| RMSE | 13.51 | 15.22 | 16.79 |
| NRMSE | 0.92 | 1.04 | 1.14 |

The correlation coefficient confidence interval shows an overall moderate agreement between measured and estimated daily $PM_{10}$ concentrations, varying between 0.61 and 0.78. $R^2$ values indicate that Model A explains between 37% and 61% of the $PM_{10}$ variance and RMSE values vary between 13.51 and 16.79 $\mu g/m^3$. Nevertheless, NRMSE values are high, with a 95% confidence interval between 0.92 and 1.14. This is mainly due to the high incidence of low $PM_{10}$ values, mentioned in the earlier sections, with 63% of the values below the 15.22 $\mu g/m^3$ all dataset RMSE value).

According to the review paper presented by Hoff and Sundar (2009), the 110.51-152.17 AOT correlation coefficient interval presented here is in agreement with the regression coefficient found by Gupta *et al.* (2006) ($\beta_1$=141), when correlating AOT and daily concentrations of $PM_{10}$, but it is lower than the 214 coefficient found by Koelemeijer *et al.* (2006). This last work also presented a significant y axis offset (42.3), indicating a possible low AOT sensitivity to small $PM_{10}$ concentration values. The 0.5 slope value presented in Figure 4.18 indicates a tendency for $PM_{10}$ underestimation for values higher than 15-20 $\mu g/m^3$ and overestimation for lower values.

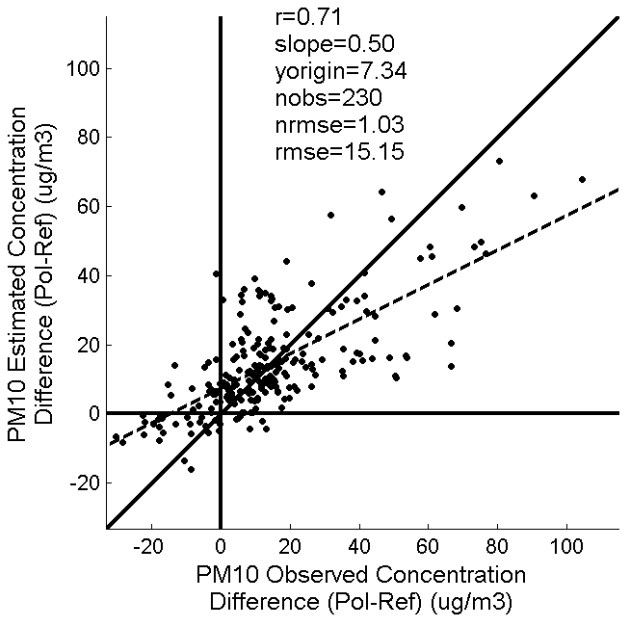


**Figure 4.18 – Scatter plot of measured against estimated daily average $PM_{10}$ concentration differences for Model A**

Histograms presented in Figure 4.19 complement the information given in the previous table and show that confidence intervals for all regression parameters are well constrained. AOT regression coefficients are positive for all bootstrapped datasets. This in accordance with theory, since an increase in PM leads to an increased extinction in the total atmospheric column and thus to an increase in AOT.

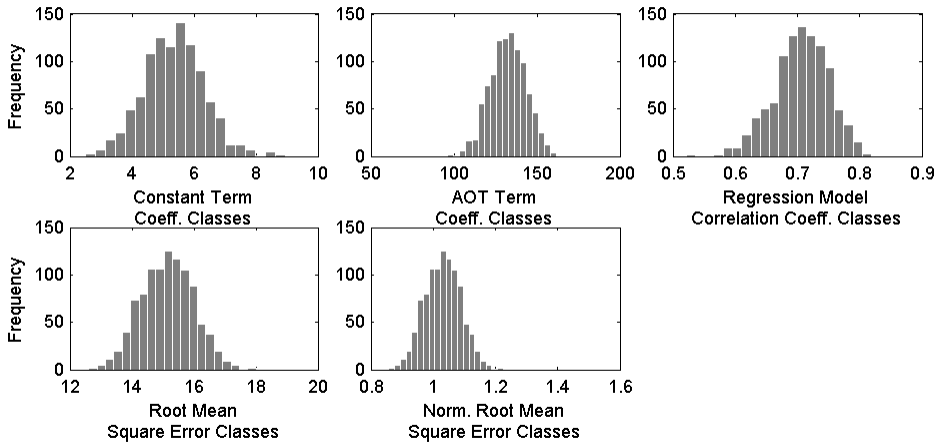


**Figure 4.19 – Histograms for all bootstrap derived multilinear regression coefficients and correlation and error statistics for Model A.**

Figure 4.20 displays a scatter plot of standardized residuals (residuals divided by their standard deviation) against estimated $PM_{10}$ daily concentrations and the independent variable AOT. The graphs provide information on error homoscedasticity (constant variance) over the entire result domain, a desired property for all regression models. Scatter plots against all meteorological variables introduced in the previous section are also included to investigate possible error dependence on those external variables.

Before analysing the results, it should be stated that residuals are calculated using the formula $[PM_{10}]_{measured}$-$[PM_{10}]_{estimated}$, meaning a positive residual refers to an underestimation and a negative to an overestimation.

The first two scatter plots (starting from the top left) demonstrated an homogeneous residual variance for all estimates and independent variable domain. Nevertheless a small increase in residuals' spread is observed for $PM_{10}$ estimated concentrations higher than 15 $\mu g/m^3$ (AOT>0.05).

Some error dependence were found for meteorological variables, especially wind speed, mean air temperature and atmospheric pressure:

a) $PM_{10}$ underestimation for low wind speed conditions and overestimation for high, following a significant linear negative correlation with a coefficient of -0.37;

b) $PM_{10}$ underestimation for days with low mean air temperature (relatively low negative correlation, r=-0.19) and high atmospheric pressure (second highest correlation, r=0.29);

c) $PM_{10}$ underestimation for high relative humidity (>70%) and mixing layer heights in both extremes (<750m and >2000m), although both with low linear correlation coefficients.

These results are comparable to the ones obtained between $PM_{10}$ and the same meteorological variables in the previous section. Although correlation coefficient values are low, they imply some influence from these variables in the estimation of $PM_{10}$ concentrations, justifying their inclusion in the models presented in the next sections.

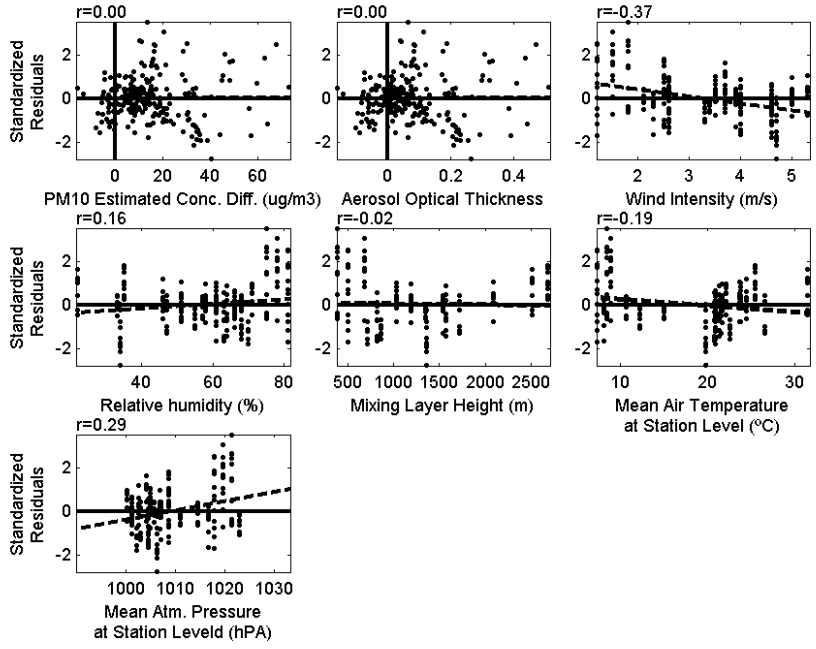


**Figure 4.20 – Model A standardized residuals plotted against the estimated $PM_{10}$ daily average concentrations differences (top graph), AOT and all considered meteorological variables.**

Finally a station analysis was performed to infer possible $PM_{10}$ estimation performance differences (Table 4.10). The bootstrapped stations datasets are relatively small and can be more affected by the resampling process causing the respective confidence intervals to be less consisted.

In fact this is confirmed by comparing the overall dataset RMSE and NRMSE confidence intervals with the stations confidence intervals, which are consistently wider and sometimes not as well centred around the values for the original dataset (with no bootstrap). This implies an ill constrained confidence interval that might arise from higher sensitivity to sample variability during the bootstrapping procedure.

RMSE confidence intervals lower and upper bounds vary respectively from 6.72 and 13.04 $\mu g/m^3$ in Loures (LOU) to 13.96 to 26.7 $\mu g/m^3$ in Entrecampos (ENT). NRMSE confidence interval bounds, on the other hand, vary from 0.24 and 0.93 in Quinta do Marquês (MAR) to 1.05 and 3.49 Mem-Martins (MEM).

Looking only at the NRMSE results as a comparative measure of station performance, the best results are achieved in two background stations, Quinta do Marquês, Olivais (OLV) and Lavradio (LAV) an industrial station. All show confidence intervals bounds lower than the ones presented for the entire dataset (Table 4.9). The other industrial station, Escavadeira (ESC), also demonstrates a good performance but presents a wider confidence interval and a higher bound than the overall dataset. This behaviour is also seen in Laranjeiro (LAR), Reboleira (REB), and all traffic stations, Cascais (CAS), Entrecampos e Avenida da Liberdade (LIB). The worst performing stations are Odivelas (ODV) and Mem-Martins, with almost both confidence intervals bounds higher than the NRMSE upper bound for the overall dataset. The good performance of the regression model for the two industrial stations was unexpected due to their lower spatial representativity, higher variability and DTA's AOT coarse resolution (20 km).

**Table 4.10 – Model A RMSE and NRMSE confidence intervals for all Lisbon Metropolitan Area air quality stations**

| | RMSE | | | NRMSE | | |
|---|---|---|---|---|---|---|
| | 2.5th Percentile | Original dataset | 97.5th Percentile | 2.5th Percentile | Original dataset | 97.5th Percentile |
| LAR | 10.70 | 14.94 | 18.67 | 0.82 | 1.15 | 1.78 |
| LOU | 6.72 | 10.15 | 13.04 | 0.59 | 0.98 | 1.63 |
| MAR | 7.54 | 11.62 | 15.07 | 0.21 | 0.45 | 0.93 |
| MEM | 9.86 | 15.64 | 20.66 | 1.05 | 1.93 | 3.49 |
| ODV | 8.54 | 18.31 | 24.99 | 1.00 | 1.76 | 3.05 |
| OLV | 11.83 | 17.97 | 22.56 | 0.43 | 0.69 | 1.06 |
| REB | 6.76 | 9.97 | 13.07 | 0.55 | 0.94 | 1.85 |
| CAS | 6.98 | 12.52 | 16.46 | 0.62 | 1.06 | 2.19 |
| ENT | 13.96 | 20.29 | 26.70 | 0.76 | 1.19 | 1.89 |
| LIB | 10.90 | 15.11 | 18.46 | 0.60 | 0.90 | 1.41 |
| ESC | 8.58 | 15.39 | 20.64 | 0.50 | 0.92 | 1.42 |
| LAV | 9.81 | 14.99 | 19.61 | 0.41 | 0.64 | 1.16 |

### 4.3.5 Multi regression model for $PM_{10}$ daily average concentration estimation based on AOT and selected meteorological variables

Model B is a multivariate linear regression model where the independent variables were chosen from an initial dataset consisting of the DTA AOT and all the meteorological variables introduced earlier. The stepwise fit based methodology used to select the most significant non collinear variables is described in detail in the data and methods section. Regression model parameters confidence intervals were defined using the same bootstrapping technique used in Model A.

It should be noted that only one daily values are available for each meteorological variable. Nevertheless, introducing these variables might help explain some $PM_{10}$ concentration inter-daily variability, while AOT provides also intra-daily differentiation between stations.

A natural logarithm transformation was used for the variables wind speed, relative humidity and mean air temperature to increase linearity in their relationship with $PM_{10}$ concentration (correlation coefficient increased, in absolute value, from 0.58, 0.09 and 0.46 to 0.68, 0.18 and 0.56, respectively). The mixing layer height parameter was removed from the study since it only had valid values for 16 of the 24 days and presented a very high correlation with relative humidity.

The stepwise fit based variable selection method results are presented in Table 4.11. AOT and ln($U_{mean}$) where chosen in all runs, contrarily to the remaining variables, who were only chosen 284 times, in the case of $P_{mean}$, 71 times, for RH and 53 for $T_{mean}$. Since none of these last three variables was chosen at least 50% of the stepwise fits, AOT and ln($U_{mean}$) were the only variables included in the regression model B. The inclusion of the transformed wind speed variable was expected following the strong correlation with $PM_{10}$ identified in section 4.3.3 and the consequent high error dependence verified in the previous model.

**Table 4.11 – Number of times the stepwise fit procedure selected each variable into the multiregression linear model using the bootstrapped datasets**

| | AOT | ln($U_{mean}$) | ln(RH) | ln($T_{mean}$) | $P_{mean}$ |
|---|---|---|---|---|---|
| Nº of selections | 1000 | 1000 | 71 | 53 | 284 |

The general regression formula for Model B is given by Equation 4.2

$$[PM10]_{\mu g/m^3} = \alpha + \beta_1 AOT + \beta_2 \ln(U_{mean}) \qquad \textbf{Equation 4.2}$$

Where α, $\beta_1$ and $\beta_2$ are respectively the regression coefficients for the constant term, AOT and ln($U_{mean}$). Table 4.12 presents the confidence intervals for all regression coefficients, respective correlation and error statistics, determined using the bootstrapped dataset samples.

**Table 4.12 - Model parameters obtained for Model B and respective 2.5th and 97.5th percentile confidence intervals obtained using a bootstrapping technique.**

| | Confidence intervals | | |
|---|---|---|---|
| Model parameter | 2.5th Percentile | Original dataset | 97.5th Percentile |
| α | 21.66 | 29.72 | 38.83 |
| $\beta_1$ | 75.30 | 97.69 | 121.25 |
| $\beta_2$ | -25.50 | -19.83 | -13.61 |
| r | 0.71 | 0.78 | 0.83 |
| $r^2$ | 0.50 | 0.61 | 0.69 |
| RMSE (μg/m³) | 12.20 | 13.53 | 14.67 |
| NRMSE | 0.83 | 0.92 | 1 |

Model B correlation coefficient, RMSE and NRMSE show a significant improvement from Model A. The first increased from 0.71 to 0.78, with a confidence interval between 0.71 and 0.83, corresponding to a $PM_{10}$ explained variance (given by $r^2$) between 50%and 68%. RMSE and NRMSE confidence inter-

vals bounds decreased from 13.21-16.79 µg/m$^3$ and 0.92-1.14, respectively, to 12.20-14.67 µg/m$^3$ and 0.83-1. Although smaller than in Model A, the NRMSE value remains high due to the high incidence of very low $PM_{10}$ values.

The 2.5$^{th}$ and 97.5$^{th}$ percentile confidence intervals for all these parameters, especially correlation coefficient and RMSE, are also more constrained, when compared to Model A, showing a lower degree of uncertainty associated with the $PM_{10}$ daily average concentration estimates. Although the correlation slope between measured and estimated $PM_{10}$ concentrations has increased from Model A (0.5 to 0.61), Figure 4.21 still shows a tendency for model underestimation for particle concentrations over 15 µg/m$^3$.

AOT regression coefficient confidence interval show a decrease in the weight of this variable in the regression model, from 110.51-152.17 in Model A to 75.30-121.25 in the current model, due to the addition of wind speed as an independent variable. Wind speed presented a negative regression coefficient with a confidence interval between -25.50 and -13.61. This was expected, considering the analysis done for the regression residuals of Model A and the inverse linear relation with $PM_{10}$ determined in section 4.3.3.

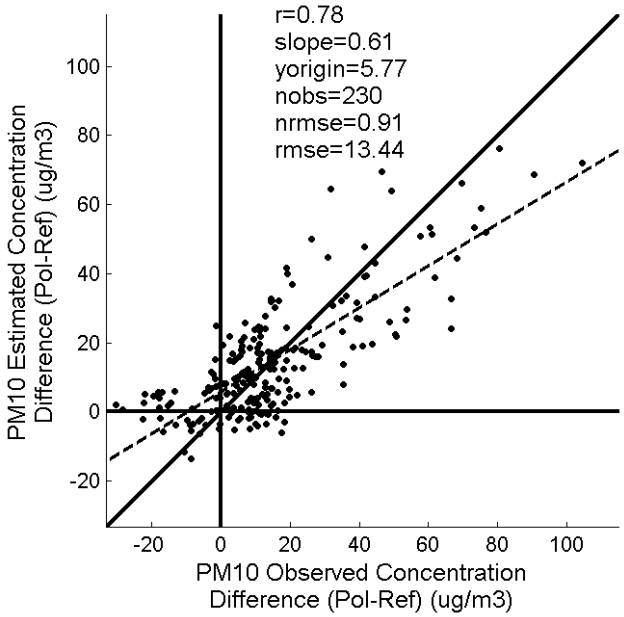


**Figure 4.21 - Scatter plot of measured against estimated daily average $PM_{10}$ concentration differences for Model B.**

The histograms (Figure 4.22) confirm the overall improvement in regression model parameters constrain and the consistency of all independent variables regression coefficients shown in Table 4.12.

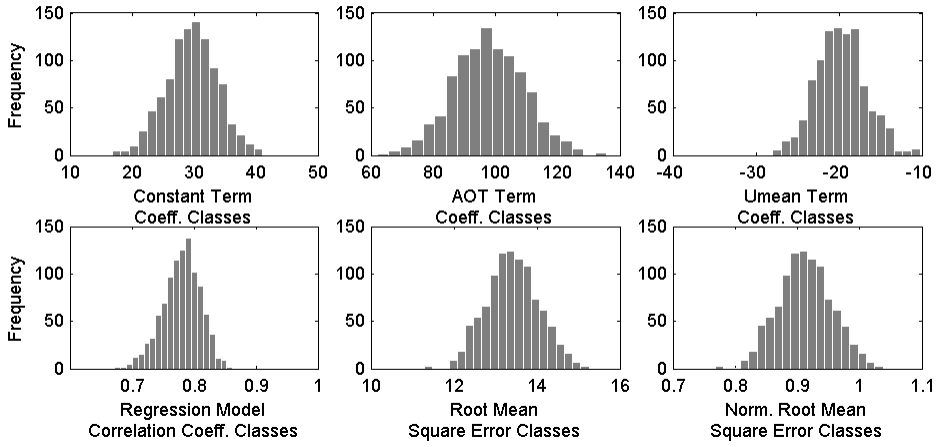


**Figure 4.22 - Histograms for all bootstrap derived multilinear regression coefficients and correlation and error statistics for Model B.**

Scatter plots of standardized residuals against estimated $PM_{10}$ concentrations, for both independent (AOT and $\ln(U_{mean})$) and remaining meteorological variables are presented in Figure 4.23. Constant error variance is verified for all independent variables, although a higher residual spread is still observable for low values of $\ln(U_{mean})$. As for the remaining meteorological variables, the dependence observed for Model A as diminished significantly, especially for mean air temperature. Nevertheless an slightly higher error variance is still distinguishable for higher ln(RH) and $P_{mean}$ values as well as for low $T_{mean}$.

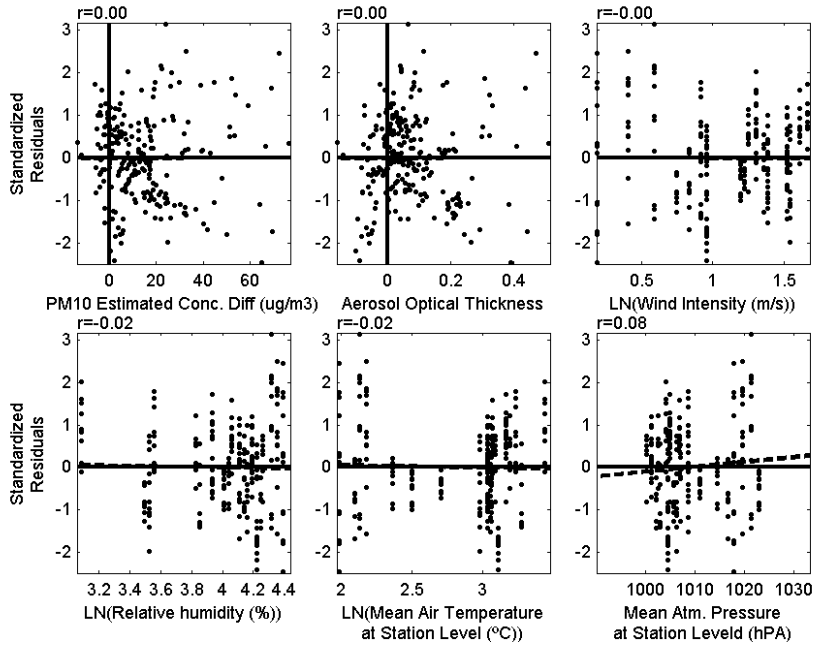


**Figure 4.23 - Model B standardized residuals plotted against the estimated $PM_{10}$ daily average concentrations differences (top graph), AOT and all considered meteorological variables.**

When compared with Model A, the lower and upper bounds of station's confidence interval decreased significantly, now varying from 6.05 to 20.46 $\mu g/m^3$ for RMSE and between 0.20 to 2.97 for NRMSE (Table 4.13).

Although Model B RMSE, NRMSE and respective confidence intervals decreased for most stations, when compared with Model A, some stations present an increase in error bounds such as Quinta do Marquês, Reboleira and Cascais. This effect was overcome by the significant improvement in Mem-Martins and Odivelas and some minor error confidence intervals decrease in Entrecampos, Escavadeira and Lavradio. The best stations continue to be Quinta do Marquês, Olivais and Lavradrio, followed by Loures, Avenida da Liberdade, Entrecampos and Reboleira and the worst are Cascais, Martins and Odivelas.

**Table 4.13 - Model B RMSE and NRMSE confidence intervals for all Lisbon Metropolitan Area air quality stations**

| | RMSE | | | NRMSE | | |
|---|---|---|---|---|---|---|
| | 2.5th Percentile | Original dataset | 97.5th Percentile | 2.5th Percentile | Original dataset | 97.5th Percentile |
| LAR | 9.61 | 12.60 | 15.23 | 0.63 | 1.01 | 1.90 |
| LOU | 6.05 | 9.41 | 12.45 | 0.51 | 0.86 | 1.69 |
| MAR | 6.28 | 11.83 | 16.67 | 0.20 | 0.45 | 1.30 |
| MEM | 9.43 | 13.13 | 16.38 | 0.85 | 1.37 | 2.49 |
| ODV | 10.93 | 15.94 | 20.46 | 0.81 | 1.28 | 2.20 |
| OLV | 8.78 | 13.52 | 17.28 | 0.34 | 0.56 | 0.91 |
| REB | 9.65 | 13.54 | 16.76 | 0.70 | 1.19 | 2.33 |
| CAS | 8.76 | 13.15 | 17.25 | 0.72 | 1.11 | 2.97 |
| ENT | 11.83 | 16.92 | 21.41 | 0.70 | 1.07 | 1.72 |
| LIB | 8.88 | 12.88 | 16.14 | 0.46 | 0.83 | 1.62 |
| ESC | 9.02 | 12.68 | 15.61 | 0.48 | 0.81 | 1.36 |
| LAV | 8.09 | 13.99 | 18.63 | 0.32 | 0.57 | 1.07 |

### 4.3.6 Multi regression model for $PM_{10}$ spatial daily average concentration estimation based on AOT and selected meteorological variables

The Lisbon Metropolitan Area daily average multiregression model (Model C) was developed using the same stepwise fit and bootstrap based variable selection and confidence interval definition methods, as described in Model B. The natural logarithm transformations for variables $U_{mean}$, RH and $T_{mean}$ are also maintained.

The stepwise fit variable selection method showed similar results to Model B. AOT was chosen almost every time (974), followed by $\ln(U_{mean})$ with 574 times. The remaining meteorological variables were chosen significantly fewer times (135 for ln(RH), 106 for $P_{mean}$ and 91 for $\ln(T_{mean})$ and were removed from the regression model

**Table 4.14 - Number of times the stepwise fit procedure selected each variable into the multiregression linear model using the bootstrapped datasets**

| | AOT | $\ln(U_{mean})$ | ln(RH) | $\ln(T_{mean})$ | $P_{mean}$ |
|---|---|---|---|---|---|
| Nº of selections | 974 | 592 | 135 | 91 | 106 |

The general regression formula for Model C, given by Equation 4.3, is therefore similar to the one presented for model B.

$$[PM10]_{\mu g/m^3} = \alpha + \beta_1 AOT + \beta_2 \ln(U_{mean}) \qquad \textbf{Equation 4.3}$$

Although results for the entire dataset, shown in the centre column of Table 4.15 and in Figure 4.24, imply a better performance for Model C, when compared with the previous models, confidence intervals for all regression parameters are significantly wider. This is due to the very small sample size available to determine this regression model (24 points).

The lower $\ln(U_{mean})$ term regression coefficient (-15.78) and respective confidence interval (between -28.62 and -2.81), compared with Model B, is compensated with higher values for the AOT regression coefficient, closer to the values shown in Model A (121.80 for the original dataset and a confidence interval between 67.45 and 171.46).

Correlation coefficient varies from 0.67 to 0.94, corresponding to an explained $PM_{10}$ variance between 44 and 88%. Although still maintaining a wider range, both RMSE and NRMSE show confidence intervals bellow the lower bounds of Model B confidence intervals, 6.73-10.60 µg/m$^3$ and 0.52-0.82, respectively.

**Table 4.15 - Model parameters obtained for Model C and respective 2.5$^{th}$ and 97.5$^{th}$ percentile confidence intervals obtained using a bootstrapping technique.**

| | Confidence intervals | | |
|---|---|---|---|
| Model parameter | 2.5$^{th}$ Percentile | Original dataset | 97.5$^{th}$ Percentile |
| α | 6.29 | 23.30 | 41.97 |
| $\beta_1$ | 67.45 | 121.80 | 171.46 |
| $\beta_2$ | -28.62 | -15.78 | -2.81 |
| r | 0.73 | 0.87 | 0.94 |
| RMSE (µg/m$^3$) | 6.73 | 9.64 | 10.60 |
| NRMSE | 0.52 | 0.75 | 0.82 |

The scatter plot in Figure 4.24 shows a good agreement between measured and estimated stations mean daily average $PM_{10}$ concentration with a correla-

tion. The slope is still under 1 but closer than either of the previous models (0.75). Nevertheless a tendency for underestimation of concentrations values higher that 15 μg/m$^3$ is still visible.

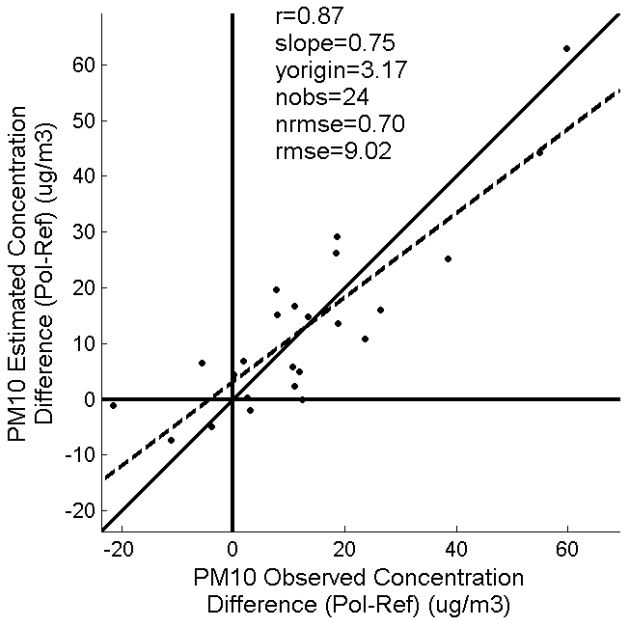


**Figure 4.24 - Scatter plot of measured against estimated daily average $PM_{10}$ concentration differences for Model C.**

The histograms in Figure 4.25 confirm the wider range of values for all regression parameters, described above. It should be noted that for the first time for all presented models a regression term presents some degree of inconsistency in terms of their contribution to the linear model. The higher end of the $\ln(U_{mean})$ histogram presents positive values, contrasting with the majority of negative regression coefficients calculated for that term. Nevertheless those positive values are outside the 95% confidence interval, as shown in Table 4.15.

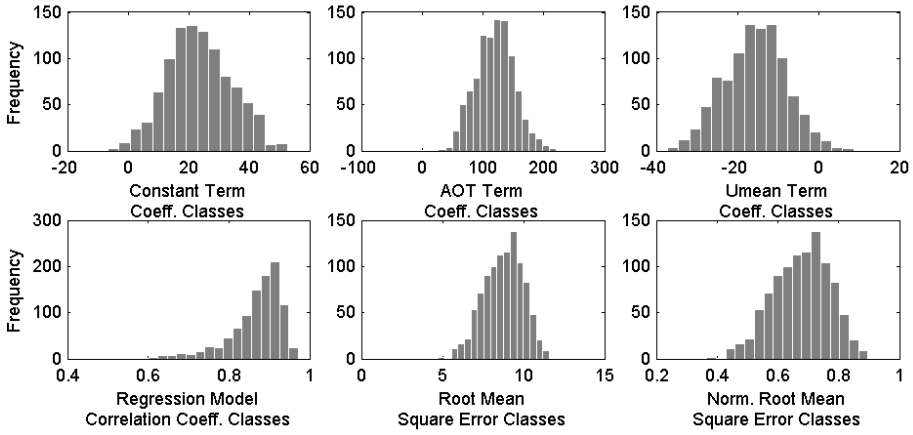


**Figure 4.25 - Histograms for all bootstrap derived multilinear regression coefficients and correlation and error statistics for Model C.**

Finally the scatter plots of standardized residuals against estimated $PM_{10}$ concentrations, for all independent variables and the remaining meteorological variables, show no evidence of error dependence within their respective domain.

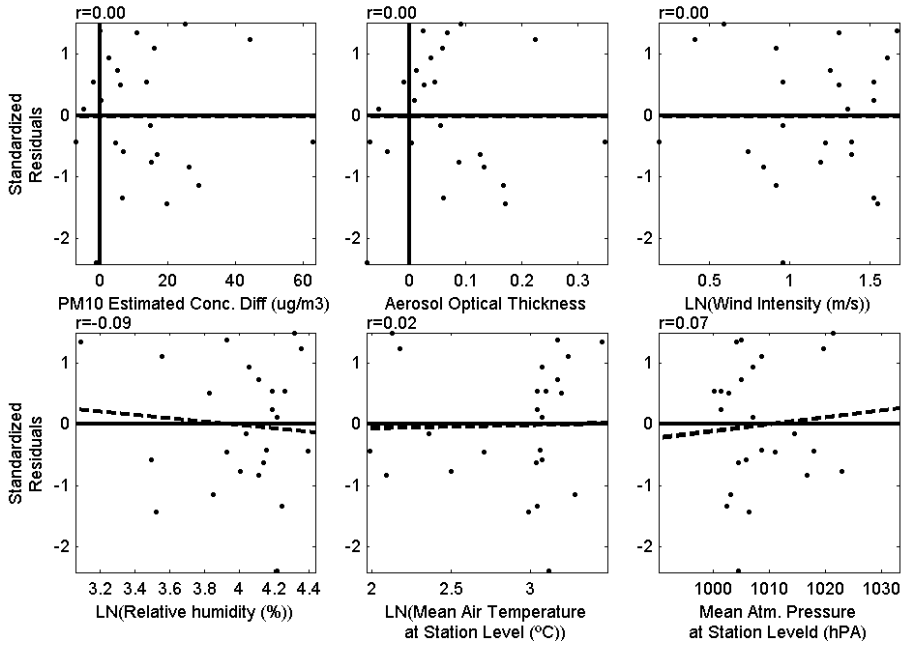


**Figure 4.26 - Model C standardized residuals plotted against the estimated $PM_{10}$ daily average concentrations differences (top graph), AOT and all meteorological variables.**

## 4.4 Conclusions

The main objective of this research is to provide a contribution to the development of a satellite AOT based PM concentration product by performing a systematic analysis of the suitability of a contrast reduction AOT algorithm for air quality studies in urban areas. The underlying hypothesis is that such a methodological approach could complement the information given by other current AOT products, which present limited capabilities in high reflective heterogeneous areas. Consequently, it is mainly focused in the algorithm's capacity to estimate $PM_{10}$ concentrations.

The evaluation of the approach is supported through the comparison of a one year dataset (2005) of DTA derived AOT values with $PM_{10}$ data from twelve air quality stations in the Lisbon Metropolitan Area. The study included a time series and correlation analysis and the definition of one univariate and two multivariate $PM_{10}$ regression models based in satellite AOT values.

The main conclusions are grouped to match the previously defined results sections with the exception being the last section, which includes the conclusions of all $PM_{10}$ estimation regression models result sections (4.3.4 to 4.3.6)

### 4.4.1 Characterization of the $PM_{10}$ and AOT datasets

The temporal/seasonal representativity of the obtained results were limited by the relatively small number of polluted images (44) included in the study. This limitation was mainly due to difficulties in finding MODIS reference/polluted image pairs with limited cloud content and similar visualization geometry. This selection process led to the elimination of several images due to high cloud cover and to the definition of 30 references images, further reducing the size of the MODIS polluted image dataset. The final number of images per month and season does not permit AOT based representations of the annual cycle. Time series analysis of daily AOT values showed a similar variation to the corresponding daily $PM_{10}$ concentration difference. A station comparison of AOT and $PM_{10}$ concentration statistics (mean and standard deviation) also revealed a similar behaviour for most stations.

This comparison highlighted some limitations of the contrast reduction algorithm for $PM_{10}$ estimation in urban environments. The difficulty in defining

several reference images of low homogeneous aerosol content, one for each image geometry cluster, leads to variations in aerosol reference content and might compromise the extraction of absolute or even spatially homogeneous AOT values. Analysis of $PM_{10}$ concentrations in reference images revealed their spatiotemporal heterogeneity, confirmed by significant variations in $PM_{10}$ content within stations and throughout the day. This characteristic compromises the ability to extract absolute $PM_{10}$ concentrations and to reproduce spatial relations between the various stations and consequently to generate $PM_{10}$ spatial patterns for the Lisbon Metropolitan Area.

The comparison between the derived AOT values and the $PM_{10}$ ground concentration differences (polluted-reference) for the Lisbon Metropolitan Area case study confirmed these limitations. The $PM_{10}$ concentrations spatial variation characteristics between the different air quality stations in polluted images changed when the $PM_{10}$ reference content was removed, attenuating, for instance, differences between traffic and background stations.

### 4.4.2 $PM_{10}$/AOT correlation

Overall results showed a moderate correlation between the two variables with a correlation coefficient equal to 0.48, when the AOT value was associated to the $PM_{10}$ value corresponding to the closest measurement hour to the satellite time of passage.

As seen in other studies (Engel-Cox *et al.*, 2004; Gupta *et al.*, 2006; Wang and Christopher, 2003), this correlation improved with time averaging, reaching a peak value of 0.58, when comparing the DTA AOT with $PM_{10}$ daily averages. The maximum correlation value (r=0.64) was achieved between $PM_{10}$ and AOT daily spatial average, referred in the study as the Lisbon Metropolitan Area daily average, which was calculated for the two variables averaging daily data from all available stations. The correlation improvement achieved with time or spatial $PM_{10}$ averaging is an expected result since it partially bridges the gap between the spatiotemporal representativity of a vertical column average variable with a 20 km spatial resolution and an hourly point ground measurement.

Another considerable increase in correlation was accomplished by only considering reference/polluted image pairs from the same season. In fact, cor-

relation between AOT and $PM_{10}$ daily average rose to 0.71 and correlation between their respective Lisbon Metropolitan Area daily averages to 0.82. This rise in correlation is related to the minimization of the negative effect of changes in surface reflectance driven by vegetation dynamics in the AOT algorithm accuracy, which were already discussed in the previous chapter. For the same reason, spring and autumn, the main transitional seasons with greater short term surface reflectance changes (Brest, 1987; Zhou *et al.*, 2003) also present the lowest correlations (0.02 and 0.07) when compared to winter and summer (0.69 and 0.58). The lower spring/autumn correlations are also related to the narrow AOT value range presented in these seasons, with a higher incidence of low AOT values.

No correlation dependency with station type was found, with very similar correlation values for background, industrial and traffic stations, ranging from 0.54 to 0.62, for the full MODIS dataset, and between 0.69 and 0.75 in the same season dataset. This result does not corroborate previous studies referred in the literature review (Gupta *et al.*, 2006; Koelemeijer *et al.*, 2006), which identified higher PM/AOT correlations in urban background stations. This apparent disagreement is partially justified by the limited number of polluted days included in the study, which doesn't provide a correct assessment of the variability and range differences between stations. This limitation is accentuated by the attenuation of $PM_{10}$ concentrations differences between traffic and background stations, already discussed in the previous section. As a result, the three station types present similar $PM_{10}$ concentration characteristics and consequently analogous $PM_{10}$/AOT correlation coefficients. Another possible explanation is related to the inherent differences between the urban areas included in those studies and the Lisbon Metropolitan Area in terms of $PM_{10}$ distribution patterns and respective station spatial representativeness. In fact, it's unlikely that differences, for instance, between background and traffic stations should be mantained across the different case studies and therefore it is possible that those differences are not as pronounced in the Lisbon Metropolitan Area, when compared with other cities.

Nevertheless some differences between individual sites were observed with lower correlations found in stations located in suburban areas to the north and northwest of Lisbon like Loures and Mem-Martins, when compared to the

ones located in the city centre (Entrecampos, Avenida da Liberdade e Olivais). This decrease in correlation is probably related to AOT retrieval errors due to the higher vegetation content present in these transitional areas. This emphasizes the higher performance of the contrast reduction method for urban surfaces but also indicates a constraint in terms of its applicability to wider areas where the urban fabric is interlaced with vegetated surfaces.

The correlation range between the contrast reduction AOT and $PM_{10}$ is within the values reported by other studies using standard MODIS aerosol product, referred in the literature review (Engel-Cox *et al.*,2004; Gupta et al, 2006; Liu et al, 2005). However, the wide range of correlation coefficient values found on those studies (from <0.5 to 0.96), reflect their diversity in scope, conditions and assumptions and limits a more detailed comparison with the work developed in this thesis.

Overall, this analysis has highlighted three important aspects to consider in future analysis: a) satellite AOT values are more more suitable for characterization of mean daily $PM_{10}$ values; b) acknowledgement of vegetation dynamics as well as other seasonal changes in surface reflectance is essential to consider; and c) the regional characteristics of different stations types may hinder straightforward algorithmic transfers between different urban areas. The potential of using AOT-based algorithms is significantly enhanced by acknowledging these three factors, has demonstrated above.

### 4.4.3 Characterization of the meteorological datasets and their relationships with $PM_{10}$ and AOT

The correlation analysis between the meteorological variables, measured at the Gago Coutinho station, and both the MODIS AOT and $PM_{10}$ datasets led to some interesting conclusions. The relation between each meteorological variable daily values and absolute daily $PM_{10}$ concentrations for the full year show that some of them might be better represented by non-linear functions. For instance, $PM_{10}$ variation with mean air temperature and mixing layer height displayed a behaviour better described by a quadratic curve. In the case of wind speed, that relationship approximated an exponential function. These findings corroborate studies done by Liu *et al.*, 2005 and Gupta *et al.*, 2009b who used,

respectively, non-linear regression models and neural networks to improve the $PM_{10}$ estimation using satellite AOTs and meteorological variables.

Another interesting finding was related to some discrepancies between the $PM_{10}$/meteorological variables relationships for the full yearly dataset and the MODIS dataset. For instance, in the case of relative humidity and mean air temperature those relationships show inverse behaviours in the two datasets. This implies that the meteorological conditions present in MODIS images final dataset might not be sufficiently representative of their annual variation. This might happen because the dataset is too small (only 24 days are available in the same season dataset) or because the specific meteorological conditions usually found in unclouded satellite images might be responsible for a sampling bias, regarding their relationship with $PM_{10}$ dispersion. To address this issue, this type of analysis should be extended, in a future, to a multi-year dataset, able to expand the number of available satellite images and retrieve more robust conclusions.

Despite these limitations the analysis for the days corresponding to the final set of MODIS images showed moderate linear correlations between both AOT and $PM_{10}$ ground concentration differences and wind speed, atmospheric pressure and mean temperature.

Neither mixing layer height nor relative humidity presented significant linear correlations with AOT values or $PM_{10}$ ground concentrations. This finding was somewhat unexpected, since several studies demonstrate the importance of these variables to correct the $PM_{10}$/AOT relation for hygroscopic aerosol growth and vertical aerosol distribution (Engel-Cox *et al.*, 2006; Flores *et al.*, 2012; Gupta *et al.* 2006; Liu *et al.*, 2005; Meier *et al.*, 2009). The small number of available polluted images in the final "same-season" dataset (24) represents an insuficient sample of the overall environmental conditions, limiting a correct assessment of the relationship between PM, AOT and the meteorological variables. The low sample dimension hampers the extraction of the significant patterns from the data and generates the lack of significant correlations.

The highest correlation coefficients (in absolute value) were established with wind speed, who showed a negative correlation with both $PM_{10}$ ($r=-0.58$) and AOT ($r=-0.44$) datasets. This relationship was expected since higher wind

intensities would favour suspended particle dispersion, decreasing their concentration.

After using a natural logarithm transformation, wind speed, relative humidity and mean air temperature showed an increase in linear correlation with $PM_{10}$ concentration differences for the MODIS dataset (correlation coefficient increased, in absolute value, from 0.58, 0.09 and 0.46 to 0.68, 0.18 and 0.56, respectively). Those transformed variables were used, in substitution of the original variables, when defining the linear regression models. This further emphasizes the possible existence of non-linear relations between $PM_{10}$ and meteorological variables and the need to include, in future studies, statistical techniques able to better reproduce those behaviours (e.g. general additive models or neural networks).

### 4.4.4 Linear regression models for $PM_{10}$ estimation using AOT and meteorological variables

The several univariate and multivariate regression models for $PM_{10}$ concentrations developed for the Lisbon Metropolitan Area air quality stations demonstrated the potential of using the contrast reduction algorithm for $PM_{10}$ estimation in urban areas. $PM_{10}$ explained variance, for a 95% confidence interval, ranged between 37 and 61% when only AOT was used as an estimator (Model A) to 50-69% when wind intensity was added (Model B).

The increase in estimation strength from Model A to Model B is in agreement with findings by other studies (Al-Saadi *et al.*, 2008; Engel-Cox *et al.*, 2006, Gupta *et al.* 2006, 2009a; Kacenelenbogen *et al.*, 2006; Liu *et al.*, 2005; Paciorek *et al.*, 2008). In those studies, adding meteorological variables, like temperature, relative humidity, mixing layer height and wind speed, enhanced the performance of the regression models. These variables improve $PM_{10}$ estimation by incorporating into the model additional information about $PM_{10}$ dispersion conditions and, as referred above, correct the $PM_{10}$/AOT relation for factors like vertical aerosol distribution and hygroscopic aerosol growth. Nevertheless, unlike most of those other studies, only wind speed added significant explanatory power to the model. This result confirmed the conclusions provided by the correlation analysis where wind speed showed the closest association with both $PM_{10}$ and AOT datasets. As said in the previous section, the small number of

included polluted images might have limited a correct assessment of the influence of the remaining meteorological variables, especially the aforementioned mixing layer height and relative humidity. A future expansion of this type of study to a multi-year dataset might correct this and establish a regression model based on AOT and these meteorological variables, applicable to wider range of vertical and horizontal $PM_{10}$ dispersion conditions.

The confidence interval of the regression coefficients confirmed a consistent positive relation with AOT in both models, with values comparable to the ones reported in other papers (Gupta *et al.*, 2006 and Koelemeijer *et al.*,2006), and a negative contribution from wind speed in the second model, driven by its role as a $PM_{10}$ dispersor factor.

Both regression models demonstrated a tendency for underestimation of $PM_{10}$ concentration differences higher than 15 $\mu g/m^3$, as highlighted by the correlation slopes lower than one between estimated and observed $PM_{10}$ concentration differences (0.5 for Model A and 0.61 for Model B). This tendency is also identified in other studies (Gupta and Sundar, 2009a, 2009b). The authors justify this tendency with the presence of multiple aerosol layers at different altitudes, leading to a divergence between the ground $PM_{10}$ measurements and the satellite AOTs. In the case of the contrast reduction AOTs, the 20 km spatial resolution limits its ability to reproduce higher ground concentration values, usually associated to traffic emissions, and therefore with a smaller area of influence.

The high NRMSE confidence intervals, from 0.92-1.14 to 0.83-1 were due to a high incidence of low AOT values (<25 $\mu g/m^3$). A low AOT value range leads to higher AOT uncertainties, as discussed previously in this thesis for the contrast reduction algorithm and reported for other AOT products (Engel-Cox *et al.*, 2004; Gupta *et al.*, 2006).

In the third model (Model C), the estimated value corresponded to the average of the $PM_{10}$ daily values for all air quality stations of the Lisbon Metropolitan Area, instead of the individual station values. This model aimed at assessing the contrast reduction based AOT's ability as an overall PM air quality indicator. Model C showed a higher explained variance in $PM_{10}$ concentrations and NRMSE confidence intervals between 44 and 88%and 0.52-0.82, respectively, when compared to the other models. The increase was expected, considering

statistical models are usually more capable of reproducing spatially or temporally averaged variables and also because of the limitations imposed by the AOT's coarse resolution. At such a coarse resolution, it's normal that the retrieved AOTs are more related to $PM_{10}$ spatial averages than the concentrations for each station. The superior model performance is also reflected by a correlation slope between estimated and observed $PM_{10}$ concentration differences closer to the unity (0.75).

5

# Chapter 5 - Conclusions

During the last ten years, several satellite based empirical $PM_{2.5}$ and $PM_{10}$ estimation models have been developed for multiple sensors and several regions with variable degrees of success. Satellite AOT retrieval accuracy in highly reflective areas, such as deserts and urban areas, is identified as one of the main sources of uncertainty for PM estimation at ground level (Engel-Cox *et al.*, 2004; Gupta *et al.*, 2006; Gupta and Sundar 2009b). Contrast reduction algorithms for AOT retrievals are based on the assessment of the aerosol contrast reduction effect on satellite images between a pair of images (one reference, and one polluted) and provide a valid alternative for those areas.

The main objective of this thesis was to explore the suitability of a contrast reduction based AOT retrieval algorithm for urban $PM_{10}$ estimation. Overall, the current research presents the first set of regression models to estimate ground level $PM_{10}$ concentrations based on satellite retrievals of AOT for the Lisbon Metropolitan Area. The results presented here are supported by a comprehensive methodology that defines optimal conditions for algorithmic application in urban areas and characterizes the $PM_{10}$/AOT correlation for Lisbon. Ultimately, the potential of AOT based models for ground level monitoring of atmospheric pollutants is emphasized.

The first part of the thesis focused on the development of a new contrast reduction algorithm, based on the Differential Texture Analysis (DTA), expanding on previous studies by optimizing several aspects of the original algorithm and providing a first systematic evaluation for an extended MODIS dataset.

The evaluation, based in a comparison with AOT values measured in five urban European AERONET sites, demonstrated the algorithm's ability to retrieve AOT values for the MODIS sensor in urban areas, with an overall correlation coefficient with ground measurements of 0.78. This ability is also emphasized by the higher number of valid measurements (192) found in the evaluation study for the algorithm considering all AERONET stations, when compared with the MODIS standard aerosol product (77 valid measurements).

The main improvements introduced in the algorithm included the definition of: a) an optimal AOT spatial resolution of approximately 20 km; b) a land cover combination of forest and urban pixels for AOT calculation, which minimizes possible retrieval errors due to surface reflectance changes related to vegetation content; and c) a sensor zenith correction term and visualization geometry clusters in order to reduce the influence in the algorithm's accuracy of target reflectance differences as a function of MODIS variable illumination geometries.

The establishment of the new algorithm supported the progress of the research to the case study of Lisbon Metropolitan Area. Using a 2005 dataset of MODIS images, the optimized AOT values were retrieved and compared with the corresponding hourly $PM_{10}$ ground concentration measurements. The calculated AOTs showed a similar behaviour for seasonal and spatial $PM_{10}$ concentration and a moderate agreement between all available $PM_{10}$ station data. The $PM_{10}$/AOT correlation analysis emphasized the need to: a) reduce the spatio-temporal gap between the coarse and vertically integrated AOT values and point ground measurements through temporal and spatial averaging and; b) further restrict the contribution of vegetation related changes in surface reflectance to increase AOT's accuracy. The joint analysis between the meteorological variables and $PM_{10}$ identified moderate/low correlations for wind speed, mean atmospheric pressure and mean air temperature, highlighting the existence of non-linear relations with some of those variables.

Following the previous analysis, the three linear regression models of $PM_{10}$ based on AOT and meteorological variables determined in the final thesis section were defined for: a) $PM_{10}$ daily averages; b) using only reference/polluted image pairs from the same season; c) applying a natural loga-

rithmic transformation to some meteorological variables, to linearize their relation with $PM_{10}$ concentrations.

The linear regression results demonstrated the ability of the contrast reduction AOT's to reproduce ground based observations of $PM_{10}$ concentrations in urban areas. The introduction of wind speed as an independent variable enhances model performance by better defining the dispersion conditions of $PM_{10}$. In fact, when used in a univariate approach, AOT explained between 37% and 61% of the total variance in $PM_{10}$ ground concentration; a percentage that increased to 50-68% with the addition of wind speed. Those results show that the main quantitative contribution for $PM_{10}$ estimation is given by AOT, since the improvement given by wind speed is marginal by comparison, although significant. The consistency of those results is further enhanced by the fact that AOT's regression coefficient confidence interval between 110.51 and 152.17 is comparable to values found in other studies (Gupta *et al.*, 2006; Koelemeijer *et al.*, 2006). This fact is particularly promising in a research field where results are very heterogeneous, dependent on site location and therefore more difficult to generalize, as can be confirmed by the literature review given in section 2.2.3. Another relevant aspect of the models developed here, is the similar behaviour found for all stations within the study area. However, as expected, some background station concentrations were better reproduced due to their wider spatial representativeness, while others that were located in the fringe of urban centres presented a higher error, probably due to the loss in algorithm's accuracy related to an increase in vegetated content.

The tendency in all models for underestimating AOT and the higher performance obtained for daily spatial averages of $PM_{10}$ estimations stresses the limitations in the AOT's ability to reproduce peak values and particular spatial variations in $PM_{10}$ concentration. This is related to the very coarse resolution provided by the algorithm for MODIS imagery, which also constrains its capability to retrieve the finer scale spatial structure of urban $PM_{10}$ distribution patterns. This also explains the higher performance seen in the last developed regression model ($PM_{10}$ explained variance between 53 and 88% and NRMSE between 0.52 and 0.82) when both daily average AOT values and $PM_{10}$ ground concentrations were aggregated for all stations. This seems to indicate that for

such coarse resolution, AOT is more representative of overall urban air quality than of station concentrations.

Other limitations regarding the algorithm performance and the methodology followed in the present work include: a) the need to extend the observational time series, in order to capture in greater detail the seasonal variations of AOT, $PM_{10}$ and meteorological variables, helping to better constraint the defined regression models; and b) the need to define several reference images, one for each image geometry cluster, with differences in the residual aerosol load, leading to the retrieval of relative AOT values, unable to provide spatially consistent distribution patterns.

To overcome these limitations, future research work regarding $PM_{10}$ estimation using satellite based AOTs derived with a contrast reduction algorithm, should provide a more in-depth analysis about the influence of meteorological variables in the definition of PM/AOT correlation and assess the algorithm's ability to extract accurately the spatial and temporal features of characteristic urban distribution patterns. To achieve this goal, a more extensive multi-year dataset should be introduced to fully incorporate seasonal variations of both $PM_{10}$ emission sources and meteorological variables. In that analysis, statistical techniques such as general additive models (GAMs) or machine learning approaches should be further explored to better resolve the apparent non-linearities present in the relationship between $PM_{10}$ concentrations and several of the meteorological variables included in this study.

Furthermore, the study should be broaden to include higher resolution sensors like ASTER (15 to 30 metre resolution) and Sentinel 2, geostationary or low orbit missions like Meteosat, GOES and Sentinel 4 and 5 and LIDAR carrying satellites, like CAPYPSO.

The first two would provide AOT results on a finer scale, able to retrieve the higher $PM_{10}$ spatial variations characteristic of urban environments and closely related to the influence of traffic and industrial emission sources.

The lower resolution (in the order of a few kilometres) geostationary satellites Meteosat Second Generation (MSG), GOES and, in the near future, Sentinel 4, able to provide imagery for a specific region at very short time intervals

(starting from half an hour), would complement the previous spatial information, by supplying intra-daily temporal $PM_{10}$ monitoring data.

The future low orbit satellite Sentinel 5, with a higher spectral resolution, capable of retrieving AOT for several spectral bands could provide more accurate aerosol size and speciation data. Finally, the integration of CALYPSO's LIDAR would give detailed information on the vertical distribution of aerosols and help correct all the $PM_{10}$ estimation models developed for the previous satellites.

However, the main focus of future developments should be on the improvements of contrast reduction algorithm. The inclusion of BRDFs would allow a better correction of view and illumination angle effects, expanding on the work developed in this thesis with the introduction of a sensor zenith correction term. This development would be particularly useful for polar orbiting satellites like Terra and Aqua who carry the MODIS sensor and scan the same region of the Earth's globe from different visualization geometries.

Another important priority should be to remove aerosol influence from reference images. This could be accomplished by either incorporating other AOT satellite products to estimate mean reference aerosol content over the study area and remove it. Alternatively a technique currently applied to geostationary satellites (Knapp *et al.*, 2005), could be applied to define a composite reference image from a MODIS image time series. If successful the definition of a "clean" reference image would allow the retrieval of absolute AOT values with lower error levels at higher resolution enabling the retrieval of meaningful spatial distribution patterns.

The work presented here helps to establish the contrast reduction technique as a viable alternative to other satellite AOT products for $PM_{10}$ estimation in urban areas. The implementation of some of these future improvements would set the standard for the development of an operational AOT product based in contrast reduction, capable of establishing a more reliable alternative for estimating $PM_{10}$ concentrations for urban areas. This product might have a significant impact on urban air quality monitoring by improving the definition of PM urban spatial and temporal dispersion patterns. Consequently it would offer more reliable information to previously unmonitored or misrepresented

areas, improving monitoring support to legislation compliance and contributing to possible ground network optimization. Furthermore it could also provide further validation for the current urban operational air quality models – physical and statistical – and even be integrated into them through data assimilation schemes.

6

# Chapter 6 - Bibliographic References

Ackerman, S. A., Frey, R., Strabala, K., Liu, Y., Gumley, L., Baum, B., and Menzel, P., 2006. Discriminating clear-sky from clouds with MODIS. Algorithm Theoretical Basis Document (MOD35), available at: http://modis-atmos.gsfc.nasa.gov/_docs/atbd_mod06.pdf, version 5.0.

Almeida S.M., Pio C.A., Freitas M.C., Reis M.A., Trancoso M.A., 2006. Source apportionment of atmospheric urban aerosol based on weekdays / weekend variability: evaluation of road re-suspended dust contribution. Atmospheric Environment 40, 2058-2067

Al-Saadi, J.A., Rosen, R., Bohnenkamp, C., Szykman, J., Chu, D.A., Hair, J., Hostetler, C., Ferrare, R., Arcemont, G., Kittaka, C., Lewis, L., 2008. Application of Satellite Aerosol Optical Depth and Airborne LIDAR Data for Monitoring Fine Particulate Formation and Transport in San Joaquin Valley, California. 10th Conference on Atmospheric Chemistry, American Meteorological Society, Boston, MA, USA.

Alves C., Gonçalves C., Fernandes A.P., Tarelho L., Pio C., 2011. Fireplace and woodstove fine particle emissions from combustion of western Mediterranean wood types. Atmospheric Research 101, 692-700.

Alves C., Vicente A., Nunes T., Gonçalves C., Fernandes A.P., Mirante F., Tarelho L., Sanchez de la Campa A., Querol X., Caseiro A., Monteiro C.,

Evtyugina M., Pio C., 2011. Summer 2009 wildfires in Portugal: emission of trace gases and aerosol composition. Atmospheric Environment 45, 641-649.

An, X., Zhu, T., Wang, Z., Li, C., Wang, Y., 2007. A Modeling Analysis of a Heavy Air Pollution Episode Occurred in Beijing; Atmos. Chem. Phys. 7, 3103-3114.

Anderson, H.R., 2009. Air pollution and mortality: a history. Atmospheric Environment 43, 142–152

APA (Portuguese Environment Agency), 2008. Evolução da qualidade do ar em Portugal entre 2001 e 2005. Lisbon, Portugal.

APA (Portuguese Environment Agency), 2011. SOER 2011 Portugal - 10 Indicators. Lisbon, Portugal.

application to Moderate Resolution Imaging Spectroradiometer aerosol retrieval over land. J. Geophys. Res. 112, D13210.

Balaguer, N.C., Denby, B.R., 2012. A survey to elicit expert opinion on the spatial representativeness of ground based monitoring data. FAIRMODE activity for WG2-SG1: Combining models and monitoring, http://fairmode.ew.eea.europa.eu/monitoring-modelling-sg1/monitoring-representativeness-survey-results-v1.pdf., accessed on 09-09-2012.

Barmpadimos, I., Hueglin, C., Keller, J., Henne, S., and Prévôt, A. S. H., 2011. Influence of meteorology on $PM_{10}$ trends and variability in Switzerland from 1991 to 2008. Atmos. Chem. Phys., 11, 1813-1835.

Barnaba, F., Putaud, J.P., Gruening, C., Dell'Acqua, A. & Dos Santos, S., 2010. Annual cycle in co-located in situ, total-column, and height-resolved aerosol observations in the Po Valley (Italy): Implications for ground-level particulate matter mass concentration estimation from remote sensing. Journal of Geophysical Research D: Atmospheres 115, D19209, 1-22.

Bell, M.L., Davis, D.L., 2001. Reassessment of the lethal London fog of 1952: Novel indicators of acute and chronic consequences of acute exposure to air pollution. Environmental Health Perspectives 109 ,389–394

Bell, M.L., Samet, J.M., Dominici, F., 2004. Time-series studies of particulate matter. Annu. Rev. Public Health 25, 247–280.

Bevan, S.L., North, P.R.J. , Los, S.O., Grey, W.M.F., 2009. Global atmospheric aerosol optical depth retrievals over land and ocean from AATSR. Ieee International Geoscience and Remote Sensing Symposium *Vols 1-5*, 3906-3909.

Borrego C., A. I. Miranda, S. Sousa, A. Carvalho, E. Sá, H. Martins, J. Valente, C. Varum and S. Jorge, 2008b. Planos e Programas para a Melhoria da Qualidade do Ar na Região Norte - Uma visão para o período 2001-2006. University of Aveiro, Portugal. AMB-QA-7/2008.

Borrego C., Carvalho A., Sá E., Sousa S., Coelho D., Lopes M., Monteiro A., Miranda A.I., 2011. Air Quality Plans for the Northern Region of Portugal: Improving Particulate Matter and Coping with Legislation, in: Nejadkoorki, F. (eds), Advanced Air Pollution. InTech.

Borrego C., Sá E., Carvalho A., Sousa S., Miranda A.I., 2010. Plans and Programmes to improve air quality over Portugal: a numerical modelling approach. Harmonization within Atmospheric Dispersion Modelling for Regulatory Purposes, Paris, France

Borrego, C., A. I. Miranda, A. Monteiro, O. Tchepel, H. Martins, R. Tavares, L. Gonçalves and P. Barbedo, 2008a. Inventário das emissões de poluentes atmosféricos da Região Norte, R3. University of Aveiro, Portugal.

Bossard, M., Feranec, J., Otahel, J., 2000. CORINE Land Cover technical guide - addendum 2000. Technical report No 40, Copenhagen.

Brás, H., 2012. Avaliação dos benefícios da implementação de Zonas de Emissões Reduzidas em Lisboa. MS Thesis. Universidade Nova de Lisboa.

Brest, C.L., 1987. Seasonal albedo of an urban/rural landscape from satellite observations. J. Climate Appl. Meteorol. 26, 1169-1187.

Brook, R.D., Rajagopalan, S., Pope, C.A. III, Brook, J.R., Bhatnagar, A., Diez-Roux, A.V., Holguin, F., Hong, Y., Luepker, R.V., Mittleman, M.A., Peters, A., Siscovick, D., Smith, S.C. Jr, Whitsel, L., Kaufman, J.D.; on behalf of the American Heart Association Council on Epidemiology and Prevention, Council on the Kidney in Cardiovascular Disease, and Council on Nutrition, Physical Activity and Metabolism, 2010. Particulate matter air pollution and cardiovascular disease: an update to the scientific statement from the American Heart Association. Circulation 121, 2331–2378

Brunekreef, B., 2003. Design of Cohort Studies for Air Pollution Health Effects; J. Toxicol. Environ. Health, Part A 66, 1723-1729.

Calvo, A.I., Fernandes, A.P., Nunes, T., Alves, C.A., Vicente, A.M., Evtyugina, M., Monteiro, A.C., Gonçalves, C.V., Tarelho, L.A.C., Pio, C. , 2011. Forest fires in Portugal in summer 2010: contribution to atmospheric pollution. Global Conference on Global Warming (GCGW-11). 11-14 July 2011, Lisbon, Portugal

Chin, M., Ginoux, P., Kinne, S., Torres, O., Holben, B. N., Duncan, B. N., Martin, R. V., Logan, J. A., Higurashi, A., Nakajima, T., 2002. Tropospheric aerosol optical thickness from the GOCART model and comparisons with satellite and Sun photometer measurements. Journal of the Atmospheric Sciences **59**, 461-483.

Chu, D. A, Kaufman, Y. J., Ichoku, C., Remer, L. A., Tanré, D., Holben, B. N., 2002. Validation of MODIS aerosol optical depth retrieval over land. Geophysical Research Letters 29 (12), 8007.

Chu, D. A., Kaufman, Y. J., Zibordi, G., Chern, J. D., Mao, J., Li, C., N. Holben, B., 2003. Global monitoring of air pollution over land from the Earth Observing System-Terra Moderate Resolution Imaging Spectroradiometer (MODIS). J. Geophys. Res. 108, 4661.

Council Directive 96/62/EC

Davies, W.H., North, P.R.J., Grey, W.M.F., Barnsley, M.J., 2010. Improvements in aerosol optical depth estimation using multi-angle CHRIS/PROBA images. IEEE Transactions on Geoscience and Remote Sensing, 48(1), 18-24.

Deschamps, P.Y., Duhaut, A., Rouquet, M.C., Tanré, D., 1984. Evidence, analysis and correction of atmospheric effects on Landsat/SPOT multispectral data. 2nd Colloque Int. sur les Signature Spectrales d'Objets en Teledetection, Colloq. 23, Inst. Natl. de la Res., Agron., Avignon, France, Bordeaux, France, pp. 709–722.

Deuzé, J. L., Breon, F. M., Devaux, C., Goloub, P., Herman, M., Lafrance, B., Maignan, F.,

Diner, D.J., Davies, R., Di Girolamo, L., Horvath, A. Moroney, C., Muller, J.-P., Paradise, S.R., Wenkert, D, and Zong, J., 1999. MISR level 2 cloud detection and classification algorithm theoretical basis. Jet Propulsion Laboratory, Pasadena, CA, USA.

Dinoi, A., Perrone, M.R., Burlizzi, P., 2010. Application of MODIS Products for Air Quality Studies Over Southeastern Italy. Remote Sens. 2, 1767-1796.

Dockery, D. W., Pope, C.A., 1996. Epidemiology of acute health effects: summary of time-series studies, in: Wilson, R., Spengler, J.D. (Eds), Particles in our air: concentration and health effects. Harvard University Press Cambridge - MA, pp. 123-147

Dockery, D.W.; Pope, C.A., III; Xu, X., Spengler, J.D., Ware, J.H., Fay, M.E., Ferris, B.G., Speizer, F.A., 1993. An Association between Air Pollution and Mortality in Six U.S. Cities; N. Engl. J. Med. 329, 1753-1759.

Draper, N. R., and Smith, H., 1998. Applied Regression Analysis. Wiley-Interscience, Hoboken, NJ, pp. 307–312

Dubovik, O. and King, M. D., 2000a. A flexible inversion algorithm for retrieval of aerosol optical properties from Sun and sky radiance measurements. J. Geophys. Res., 105, 20,673–20,696.

Dubovik, O., Holben, B., Eck, T. F., Smirnov, A., Kaufman, Y. J., King, M. D., Tanré, D., Slutsker, I., 2002. Variability of absorption and optical properties of key aerosol types observed in worldwide locations. Journal of the Atmospheric Sciences 59, pp. 590-608.

Dubovik, O., Smirnov, A., Holben, B. N., King, M.D., Kaufman, Y.J., Eck, T.F., Slutsker, I., 2000b. Accuracy assessments of aerosol optical properties retrieved from AERONET sun and sky-radiaometric measurements. J. Geophys. Res. 105, 9791–9806.

EEA (European Environment Agency), 2010. The European environment — state and outlook 2010. Copenhagen, Denmark.

EEA, 1999. Criteria for EUROAIRNET. The EEA Air Quality Monitoring and Information Network. Technical Report No. 12. European Environment Agency, Copenhagen, Denmark.

Efron, B., 1979. 1977 Rietz Lecture - Bootstrap Methods - Another Look at the Jackknife. Ann Stat, 7(1), 1-26.

Efron, B., 1982. The jackknife, the bootstrap, and other resampling plans. 38. Society of Industrial and Applied Mathematics CBMS-NSF Monographs.

Engel-Cox, J.A., Hoff, R.M., Rogers, R., Dimmick, F., Rush, A.C., Szykman, J.J.; Al-Saadi, J.; Chu, D.A.; Zell, E.R., 2006. Integrating LIDAR and Satellite Optical Depth with Ambient Monitoring for 3-Dimensional Particulate Characterization. Atmos. Environ. 40, 8056-8067.

Engel-Cox, J.A., Holloman, C.H., Coutant, B.W., Hoff R.M., 2004. Qualitative and quantitative evaluation of MODIS satellite sensor data for regional and urban scale air quality. Atmos Environ 38(16), 2495–2509.

EU, 1996. Directive 1996/62/EC of the European Parliament and of the Council of 27 September 1996 on ambient air quality assessment and management, OJ L 96, 21.11.1996, pp. 55 - 63 (http://eur-lex.europa.eu/LexUriServ/LexUriServ.do?uri=CELEX:31996L0062:EN:PDF), accessed 30 July 2011.

EU, 1999. Directive 1999/30/EC of the European Parliament and of the Council of 22 April 1999 relating to limit values for sulphur dioxide, nitrogen dioxide and oxides of nitrogen, particulate matter and lead in ambient air, OJ L 163, 29.6.1999, pp. 41–60 (http://eur-lex.europa.eu/LexUriServ/LexUriServ.do?uri=OJ:L:1999:163:0041:0060:EN:PDF), accessed 30 July 2011.

EU, 2000. Directive 2000/69/EC of the European Parliament and of the Council of 16 November 2000 relating to limit values for benzene and carbon monoxide in ambient air, OJ L 313 , 13.12.2000, pp. 12 - 21 (http://eur-lex.europa.eu/LexUriServ/LexUriServ.do?uri=CELEX:32000L0069:EN:PDF), accessed 30 July 2011.

EU, 2002. Directive 2002/03/EC of the European Parliament and of the Council of 16 November 2000 of 12 February 2002 relating to ozone in ambient air OJ L 067, 09.03.2002, pp. 14 - 30 (http://eur-lex.europa.eu/LexUriServ/LexUriServ.do?uri=CELEX:32002L0003:EN:PDF), accessed 30 July 2011.

EU, 2004. Directive 2004/107/EC of the European Parliament and of the Council of 15 December 2004 relating to arsenic, cadmium, mercury, nickel and polycyclic aromatic hydrocarbons in ambient air, OJ L 23, 26.1.2005, pp. 3–16 (http://eur-lex.europa.eu/LexUriServ/LexUriServ.do?uri=OJ:L:2005:023:0003:0016:EN:PDF), accessed 30 July 2011.

EU, 2008. Directive 2008/50/EC of the European Parliament and of the Council of 21 May 2008 on ambient air quality and cleaner air for Europe, OJ L 152, 11.06.2008 (http://eur-lex.europa.eu/LexUriServ/LexUriServ.do?uri=OJ:L:2008:152:0001:0044:EN:PDF) accessed 27 July 2011.

EU, 2008. Directive 2008/50/EC of the European Parliament and of the Council of 21 May 2008 on ambient air quality and cleaner air for Europe, OJ L 152, OJ L 152, 11.06.2008, pp. 1 - 44 (http://eur-lex.europa.eu/LexUriServ/LexUriServ.do?uri=OJ:L:2008:152:0001:0044:EN:PDF), accessed 27 July 2011.

European Comission (EC), 2011. Commission staff working paper establishing guidelines for demonstration and subtraction of exceedances attributable to natural sources under the Directive 2008/50/EC on ambient air quality and cleaner air for Europe. Brussels, Belgium.

Fernandes A.P., Alves C., Gonçalves C., Tarelho L., Pio C., Schimdl C., Bauer H., 2011. Emission factors from residential combustion appliances burning Portuguese biomass fuels. Journal of Environmental Monitoring 13, 11, 3196-3206.

Ferreira F., Tente, H., Nogueira, N., Gomes, P., 2006b. Particulate Matter Assessment in the Lisbon Region: from Diagnosis to Solutions. 15th IUAPPA regional conference, Lille, France.

Ferreira, F., Monjardino, J., 2007. Identificação e Avaliação de Eventos Naturais de 2006: Annual Report for the Portuguese Environment Agency. Lisbon, Portugal.

Ferreira, F., Monjardino, J., 2008. Identificação e Avaliação de Eventos Naturais de 2007: Annual Report for the Portuguese Environment Agency. Lisbon, Portugal.

Ferreira, F., Monjardino, J., 2009a. Identificação e Avaliação de Eventos Naturais de 2008: Annual Report for the Portuguese Environment Agency. Lisbon, Portugal.

Ferreira, F., Monjardino, J., 2010. Identificação e Avaliação de Eventos Naturais de 2009: Annual Report for the Portuguese Environment Agency. Lisbon, Portugal.

Ferreira, F., Monjardino, J., 2011. Identificação e Avaliação de Eventos Naturais de 2010: Annual Report for the Portuguese Environment Agency. Lisbon, Portugal.

Ferreira, F., Nogueira, L., Almeida, C., Tente, H., Martins, A., Monjardino, J., Neto, J., Franco, N., Pereira, P., Gomes, P., Mesquita, S., Góis Ferreira, V., Maciel, H., Torres, P., 2006a. Planos e Programas para a melhoria da qualidade do ar na Região de Lisboa e Vale do Tejo. Edição Revista de Dezembro de 2006. Environmental Sciences Department of the Science and Technology Faculty - New University of Lisbon, Lisbon Regional Coordination and Development Commission (CCDR-LVT), INVENTAR, Lisboa, Portugal.

Ferreira, F., Nogueira, L., Almeida, C., Tente, H., Martins, A., Monjardino, J., Neto, J., Franco, N., Pereira, P., Gomes, P., Mesquita, S., Góis Ferreira, V., Maciel, H., Torres, P., 2009b. Planos e Programas para a melhoria da qualidade do ar na Região de Lisboa e Vale do Tejo (período 2005 - 2007). Edição Revista de Outubro de 2009. Environmental Sciences Department of the Science and Technology Faculty - New University of Lisbon, Lisbon Regional Coordination and Development Commission (CCDR-LVT), INVENTAR, Lisboa, Portugal.

Flores, J. M., Bar-Or, R. Z., Bluvshtein, N., Abo-Riziq, A., Kostinski, A., Borrmann, S., Koren, I., and Rudich, Y., 2012. Absorbing aerosols at high relative humidity: closure between hygroscopic growth and optical properties. Atmos. Chem. Phys. Discuss., 12, 1019-1052.

Fox, J., 1997. Applied regression analysis, linear models, and related methods. Sage, Thousand Oaks, California.

Franco, N., 2008. Efeito de eventos naturais na qualidade do ar – Avaliação dos métodos de identificação. MS Thesis. Universidade Nova de Lisboa.

Garber, W., Colosio, J., Grittner, S., Larssen, S., Rasse, D., Schneider, J., Houssiau, M., 2002. Guidance on the Annexes to Decision 97/101/EC on Exchange of Information as revised by Decision 2001/752/EC for the European Commission, European Commission, DG Environment.

Gobeli, D., Schloesser, H., Pottberg, T., 2008. Met One Instruments BAM-1020 Beta Attenuation Mass Monitor US-EPA $PM_{2.5}$ Federal Equivalent Method Field Test Results. Paper # 2008-A-485-AWMA

Góis, V., Nogueira, L., Almeida, C., Maciel, H., Torres, P., 2005. Using aerial photographic data for inventory of air emissions from road traffic sources: case study in the city of Lisbon. WIT Transactions on Ecology and the Environment 82, 337-347.

Gois, V., Torres, P., Nogueira, L., Maciel, H., Almeida, C., 2006. Inventário de Emissões Atmosféricas da Região de Lisboa e Vale do Tejo 2000-2001. Inventar, Estudos e Projectos Unip. Lda., CCDR-LVT (eds), Lisboa, Portugal.

Goloub, P., Tanré, D., Deuzé, J. L., Herman, M., Marchand, A., Breon, F. M., 1999. Validation of the first algorithm applied for deriving the aerosol properties over the ocean using the POLDER ADEOS measurements. Ieee Transactions on Geoscience and Remote Sensing 37,1586-1596.

Gonçalves, C., Alves C., Fernandes A.P., Monteiro C., Tarelho L., Evtyugina M., Pio C., 2011. Organic compounds in $PM_{2.5}$ emitted from fireplace and woodstove combustion of typical Portuguese wood species. Atmospheric Environment 45, 4533-4545.

Grey, W.M.F., North, P.R.J., Los, S.O., Mitchell, R.M., 2006. Aerosol optical depth and land surface reflectance from Multiangle AATSR measurements: Global validation and intersensor comparisons. IEEE Transactions on Geoscience and Remote Sensing 44, 2184-2197.

Grosso, N., Ferreira, F., Mesquita, S., 2006. Chapter 3.1 Improvement in particles ($PM_{10}$) urban air quality mapping interpolation using remote sensing

data. Air Pollution Modeling and Its Application XVIII, 265-274, Borrego, C. and Renner, E. (eds), Leipzig, Germany.

Grosso, N., Paronis, D., 2011. Comparison of contrast reduction based MODIS AOT estimates with AERONET measurements. Atmospheric Research 116, 33-45.

Gupta, P., and Christopher, S. A., 2009a. Particulate matter air quality assessment using integrated surface, satellite, and meteorological products: Multiple regression approach. J. Geophys. Res. 114, D14205.

Gupta, P., Christopher, S. A., 2009b. Particulate matter air quality assessment using integrated surface, satellite, and meteorological products: 2. A neural network approach. J. Geophys. Res. 114, D20205.

Gupta, P., Christopher, S.A., Wang, J., Gehrig, R., Lee, Y.C., Kumar, N., 2006. Satellite remote sensing of particulate matter and air quality over global cities. Atmospheric Environment, 40, 5880-5892.

Hoff, R., Christopher, S.A., 2009. Remote sensing of particulate matter air pollution from space : Have we reached the promised land. Journal of Air & Waste Management Association, 59, 642-675.

Hogg, R.V., Ledolter, J., 1987. Engineering Statistics. MacMillan, New York.

Holben, B. N., Eck, T. F., Slutsker, I., Tanré, D., Buis, J. P., Setzer, A., Vermote, E., Reagan, J. A., Kaufman, Y. J., Nakajima, T., Lavenu, F., Jankowiak, I., Smirnov, A., 1998. AERONET - A federated instrument network and data archive for aerosol characterization. Remote Sensing of Environment 66, 1-16.

Holben, B., Vermote, E., Kaufman, Y.J., Tanré, D., Kalb, V., 1992. Aerosol retrieval over land from AVHRR data - application for atmospheric correction. Ieee Transactions on Geoscience and Remote Sensing 30, 212-222.

Holben, B.N., Tanré, D., Smirnov, A., Eck, T.F., Slutsker, I., Abuhassan, N., Newcomb, W.W., Schafer, J., Chatenet, B., Lavenu, F., Kaufman, Y.J., Vande Castle, J., Setzer, A., Markham, B., Clark, D., Frouin, R., Halthore, R., Karnieli, A., O'Neill, N.T., Pietras, C., Pinker, R.T., Voss, K., Zibordi, G. , 2001. An emerging ground-based aerosol climatology: Aerosol Optical Depth from AERONET. J. Geophys. Res. 106, 12067-12097.

Hooyberghs, J., Mensink, C., Dumont, G., Fierens, F., and Brasseur, O., 2005. A neural network forecast for daily average $PM_{10}$ concentrations in Belgium. Atmos. Environ., 39, 3279–3289.

Hsu, N.C., Tsay, S.C., King, M.D., Herman, J.R. 2006. Deep blue retrievals of Asian aerosol properties during ACE-Asia. IEEE Transactions on Geoscience and Remote Sensing, 44(11), 3180-3195.

Huang W., Tan J., Kan H., Zhao N., Song W., Song G., Chen G., Jiang L., Jiang C., Chen R., Chen B., 2009. Visibility, air quality and daily mortality in Shanghai, China. Sci Total Environ 407(10), 3295-300

Husar, R. B., Halloway, J. M., Patterson, D. E., Wilson, W. E., 1981. Spatial and temporal pattern of eastern U.S. haziness: A summary. Atmos. Environ., 15, 1919-1928.

Hyslop, N.P., 2009. Impaired visibility: The air pollution people see. Atmos. Environ. 43, 182-195.

Ichoku, C., Kaufman, Y. J., Remer, L. A., Levy, R., 2004. Global aerosol remote sensing from MODIS. Advances in Space Research 34, 820-827.

INE, 2001. Recenseamento Geral da População e da Habitação - Censos 2001. Instituto Nacional de Estatística, Lisbon, Portugal.

IPCC, 2007: Climate Change 2007: The Physical Science Basis. Contribution of Working Group I to the Fourth Assessment Report of the Intergovernmental Panel on Climate Change [Solomon, S., D. Qin, M. Manning, Z. Chen, M. Marquis, K.B. Averyt, M.Tignor and H.L. Miller (eds.)]. Cambridge University Press, Cambridge, United Kingdom and New York, NY, USA.

Jerrett, M., Finkelstein, M., 2005. Geographies of Risk in Studies Linking Chronic Air Pollution Exposure to Health Outcomes. J. Toxicol. Environ. Health A 68, 1207-1242.

Joint WHO/Convention Task Force on the Health Aspects of Air Pollution, 2006. Health risks of particulate matter from long-range transboundary air pollution. WHO Regional Office for Europe, Copenhagen, Denmark.

Kacenelenbogen, M., Leon, J.F., Chiapello, I., Tanre, D., 2006. Characterization of Aerosol Pollution Events in France Using Ground-Based and POLDER-2 Satellite Data. Atmos. Chem. Phys. 6, 4843-4849.

Kahn, R. A., Gaitley, B. J., Martonchik, J. V., Diner, D. J., Crean, K. A., Holben, B., 2005. Multiangle Imaging Spectroradiometer (MISR) global aerosol optical depth validation based on 2 years of coincident Aerosol Robotic Network (AERONET) observations. Journal of Geophysical Research-Atmospheres 110, 16.

Kambezidis, H. D., Kaskaoutis, D. G. Aerosol climatology over four AERONET sites: An overview. Atmospheric Environment 42, 1892-1906.

Kaskaoutis, D.G., Kosmopoulos, P., Kambezidis, H.D., Nastos, P.T., 2007. Aerosol climatology and discrimination of different types over Athens, Greece, based on MODIS data. Atmospheric Environment 41, 7315-7329.

Kaufman, Y.J., Tanré, D., Boucher, O., 2002. A satellite view of aerosols in the climate system. Nature 419, 215-223.

Kim, Y., Sartelet, K., and Seigneur, C., 2011. Formation of secondary aerosols over Europe: comparison of two gas-phase chemical mechanisms, Atmos. Chem. Phys. 11, 583–598.

King, M.D., Kaufman, Y.J., Tanré, D. T, Nakajima, T., 1999. Remote sensing of tropospheric aerosols from space: Past, present, and future. Bulletin of the American Meteorological Society 80, 2229-2259.

Kleinman, M.T., Phalen, R.F., Mautz, W.J., Mannix, R.C., McClure, T.R., Crocker, T.T., 1989. Health effects of acid aerosols formed by atmospheric mixtures. Environmental Health Perspectives 79:137-45.

Knapp, K. P., Frouin, R., Kondragunta, S., Prados, A., 2005. Toward aerosol optical depth retrieval over land from GOES visible radiances: determining surface reflectance, Int. J. Remote Sens. 26, 4097–4116

Koelemeijer, R.B.A.; Homan, C.D.; Matthijsen, J., 2006. Comparison of Spatial and Temporal Variations of Aerosol Optical Thickness and Particulate Matter over Europe. Atmospheric Environment, 40, 5304-5315.

Kokhanovsky, A. A., Breon, F. M., Cacciari, A., Carboni, E., Diner, D., Di

Nicolantonio, W., Grainger, R. G., Grey, W. M. F., Holler, R., Lee, K. H., Li, Z., North, P. R. J., Sayer, A. M., Thomas, G. E., von Hoyningen-Huene, W, 2007. Aerosol remote sensing over land: A comparison of satellite retrievals using different algorithms and instruments. Atmospheric Research 85, 372-394.

Kreidenweis, S.M., Remer, L.A., Bruintjes, R., Dubovik, O., 2001. Smoke aerosol from biomass burning in Mexico: Hygroscopic smoke optical model. Journal of Geophysical Research-Atmospheres 106, 4831-4844.

Krewski, D., Burnett, R.T., Goldberg, M.S., Hoover, K., Siemiatycki, J., Jerrett, M.,Abrahamowicz, A. and White, W.H., 2000. Reanalysis of the Harvard Six Cities Study and the American Cancer Society Study of Particulate Air Pollution and Mortality, A Special Report of the Institute's Particle Epidemiology Reanalysis Project, Health Effects Institute, Cambridge, MA, USA.

Levy, R.C., Remer, L.A., and Dubovik, O., 2007. Global aerosol optical properties and

Lin, T.H., Chen, A.J., Liu, G.R., Kuo, T.H., 2002. Monitoring the atmospheric aerosol optical depth with SPOT data in complex terrain. International Journal of Remote Sensing 23, 647-659.

Lippmann, M., 2001. Human Health: Effects of Ambient Air Particulate Matter. Presentation made for "Acid Rain: Are the Problems Solved?", Center for Environmental Information, Washington DC, USA.

Liu, G.R., Lin, T.H., Kuo, T.H., 2002. Estimation of aerosol optical depth by applying the optimal distance number to NOAA AVHRR data. Remote Sensing of Environment 81, 247-252.

Liu, Y., Sarnat, J.A., Kilaru, A., Jacob, D.J., Koutrakis, P., 2005. Estimating Ground-Level $PM_{2.5}$ in the Eastern United States Using Satellite Remote Sensing. Environ. Sci. Technol. 39, 3269-3278.

Malm, W. C., Day, D. E., Kreidenweis, S.M., 2000. Light scattering characteristics for aerosols as a function of relative humidity: part I: A comparison of measured scattering and aerosol concentrations unsing the theoretical models.J. Air Waste Manage. Assoc. 50, 686-700.

MAOT (Ministério do Ambiente e do Ordenamento do Território), 1999. Decreto-Lei n.º 276/99, Diário da República, 170, 23.07.1999, pp. 4599-4604 (http://dre.pt/pdfgratis/1999/07/170A00.PDF), accessed 27 August 2012.

MAOT (Ministério do Ambiente e do Ordenamento do Território), 2002. Decreto-Lei n.º 111/2002, Diário da República, 89, 16.04.2002, pp. 3711-2722 (http://www.dre.pt/pdf1sdip/2002/04/089A00/37113722.PDF), accessed 27 August 2012.

MAOT (Ministério do Ambiente e do Ordenamento do Território), 2003. Decreto-Lei n.º 320/2003, Diário da República, 293, 20.12.2003, pp. 8512-8521 (http://www.dre.pt/pdf1sdip/2003/12/293A00/85128521.PDF), accessed 27 August 2012.

MAOT (Ministério do Ambiente e do Ordenamento do Território), 2010. Decreto-Lei n.º 102/2010, Diário da República, 186, 23.09.2010, pp. 4177-4205 (http://www.dre.pt/pdf1s/2010/09/18600/0417704205.pdf), accessed 27 August 2012.

Marques, F., Cassmassi, J. , Ferreira, F., Mesquita, S., 2006. Air quality forecast for Lisbon, Portugal: from data analysis to outreach. 2006 National Air Quality Conferences: Air Quality Forecasting, Mapping, and Monitoring and Communicating Air Quality and Communities in Motion "Quality of Air Means Quality of Life", San Antonio, Texas, USA.

Martins V., Miranda A.I., Carvalho A., Schaap M., Borrego C., Sá E., 2012. Impact of forest fires on particulate matter and ozone levels during the 2003, 2004 and 2005 fire seasons in Portugal. Science of the Total Environment, 414, 53-62.

Martonchik, J. V., Diner, D. J., 1992. Retrieval of aerosol optical properties from multiangle satellite imagery. IEEE Transactions on Geoscience and Remote Sensing, 30, 223-230.

Masmoudi, M., Chaabane, M., Tanré, D., Gouloup, P., Blarel, L., Elleuch, F., 2003. Spatial and temporal variability of aerosol: size distribution and optical properties. Atmospheric Research 66, 1-19.

Meier, J., Wehner, B., Massling, A., Birmili, W., Nowak, A., Gnauk, T., Brüggemann, E., Herrmann, H., Min, H., and Wiedensohler, A., 2009. Hygro-

scopic growth of urban aerosol particles in Beijing (China) during wintertime: a comparison of three experimental methods. Atmos. Chem. Phys. Discuss., 9, 6889-6927.

Mekler, Y., Kaufman, Y.J., 1982. Contrast reduction by the atmosphere and retrieval of nonuniform surface reflectance. Applied Optics 21, 310-316.

MODIS Characterization Support Team, 2006. MODIS Level 1B Product User's Guide For Level 1B Version 5.0.6 (Terra) and Version 5.0.7 (Aqua). (Available at http://mcst.gsfc.nasa.gov/sites/mcst.gsfc/files/file_attachments/M1054.pdf)

Neto, J., Ferreira, F., Torres, P.M., Boavida, F., 2009. Lisbon air quality forecast using statistical methods. International Journal of Environment and Pollution, 39(3/4), 333 - 339.

Neto, J., Torres, P. & Ferreira, F., 2004. Previsão da qualidade do ar para Lisboa – a abordagem estatística. 8th National Environment Conference, Lisbon. CD-ROM, pp. 11.

Neto, J., Torres, P., Ferreira F., Boavida, F., 2005. Lisbon air quality forecast using statistical methods. Proceedings of the Third International Symposium on Air Quality Management at Urban, Regional and Global Scales, pp. 591-597, Istanbul, Turkey.

Paciorek, C.J., Liu, Y., Moreno-Macias, H., Kondragunta, S., 2008. Spatiotemporal Associations between GOES Aerosol Optical Depth Retrievals and Ground-Level $PM_{2.5}$. Environ. Sci. Technol. 42, 5800-5806.

Pandolfi, M., Cusack, M., Alastuey, A., and Querol, X., 2011. Variability of aerosol optical properties in the Western Mediterranean Basin. Atmos. Chem. Phys., 11, 8189-8203.

Paronis, D., Sifakis, N., 2003. Satellite aerosol optical thickness retrieval over land with contrast reduction analysis using a variable window size. Igarss 2003: Ieee International Geoscience and Remote Sensing Symposium, Vols I - Vii, Proceedings - Learning from Earth's Shapes and Sizes, Ieee, New York, pp. 1276-1278.

Pateraki S., Asimakopoulos, D.N., Flocas, H.A., Maggos, T., Vasilakos, C., 2012. The role of meteorology on different sized aerosol fractions ($PM_{10}$, $PM_{2.5}$ and $PM_{2.5-10}$). Sci Total Environ 419, 124-35.

Pelletier, B., Santer, R. & Vidot, J., 2007. Retrieving of particulate matter from optical measurements: A semiparametric approach. Journal of Geophysical Research D: Atmospheres 112, D06208, 1-18.

Pereira, L., 2008. Contribuição dos aerossóis para os processos físico-químicos da atmosfera. MS Thesis. Faculdade de Ciências da Universidade de Lisboa.

Pope III, C.A., Dockery, W.D., 1999. Epidemiology of Particle Effects, In: Stephen T. Holgate, Jonathan M. Samet, Hillel S. Koren and Robert L. Maynard, Editor(s), Air Pollution and Health. Academic Press, London, pp. 673-705.

Pope, C.A. III, Burnett R.T., Turner, M.C., Cohen, A., Krewski, D., Jerrett, M., Gapstur, S.M., Thun, M.J., 2011. Lung Cancer and Cardiovascular Disease Mortality Associated with Ambient Air Pollution and Cigarette Smoke: Shape of the Exposure–Response Relationships. Environ Health Perspect 119(11), 1616-21

Pope, C.A. III, Dockery, D.W., 2006. Health effects of fine particulate air pollution: lines that connect. J Air Waste Manag Assoc. 56(6), 709-42.

Pope, C.A., III, Thun, M.J., Namboodiri, M.M., Dockery, D.W., Evans, J.S., Speizer, F.E., Heath, J.C.W., 1995. Particulate Air Pollution as a Predictor of Mortality in a Prospective Study of U.S. Adults. Am. J. Respir. Crit. Care. Med. 151, 669-674.

Prospero, J.M., 1999. Long-term measurements of the transport of African mineral dust to the southeastern United States: Implications for regional air quality. Journal of Geophysical Research-Atmospheres 104, 15917-15927.

Putaud, J.-P., van Dingenen, R., Alastuey, A., Bauer, H., Birmili, W., Cyrys, J., Flentje, H., Fuzzi, S., Gehrig, R., Hansson, H., Harrison, R., Herrmann, H., Hitzenberger, R., Huglin, C., ¨Jones, A., Kasper-Giebl, A., Kiss, G., Kousa, A., Kuhlbusch, T.,Loschau, G., Maenhaut, W., Molnar, A., Moreno, T., Pekkanen, J., Perrino, C., Pitz, M., Puxbaum, H., Querol, X., Rodriguez, S., Salma, I., Schwarz, J., Smolik, J., Schneider, J., Spindler, G., ten Brink, H., Tursic, J., Viana, M.,

Wiedensohler, A., and Raes, F., 2010. A European aerosol phenomenology - 3: Physical and chemical characteristics of particulate matter from 60 rural, urban, and kerbside sites across Europe, Atmos. Environ. 44, 1308–1320.

Querol, X., Alastuey, A., Pey, J., Escudero, M., Castillo, S., Gonzalez Ortiz, A., Pallarés, M., Jiménez, S., Cristóbal, A., Ferreira, F., Marques, F., Monjardino, J., Cuevas, E., Alonso, S., Artíñano, B., Salvador, P., de la Rosa, J., 2009. Methodology for the identification of natural episodes in $PM_{10}$ and $PM_{2.5}$, and justification with regards to the exceedances of the $PM_{10}$ daily limit value. Instituto de Diagnóstico Ambiental Y Estudios del Agua – CSIC - Ministerio de Ciencia e Innovación, Universidad Nova de Lisboa, AEMet-Izaña, CIEMAT, Universidad de Huelva. IDEA/CSIC, Barcelona, Spain.

Remer L., Kleidman R., Levy R., Kaufman Y., Tanre D., Mattoo S., Martins J., Ichoku C., Koren I., Yu H., Holben B., 2008. Global aerosol climatology from the MODIS satellite sensors. J. Geophys. Res., 113, D14S07.

Remer, L. A., Kaufman, Y. J., Tanre, D., Mattoo, S., Chu, D. A., Martins, J. V., Li, R. R., Ichoku, C., Levy, R. C., Kleidman, R. G., Eck, T. F., Vermote, E., and Holben, B. N., 2005. The MODIS aerosol algorithm, products, and validation. J. Atmos. Sci. 62, 947–973.

Remer, L. A., Kleidman, R. G., Levy, R. C., Kaufman, Y. J., Tanré, D., Mattoo, S., Martins, J. V., Ichoku, C., Koren, I., Yu, H. B., Holben, B. N., 2008. Global aerosol climatology from the MODIS satellite sensors. Journal of Geophysical Research-Atmospheres 113, 18.

Remer, L. A., Tanre, D., Kaufman, Y. J., Levy, R., Mattoo, S., 2006. Algorithm for remote sensing of Tropospheric aerosol from MODIS: Collection 005. Product ID MOD04/MYD04 Ref. No. ATBD-MOD-96. (Available at http://modis-atmos.gsfc.nasa.gov/_docs/MOD04:-MYD04_ATBD_C005_revl.pdf).

Renard, J. B., Brogniez, C., Berthet, G., Bourgeois, Q., Gaubicher, B., Chartier, M., Balois, J. Y., Verwaerde, C., Auriol, F., Francois, P., Daugeron, D., Engrand, C., 2008. Vertical distribution of the different types of aerosols in the stratosphere: Detection of solid particles and analysis of their spatial variability. Journal of Geophysical Research-Atmospheres 113, 17.

Retalis, A., Sifakis, N., 2010. Urban aerosol mapping over Athens using the differential textural analysis (DTA) algorithm on MERIS-ENVISAT data. Isprs Journal of Photogrammetry and Remote Sensing 65, 17-25.

Retalis, A., Sifakis, N., Grosso, N., Paronis, D., Sarigiannis, D., 2003. Aerosol optical thickness retrieval from AVHRR images over the Athens urban area. Igarss 2003: Ieee International Geoscience and Remote Sensing Symposium, Vols I - Vii, Proceedings - Learning from Earth's Shapes and Sizes, Ieee, New York, pp. 2182-2184.

Robles González, C. Schaap, M. de Leeuw, G., Builtjes, P. J. H., van Loon, M., 2003. Spatial variation of aerosol properties over Europe derived from satellite observations and comparison with model calculations. Atmos. Chem. Phys., 3, 521–533.

Rohen, G. J., von Hoyningen-Huene, W., Kokhanovsky, A., Dinter, T., Vountas, M., Burrows, J. P., 2011. Atmospheric Measurement Techniques 4(3), 523-534.

Rost J., Holst, T., Sähn, E., Klingner, M., Anke, K., Ahrens, D., Mayer, H., 2009. Variability of $PM_{10}$ concentrations dependent on meteorological conditions. Int J Environ Pollut 36, 3-18.

S. Rodríguez, Querol, X., Alastuey, A., Kallos, G., Kakaliagou, O., 2001. Saharan dust contributions to $PM_{10}$ and TSP levels in Southern and Eastern Spain Atmos Environ 35, 2433–2447.

Santos, D., Costa, M. J., and Silva, A. M., 2008. Direct SW aerosol radiative forcing over Portugal. Atmos. Chem. Phys., 8, 5771-5786.

Santos, D., M.J. Costa and A.M. Silva, 2007. Local Direct SW Radiative Forcing by Saharan Dust and Forest Fire Aerosols over Portugal. European Aerosol Conference, Salzburg, Abstract T20A004

Scarrow, H. A., 1972. The impact of British domestic air pollution legislation. Brit. J. Pol. Sci., 2(3), 261–282.

Seinfeld, J.H., Pandis, S.N., 2006. Atmospheric Chemistry and Physics: From Air Pollution to Climate Change. John Wiley & Sons, Inc (eds), Hoboken, New Jersey, USA.

Sifakis, N., Deschamps, P.Y., 1992. Mapping of air-pollution using SPOT satellite data, Photogrammetric Engineering and Remote Sensing 58, 1433-1437.

Sifakis, N., Soulakellis, N. A., Paronis, D. K., 1998. Quantitative mapping of air pollution density using earth observations: a new processing method and application to an urban area, International Journal of Remote Sensing 19, 3289-3300.

Solomon, S., Qin, D., Manning, M., Chen, Z., Marquis, M., Averyt, K.B., Tignor, M., Miller, H.L., 2007. Contribution of Working Group I to the Fourth Assessment Report of the Intergovernmental Panel on Climate Change, Cambridge University Press, New York.

Spangl, W., 2007. Representativeness and Classification of Air Quality Monitoring Stations: Final Report. Umweltbundesamt, Vienna.

Tanré, D., Deschamps, P.Y., Devaux, C., Herman, M., 1988. Estimation of saharan aerosol optical-thickness from blurring effects in Thematic Mapper data. Journal of Geophysical Research-Atmospheres 93, 15955-15964.

Tanré, D., Kaufman, Y. J., Holben, B. N., Chatenet, B., Karnieli, A., Lavenu, F., Blarel, L., Dubovik, O., Remer, L. A., Smirnov, A., 2001. Climatology of dust aerosol size distribution and optical properties derived from remotely sensed data in the solar spectrum. Journal of Geophysical Research-Atmospheres 106, 18205-18217.

Tanré, D., Vermote, E., Holben, B.N., Kaufman, Y.J., 1992. Satellite aerosols retrieval over land surfaces using the structure functions, Geoscience and Remote Sensing Symposium, 1992, New York, pp. 1474-1477.

Tente, H., 2005. Impacte das partículas em suspensão sobre a saúde humana: uma abordagem multidisciplinar para a cidade de Lisboa. MS Thesis. Universidade de Aveiro. Print.

Tran, H. T., Alvarado, A., Garcia, C., Motallebi, N., Miyasato, L., Vance, W. 2008. Methodology for Estimating Premature Deaths Associated with Long-term Exposure to Fine Airborne Particulate Matter in California, California Environmental Protection Agency, Air Resources Board, Sacramento, CA, USA.

van den Hout, D., Larssen, S., 2006. Representativeness and network design. Project Air4EU - M.3 report, http://www.air4eu.nl/reports_products.html, accessed on 01-08.2012.

van Donkelaar, A.; Martin, R.V.; Park, R.J., 2006. Estimating Ground-Level $PM_{2.5}$ Using Aerosol Optical Depth Determined from Satellite Remote Sensing. J. Geophys. Res. Atmos. 111, D21201.

Veffkind, P., van Hoss, R.F., Eskes, H., Borowiak, A., Dentener, F. and Wilson, J., 2007. The applicability of remote sensing in the field of air pollution. European Commission/Directorate-General Joint Research Centre, Institute for Environment and Sustaintability,

Vidot, J., Santer, R. & Ramon, D., 2007. Atmospheric particulate matter (PM) estimation from SeaWiFS imagery. Remote Sensing Environment 111, 1-10.

Vidot, J., Santer, R., Aznay, O., 2008. Evaluation of the MERIS aerosol product over land with AERONET. Atmospheric Chemistry and Physics 8, 7603-7617.

von Hoyningen-Huene, W., Kokhanovsky, A. A., Burrows, J. P., Bruniquel-Pinel, V., Regner, P., Baret, F., 2006. Simultaneous determination of aerosol- and surface characteristics from top-of-atmosphere reflectance using MERIS on board of ENVISAT, Atmospheric Remote Sensing: Earth's Surface, Troposphere, Stratosphere and Mesosphere - Ii, Elsevier Science Ltd, Oxford, pp. 2172-2177.

Wang, J., Christopher, S. A., 2003. Intercomparison between satellite-derived aerosol optical thickness and $PM_{2.5}$ mass: Implications for air quality studies, Geophys. Res. Lett. 30(21), 2095.

Wang, Z., Chen, L., Tao, J., Zhang, Y. & Su, L., 2010. Satellite-based estimation of regional particulate matter (PM) in Beijing using vertical-and-RH correcting method. Remote Sensing of Environment 114, 50-63.

WHO, 2003. The World health report : 2003 : shaping the future. World Health Organization, Geneva, Switzerland.

WHO, 2004. Health Aspects of Air Pollution - Results from the WHO Project "Systematic Review of Health Aspects of Air Pollution in Europe". WHO

Regional Office for Europe. Copenhagen, Denmark.

Winkler, H., Formenti, P., Esterhuyse, D. J., Swap, R. J., Helas, G., Annegarn, H. J., Andreae, M. O., 2008. Evidence for large-scale transport of biomass burning aerosols from sunphotometry at a remote South African site. Atmospheric Environment 42, 5569-5578.

Xia, X.A., Chen, H.B., Wang, P.C., Zhang, W.X., Goloub, P., Chatenet, B., Eck, T.F. & Holben, B.N., 2006. Variation of column-integrated aerosol properties in a Chinese urban region. J. Geophys. Res. 111, D05204, 1-10.

Zhou, L., Dickinson, R.E., Tian, Y., Zeng, X., Dai, Y., Yang, Z., Schaaf, C.B., Gao, F., Jin, Y., Strahler, A., Myneni, R.B., Yu, H., Wu, W., Shaikh, M., 2003. Comparison of seasonal and spatial variations of albedos from Moderate-Resolution Imaging Spectroradiometer (MODIS) and Common Land Model. Journal of Geophysical Research – Atmospheres 108, 4488.